POLITECNICO DI MILANO

Department of Electronics, Information and Bioengineering
Master degree in Automation and Control Engineering

SELF-TUNING ALGORITHMS FOR OUTSIDE TEMPERATURE REJECTION FOR RADIANT PANEL HEATING SYSTEMS

Thesis presented by:

Riccardo Babini, 833504

Supervisor:
Prof. Luca Ferrarini

Correlator:
Ing. Anacleto Petretti

2015/2016

PAGE INTENTIONALLY LEFT BLANK

INDEX

INDEX 3
SOMMARIO 7
RINGRAZIAMENTI 9
ABSTRACT 11
1. INTRODUCTION 13
1.a State of Art analysis 13
1.b Thesis objectives 15
1.c Document structure 16
2. MODELING 17
2.a State of the art modeling techniques 17
2.b 4-states Model 19
2.b.1 System outline 19
2.b.2 State variables and inputs 20
2.b.3 Heat exchange equations and state-space model 23
2.b.4 Pipe heat exchange 29
2.c Effect of saturations 31
2.c.1 Saturation on the inlet water temperature set-point 31
2.c.2 Saturation of the mixing valve 33
2.d Model testing 36
2.e Extending the model 38
2.f Chapter 2 conclusions 40
3. CONTROL 41
3.a Zone temperature PID control 41
3.b Mixing valve control 46

3.c Anti-windup 48
3.d Safety hysteresis 51
3.e Outside temperature compensator 54
3.e.1 Compensator structure 54
3.e.2 Typical outside temperature profile 56
3.e.3 1-pole 1-zero approximation of M(s) 58
3.e.4 Updating the anti-windup 59
3.f Chapter 3 conclusions 61
4. PLANT ANALYSIS AND IDENTIFICATION 63
4.a Main thermo-physical parameters 63
4.a.1 Parameters choice 64
4.a.2 Range for the main thermo-physical parameters 67
4.a.3 Representative rooms and limit cases 70
4.b G(s), H(s) and M(s) analysis 73
4.b.1 G(s) and H(s) 73
4.b.2 M(s) 76
4.c Plant identification 77
4.c.1 Identification algorithm 77
4.c.2 G(s) estimation 78
4.c.3 G(s) gain estimation refinement 87
4.c.4 H(s) estimation 88
4.d Estimated G(s) and H(s) analysis 90
4.e Chapter 4 conclusions 93
5. ADAPTIVE TUNING 95
5.a PID adaptive tuning 95
5.b M(s) adaptive tuning 97
5.b.1 M(s) gain 98
5.b.2 M(s) zero 99
5.b.3 M(s) pole 101
5.c Adaptive tuning algorithms 111
5.d Applicability limits 119
5.d.1 Room dimensions 120
5.d.2 Radiant panel parameters 125
5.d.3 Conclusions on the applicability limits 127
5.e Chapter 5 conclusions 128

6. SOLAR RADIATION 129
6.a Transfer functions analysis 129
6.a.1 J(s) analysis 130
6.a.2 K(s) analysis 131
6.a.3 Conclusions on the solar radiation transfer functions 133
6.b Solar radiation effect on M(s) 134
6.b.1 M(s) gain 134
6.b.2 M(s) zero 135
6.b.3 M(s) pole 135
6.b.4 Conclusions on the solar radiation effect on M(s) 138
6.c Solar radiation compensator idea 138
6.d Chapter 6 conclusions 141
7. FAULTS 143
7.a Mixing valve fault 144
7.b Inlet water temperature sensor fault 146
7.b.1 Positive offset 147
7.b.2 Negative offset 153
7.b.3 Conclusions on this fault 156
7.c Chapter 7 conclusions 156
8. SIMULATIONS 157
8.a G(s) estimation 157
8.a.1 G(s) Closed loop 157
8.a.2 G(s) Open loop 160
8.a.3 G(s) estimation in open loop exploiting H(s) estimation 162
8.b H(s) estimation 166
8.c Adaptive tuning algorithms 168
8.c.1 Algorithm 1 170
8.c.2 Algorithm 2 171
8.c.3 Algorithm 3 172
8.c.4 Algorithm 4 173
8.c.5 Algorithm 5 174
8.c.6 Algorithm 6 175
8.c.7 Algorithm 7 176
8.c.8 Conclusions on the tuning algorithms 177
8.d Chapter 8 conclusions 177

9. CONCLUSIONS 179
9.a Main achievements 179
9.b Limitations and future developments 180
List of figures 183
List of tables 187
Bibliography 189

RINGRAZIAMENTI

Ringrazio innanzitutto il Prof. Ferrarini ed il team del Daisy Lab per la collaborazione e frequente supporto che han reso possibile questo lavoro di tesi.

Per il resto, la lista si farebbe lunga. Onestamente, non sarei riuscito a concludere questo percorso senza la forza della rete sociale di cui dovrei esser sempre grato. Poi ti ritrovi a realizzare queste fortune solo quando hai l'occasione di doverci pensare, ma va bene così.

La famiglia si ringrazia sempre per prima o per ultima. Ringraziamola per prima. Per quanto in casa io sia freddo e burbero, i sentimenti stanno sempre sotto superficie. Ma a voi non serve spiegarlo, siamo fatti della stessa pasta.

Tutti gli altri rapporti vanno e vengono. Di persone che han lasciato il segno ne son passate, e anche se non dovessi citarle personalmente non se ne abbiano a male, non sono state dimenticate. Per necessità, qui ringrazio solo chi è presente tutt'ora. Inizio con il buon Fausto, la persona che più rappresenta l'idea di saggezza ai miei occhi. Poi viene tutto il gruppo Pornaccin. I 3 Forse Laureati, e così resterete a vita, rompi-cocci che non siete altro. Quella pisquana dell'Eli, che ci cresci insieme e ti ci affezioni. La Silviona e la Batterista (resterò sempre il tuo bhrem-bhrem). I compagni di corso, con particolare attenzione a Ja e Tia. Ringrazio anche Loris per la sua pazienza e apertura, ma soprattutto per la sua famigerata umiltà. La Chiara, meglio conosciuta come Mrs. Doubtfire, di un altruismo poco manifesto ma immenso. Il buon moffettone Nico, che si laurea oggi (se tutto è andato bene!). Il Gabri, che non tiri giù manco a cannonate. Tutto il "gruppo di Mariano" con cui ho condiviso momenti di pacifico divertimento. Il signor Pipero, sempre lì a Milàn a fa' su i danè. Il mitico (p)Icio, sempre sorridente come si dovrebbe essere, e i due cervelloni delle Riva sisters.

L'ultimo paragrafo va a tutti i compagni di viaggio passati, sperando che le nostre strade un giorno si rincontrino con la stessa perfetta casualità della prima volta.

PAGE INTENTIONALLY LEFT BLANK

SOMMARIO

La presente tesi è dedicata allo sviluppo di una nuova strategia di taratura adattiva nel contesto del controllo del sistema di riscaldamento a pannelli radianti. Questa strategia di taratura adattiva è programmata per adattarsi alla variazione dei parametri termo-fisici della stanza sotto controllo. Questi parametri sono difficilmente identificabili da un'analisi manuale a causa della loro dipendenza dai materiali costruttivi e dalle condizioni ambientali generali della stanza. Nonostante ciò, l'adeguata taratura del sistema di controllo dipende fortemente da questi parametri termo-fisici, rendendone necessaria l'identificazione al fine di raggiungere adeguate performance in termini di comfort termico. A causa della scarsità di sensori in dotazione di questo sistema di riscaldamento, la strategia di taratura adattiva presenta una combinazione di procedure di identificazione tradizionali e ragionamenti di livello sistemico.

La ricerca è stata sviluppata basandosi su un modello a parametri concentrati simulato in ambiente Simulink. Questo modello semplificato è sufficientemente dettagliato da riuscire a descrivere le dinamiche dominanti del sistema sotto controllo. Inoltre questa scelta modellistica permette una maggiore rappresentatività fisica dei risultati sulla base dei quali la strategia adattiva sarà sviluppata. A causa delle tipiche restrizioni tecnologiche imposte dal mercato, le strategie di controllo più avanzate sono state scartate in favore di approcci più tradizionali, quali controllori PID affiancati da un compensatore in anello aperto per il disturbo causato dalla temperatura esterna. Dopo aver presentato il modello e la struttura di controllo adottate, il focus della tesi viene spostato sullo sviluppo della strategia di controllo adattiva. Infine vengono presentate due analisi aggiuntive: la prima riguardante l'effetto stimato della radiazione solare sulla strategia adattiva proposta, la seconda contenente un'analisi dei guasti volta a sottolineare i principali punti deboli del sistema a pannelli radianti.

PAGE INTENTIONALLY LEFT BLANK

ABSTRACT

In this thesis a simple and robust adaptive tuning strategy is presented in the context of the control of a room endowed with a radiant panel heating system. The proposed adaptive tuning strategy is required to adapt the control parameters with respect to any variation of the thermo-physical parameters of the system. The latter ones are hardly identifiable by an external operator because of their dependency from the constructive materials and general environmental conditions. Nevertheless, the correct tuning of the control structure strongly depend on those parameters, thus making their identification a necessary step to obtain high thermal comfort performances. Because of the few sensors equipped in this kind of heating system, some high-level reasoning is combined with the traditional identification methods in order to correctly adapt the control parameters to the actual controlled plant.

The research is developed based on a lumped parameters model simulated in the Simulink environment. The simplified model is detailed enough to catch all the relevant dynamics affecting the thermal system under control. Moreover, this modeling choice allows a better physical representativeness of the results by which the obtained conclusions can be logically explained. Due to the typical restrictions imposed by the market, advanced control strategies are discarded in favor of more traditional ones such as PID controllers and a simple open loop compensator for the outside air temperature disturbance. After describing the modeling and the control structure adopted, the thesis focuses on the development and testing of such adaptive tuning strategies. Finally, two additional analyses are presented: the first concerning the estimated effect of the solar radiation disturbance on the proposed adaptive tuning strategy and the second discussing the main weaknesses of the radiant panel heating system through a fault analysis.

PAGE INTENTIONALLY LEFT BLANK

1. INTRODUCTION

This chapter is dedicated to the reasoning behind this thesis work. In the first section 1.a a state of art analysis is carried out. Then, the thesis main objective – based on the requirements that were imposed by the research commissioner – is presented in section 1.b. Finally, the structure of the thesis document is described in section 1.c in order to ease its fruition to the reader.

1.a State of Art analysis

Different building temperature control strategies have been developed especially in the last decade because of the increasing interest in building energy efficiency. Among these strategies, many concern advanced control methods such as MPC, artificial neural networks and so on. In most of the applications, these control strategies are supported by an adaptive component which aims at reducing the uncertainties on the model of the controlled plant. The technical literature is dense of theories and applications of the adaptive approach. A valid reference to include the majority of this field background is “Astrom & Wittenmark” [1]. An example of adaptive-based control of a heating system is [2], in which an adaptive control strategy based on the Recursive Least Square identification method has been developed for a multizone airhandling unit. However, as anticipated in the abstract, the mere application of the identification procedures alone does not provide a solution for the control task tackled in this thesis because of the lack of available measurements.

A more sophisticated study is produced in [3], in which an integration of adaptive control and model predictive control has been developed, but the main focus is on the occupant behavior and discomfort aspects. In [4] an ANN-based (Artificial Neural Network) model has been integrated with a predictive and adaptive thermal control with the focus on disturbance rejection. Very satisfactory results characterized the performances of both these studies. However, their sophisticated control theories are not suitable for the typical market restrictions. Moreover, the results of these studies strongly depend on the quality of the prediction and the estimation, which cannot be guaranteed generally due to the typical uncertainties and disturbances acting on the building. In addition, these techniques lack of

the high reliability required by the market because the stability, the quality of estimation and the convergence rate of these methods are affected by the initial control configuration.

Less sophisticated control techniques have been developed in the context of the control of a single room endowed with a heating device. In [5] the adaptive control strategy is used for a radiator heating system. In this study, an operator decision is required to adapt the control scheme. These methods are usually called “push-button”, which are not so user-friendly. Other studies [6] [7] [8] applied an adaptive procedure on a constrained MIMO (Multi-Input Multi-Output) system. The control had to deal with saturation constraints on the input – such as the valve saturations – similarly to what will be carried on in this thesis. However, these methods rely on a fixed state-space plant model and present some convergence issues.

One way to tackle the problem proposed in this thesis could be to extend the sophisticated control strategies (MPC, ANN…) to the current application. In the majority of the current market realities, however, the control structure installed on a generic heating system is simply constituted of a feedback control loop endowed with a PID regulator. This simple control structure is chosen because of the well-known reliability of the PID controllers, in spite of not exceptional obtainable performance. In some cases, this control is helped with a compensator meant to reject the effect of the outside air temperature. The outside air temperature is the most commonly compensated disturbance because of its easy measurability. The focus of this thesis will be on developing an efficient adaptive tuning strategy for both the PID controller and the outside air temperature compensator. The current PID and compensator tuning strategies involve the use of a single time constant related to the building under control. This time constant is then implemented in a fixed control algorithm that was proven to return a sufficiently increased thermal comfort in the common heating systems scenarios. However, this approach presents two main weakness. First, it simplifies too much the thermal dynamics of the building by associating a single time constant to the whole system. Second, it loses almost completely any physical representativeness and thus trusts only an empirical evidence obtained from a testing campaign.

1.b Thesis objectives

Some of the advanced control solutions (MPC, ANN etc…) already present a potentially high improvement in terms of thermal comfort with respect to the state of the art PID-based technology installed on the current radiant panel systems. However, those solutions are based on complex theories that are hardly implementable on the simple controllers dedicated to the home-scale reality of this heating system. A simple and reliable adaptive tuning strategy was preferred, so its development and first testing is presented in this thesis.

The objective of this research is then to propose an improved and robust adaptive tuning strategy for the existing PID-based control typically installed on the radiant panel heating systems. The adaptive nature of this proposed control strategy is required because of the strong influence that the physical parameters of the controlled system have on the control tuning performances. A single robust control tuning for all the possible system configurations would result in a severe restriction on the obtainable performances. It is then vital to adapt the control parameters on the controlled system physical parameters in order to obtain an appreciable overall heating performance.

The controlled system is characterized by a multitude of different physical parameters. Most of these parameters cannot be neglected when deciding the control tuning. Some of these parameters are easily measureable and can then be easily considered in the control tuning. However, other parameters are characterized by a thermo-physical nature that makes them both hardly identifiable and strongly affecting the system dynamics. For these reasons, a particular combination of known identification procedures and high-level reasoning needs to be developed to overcome this obstacle. This complete strategy presented in the current thesis is required to perform its adaptive task in a reasonable time span. This quality is intended both to meet with the user thermal comfort requirements and to grant the possibility of a retuning in case of relevant variations on the controlled system conditions.

The presented research is based on a lumped parameters model developed in Simulink environment. This model has been developed so to capture the main dynamics of the controlled system while maintaining the physical representativeness of the quantities involved. The model has been verified on a testing room made available by a company involved in the production of radiant panel heating systems.

1.c Document structure

A new modeling and control structure is proposed together with a special adaptive tuning strategy. The modeling adopted in this thesis is presented in chapter 2. The following chapter 3 is dedicated to the presentation of the control structure. This structure relies on the same typical hardware installed on radiant panel systems. The analysis continues with chapter 4 where some relevant plant identification procedures are presented together with a set of sensitivity analyses that will serve the adaptive tuning strategy. Finally, the adaptive tuning strategy is presented in chapter 5 declined into seven different algorithms together with their applicability limits. The thesis continues in chapter 6 with a discursive analysis on the expected impact of the solar radiation on the tuning algorithms here presented. Another chapter 7 presents a brief fault analysis to highlight some critical points of the hardware set of the radiant panel system. The chapter 8 presents some relevant results taken from the adaptive tuning algorithms testing campaign. A final chapter 9 gathers the results of the thesis to draw its conclusions, describing the main achievements obtained the limitations of this approach and its future developments.

In this thesis, each section of each chapter presents a brief summary of the content of the section itself. In this way, the reader can easily focus on the parts of more interest. Each chapter, with exception of chapter 1 and chapter 9, is then closed by a conclusion section which collects the relevant results of the chapter itself.

2. MODELING

In this chapter, the model used for this thesis is developed in section 2.b. Before that, a brief analysis of the modeling techniques common of this field is listed in section 2.a. This step is necessary to justify the adoption of the modelling technique of this work. After the model designing, a discussion will be held in section 2.c about the effect on the system performance of the saturations imposed on the plant. The fourth section 2.d is dedicated to the model verification on an existing small testing room. A final section 2.e discusses the possible extension of the model by adding a fifth state.

2.a State of the art modeling techniques

A vast range of modeling techniques are already present in the literature to capture the thermal behavior of a building. Without entering too much into detail, a list of known techniques is presented together with a quick review of their advantages and disadvantages:

- Static or quasi-static models: these models are used mainly for building load estimation. This problem is of increasing concern in energy efficiency building regulations. For this reason, various calculation methods are continuously developed according to the newest EU regulations, granting an up-to-date range of analytical tools [9] [10] [11].
  However, these models are too simplified for this thesis purpose since they focus only on the thermal load of the building neglecting most of the transient behavior. For this reason, this excessively simplified modeling cannot be adopted.
- Simulation software: an extremely wide scenario of simulation packages is currently available. It would take too much to describe all the different shades that each software focuses on, so only the main characteristic of this approach will be discussed. The simulation software distinguishes itself for the complexity of the model that it uses. Exploiting a high number of variables and parameters, the simulation software can usually obtain a remarkable accuracy with respect to the real plant. For this reason, the simulation software is of great aid during the building design phase – when no measurement data is available – to perform a sensitivity analysis with respect to different constructive choices. One of the most famous software packages in this context is EnergyPlus, a tool that is able to integrate all the

main aspects of the plant-building system, from indoor environment thermal loads to HVAC plants and heating and cooling generation system.

However, this modeling approach is commonly discarded when coming to the designing of the control strategy exactly because of its excessive complexity: during the control designing, it is preferable to rely only on a restricted set of important quantities in order to easily verify its performance properties. Moreover, the thesis scenario will be characterized by a major uncertainty on the main thermal-related parameters, making it useless to exaggerate the accuracy level of our modeling.

- Black-box modeling: this category represents one of the simplest modeling approaches seen in literature. This kind of technique tries to reproduce the thermal behavior of the building by extrapolating ARX/ARMAX/Artificial Neural Network models from data [12] [13] [14].The advantage of this approach lays on its easy implementation and low computational effort due to its long-affirmed literature and algorithms.

  However, these techniques cannot be adopted in our context because the obtained model lacks of physical representation, a fact that would prevent us from developing robust control tuning strategies.

- Lumped Parameters Modeling: this strategy is usually the preferred approach when studying the main dynamics of a thermal system. With this approach, the theoretically infinite state variables of our system are grouped in a small set of representative variables, i.e. we consider a single state variable is adopted to describe the temperature of an entire wall, another one to describe the air temperature and so on. Of course, this approximation introduces a more or less severe inaccuracy with respect to the real plant behavior, but it also allows to establish physical/logical connections between the thermal phenomena thus making it a powerful tool to design the control structure and the control tuning procedures.

  Moreover, by adopting a lumped parameter model for a simple thermal system it is possible to exploit the RC equivalent circuit to further simplify the analysis of the system: a thermal capacity will be associated with a capacitor and a thermal conductance with a resistor, obtaining an electric circuit whose passive components are resistances and capacitors only. This RC modeling is widely used even to develop high order models [15], since its accuracy has been proven to be sufficiently high in most of the common study applications. In this thesis, the RC equivalent will be

exploited to easily prove some characteristics of our plant in both section 4.b.1 and 6.a.

Among the previously presented modeling techniques, the lumped parameters modeling is adopted in this thesis because of its adequacy to the proposed purposes, i.e. control designing and tuning.

2.b 4-states Model

In this section, the model adopted for this thesis is developed. First, a quick description of the system nature and functioning will be held in section 2.b.1. Then the state variables and the inputs of the model will be listed and described in section 2.b.2. Lastly, the equations describing the heat exchanges considered in this system will be presented in section 2.b.3. The pipe heat exchanges equations are deeply analyzed in section 2.b.4.

2.b.1 System outline

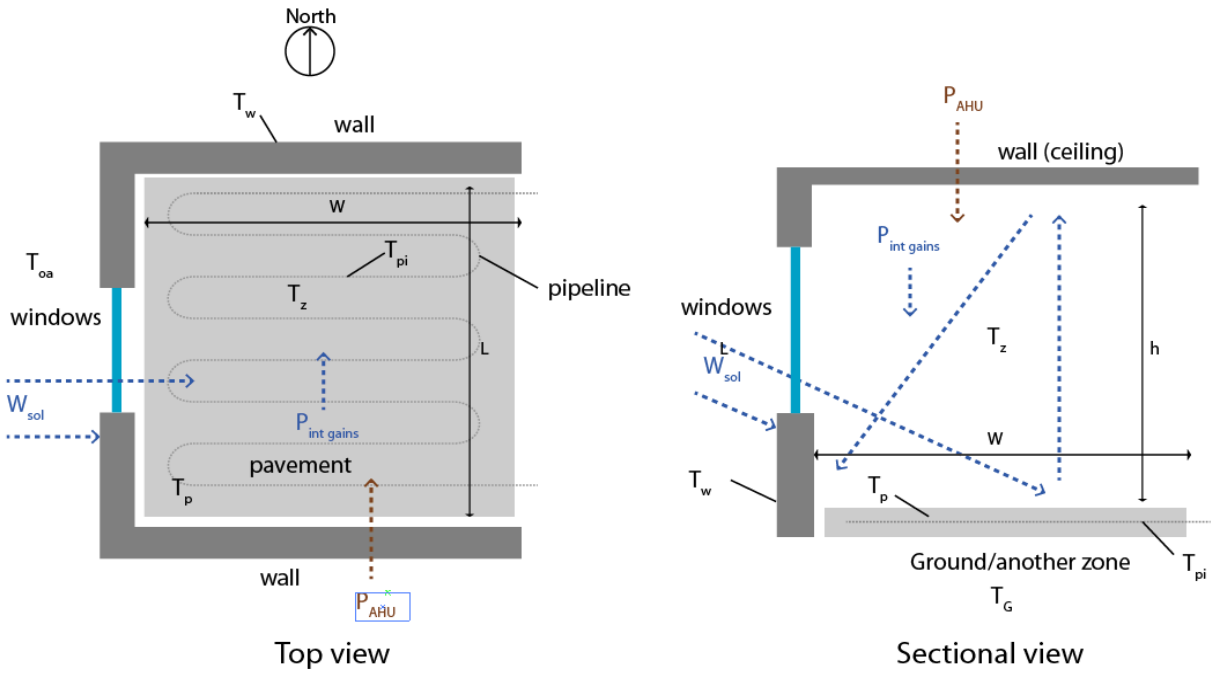

Fig. 2.1: Room endowed with radiant panel heating system

The system is schematically represented in Fig. 2.1 along with its inputs and state variables. As preannounced in the introduction, this system is endowed with a radiant panel heating system installed inside the pavement. A brief description of its functioning will be now given.

When the system is activated, a pump ensures a constant water flow inside a pipeline that is installed under the pavement. The temperature inside the pipeline is controlled as to release heat to the pavement, that in turn will heat the controlled air volume. Usually a screed ("massetto") is installed in the pavement together with the pipeline in order to support it with a big thermal inertia and guarantee a long-lasting mild warmth to the user. The temperature of the water at the inlet of the pipeline is controlled with a three-way mixing valve: the water outgoing the pipeline is recovered in this valve and is then mixed with an additional amount of hot water coming from a boiler, in order to meet an imposed inlet temperature set-point. The functioning of the valve is tackled more in detail in section 2.c.2.

The system can then be deactivated: in this OFF state, an electronically controlled shut-off valve installed on the pipeline is closed and the water will quickly stop flowing. Moreover, the mixing valve cuts off the hot water source and the regulators stop outputting their control action. The deactivation of the system can occur even during its normal functioning for safety reasons: in the control chapter 3 we will introduce a safety hysteresis cycle that deactivates the system in case of over-heating of the control volume. The heat exchange phenomena taking place when the system is deactivated will be different from the flowing water case, but this distinction will be addressed later on in the 2.b.4 paragraph.

2.b.2 State variables and inputs

First, the thermal load under control is considered as a single thermal volume. This assumption is made in agreement with the modeling strategy chosen (Lumped Parameters Modeling) by which any non-severe simplification is expected. Multiple thermal volumes could have been considered to account for the stratification of the air or other thermal phenomena. However, in this work it is assumed that the thermal load is sufficiently small – like a residential room and similar volumes – so that such phenomena represent a negligible effect.

Following this lumped parameter modeling strategy, the model of this system is characterized by 4 state variables, as listed below:

- T_Z Zone temperature: the temperature of the controlled thermal volume (room interior), assumed to be uniform.
- T_W Walls temperature: the temperature of the walls, including the ceiling. As for the zone temperature, it is assumed to be uniform along all the walls. This element has

been considered separately from the controlled thermal volume because of its essential insulation function.

- T_{Pav} Pavement temperature: the temperature of the pavement. This has been considered separately from the previous two because the thermal capacitance associated to the pavement can reach high values on its own, especially when the radiant panel system is endowed with a screed ("massetto"). Moreover, the pavement is the first relevant thermal volume that interacts with the radiant panel: combined with its non-negligible thermal inertia, this makes the pavement deserve a state variable of its own.
- T_{Pi} Pipe temperature: this is the average temperature of the pipeline, including both the water and the metal conduct. To represent accurately the dynamic behavior of this heat exchanger, one should at least differentiate the two thermal inertiae (water and metal). However, the dynamics associated to the heat exchanger would definitely be faster than the dominant dynamics of our thermal system in its entirety, and thus negligible.

Each of these state variables is associated to a thermal inertia, respectively:

- C_Z is the thermal inertia of the zone, i.e. the controlled thermal volume. This quantity encompasses even the thermal inertia of any furniture/object inside the controlled zone itself that is not represented by the other thermal inertiae presented below.
- C_W is the thermal inertia of the walls, including the ceiling.
- C_{Pav} is the thermal inertia of the pavement, including the eventual screed but excluding the pipeline.
- C_{pi} is the thermal inertia of the pipeline, including both the water and the metal conduct. However, this C_{pi} will be computed on the water mass only, since the thermal inertia of the metal conduct is negligible with respect to the thermal inertia of the water.

The system is subject to both controllable and uncontrollable inputs.

The only controllable input considered in this thesis is the temperature of the water at the inlet of the pipeline, that from now on will be referred to as "inlet water temperature" for simplicity. The notation associated to this input is T_M.
There can be other controllable inputs associated to different heating systems, like the

thermal power of an air handling units (AHU) P_{AHU}. These kind of thermal devices won't be considered in this thesis, so no further attention will be given to this topic.

Conversely there are many uncontrollable inputs (disturbances) that can influence the system. Some of them can be considered as measurable:

- Temperature of the outside air T_{oa}: this is the temperature of the environment external to the thermal system considered. It is considered to be reasonably uniform along all the boundaries of our room.
  This disturbance can be considered as measurable since an external temperature sensor would be an economic addition to our control structure. In the following chapters it will be clear that a measure of this disturbance – or its efficient estimation – is required to compensate its effect on the control volume temperature T_Z.
- Solar radiation W_{Sol}: this is another input that generally affects the room temperature. While the solar radiation flux density W_{Sol} [$^{W}/_{m^2}$] is considered as a uniform input, the thermal power resulting from this input depends on the incident surface and the absorption coefficient of the body invested by this flux. For this reason, its provision will be considered distinctly depending on the nature of the body invested (window, wall, pavement) and the orientation of the façade (north, south, east, west).
  This input can be considered only partially measurable, because a pyranometer can measure the solar radiation flux density, while the incident surface of any body invested by this flux cannot be directly measured. There are various methods in the literature addressed to the estimation of the incident surface. Some of them involve easy linear approximations that can easily be implemented in a control scheme. However, in this thesis no particular focus will be made on the compensation of this kind of disturbance. A separate chapter 6 will be dedicated to further analysis of this topic.

Other disturbances are considered as non-measurable and unfit for estimation, such as:

- Ground Temperature T_G: this term can be conceptually extended to the temperature of the confining zone under our pavement. Its effect can be relevant because of the relatively high temperature that the pavement can reach during its heating phase. However a sufficiently good insulation can prevent enough this kind of heat dispersion. In this thesis the effect of this dispersion will be neglected under the hypothesis of good pavement insulation.

- Internal Gains P_{Int}: this kind of input is widely (in)famous in building thermal control. Under this name are grouped the thermal powers produced by any kind of device functioning, human metabolism and any other uncontrollable sources. The difficulty in the estimation of this input is well known in literature. No particular attention will be given to the estimation and compensation of this disturbance in this thesis.

2.b.3 Heat exchange equations and state-space model

The heat exchange phenomena involved can be divided in three categories:

- Convective heat exchanges: this type of heat exchange is the most frequent in the room model. The convective conductance coefficient U is considered constant because of the regularity of its application, i.e. no significant contortion of our working conditions is expected in our system. This heat exchange generally reads:

  $$C_X \dot{T_X} = U_{XY}(T_Y - T_X)$$

  considering for example the energy balance equation of the body X, where X and Y are the bodies among which the convective heat exchange is taking place.
- Direct injection of thermal power: in this type of heat exchange it is assumed that a body Y brings a certain amount of thermal power P_{XY} to the body X that does not depend on the state of the receiving body X. This heat exchange reads:

  $$C_X \dot{T_X} = P_{XY}$$

  This type of heat exchange modeling will be used for the solar radiation.
- Heat transfer from water to pavement: this particular heat exchange phenomenon will be analyzed separately in section 2.b.4 for its greater complexity with respect to the other two.

Now the energy balance equations for each state variable will be presented. These equations will be the ones constituting the dynamic model. Two of these equations – the pavement and the pipe ones – change when the system is shut OFF (i.e. the water is not circulating), so both versions will be presented:

- Zone temperature T_Z:

$$C_Z\dot{T_Z} = U_{wall}(T_W - T_Z) + U_{win}(T_{oa} - T_Z) + U_{pav}(T_{Pav} - T_Z) + \dot{m_{sa}}c_{pa}(T_{oa} - T_Z) + P_{Int}$$

with:

  - C_Z : zone air mass thermal capacity [J/K]
  - $U_{wall} = u_{wall}S_{Wall}$: average internal convective conductance of walls (ceiling) [W/K]
  - U_{win} : convective conductance of transparent surface [W/K]
  - $U_{pav} = u_{pav}S_{Pav}$: air-pavement convective transmittance [W/K]
  - c_{pa} : air specific heat [J/KgK]
  - $\dot{m_{sa}}$: air mass flow of AHU unit [Kg/s]

The temperature control of this body is our main control objective. This body is affected by three convective heat exchanges – with the walls, with the pavement and with the windows – and by two thermal power injections: one related to an eventual air handling unit (AHU) and one to the internal gains (discussed in the previous section).

NOTE: the convective conductance of both the walls (U_{wi}) and the pavement (U_{pav}) have been expanded to their full form (respectively $u_{wi}S_{Wall}$ and $u_{pav}S_{Pav}$) to ease the plant analysis of chapter 4.

- Walls temperature T_W:

$$C_{Wall}\dot{T_W} = U_{wall}(T_Z - T_W) + U_{wall}(T_{OA} - T_W) + U_{wG}(T_G - T_W) + + k_{Wall}\sum_{i=N,S,W,E,Ceil} W_{Sol,i}S_{Op,i} + \frac{1}{2}k_{Sol,Tr} * \sum_{i=N,S,W,E,Ceil} W_{Sol,i}S_{Tr,i}$$

with:

  - C_{Wall} : walls (including ceiling) mass thermal capacity [J/K]
  - U_{wG}: average convective conductance of walls with the ground [W/K]
  - k_{Wall} : coefficient of solar radiation effect on opaque area [#]
  - $W_{Sol,i}$: solar radiation on i-th façade [W/m^2]
  - $S_{Op,i}$:opaque area of i-th façade affected by solar radiation [m^2]
  - $k_{Sol,Tr}$: coefficient of solar radiation effect on transparent area [#]
  - $S_{Op,i}$: transparent area of i-th façade affected by solar radiation [m^2]

This body is affected by three convective heat exchanges – with the zone, with the outside air and with the ground – and by the power injection caused by the solar

radiation, divided into two contributions: one for the invested opaque area (walls and similar) and one for the transparent area (windows).

- Pavement temperature T_{Pav}:

  with system ON:

$$C_{Pav}\dot{T_{Pav}} = U_{Pav}(T_Z - T_{Pav}) + U_{PavG}(T_G - T_W) +$$
$$+\frac{1}{2}k_{Sol,Tr}\sum_{i=N,S,W,E,Ceil} W_{Sol,i}S_{Tr,i} + U_1 A_p L\left(\frac{1-e^{-\alpha}}{\alpha}\right)(T_M - T_{Pav})$$

  with system OFF:

$$C_{Pav}\dot{T_{Pav}} = U_{Pav}(T_Z - T_{Pav}) + U_{PavG}(T_G - T_W) +$$
$$+\frac{1}{2}k_{Sol,Tr}\sum_{i=N,S,W,E,Ceil} W_{Sol,i}S_{Tr,i} + U_1 A_p L(T_{Pi} - T_{Pav})$$

  with:

  - C_{Pav} : pavement mass thermal capacity [J/K]
  - U_{PavG}: average convective conductance of pavement with the ground [W/K]
  - U_1 : constant heat transfer coefficient between pavement and pipeline [W/K]
  - A_p : external perimeter of the pipe [m]
  - L : length of the pipeline [m]
  - α : N.T.U. of the pipeline [#]

  In both system ON and OFF cases, the pavement is affected by two convective heat exchanges – with the zone and with the ground – by the solar radiation passing through the windows and by a particular heat exchange with the pipeline, which is explained in detail in section 2.b.4.

- Pipe temperature T_{Pi}:

  with system ON:

$$C_{Pi}\dot{T_{Pi}} = [U_1 A_p L\left(\frac{1-e^{-\alpha}}{\alpha}\right) + wC_{p-aq}(e^{-\alpha} - \frac{1-e^{-\alpha}}{\alpha})](T_{Pav} - T_M)$$
$$+ wC_{p-aq}(T_M - T_{Pi})$$

  with system OFF:

$$C_{Pi}\dot{T_{Pi}} = U_1 A_p L(T_{Pav} - T_{Pi})$$

  with:

  - C_{Pi} : pipeline water mass thermal capacity [J/K]. The thermal capacity of the metal structure of the pipeline is negligible with respect to the water thermal capacity.

- w : water mass flow in the pipeline [kg/s]
- C_{p-aq} : specific heat of water [J/kgK]

The heat exchanges affecting the pipeline are explained in detail in section 2.b.4.

Now that the differential equations of the dynamic system have been presented, it is possible to explicit the matrices [A B C D] to reformulate the system into state-space form. This operation will be done for both the ON/OFF functioning states.

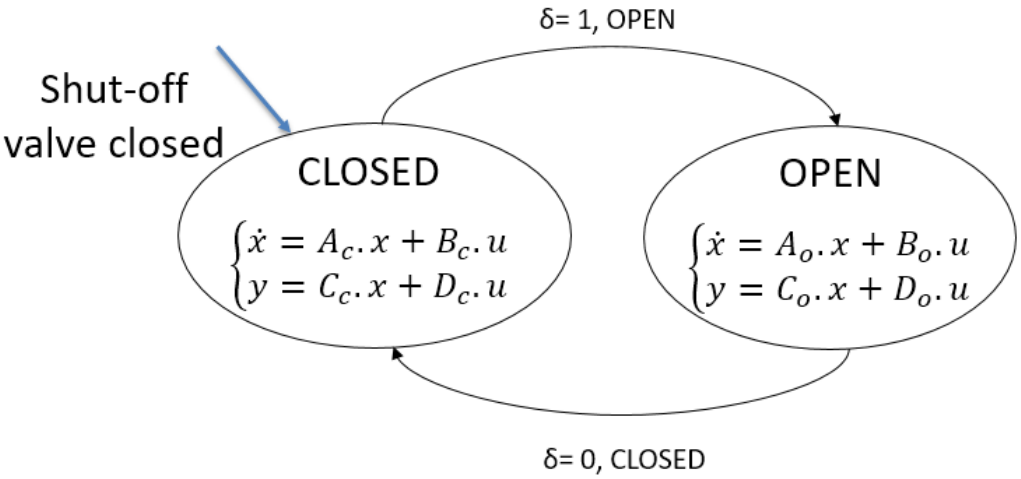

Fig. 2.2: Open/closed valve switching system

First, the state vector x and the input vector u are defined:

$$x = \begin{bmatrix} T_W \\ T_Z \\ T_{Pav} \\ T_{Pi} \end{bmatrix} \qquad u = \begin{bmatrix} T_{oa} \\ W_{sol,N} \\ W_{sol,S} \\ W_{sol,W} \\ W_{sol,E} \\ W_{sol,ceil} \\ T_G \\ P_{int} \\ T_M \end{bmatrix}$$

Then the matrices are presented:

- System ON:

$$A_o=\begin{bmatrix} -\frac{1}{C_{WC}}(\mathrm{U}_{wce}+\mathrm{U}_{wci}+\mathrm{U}_{weG}) & \frac{1}{C_{WC}}\mathrm{U}_{wci} & 0 & 0 \\ \frac{1}{C_Z}\mathrm{U}_{wci} & -\frac{1}{C_Z}(\mathrm{U}_{wci}+\mathrm{U}_{win}+U_{pavi}+\mathrm{U}_{sa}) & \frac{1}{C_Z}U_{pavi} & 0 \\ 0 & \frac{1}{C_P}U_{pavi} & -\frac{1}{C_P}(U_{pavi}+U_{pavG}+U_1.A_p.L.(\frac{1-e^{-\alpha}}{\alpha})) & 0 \\ 0 & 0 & \frac{1}{C_{aq}}(w.C_{p-aq}.(e^{-\alpha}-\frac{1-e^{-\alpha}}{\alpha})+U_1.A_p.L.(\frac{1-e^{-\alpha}}{\alpha})) & -\frac{1}{C_{aq}}w.C_{p-aq} \end{bmatrix}_{4\times4}$$

$$B_o=\begin{bmatrix} b11 & b12 & b13 & b14 & b15 & b16 & b17 & b18 & b19 \\ b21 & b22 & b23 & b24 & b25 & b26 & b27 & b28 & b29 \\ b31 & b32 & b33 & b34 & b35 & b36 & b37 & b38 & b39 \\ b41 & b42 & b43 & b44 & b45 & b46 & b47 & b48 & b49 \end{bmatrix}_{4\times9} \qquad C_o=\begin{bmatrix} 1 & 0 & 0 & 0 \\ 0 & 1 & 0 & 0 \\ 0 & 0 & 1 & 0 \\ 0 & 0 & 0 & 1 \end{bmatrix}_{4\times4}$$

$$b11=\frac{1}{C_{WC}}\mathrm{U}_{wcsO}$$

$$b12=\frac{1}{C_{WC}}(k_{wall}S_{op,N}+\frac{1}{2}K_{sol,tr}S_{tr,N})$$

$$b13=\frac{1}{C_{WC}}(k_{wall}S_{op,\mathrm{S}}+\frac{1}{2}K_{sol,tr}S_{tr,\mathrm{S}})$$

$$b14=\frac{1}{C_{WC}}(k_{wall}S_{op,\mathrm{W}}+\frac{1}{2}K_{sol,tr}S_{tr,W})$$

$$b15=\frac{1}{C_{WC}}(k_{wall}S_{op,\mathrm{E}}+\frac{1}{2}K_{sol,tr}S_{tr,\mathrm{E}})$$

$$b16=\frac{1}{C_{WC}}k_{wall}S_{op,\mathrm{ceil}}$$

$$b17=\frac{1}{C_{WC}}U_{wsG}$$

$$b18=0$$

$$b19=0$$

$$b21=\frac{1}{C_Z}(\mathrm{U}_{win}+\mathrm{U}_{sa})$$

$$b22=0$$

$$b23=0$$

$$b24=0$$

$$b25=0$$

$$b26=0$$

$$b27=0$$

$$b28=\frac{1}{C_Z}S_{pavi}$$

$$b29=0$$

$$b31=0$$

$$b32=\frac{1}{2C_P}K_{sol,tr}S_{tr,N}$$

$$b33=\frac{1}{2C_P}K_{sol,tr}S_{tr,\mathrm{S}}$$

$$b34=\frac{1}{2C_P}K_{sol,tr}S_{tr,\mathrm{W}}$$

$$b35=\frac{1}{2C_P}K_{sol,tr}S_{tr,\mathrm{E}}$$

$$b36=\frac{1}{2C_P}K_{sol,tr}S_{tr,\mathrm{ceil}}$$

$$b37=\frac{1}{C_P}U_{pavG}$$

$$b38=0$$

$$b39=\frac{1}{C_{aq}}U_1.A_p.L.(\frac{1-e^{-\alpha}}{\alpha})$$

$$b41=0$$

$$b42=0$$

$$b43=0$$

$$b44=0$$

$$b45=0$$

$$b46=0$$

$$b47=0$$

$$b48=0$$

$$b49=w.C_{p-aq}-w.C_{p-aq}.(e^{-\alpha}-\frac{1-e^{-\alpha}}{\alpha})-U_1.A_p.L(\frac{1-e^{-\alpha}}{\alpha})$$

$$D_o=\begin{bmatrix} 0 & 0 & 0 & 0 & 0 & 0 & 0 & 0 & 0 \\ 0 & 0 & 0 & 0 & 0 & 0 & 0 & 0 & 0 \\ 0 & 0 & 0 & 0 & 0 & 0 & 0 & 0 & 0 \\ 0 & 0 & 0 & 0 & 0 & 0 & 0 & 0 & 0 \end{bmatrix}_{4\times9}$$

- System OFF:

$$A_c = \begin{bmatrix} -\frac{1}{C_{WC}}(\mathrm{U}_{wcs}+\mathrm{U}_{wci}+\mathrm{U}_{wsG}) & \frac{1}{C_{WC}}\mathrm{U}_{wci} & 0 & 0 \\ \frac{1}{C_Z}\mathrm{U}_{wci} & -\frac{1}{C_Z}(\mathrm{U}_{wci}+\mathrm{U}_{win}+U_{pavi}+\mathrm{U}_{sa}) & \frac{1}{C_Z}U_{pavi} & 0 \\ 0 & \frac{1}{C_P}U_{pavi} & -\frac{1}{C_P}(U_{pavi}+U_{pavG}+U_1.A_p.L) & \frac{1}{C_P}U_1.A_p.L \\ 0 & 0 & \frac{1}{C_{aq}}.U_1.A_p.L & -\frac{1}{C_{aq}}U_1.A_p.L \end{bmatrix}_{4\times4}$$

$$B_c = \begin{bmatrix} b11 & b12 & b13 & b14 & b15 & b16 & b17 & b18 & b19 \\ b21 & b22 & b23 & b24 & b25 & b26 & b27 & b28 & b29 \\ b31 & b32 & b33 & b34 & b35 & b36 & b37 & b38 & b39 \\ b41 & b42 & b43 & b44 & b45 & b46 & b47 & b48 & b49 \end{bmatrix}_{4\times9} \qquad C_c = \begin{bmatrix} 1 & 0 & 0 & 0 \\ 0 & 1 & 0 & 0 \\ 0 & 0 & 1 & 0 \\ 0 & 0 & 0 & 1 \end{bmatrix}_{4\times4}$$

$$b11 = \frac{1}{C_{WC}}\mathrm{U}_{wcsO}$$
$$b12 = \frac{1}{C_{WC}}(k_{wall}S_{op,N} + \frac{1}{2}K_{sol,tr}S_{tr,N})$$
$$b13 = \frac{1}{C_{WC}}(k_{wall}S_{op,S} + \frac{1}{2}K_{sol,tr}S_{tr,S})$$
$$b14 = \frac{1}{C_{WC}}(k_{wall}S_{op,W} + \frac{1}{2}K_{sol,tr}S_{tr,W})$$
$$b15 = \frac{1}{C_{WC}}(k_{wall}S_{op,E} + \frac{1}{2}K_{sol,tr}S_{tr,E})$$
$$b16 = \frac{1}{C_{WC}}k_{wall}S_{op,ceil}$$
$$b17 = \frac{1}{C_{WC}}U_{wsG}$$
$$b18 = 0$$
$$b19 = 0$$

$$b21 = \frac{1}{C_Z}(\mathrm{U}_{win}+\mathrm{U}_{sa})$$
$$b22 = 0$$
$$b23 = 0$$
$$b24 = 0$$
$$b25 = 0$$
$$b26 = 0$$
$$b27 = 0$$
$$b28 = \frac{1}{C_Z}S_{pavi}$$
$$b29 = 0$$

$$b41 = 0$$
$$b42 = 0$$
$$b43 = 0$$
$$b44 = 0$$
$$b45 = 0$$
$$b46 = 0$$
$$b47 = 0$$
$$b48 = 0$$
$$b49 = 0$$

$$b31 = 0$$
$$b32 = \frac{1}{2C_P}K_{sol,tr}S_{tr,N}$$
$$b33 = \frac{1}{2C_P}K_{sol,tr}S_{tr,S}$$
$$b34 = \frac{1}{2C_P}K_{sol,tr}S_{tr,W}$$
$$b35 = \frac{1}{2C_P}K_{sol,tr}S_{tr,E}$$
$$b36 = \frac{1}{2C_P}K_{sol,tr}S_{tr,ceil}$$
$$b37 = \frac{1}{C_P}U_{pavG}$$
$$b38 = 0$$
$$b39 = 0$$

$$D_c = \begin{bmatrix} 0 & 0 & 0 & 0 & 0 & 0 & 0 & 0 & 0 \\ 0 & 0 & 0 & 0 & 0 & 0 & 0 & 0 & 0 \\ 0 & 0 & 0 & 0 & 0 & 0 & 0 & 0 & 0 \\ 0 & 0 & 0 & 0 & 0 & 0 & 0 & 0 & 0 \end{bmatrix}_{4\times9}$$

2.b.4 Pipe heat exchange

This type of exchange was treated separately for its complexity. The model proposed is based on the known theory about heat exchangers [16], no innovative concepts are introduced. However, since this heat exchange is the phenomenon of main interest in the whole system, a small section describing the main logics behind this model is presented to complete the picture.

Assuming that the pipeline exchanges heat only – or at least mainly – with the pavement, its energy balance reads:

$$C_{Pi}\dot{T_{Pi}} = Q_{inlet} - Q_{outlet} - Q_{Pipe \to Pav}$$

with:

- Q_{inlet}: the heat associated to the water entering the pipeline. This quantity can be written as:

  $$Q_{inlet} = wC_{p-aq}T_M$$

  when the system is ON. Instead, it is null when the system is OFF.
- Q_{outlet}: the heat associated to the water outgoing the pipeline. This quantity can be written as:

  $$Q_{inlet} = wC_{p-aq}T_O$$

  when the system is ON, with T_O=temperature of water outgoing the pipeline. Instead, it is null when the system is OFF. The temperature T_O will be computed soon.
- $Q_{Pipe \to Pav}$: the heat transferred to the pavement. The focus of this section is on the modeling of this quantity.

By considering a small slice of pipeline of length dx, the amount of heat Δq_W contained in that specific amount of water Adx of temperature T_x is:

$$\Delta q_W = \rho A dx C_p T_x$$

Its temperature is reduced because of the warming up of the pavement. The heat transfer loss in a very short time is then expressed as:

$$d\Delta q_W = -\rho A dx C_p dT_x$$

This heat is received by the pavement as follows:

$$d\Delta q_{Pav} = U_1 A_p (T_x - T_{Pav}) dx dt$$

Resulting in:

$$d\Delta q_W = \rho A dx C_p T_x = U_1 A_p (T_x - T_{Pav}) dx dt = d\Delta q_{Pav}$$

Now, considering the system ON, the following assumptions can be made:

- The pavement temperature is constant in a short time
- The flow velocity is constant ($\frac{dx}{dt} = \theta = const$)
- $T_x(x = 0) = T_M$

The previous equivalence can be rewritten as:

$$-\rho A \frac{dx}{dt} C_p \frac{dT_x}{dx} = -\rho A \theta C_p \frac{dT_x}{dx} = U_1 A_p (T_x - T_{Pav})$$

So that, by solving this differential equation:

$$T_x = T_{Pav} + (T_M - T_{Pav}) e^{-\frac{U_1 A_p x}{\rho A \vartheta C_p}}$$

The average temperature of the pipe T_{Pi} can be found by solving the integration of T_x over the length of the pipeline:

$$T_{Pi} = \frac{1}{L} \int_0^L T_x dx = T_{Pav} + (T_M - T_{Pav}) \left(\frac{1 - e^{-D\frac{L}{\theta}}}{D\frac{L}{\theta}} \right) = T_{Pav} + (T_M - T_{Pav}) \left(\frac{1 - e^{-\alpha}}{\alpha} \right)$$

with $D = \frac{U_1 A_p}{\rho A C_p}$ and $\alpha = D\frac{L}{\theta}$ = Number of Transferred Units (N.T.U.), that is a characteristic parameter of an heat exchanger. The average temperature of the pipe T_{Pi} is then exploited to compute the heat transfer rate $Q_{Pipe \to Pav}$:

$$Q_{Pipe \to Pav} = \int_0^L U_1 A_p (T_x - T_{Pav}) dx = U_1 A_p L (T_{Pi} - T_{Pav})$$

$$= U_1 A_p L (T_M - T_{Pav}) \left(\frac{1 - e^{-\alpha}}{\alpha} \right)$$

Moreover, the temperature of the water outgoing the pipeline is computed. This quantity is needed both for the computation of Q_{outlet} and by the mixing valve in the simulation model:

$$T_O = T_x|_{x=L} = T_{Pav} + (T_M - T_{Pav}) e^{-\frac{U_1 A_p L}{\rho A \vartheta C_p}} = T_{Pi} + (T_M - T_{Pav})(e^{-\alpha} - \frac{1 - e^{-\alpha}}{\alpha})$$

The complete pipeline energy balance with the system ON reads:

$$C_{Pi} \dot{T_{Pi}} = Q_{inlet} - Q_{outlet} - Q_{Pipe \to Pav} =$$

$$w C_{p-aq} T_M - w C_{p-aq} \left(T_{Pi} + (T_M - T_{Pav}) \left(e^{-\alpha} - \frac{1 - e^{-\alpha}}{\alpha} \right) \right) - U_1 A_p L (T_M - T_{Pav}) \left(\frac{1 - e^{-\alpha}}{\alpha} \right)$$

Now, considering the system OFF instead, the following assumptions can be made:

- The pavement temperature is constant in a short time
- The flow velocity is zero

- $T_x(x = 0)$ is the initial temperature at point x when the valve has just been closed

The equivalence $d\Delta q_W = d\Delta q_{Pav}$ can then be rewritten as:

$$-\rho A C_p \frac{dT_x}{dt} = U_1 A_p (T_x - T_{Pav})$$

So that, by solving this differential equation:

$$T_x = T_{Pav} + (T_{X_0} - T_{Pav}) e^{-\frac{U_1 A_p t}{\rho A \vartheta C_p}}$$

And then the heat transfer rate $Q_{Pipe \to Pav}$ is computed as:

$$Q_{Pipe \to Pav} = \int_0^L U_1 A_p (T_{x,t} - T_{Pav}) dx = U_1 A_p L (T_{Pi} - T_{Pav})$$

In this way, the complete pipeline energy balance with the system OFF reads:

$$C_{Pi} \dot{T_{Pi}} = -Q_{Pipe \to Pav} = -U_1 A_p L (T_{Pi} - T_{Pav})$$

2.c Effect of saturations

Before proceeding with the control-related studies of this thesis, an analysis of the effect of the saturations characterizing this heating system is noteworthy. There are two saturations affecting the system: the saturation imposed on the inlet water temperature set-point $T_{M,rif}$ and the saturation resulting from the physical limits of the mixing valve (fully open – fully close).

NOTE: it is not relevant to be aware of the control structure now to catch the effect of the saturation under analysis. The control structure will be presented in the next chapter 3.

2.c.1 Saturation on the inlet water temperature set-point

The inlet water temperature set-point $T_{M,rif}$ is both superiorly and inferiorly limited to some safety values. The upper limit is imposed to avoid over-heating of the pavement itself, resulting in thermal discomfort for the user. The lower limit is imposed to prevent condensation phenomena in the heating system. In this thesis work the values adopted for these boundaries are [20°C ; 40°C]. These values have been chosen based on an existing heating system on the market.

This saturation will mainly affect the speed of the system both in the heating and cooling phases. Moreover, as most saturations do, it will be necessary to introduce an anti-windup system in our control structure.

In Fig. 2.3 a representative comparison is presented between the heating system without any saturation and the same heating system (i.e. with the same physical parameters and everything) endowed with a saturation [20°C ; 40°C] on the inlet water temperature set-point $T_{M,rif}$, as previously said. In both cases, the room started with an initial temperature $X_0 = 10°C$ for all the state variables T_Z, T_W, T_{Pav} and T_{Pi}. Then a set-point $T_{Z,rif} = 23°C$ was imposed on the zone temperature T_Z, triggering a heating response from the controller that is observed for a time span of 1 day.

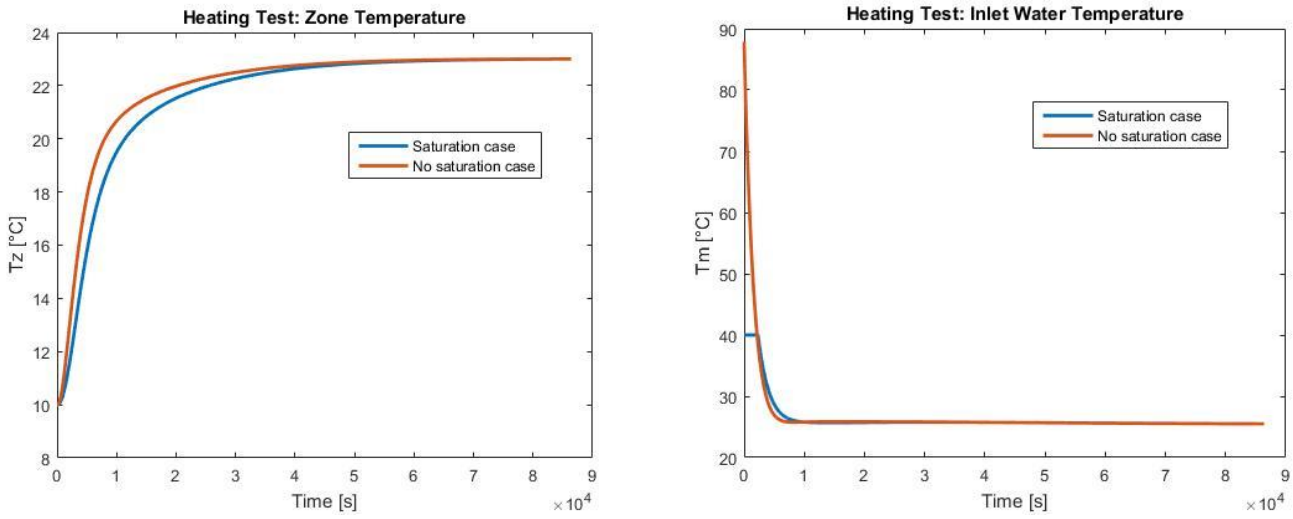

Fig. 2.3: Heating test to highlight the effect of the inlet water temperature set-point saturation

As it can be seen from the profile of the zone temperature T_Z, the heating phase is definitely faster in the "no saturation" case. This is justified by the profile of the inlet water temperature T_M, in which it is possible to see that the "no saturation" controller is able to exaggeratedly modify its value very quickly.

The effect of the saturation [20°C ; 40°C] on the inlet water temperature set-point $T_{M,rif}$ can be noticed even in a cooling test, presented in Fig. 2.4. In this test the room started (in both "no saturation" and "saturation" cases) with an initial temperature $X_0 = 23°C$ for all the state variables. Then a set-point $T_{Z,rif} = 18°C$ was imposed on the zone temperature T_Z, triggering a cooling response from the controller that is observed for a time span of 1 day.

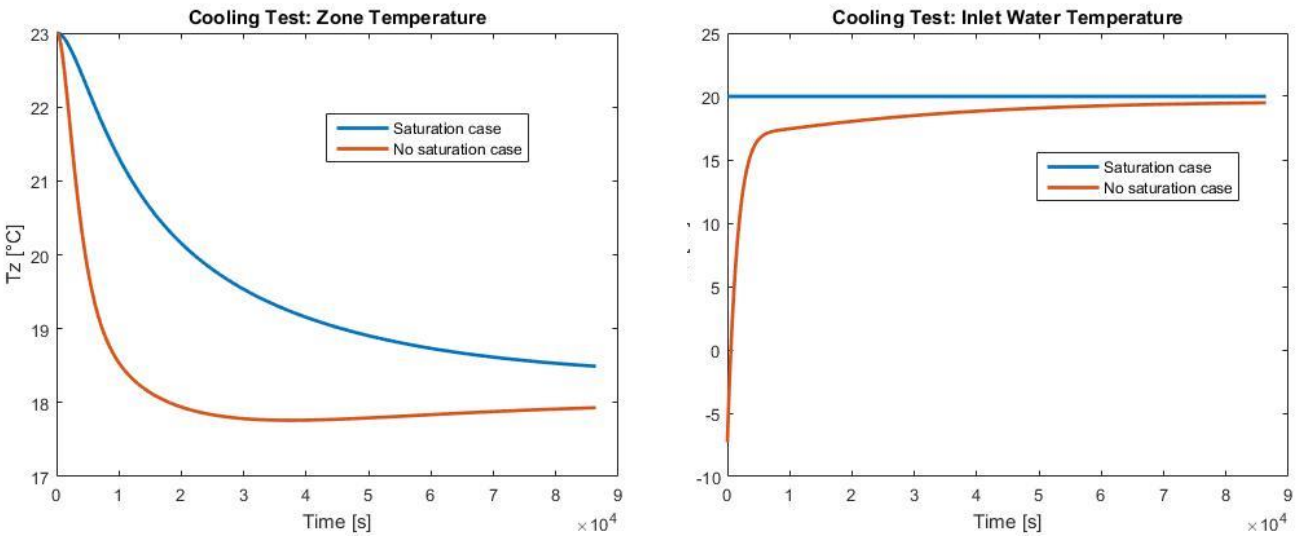

Fig. 2.4: Cooling test to highlight the effect of the inlet water temperature set-point saturation

Similarly to the previous heating test, the response is faster in the "no saturation" case. The reasons are exactly the same exposed for the previous test, as it can be seen from the profile of the inlet water temperature T_M.

2.c.2 Saturation of the mixing valve

The presence of the mixing valve at the inlet of the heating pipeline does not allow the inlet water temperature to arbitrarily assume a desired value. The inlet water temperature is the result of the mixing taking place into the mixing valve. As previously described in the section 2.b.1, the mixing valve recovers the water outgoing the pipeline and mix it with a variable amount of hot water coming from a boiler. In this thesis, the hot water source will be considered at 56°C constant.

The mixing process in the valve will inevitably involve some dynamics. The mixing volume of the valve is assumed sufficiently small so that the mixing dynamics can be neglected, i.e. the water in the valve has only one temperature. This temperature is the result of the average between the temperature of the water outgoing the pipeline and the temperature of the water coming from the boiler, both weighted by its mass flow. In formula:

$$T_M = \frac{T_O * w_O + T_B * w_B}{w_O + w_B}$$

With:

- T_O: temperature of the water ougoing the pipeline

- w_O: mass flow of the water outgoing the pipeline, that is equal to the mass flow imposed by the recirculating pump w
- T_B: temperature of the water coming from the boiler
- w_B: mass flow of the water coming from the boiler

Ultimately, the inlet water temperature T_M is controlled by adjusting the mass flow w_B, which in turn is controlled by the position of the valve X_V. In this work, X_V is a variable in the range [0 ; 1] that represents how much the way connected to the boiler is opened: 0 means that it is completely shut, while 1 means that it is fully open. Since the total amount of water in the pipeline should be kept constant, an addition of water coming from the boiler must correspond to an extraction of water coming from the pipeline: in this way, the two mass flows w_O and w_B are connected such that $w_O + w_B = w = const$. It is possible then to reformulate the previous relationship among T_M, T_O and T_B using only the position of the valve X_V:

$$T_M = X_V * T_B + (1 - X_V) * T_O$$

The opening/closing of the valve is characterized by its actuator dynamics. Without entering too much into detail on the mixing valve, the actuation dynamics (i.e. the relationship between the valve position set-point $X_{V,rif}$ and its current position X_V) are considered to be linear. The time constant of the transfer function associated to this linear dynamics is set to 1 minute, so that a complete change of set-point is obtained approximately in 5 minutes. This value has been chosen based on a mixing valve exploited in a real radiant panel heating system. The block diagram associated to this actuation dynamics is visible in Fig. 2.5.

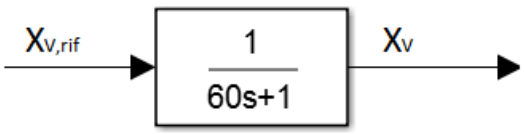

Fig. 2.5: Mixing valve actuator block diagram

Two apparent consequences are resulting from this mixing valve:

- The water into the pipeline cannot be heated instantaneously
- The water into the pipeline can be forcedly heated, but not forcedly cooled: if the inlet water temperature set-point $T_{M,rif}$ should get lower than the current inlet water

temperature T_M, the only control action possible is to close the mixing valve (i.e. close the way connected to the boiler) and let the temperature T_M fall for heat dispersion with the environment. This process can take a very long time, depending on different factors such as: current temperature values for the states and the inputs, insulation of the room, thermal inertia of the pavement, average conductance between the pavement and the zone, characteristics of the pipeline etc…

Both of these consequences concern the speed of the transient from T_M to $T_{M,rif}$. The heating speed is mostly a negligible problem, since it depends only on how fast the valve can change its position, i.e. 5 minutes tops. The second problem is more limiting and can really affect the system performances in the cooling case. To prove this point, a cooling test is presented in Fig. 2.6 that compares a room endowed with a mixing valve with a room in which the inlet water temperature T_M is simply imposed (i.e. $T_M = T_{M,rif}$ at any time). In this test the room started (in both "no valve" and "valve" cases) with an initial temperature $X_0 = 23°C$ for all the state variables. Then a set-point $T_{Z,rif} = 18°C$ was imposed on the zone temperature T_Z, triggering a cooling response from the controller.

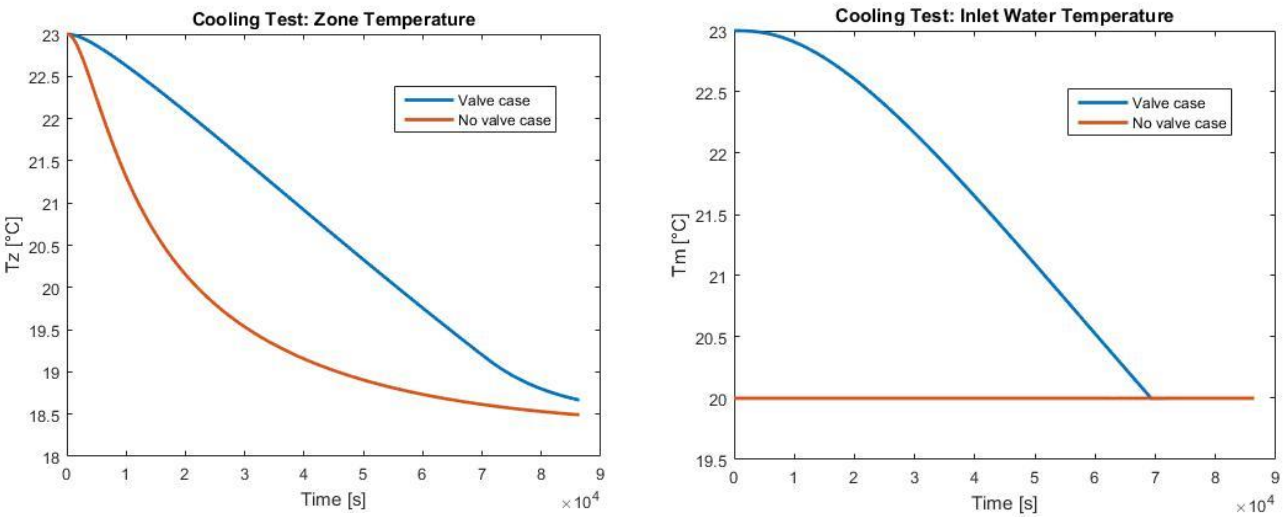

Fig. 2.6: Cooling test to highlight the effect of the mixing valve saturation

The zone temperature profile T_Z in the "valve" case is slower than the one in the "no valve" case. This is a result of the inlet water temperature profile T_M in which it is possible to see the slow cooling of T_M in the "valve" case.

2.d Model testing

In order to verify the model proposed in this chapter, a testing campaign was performed on a test room. In particular, the task consisted in performing a fitting of the data measured in the test room with the proposed model. The objective of this task is to verify if the simplified model adopted was suitable to describe the dynamics of a real room endowed with a radiant panel floor. The map of this test room, made available by an Italian company involved in the production of radiant panel systems, is schematically represented in Fig. 2.7.

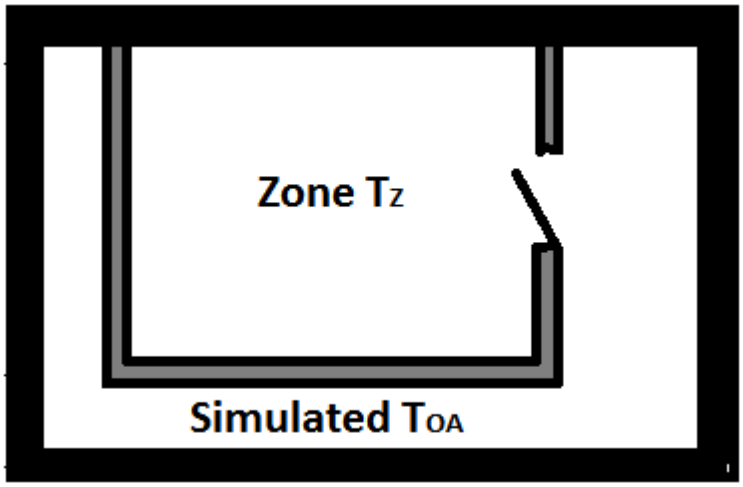

Fig. 2.7: Test room map

The characteristics of this room are listed below:

- Three walls of this room are facing an environment characterized by an imposed temperature. This imposed temperature assumes the role of the outside temperature T_{OA}. For technical limitations, this imposed temperature could only work on constant values.
- The other wall and the ceiling of the room were granted to be perfectly insulated, so that its contribution can be neglected.
- There are no windows.
- Even the pavement was considered insulated from the ground, so that such heat dispersion could be neglected.
- The sensors available are: zone temperature T_Z, inlet water temperature T_M and pavement temperature T_{Pav}. Of course, these sensors couldn't measure the average zone temperature nor the average pavement temperature, but only one particular point

of those masses. The positioning of the sensors was done in order to capture a reliable measure, i.e. avoiding corners as much as possible.

Because of the characteristics of this test room, some limitations on our modeling are imposed:

- The ground temperature disturbance was removed, thanks to the insulation of the test room.
- The solar radiation disturbance was removed, since there was no device that could reproduce its effect.
- Since no significant heating device or human presence was influencing the tests, any internal gains contribution was neglected.

The resulting model on which the data fitting was performed is:

$$\begin{cases} C_Z\dot{T_Z} = U_{wall}(T_W - T_Z) + U_{pav}(T_{Pav} - T_Z) \\ C_{Wall}\dot{T_W} = U_{wall}(T_Z - T_W) + U_{wall}(T_{OA} - T_W) \\ C_{Pav}\dot{T_{Pav}} = U_{Pav}(T_Z - T_{Pav}) + U_1 A_p L(\frac{1 - e^{-\alpha}}{\alpha})(T_M - T_{Pav}) \\ C_{Pi}\dot{T_{Pi}} = [U_1 A_p L\left(\frac{1 - e^{-\alpha}}{\alpha}\right) + wC_{p-aq}(e^{-\alpha} - \frac{1 - e^{-\alpha}}{\alpha})](T_{Pav} - T_M) + wC_{p-aq}(T_M - T_{Pi}) \end{cases}$$

Because of the testing nature of the room under analysis, some parameters were already known by construction. These are listed below:

- $U_{wall} = 0.28\ \mathrm{W/m2K}$
- $c_{p,Wall} = 13\ \mathrm{kJ/m2K}$

The other parameters were fitted on the data sets provided by the tests. The obtained fitting granted a satisfactory repeatability over the whole data set, confirming the validity of the proposed modeling. In Fig. 2.8 a specific data set is plotted to present the typical behavior of the control system of the thesis, with T_Z zone temperature, T_{del} inlet water temperature and $T_{del}SP$ the set point of the latter.

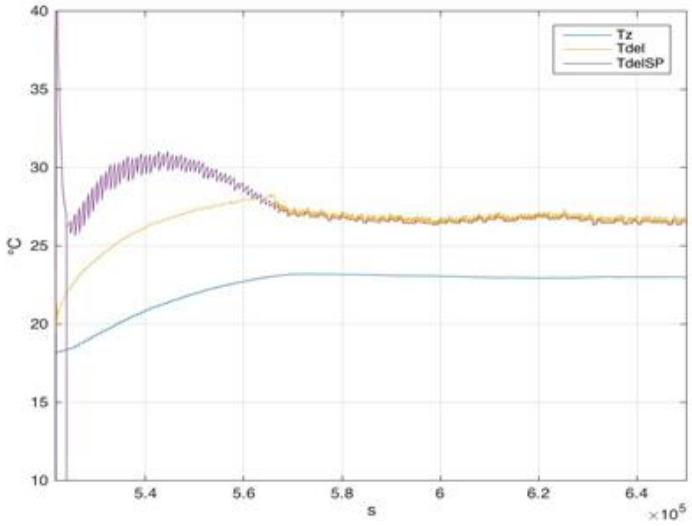

Fig. 2.8: Sperimental data collected in the fitting phase

The control strategy will be presented in the next chapter. For now, we can say that the absence of overshooting and the settling time of 10 hours are confirming the expected functioning of the system.

2.e Extending the model

In the presented model, only four states have been identified to suitably describe the main dynamics of the system under control. In this section, a brief analysis is discussed about the possible extension of the model so to further distinguish the thermal behavior of the walls exchanging heat with the outside air from the non-exchanging walls.

To easily understand the nature of these non-exchanging walls, it is possible to consider an apartment in a residential building. Focusing on the room endowed with the radiant panel heating system, some walls will be facing the outside environment, and these will represent the exchanging walls as described in the 4-states model equations. There will be however some inner walls that confine with an adjacent room. These walls won't be affected by the heat exchange with the outside air. Moreover, it is possible to say that the heat exchange concerning these walls is negligible under the realistic hypothesis that the confining room has a temperature close enough to the zone temperature of the room under control. In this way, these walls are called non-exchanging walls and are simply considered adiabatic. The contribution of the non-exchanging walls, however, is not insignificant. Their effect can be assimilated to an additive thermal inertia for the controlled zone volume. This means that the

thermal inertia of the zone C_Z encompasses the contribution of the non-exchanging walls – together with the contribution of any other room furniture as previously indicated in 2.b.3.

A fifth state was introduced to describe the thermal behavior of the non-exchanging walls. The extended model equations read:

$$\begin{cases} C_Z\dot{T_Z} = U_{wall}(T_W - T_Z) + U_{pav}(T_{Pav} - T_Z) \\ C_{Wall}\dot{T_W} = U_{wall}(T_Z - T_W) + U_{wall}(T_{OA} - T_W) \\ C_{Pav}\dot{T_{Pav}} = U_{Pav}(T_Z - T_{Pav}) + U_1 A_p L\left(\frac{1 - e^{-\alpha}}{\alpha}\right)(T_M - T_{Pav}) \\ C_{Pi}\dot{T_{Pi}} = \left[U_1 A_p L\left(\frac{1 - e^{-\alpha}}{\alpha}\right) + wC_{p-aq}\left(e^{-\alpha} - \frac{1 - e^{-\alpha}}{\alpha}\right)\right](T_{Pav} - T_M) + wC_{p-aq}(T_M - T_{Pi}) \\ C_{Wall,NE}\dot{T_{W,NE}} = U_{wall}\left(T_Z - T_{W,NE}\right) \end{cases}$$

Where the notation $T_{W,NE}$ stands for the temperature of the non-exchanging walls, with the relative thermal capacitance $C_{Wall,NE}$. It can be easily seen that the fifth equation describing the non-exchanging walls forces the convergence of the temperature $T_{W,NE}$ to the temperature T_Z. Once any possible offset between the initial states of $T_{W,NE}$ and T_Z is canceled, if the dynamics of the heat exchange between the non-exchanging walls and the zone volume are fast enough, then the thermal inertia $C_{Wall,NE}$ can be considered as an additive contribution to the thermal inertia C_Z, confirming the previous reasoning.

The model fitting procedure mentioned in the previous section has been carried out even on this 5-states model to verify any possible improvement in the model adherence to the real data. Focusing on the exploited testing room, the fifth state was associated to the wall and ceiling that were considered adiabatic. However, no appreciable difference was obtained in the fitting quality by considering the fifth state. This test outcome allowed the adoption of the simpler 4-states model in the developing of this thesis.

2.f Chapter 2 conclusions

These chapter described the model that will be adopted in this thesis. After quickly analyzing the modeling strategies currently adopted for this scope by the literature, the lumped parameter modeling was adopted for its simplicity and representativeness with the physical nature of the model parameters. A 4-states model was then developed in its entirety and, after analyzing the effect of the saturations on the system performances, the adequacy of the proposed model was verified through a model testing campaign performed in a real testing room. The possible extension of this model to a 5-states one has been tested. However the introduction of the fifth state – aimed at describing the thermal behavior of the non-exchanging walls – did not produce any relevant improvement.

The model presented initially was affected by more inputs than the ones that are considered after the model testing section. The choice of neglecting some disturbances has been made mainly for two reasons. The first is the impossibility of verifying the capacity of the proposed model to capture the real behavior of these disturbances because of the technological limits of the testing room. The second one is to focus the attention of the thesis on the compensation of one disturbance, i.e. the outside air temperature T_{OA}, that is known to be usually the most influent in the building heating topic. Anyway, the model adopted in the thesis is the one presented in the model testing section 2.b.4, which has as only inputs the inlet water temperature T_M and the outside air temperature T_{OA}. A separate chapter 6 will be dedicated to the estimated effect of the solar radiation disturbance.

3. CONTROL

In this chapter, the control strategy proposed for this heating system is developed. First, a control loop governed by a PID will be closed on the zone temperature measurement T_Z in section 3.a in order to obtain the classic control performances on the controlled system. Then, another simple control loop will be imposed on the mixing valve in section 3.b to guarantee a fast convergence of the inlet water temperature T_M to its set-point $T_{M,rif}$. For both the control loops, an anti-windup system is designed in order to overcome the typical problems related to the saturations (see 2.c) in section 3.c. An hysteresis high-level control is then added in section 3.d to the system to ensure that the heating system does not provoke any serious over-heating phenomena.

After having outlined the zone temperature control, an open-loop compensator is introduced in section 3.e to mitigate the effect of the external temperature T_{OA} on the zone temperature T_Z.

3.a Zone temperature PID control

A simple PID was found to be sufficiently performing to control the zone temperature T_Z with a set-point $T_{Z,rif}$. The PID control does not represent an innovative solution, as many books concerning all the various PID applications and common issues have already been published, among which we can mention [17] and [18] as example.

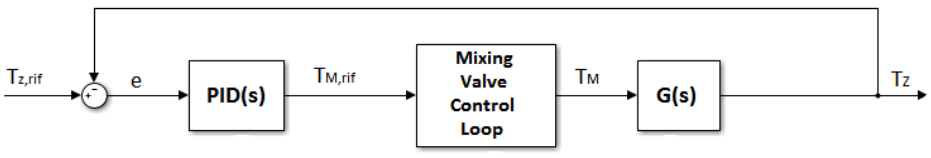

Fig. 3.1: Block diagram of the outer control loop endowed with a PID regulator

The structure of this control loop endowed with a PID regulator is presented in Fig. 3.1. The PID is fed with the error on the zone temperature $e = T_{Z,rif} - T_Z$ and outputs the inlet water temperature set-point $T_{M,rif}$ as its control action. This set-point will be received by the mixing valve control loop, which is analyzed later on in section 3.b. The mixing valve

control loop will output the actual inlet water temperature T_M entering the G(s) transfer function, that in turn outputs the zone temperature T_Z.

Some more words deserve to be spent on the tuning of this PID. In fact, in order to ease the tuning of the PID for the adaptive case – that represents the main point of this thesis and will be addressed in the chapter 5 – a particular tuning strategy has been defined.
Starting from the transfer function $PID(s)$ associated to this PID regulator, it reads:

$$PID(s) = P + I * \frac{1}{s} + D * \frac{N}{1 + N * \frac{1}{s}}$$

That can be reformulated making explicit its gain, poles and zeroes as:

$$PID(s) = k \frac{(1 + s\tau_1) * (1 + s\tau_2)}{s * (1 + s\tau_3)}$$

With:

- $I = k$
- $N = \frac{1}{\tau_3}$
- $P = \frac{(\tau_1 + \tau_2) * N * I - I}{N}$
- $D = \frac{(\tau_1 * \tau_2) * N * I - P}{N}$

This representation allows a quick tuning once k, τ_1, τ_2 and τ_3 have been chosen. These quantities depends of course from the plant we are controlling. The plant transfer function controlled by this PID is G(s). The typical shape of the Bode diagram associated to G(s) is represented in Fig. 3.2. As it can be seen, there are no particular irregularities (like resonant peaks, positive slopes etc…) in the frequency response of this system. This bland behavior of the system is attributable to its energetic nature and intrinsically slow dynamics.

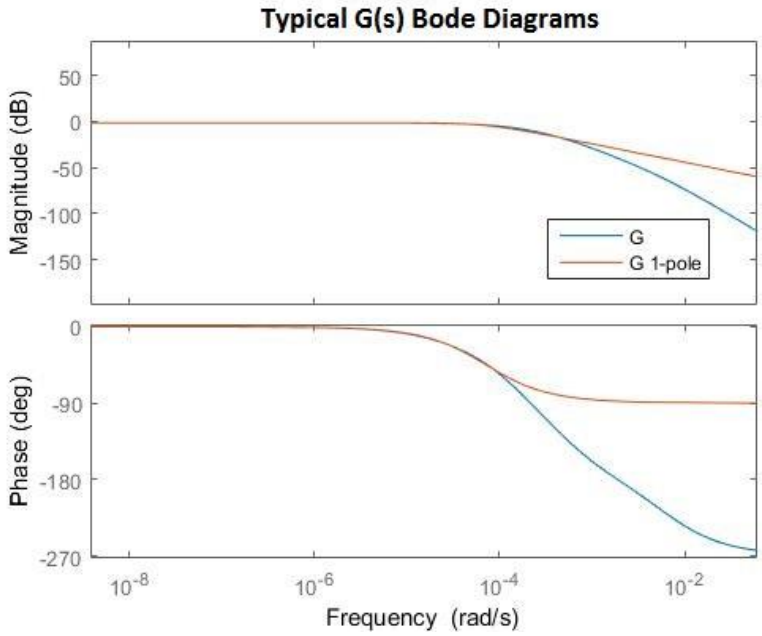

Fig. 3.2: Typical shape of the Bode diagrams of the G(s) transfer function with its 1-pole approximation

Thanks to its just analyzed typical frequency response, G(s) can be reasonably reduced to its first order approximation:

$$G(s) \approx \mu_G * \frac{1}{1 + s\tau_G}$$

This simplification is justifiable only in the low-frequency domain, as it can be seen in Fig. 3.2. Since the proposed PID tuning is very conservative, the resulting cut-off frequency always falls in the low-frequency range in which we can use the G(s) 1-pole approximation. With this assumption, the loop function resulting is:

$$L(s) = PID(s) * G(s) = k\frac{(1 + s\tau_1) * (1 + s\tau_2)}{s * (1 + s\tau_3)} * \mu_G * \frac{1}{1 + s\tau_G}$$

NOTE: the dynamics associated to the mixing valve have been neglected in the loop transfer function. This is because those dynamics are way faster than the typical dynamics of G(s). Anyway, this simplification is discussed more in the next section 3.b.

Now, the PID values for k, τ_1, τ_2 and τ_3 are set:

- τ_1 is set equal to τ_G in order to have a virtual cancellation – since τ_G is not a real time constant of G(s) but only the result of an approximation – between those two singularities.

- τ_2 is set empirically: $\tau_2 = \frac{\tau_G}{5}$
- τ_3 is connected to the filtering action imposed to the derivative action of the PID, a necessary component for the PID feasibility. It is empirically set: $\tau_3 = \frac{1}{1000}$
- k is set empirically as $k = \frac{2}{\mu_G}$. This parameter of the PID is strongly affecting the cut-off frequency of the closed loop system. By increasing the value of the cut-off frequency it is easy to incur into overshooting phenomena (i.e. the closed loop system is too fast) represented in Fig. 3.3. On the other hand, by reducing too much the cut-off frequency the system can end up as excessively slow. The choice of value of k proposed, together with the choice for the other PID parameters, has proved to return a very good trade-off between the system performance and the avoidance of overshoots.

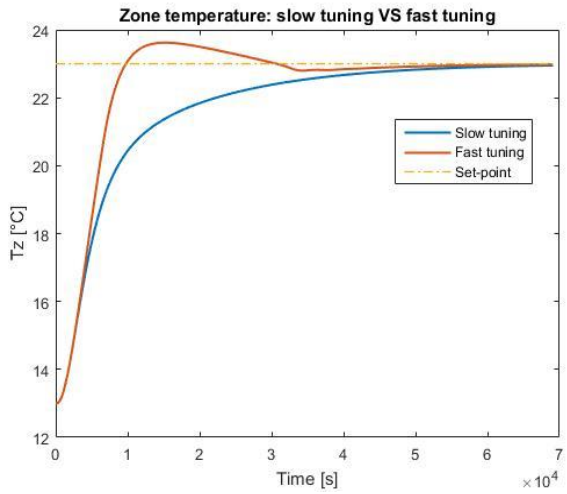

Fig. 3.3: Effect of different PID tuning strategies

A purely theoretical PID tuning approach would not have been an efficient choice in this case, since the plant G(s) is characterized by too many singularities with no strong physical representativeness per se. It is preferable to refer to some overall characteristics of the controlled plant instead. In this way, the presented PID tuning is mostly based on an empirical use of the quantities τ_G and μ_G of the 1-pole approximation of G(s). The dependency of the PID tuning on these two quantities only will be exploited in the adaptive part of chapter 5.

This empirical approach has been developed starting from the Matlab PID tune toolbox [19]. This toolbox allows the user to tune the PID according to two performance indexes, i.e. the response time and the transient behavior. The response time index is self-explanatory and it

represents the system reaction quickness to a set-point imposition. The transient behavior index represents the behavior of the transition, which varies in a qualitative scale from “aggressive response” to “robust response”. The aggressive response aims at reaching the set point quickly and then stabilizing with a series of damped oscillations, thus generating overshooting phenomena. The robust response tends to slow down as the controlled variable reaches its set point in order to ensure a clean and smooth settling even under relevant uncertainties on the controlled plant.

The proposed tuning strategy is more focused on its robustness with respect to the response time. For this reason, while exploiting the Matlab PID tuning toolbox the response time performance index has been fixed to the standard middle value and the transient behavior has been set to the “robust response” extreme. An example of the resulting tuning is visible in Fig. 3.4, compared with the relative empirical one developed in the thesis.

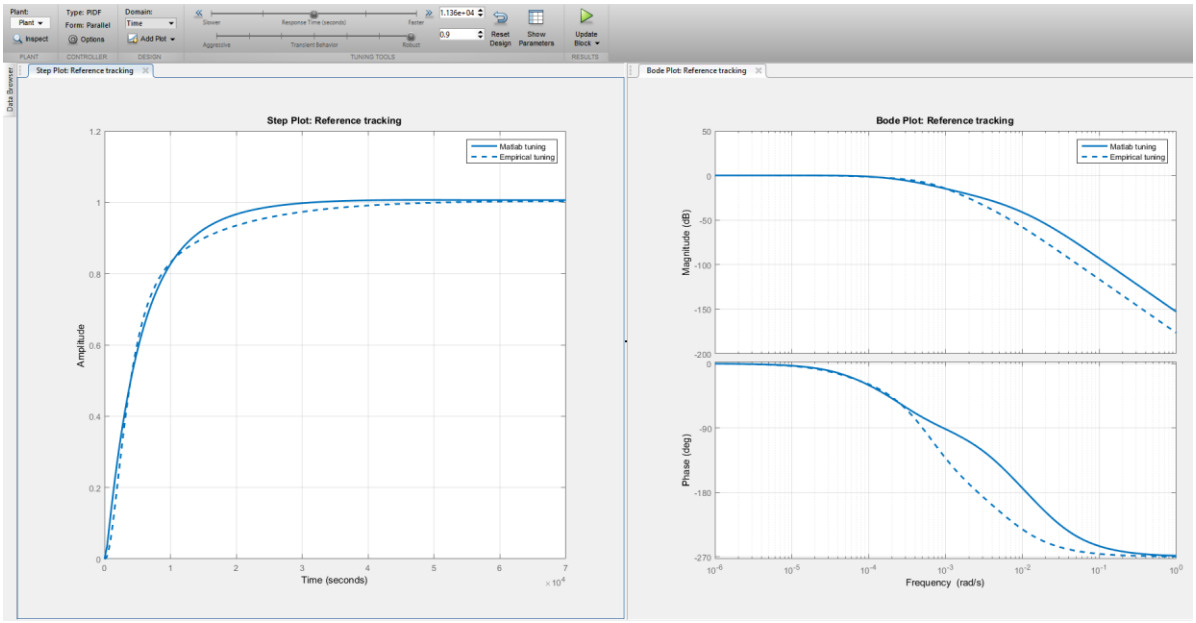

Fig. 3.4: Matlab PIDtune toolbox - comparison between the PID tuning proposed by Matlab and the PID tuning resulting from the proposed strategy

After manually analyzing the PID tuning resulting from this Matlab toolbox along different room configurations, the empirical tuning was obtained as a variation on the tuning proposed by the toolbox. The two main objectives of this variation are presented below:

- Express the controller parameters P, I, D and N in function of some determined parameters of the controlled plant G(s) while maintaining the appreciable behavior of the tuning proposed by the Matlab toolbox. In this way, a systematic tuning approach can be exploited by the adaptation mechanism that will be presented in chapter 5.

- Further increase the robustness of the PID tuning by slowing down the final phase of the system reference tracking response. Referring to Fig. 3.4, it is possible to see that the empirical tuning presents a smoother settling with respect to the Matlab tuning. That slow final settling phase refers to the slowest dynamics of the plant G(s), i.e. the ones describing the heating of the walls. By keeping a cautious final approach to the set point, the system is able to robustly adapt to the plant uncertainties minimizing the risk of overshoots. The proposed final settling slowdown is possible in this kind of control application because it is not important to strictly reach the set point in a small amount of time. In terms of thermal comfort, it is preferable to avoid overshoots and quickly reaching just the neighborhood of the zone temperature set point.

3.b Mixing valve control

The mixing valve control loop aims at driving the inlet water temperature T_M towards its set-point $T_{M,rif}$ that was imposed by the zone temperature PID just discussed.

This loop, which ultimately acts as an inner control loop, is imposed not for performance reasons but for the very functioning of the mixing valve itself. In fact, the inlet water temperature set-point $T_{M,rif}$ can be converted in an exact valve position set-point $X_{V,rif}$ only by knowing both the temperature of both the water outgoing the pipeline and the water coming from the boiler. However, our system is assumed to be devoid of such sensors, thus making this conversion $T_{M,rif} \rightarrow X_{V,rif}$ impossible.

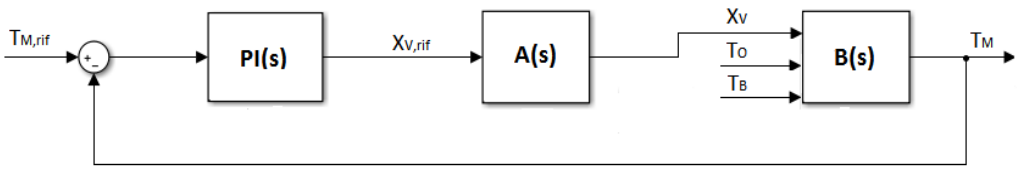

Fig. 3.5: Block diagram of the inner control loop endowed with a PI regulator

To solve this problem, a control loop is closed on the T_M itself, leading to the structure presented in Fig. 3.5. The block B(s) represents the conversion from the position of the valve, the temperature of the water outgoing the pipeline T_O to the actual T_M. This block is of

algebraic nature for the perfect mixing hypothesis introduced in section 2.c.2. Its expression reads:

$$T_M = X_V * T_B + (1 - X_V) * T_O$$

This block can be interpreted as an uncertainty on the gain of the mixing valve loop transfer function:

$$L(s) = PI(s) * A(s) * B(s, T_O, T_B)$$

This uncertainty will unpredictably increase or decrease the cut-off frequency. However, by choosing a PI regulator, any choice for its tuning cannot lead to instability. In fact, the actuator transfer function A(s) is characterized by one pole, while the PI(s) transfer function is characterized by a pole in the origin and a zero. This means that, in a purely theoretical fashion, the phase margin of this loop transfer function cannot be negative for any choice of the cut-off frequency.

However, the choice of a PI regulator is not forced by the robustness issue just discussed. In fact, a PI control turned out to be performing enough for this inner control loop. The derivative action of a typical PID was not needed in this case, since there are no severe speed requirements. That is because the valve actuator discussed in section 2.c.2 has a time constant of 1 minute, so the dynamics of the closed-loop mixing valve system are already be much faster than the dynamics of the entire heating system, which are set on the order of magnitude of the hours. Moreover, this consideration justifies the choice of neglecting the dynamics of the inner control loop when designing the outer control loop (i.e. the PID for T_Z discussed in the previous section 3.a).

About the tuning of the PI, its zero is set equal to the nominal pole of the valve actuator in order to achieve their theoretical cancellation. The gain of the PI will then coincide with the cut-off frequency. Its value has been set to 0.01 in order to ensure two properties:

- The dynamics of the closed-loop mixing valve system are still very fast compared to the dynamics of G(s) and can thus be neglected
- Despite the theoretical assurance that there is no risk of instability, the cut-off frequency was kept reasonably small so to guarantee both a sufficiently good performance and a robust phase margin.

3.c Anti-windup

As previously said in section 2.c, there are 2 saturations affecting the system. The first one is an imposed saturation on the inlet water temperature set-point $T_{M,rif}$ which can assume a value only in the range [20°C ; 40°C]. This saturation will affect the functioning of the PID in control of the outer loop (i.e. of the zone temperature T_Z), provoking wind-up phenomena. The second saturation is due to the physical limitations of the mixing valve, which has obvious limits on its water mass flow. This saturation will cause wind-up phenomena on the PI in control of the inner loop (i.e. of the inlet water temperature T_M).

Windup effects and anti-windup strategies are presented in many books, among which we can mention [17] and [18]. In this section, the focus will be given to two anti-windup schemes: the back-calculation scheme and the clamping scheme. These schemes are the one offered in the Simulink environment, as well as the most commonly adopted in the ordinary PID applications.

- Back-calculation:
  the structure of a PID endowed with this anti-windup scheme is proposed in Fig. 3.6. The back-calculation part of the whole configuration is highlighted in red.

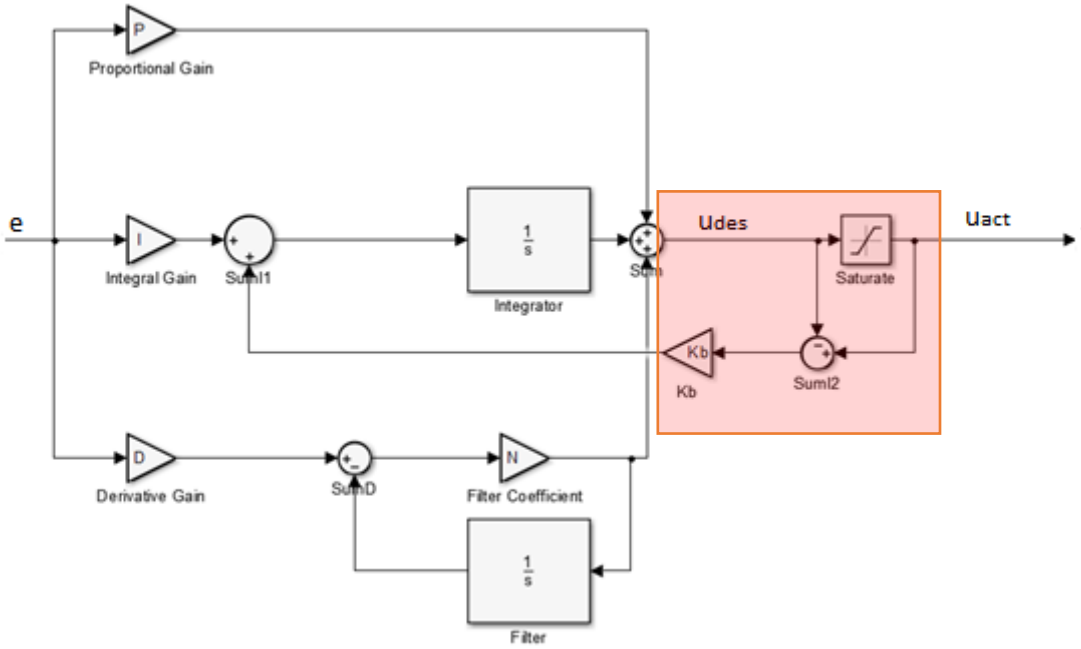

Fig. 3.6: Back-calculation anti-windup scheme

This scheme is intended to prevent an excessive growth of the integral action, which is resized based on how much the PID desired control action u_{Des} is different from

the actual control action u_{Act} (i.e. the one that was possibly adjusted to fit the saturation limits). In fact, the difference between u_{Act} and u_{Des} is weighted with a back-calculation coefficient k_B and then sent as input for the integral block of the PID.

The k_B coefficient has an important role in this anti-windup strategy. This k_B will in fact determine how much the integrator will fall into a wind-up state: if a constant error e feeds the PID, then its control action u_{Des} will exceed the saturation limit by:

$$u_{Des} - u_{Act} = \frac{I}{k_B} * e$$

so a high value of k_B would minimize the anti-windup magnitude. The coefficient k_B has even a different role: $\frac{1}{k_B}$ is the time constant by which the integrator will be reset from a wind-up state [18]

For both these factors, it looks like an high value for the back-calculation coefficient is preferable. However, a high value of k_B can cause the derivative action to negatively interfere with the integral action: the initially high saturation caused by the response of the derivative action to a step variation of the zone temperature set-point $T_{Z,rif}$ would be uselessly compensated on the integral part of the PID. In order to avoid this occurrence, it is advisable to set $\frac{1}{k_B}$ between the derivative time constant τ_D and the integral time constant τ_I:

$$\tau_D < \frac{1}{k_B} < \tau_I$$

In particular, a generally good value is the geometrical average of those two time constants:

$$\frac{1}{k_B} = \sqrt{\tau_I * \tau_D}$$

- Clamping:

  the structure of a PID endowed with this anti-windup scheme is proposed in Fig. 3.7. The clamping circuit is highlighted in red.

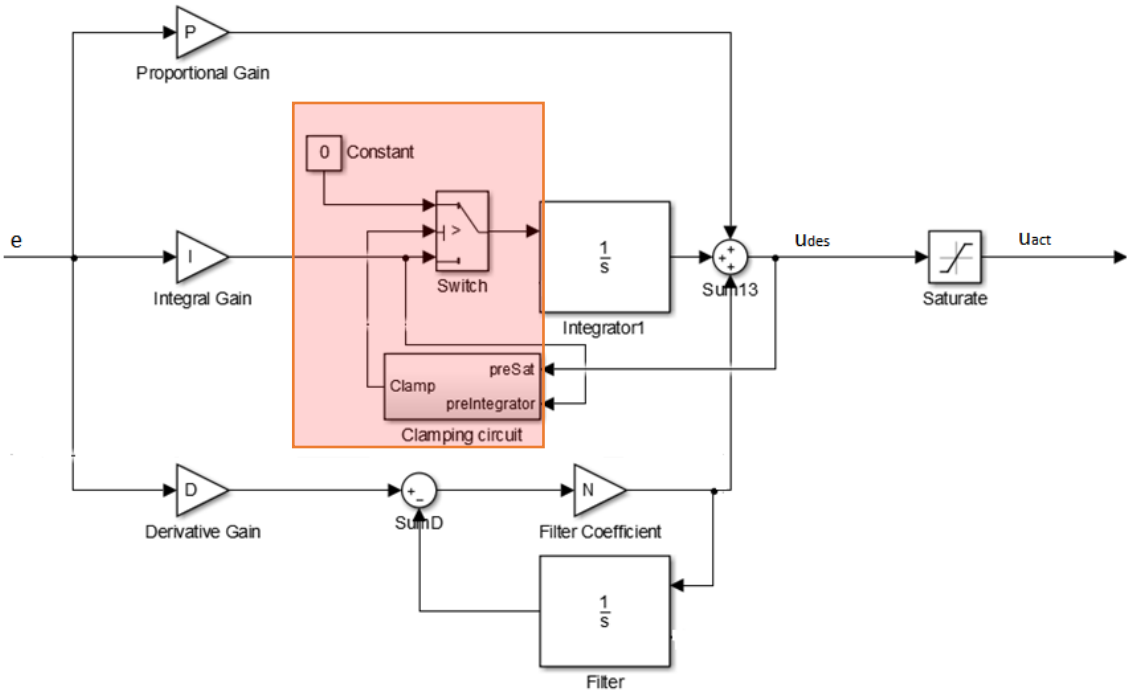

Fig. 3.7: Clamping anti-windup scheme

This scheme acts in a more logic-based way. A switch decides the input of the PID integrator. This switch forces the input to be zero when u_{Des} exceeds the saturation limits and has the same sign of the error signal e. In the opposite case, the input is just set to $e * I$ as normal functioning.

The clamping anti-windup scheme has three advantages with respect to the other solution presented. First, it does not need a tuning, making it a more robust solution. Second, it theoretically never enters in a windup state. Lastly, it does not interfere with the derivative action in any way. For these three reasons, this configuration is preferable over the back-calculation one and thereafter will be adopted in this work.

The clamping anti-windup circuit will be installed both on the PID controller of the outer loop and on the PI controller of the mixing valve. There are no particular consideration to be outlined in the installation of this anti-windup scheme, since it doesn't need tuning.

3.d Safety hysteresis

In order to prevent any kind of severe over-heating caused by the radiant panel system, an electronically controlled shut-off valve is installed in the pipeline. This valve is associated to the status of the system that was previously described in section 2.b: when the system is ON and the control is working normally, the valve is open; when the system is OFF and all controls are inhibited, the valve is closed in order to stop the water from flowing along the pipeline.

The switching between ON and OFF, as well as the position of the shut-off valve, is decided by an hysteresis cycle imposed over the zone temperature error $e = T_{Z,rif} - T_Z$. This hysteresis cycle is presented graphically in Fig. 3.8. Its functioning can be easily defined in words:

- The system is shut off when the error $e = T_{Z,rif} - T_Z$ becomes lower than 0.5°C
- The system is turned on when the error $e = T_{Z,rif} - T_Z$ becomes higher than 0.5°C

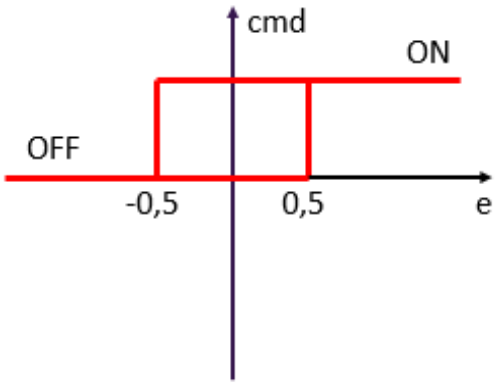

Fig. 3.8: Safety hysteresis diagram

The effect of this ON/OFF switching on our control structure needs to be analyzed. If the controller (this is valid both for the outer PID and for the inner PI) keeps computing its control action during an OFF phase of the system, its value will lose any sense. This consideration is valid both for the outer PID and for the inner PI. An example concerning the outer PID is presented in Fig. 3.9, in which the $T_{Z,rif}$ value is reduced of 3°C, causing the hysteresis switch to turn OFF the system. While the system is OFF the zone temperature starts to decrease because of the heat dispersion towards the external environment (phase 1). At some point, the zone temperature falls below its set-point $T_{Z,rif}$, making the PID output

uselessly rise to a potentially high value (phase 2). Once the system is turned back ON (phase 3), the PID applies an exaggerated control action (i.e. setting $T_{M,rif}$ too high) that in term produces an overheating of the system. If this overheating phenomenon is too high, the zone temperature could rise above its set-point of 0.5°C, triggering again the hysteresis safety cycle and starting a potentially infinite ON/OFF cycle.

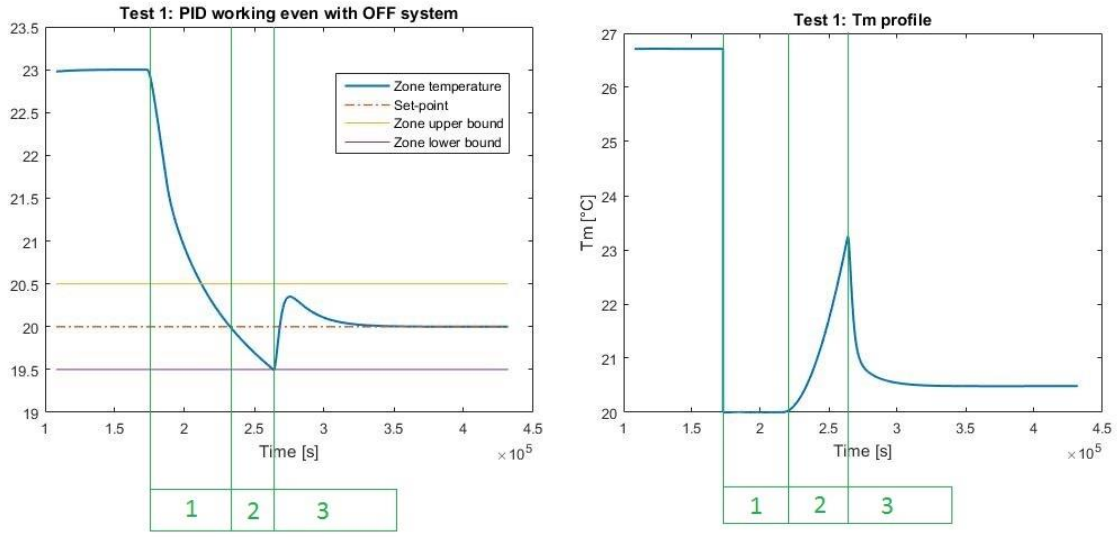

Fig. 3.9: System behavior if the outer loop PID is left computing while the system if OFF

To prevent this over-reaction of the controller in the OFF→ON switching, one could chose to turn off the controller while the system is OFF and simply restart it from zero then the system is turned back on. However, even this approach presents some problems. In Fig. 3.10 the same example proposed previously is considered ($T_{Z,rif}$ lowered of 3°C) but with a complete reset of the PID controller when the system is turned OFF→ON. After the normal fall of the zone temperature (phase 1), when the system is turned ON and the PID reset to zero the zone temperature keeps falling for a long time (phase 2) before starting to rise again (phase 3). This is caused by the reset of the PID, which has to slowly charge its integral action to a suitable amount before starting to move the zone temperature towards its set-point.

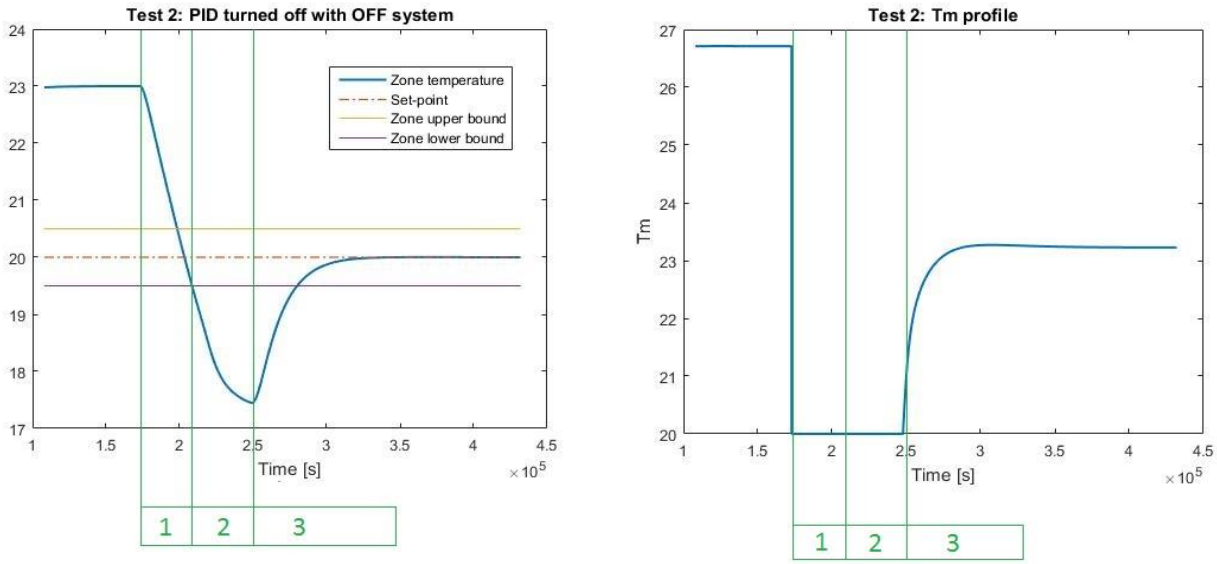

Fig. 3.10: System behavior if the outer loop PID is turned OFF while the system if OFF

The solution to this problem is found in a correct initialization of the integral action. When the system is turned back ON, the PID is reset but with an initial value on the integral action. This initial value was imposed equal to the zone temperature itself, weighted by a 0.7 factor that was empirically found to be efficient. The performance of the integral action initialization is presented in Fig. 3.11, compared with the performance of the pure reset of the PID (i.e. with no initialization on the integral action).

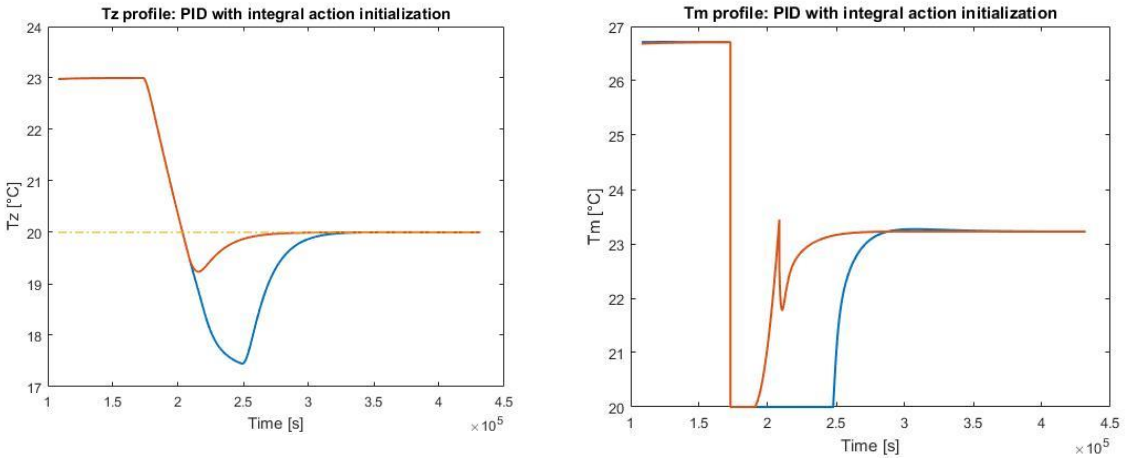

Fig. 3.11: System behavior if the outer loop PID integral action is initialized when the system is turned ON

3.e Outside temperature compensator

Now that the system functioning and overall control structure has been decided, the compensator of the outside temperature will be introduced. In the first section 3.e.1 the typical open-loop compensator structure is described and adopted for our compensator. Then in section 3.e.2 the typical profile of the external temperature is analyzed in order to estimate its average frequency spectrum. After this analysis, the theoretical compensator initially proposed is suitably simplified in section 3.e.3. Finally, the anti-windup scheme is updated to account for the compensator in section 3.e.4.

3.e.1 Compensator structure

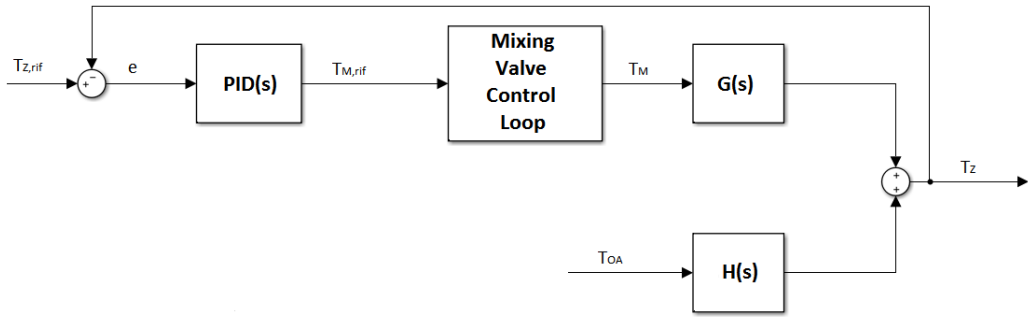

Fig. 3.12: Block diagram of the system until now

The overall system affected by both the radiant panel and the outside temperature inputs is represented in its block diagram form in Fig. 3.12. As it can be seen, the outside temperature T_{OA} affects the zone temperature T_Z (i.e. the controlled variable) through its transfer function $H(s)$. A representative case for the effect of the outside temperature on the zone temperature is shown in Fig. 3.13, with $T_{OA}[°C] = 8 + 5 * \sin(\frac{2\pi}{86400} t)$.

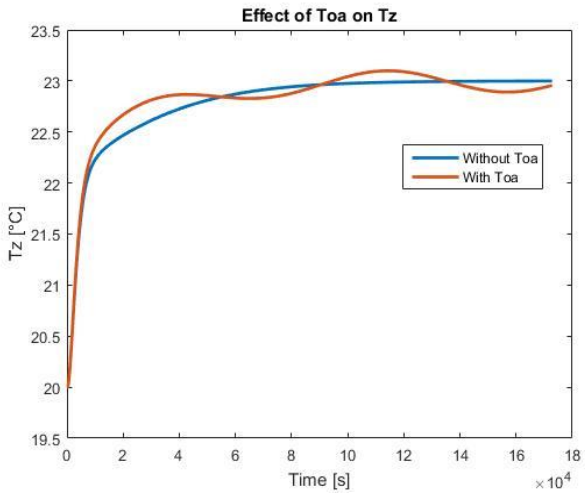

Fig. 3.13: Effect of the outside air temperature on the zone temperature

The outer control loop will eventually compensate the effect of this disturbance on T_Z, since the PID asymptotically imposes a zero error $e = T_{Z,rif} - T_Z$. However, the outside temperature is, by its nature, a variable disturbance. This means that the outer loop will reasonably compensate the effect of the quasi-static component of this disturbance (outside temperature average), but not the effect of the variable part (daily temperature range). This effect will never be definitely removed, but only muffled or strengthened by the PID action. The positive or negative contribution of the PID on the effect of T_{OA} depends on the well-known sensitivity function [20]:

$$S(s) = \frac{1}{1 + PID(s) * G(s)}$$

To reduce the effect of T_{OA}, is advisable to tune the PID controller such that the sensitivity function $S(s)$ has a negative magnitude (dB) for the typical frequencies characterizing the disturbance, i.e. the control bandwidth [0 , ω_C] should encompass the frequency range of T_{OA}. The PID tuning previously proposed turned out to be conservative enough to produce a damping effect on T_{OA} in all the test cases.

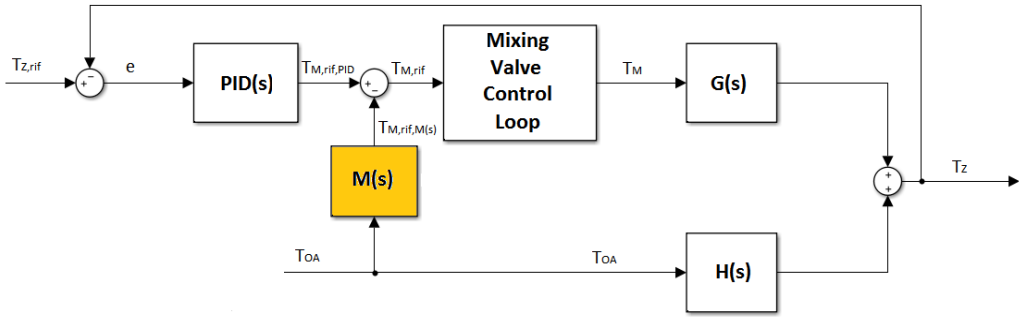

Fig. 3.14: Block diagram of the system endowed with an open loop outside air temperature compensator

Beside the damping effect of the outer loop, a dedicated compensator would improve the disturbance rejection. By assuming the outside temperature measurability, it is possible to install an open-loop compensator M(s) visible in Fig. 3.14. In order to obtain a theoretical perfect compensation of the outside temperature disturbance, the transfer function of this open-loop compensator should read:

$$M(s) = \frac{H(s)}{G(s)}$$

This structure can have some known feasibility issues, such as [20]:

- Improper system, i.e. number of zeroes greater than number of poles
- The difference between an eventual time delay on H(s) and on G(s) is negative, i.e.:

$$delay[H(s)] - delay[G(s)] < 0 \rightarrow Not\ feasible$$

- Unstable system, i.e. one or more poles of $M(s)$ have positive real part.

In section 4.b.1, an analysis of G(s) and H(s) will prove that M(s) never ends up being unstable. Even the time delay point is not an issue in this work, since no time delays have been modeled. The “improper system” issue is addressed later on in section 3.e.3.

3.e.2 Typical outside temperature profile

The most common assumption adopted for the outside temperature profile approximates it to a sinusoid of period 24 hours. This simplification captures most of the behavior of a typical external temperature profile, as it can be seen in Fig. 3.15. The presented profile has been representatively chosen from a meteorological website [21]. It describes the behavior of the outside temperature in a winter partially cloudy day of an Italian hill town.

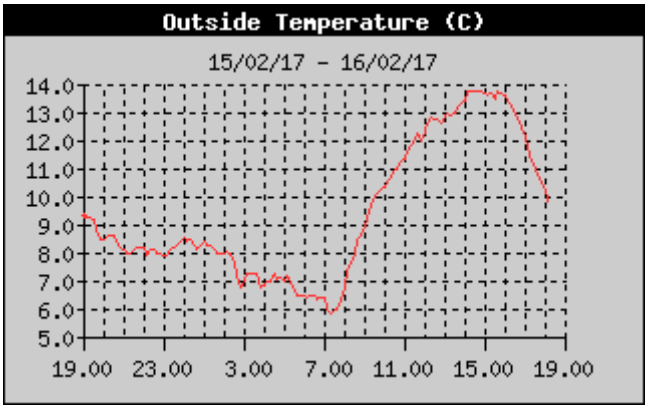

Fig. 3.15: Typical outside air temperature profile

In this thesis, a more reliable profile of the external temperature was designed by exploiting the Simulink library blocks. A continuous-time voltage-controlled oscillator (VCO) was able to distort the base sine wave of period 24-h to resemble more accurately the typical profile of the outside temperature which is exemplified in Fig. 3.15. This profile is characterized by a faster rising slope – associated to the morning – and a slower descending slope – associated to the late afternoon and evening. This newly obtained profile is presented in Fig. 3.16.

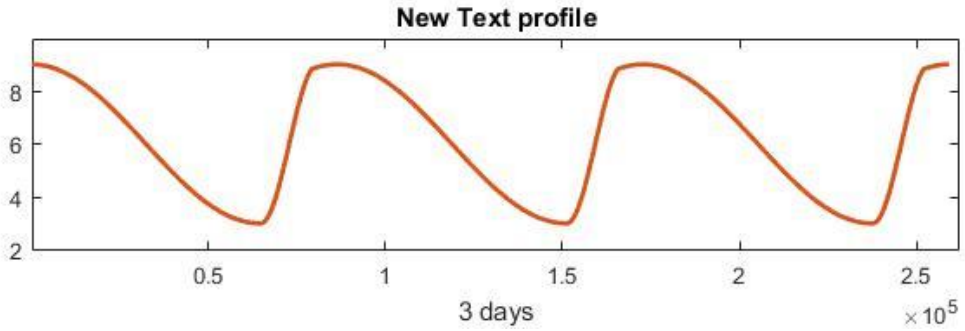

Fig. 3.16: Realistic approximation of the outside air temperature profile

Having obtained an improved approximation of the typical outside temperature profile, the next step was to analyze its frequency spectrum. Presented in Fig. 3.17, this spectrum has its main contribution around the 24-h frequency and then it quickly decreases as the frequency rises. The last significant frequency can be set at $\approx 7e^{-5}Hz = 4{,}4e^{-4}\frac{rad}{s}$.

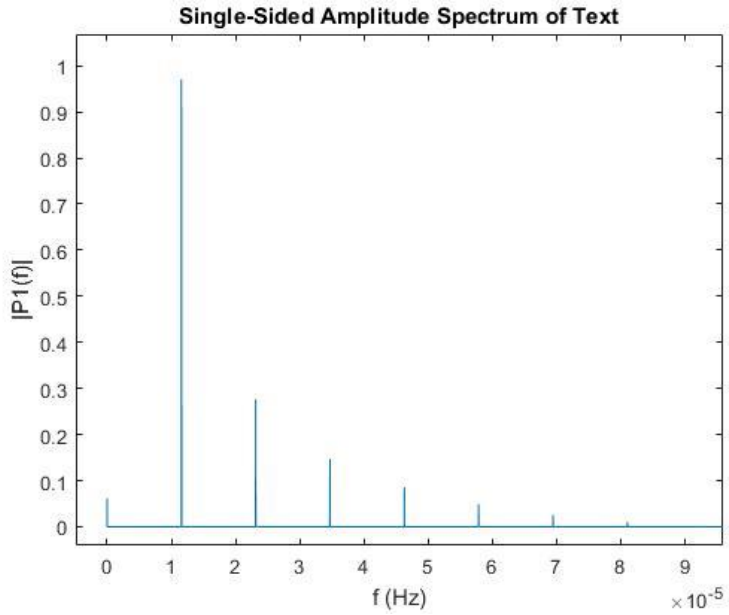

Fig. 3.17: Frequency spectrum of the outside air temperature approximation

3.e.3 1-pole 1-zero approximation of M(s)

The feasibility issue of the compensator M(s) proposed is not solved yet. Without entering too much into detail on the relationship between G(s) and H(s) – a topic broadly discussed in chapter 4 – the typical profile of the Bode diagram of M(s) is represented in Fig. 3.18. There is an evident problem of feasibility, since the final slope of this diagram is +1, meaning that the number of zeroes in M(s) is greater than the number of its poles.

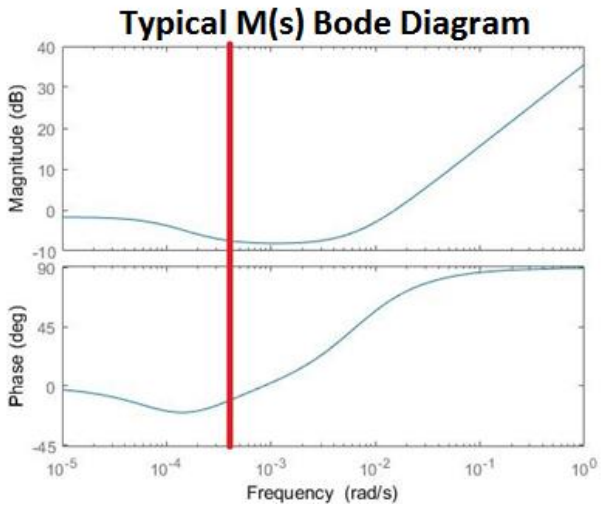

Fig. 3.18: Typical shape of the Bode diagrams of the ideal compensator M(s)

The easy solution adopted in this work is to approximate M(s) with its dominant pole and dominant zero only, i.e. taking only the pole and the zero with the lowest frequency. This

simplification is possible if the ideal M(s) and the approximated one are close enough – in both magnitude and phase – in the frequency range of the disturbance at issue, i.e. T_{OA}. By comparing the frequency spectrum of the typical outside temperature profile (obtained in the previous section) with the Bode diagrams of M(s), this simplification proved to be reasonably applicable in all the tested cases. An example of this comparison is presented in Fig. 3.19.

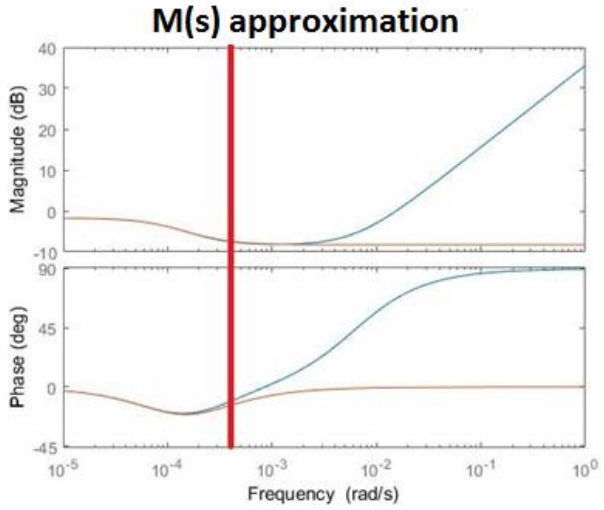

Fig. 3.19: 1-pole 1-zero approximation of the M(s) compensator.
The red vertical line represents the last significant frequency of the outside air temperature profile

3.e.4 Updating the anti-windup

The presence of the compensator additive action on the inlet water temperature set-point $T_{M,rif}$ poses a problem regarding the PID anti-windup. The PID output limits should account in real time even for the contribution of the compensator in order to ensure that $T_{M,rif}$ – that is composed of both the PID output and the compensator output – is kept in the range [20°C ; 40°C]. By referring to Fig. 3.14, the imposed saturation will now read:

$$T_{M,rif} = (T_{M,rif,PID} - T_{M,rif,M(s)}) \in [20°C\,;40°C]$$

To apply these boundaries, the saturation limit imposed on the PID output must read:

$$u_{PID,max}(t) = 40°C + T_{M,rif,M(s)}(t)$$

$$u_{PID,min}(t) = 20°C + T_{M,rif,M(s)}(t)$$

The PID saturation limits are now variable. There is an operative problem with the simulation environment, since Simulink clamping anti-windup scheme accepts only fixed

saturation limits. To bypass this limitation, a new clamping anti-windup scheme was developed starting from the Simulink clamping anti-windup scheme. The Simulink scheme is presented in comparison with the new scheme in Fig. 3.20. There are only two differences between the schemes:

- The saturation block on the output of the PID was changed from a static saturation block to a dynamic saturation block, which accepts time-variant values for its upper and lower limits.
- The “Clamping Circuit” was updated. The dead zone block was changed from a static block to a dynamic block, which accepts time-variant values for its upper and lower limits.

With this updated anti-windup scheme, the compensator M(s) can be introduced in our control strategy.

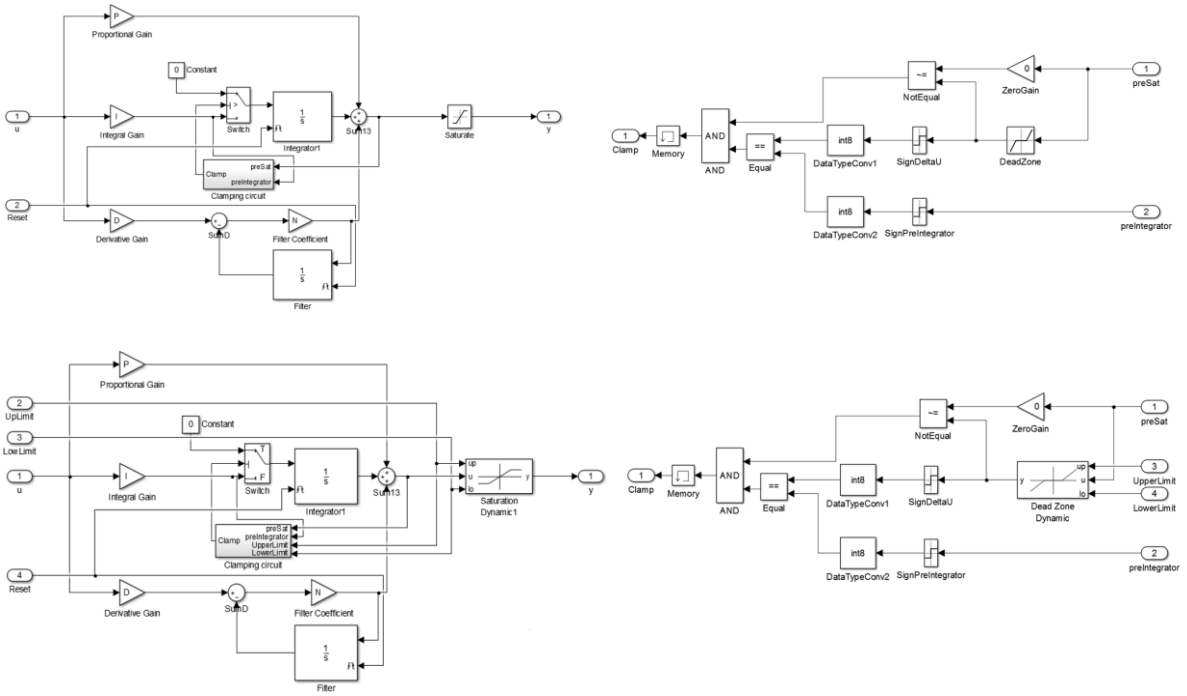

Fig. 3.20: Classic clamping anti-windup block scheme (upper) in comparison with the new clamping anti-windup scheme which accounts for the variable saturation boundaries (lower)

3.f Chapter 3 conclusions

In this chapter, the overall control strategy of the radiant panel heating system was defined. In short, an outer control loop was closed on the zone temperature T_Z equipped with a PID regulator. Then an inner control loop was closed on the inlet water temperature T_M – equipped with a PI regulator – in order to robustly control the mixing valve in presence of variation of the boiler water temperature and/or the temperature of the water outgoing the pipeline. Both the PID and the PI regulator were provided with a clamping anti-windup to account each one for its saturation, which were introduced in the previous chapter.

After this two control loops, an open-loop compensator M(s) for the outside temperature was designed. The frequency spectrum of the typical outside temperature profile was then studied in order to justify a low-order approximation of the ideal open-loop compensator. The anti-windup scheme was finally adapted in order to account for the action of the compensator.

The control structure proposed does not represent an innovation per se. It is, in fact, just the combination of easy and well-known control strategies. A more complicated control structure could achieve higher performances indeed. However, the simplicity of this control structure was preferred for two main reasons. First, a simple control structure shows more reliability and robustness than a complex one. This advantage is of paramount importance in our context, which is known to be dictated by a wide uncertainty on its main physical parameters. Second, this easy control structure will serve as support for the adaptive algorithms that will soon be presented. A too complicated control structure would have needed a fine tuning, which hardly maintains its physical representativeness and thus could lack of sufficient reliability.

PAGE INTENTIONALLY LEFT BLANK

4. PLANT ANALYSIS AND IDENTIFICATION

The previous chapters dealt with the control of the heating system with fixed parameters. In this chapter, the variation of some of the model parameters is introduced. The control strategy will then need an adaptive component to deal with these parameter variations, since the performance of the controller depend indeed on the plant it is assuming to control.

This chapter lays the basis for the adaptive-based control of the radiant panel heating system. The analysis of both the plant and the outside temperature compensator M(s) transfer functions will be combined with different plant identification strategies in order to propose a range of tuning algorithms for the controller, which will be developed in the next chapter 5. The current chapter is mainly dedicated to the plant identification procedures, together with the sensibility analysis of such identified models to the main thermo-physical parameters of the system.

The first section 4.a deals with the definition of the main thermo-physical parameter. These are the parameters that will be let vary in our model, i.e. the parameters according which our adaptive methods have to tune. The choice of these particular parameters will be explained, together with the range in which each parameter will be considered. The second section 4.b deals with the analysis of the plant transfer functions G(s) and H(s) and the outside air temperature compensator M(s). Then, in the third section 4.c different plant identification methods are proposed, along with their strength points, weaknesses and suitable context of application. The fourth and final section 4.d will deal with the sensibility analysis of these identified models. These sensibility analyses will be exploited in the next chapter 5 in the development of the control tuning algorithms.

4.a Main thermo-physical parameters

This section defines the thermo-physical parameters that will be let vary, i.e. the ones on which the control tuning algorithms will perform their adaptation. In the first part 4.a.1, the choice of such parameters will be explained. The following part 4.a.2 will determine the

variation range considered for these parameters, according to statistical inferences. The final section 4.a.3 will define a set of 39 room configurations that will be exploited in most of the tests of this thesis.

4.a.1 Parameters choice

The room model adopted in this work has many physical parameters that can vary depending on the room and heating system characteristics. Among these, for example: three room dimensions, transmittances of each thermal body, thermal inertias, walls thickness, windows, number of walls exposed to the outside environment, pipeline dimensions etc… Most of these parameters have a discrete impact on the controller tuning, i.e. a variation in such parameters should correspond to a variation in the controller values, especially for the outside temperature compensator M(s).

The optimal solution would then be to detect any variation of all the model parameters and re-tune the controller by consequence. The measures at our disposal are, however, limited: zone temperature T_Z, inlet water temperature T_M, outside air temperature T_{OA}. Here the problem arises: many different variation of the plant parameters – that in turn should correspond to different re-turning of the controller – have the same visible effect on the measured variables. This means that, by observing a determinate variation on one measured variable, there is no way to determine the specific cause that generated that phenomenon and thus there is no way to apply the correct re-tuning to the controller. This situation is exemplified in Fig 4.1.

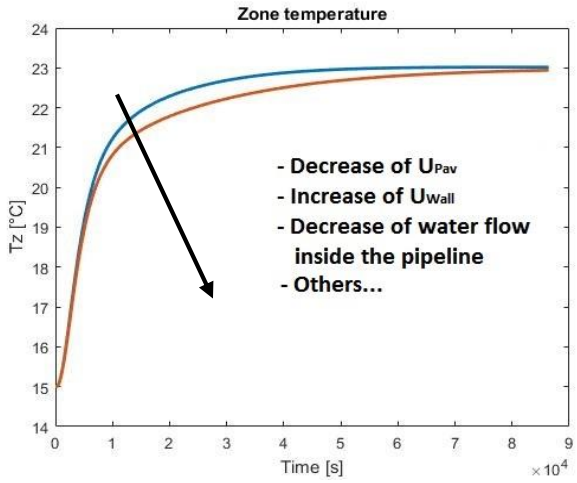

Fig 4.1: Variations on the system measured variables caused by different factors

It will be then necessary to design the adaptive strategy as capable of identifying a variation into a limited specific set of model parameters, and therefore apply the related re-tuning action. With this approach, some parameters variation will be neglected in this adaptive task. This means that those "discarded" parameters will be considered constant, assuming a nominal representative value. Despite the fact that all the parameters have a more or less severe impact on the ideal controller tuning, there are some parameters that have more reason to be neglected with respect to others. These are the ones that can be more easily identified and/or controlled in the design phase: it would be "a waste of measures" to focus our adaptation strategies on these parameters – that are somehow identifiable – instead of some other influent and less identifiable parameters. Before introducing the parameters on which the adaptation will focus, i.e. the main thermo-physical parameters, a description of the neglected parameters is given below:

- Room dimensions: these parameters are, among the one characterizing the room model, the easiest to verify. Moreover, the re-tuning algorithms will present a discrete robustness with respect to the variation of the room dimensions. In presence of big variations of these parameters with respect to their nominal values, the tuning algorithms will just need an easy numerical correction to work properly, but still maintaining their structure. For this reason, since an external gross estimation of the room dimension is sufficient to perform that numerical correction, the "room dimensions" parameters won't be object of the adaptation procedures. See section 5.d for more details.
- Heating system parameters: under this category are grouped all the parameters defining the pipeline dimensions, its thermal characteristics, the recirculating pump and everything else related to the radiant panel system itself. All the multitude of parameters falling under this category are justifiably excluded from the adaptation task. This is because the characteristics of the radiant panel system are usually known to the producer, so its identification would be meaningless. In section 5.d the validity of the tuning algorithm will be proven even with different parameters of the radiant panel system: as for the big variations of the room dimensions discussed before, only a simple numerical correction in the algorithm is needed. This numerical correction is even less invasive than the one proposed for the "room dimensions" parameters, since it would be performed in the production phase of the controller itself (depending on the physical configuration of the heating system).

For the listed reasons, these parameters will be kept to their nominal representative values. The values adopted are the one characterizing the test room presented in section 2.d:

- Room dimensions:
  - Height: 2.85 [m]
  - Length: 3.6 [m]
  - Width: 2.5 [m]
- Heating system parameters (referring to the notation presented in chapter 2):
  - $L = S_{Pav}/0.15$ [m] with a nominal surface/length ratio of 0.15; this parameter is then in function of the pavement surface.
  - D_e external diameter of the pipe : 0.017 m → A_p : 0.053 [m]
  - D_i internal diameter of the pipe : 0.013 m
  - θ : 0.377 [m/s]
  - ρ : 996 [kg/m^3]
  - $w = \theta \rho A_p$: 0.05 [kg/s]
  - C_{p-aq} : 4180 [J/kgK]
  - $C_{Pi} = C_{p-aq} A_p L \rho$ [J/K]
  - U_1 : 24.741 [W/K]

At last, the main thermo-physical parameters chosen are:

- The walls average convective heat transfer coefficient u_{wall}: this parameter, combined with the conductive surface of the walls S_{Wall} represents the walls thermal conductance U_{Wall}. The parameter U_{Wall} of an existent building is indeed hard to identify, but its variation have big repercussions on the correct compensator tuning: it is then a good choice to focus the adaptive task on this parameter.
  The adaptation to any variation on the parameters u_{wall} and S_{Wall} results then in the adaptation to the variation of the whole U_{Wall}. However, it is not necessary to perform a separate adaptation between an S_{Wall} variation – which in turn is correlated to the room dimensions and the number of walls exposed to the outside environment – or an u_{wall} variation, because in the walls energy balance adopted after the model testing of section 2.d:
  $$C_W \dot{T_W} = U_{Wall}(T_Z - T_W) + U_{Wall}(T_{OA} - T_W)$$
  the parameters u_{wall} and S_{Wall} are always combined together into U_{Wall}. This means that a variation of u_{wall} has the same effect of an equivalent variation of S_{Wall}, so we can focus our adaptation on the variation of just one of the two parameters. Any variation of the second parameter will be assimilated into a variation of the first, so in the end the variation of the whole U_{Wall} is correctly addressed and compensated.

Moreover, the parameter S_{Wall} is easily identified manually, just like the room dimensions.

A more straightforward way would have directed the adaptation on the whole U_{Wall} parameter. However, in this thesis the choice of identifying the u_{wall} parameter instead was preferred in order to define the boundaries (see the next section 4.a.2) of this parameter only in function of the material quality of the walls, resulting in more representative independence from the easily identifiable dimensions of the model (S_{Wall}).

- The walls specific heat capacity $c_{p,Wall}$: this parameter, multiplied by the walls mass, results in the walls mass thermal inertia C_{Wall}. Similarly to U_{Wall}, even this parameter is hard to identify and has a strong effect on the correct tuning of the compensator M(s). The same conclusions on u_{wall} and S_{Wall} exposed before can be extended to the parameters in current object, i.e. $c_{p,Wall}$ and the walls mass. Combined with the previous parameter, this one closes the picture on the walls thermal properties in our model.
- The pavement average convective heat transfer coefficient u_{Pav}
- The pavement specific heat capacity $c_{p,Pav}$: u_{Pav} and $c_{p,Pav}$ define the thermal properties of the pavement, similarly to u_{Wall} and $c_{p,Wall}$. The same conclusion discussed about the walls can be drawn regarding the dimensions of the pavement implicated into these two parameters.

These four parameters have been preferred to others because of their strong impact on both the dynamics of the system and the ideal tuning of the controllers. Moreover, being those parameters of thermal nature, their identification is often very hard to perform manually, making them the perfect candidates for the adaptive tuning strategy.

4.a.2 Range for the main thermo-physical parameters

Now that the main thermo-physical parameters are defined, the focus shifts on the boundaries that will be applied to their values. Since these parameters are left to vary, it is advisable to decide an admissible range for the values they are allowed to take in order to perform a well-defined test campaign. An analysis of the typical values of these constructive materials is performed.

This analysis is divided into the walls parameters and the pavement parameters:

- WALLS:

  To identify a reliable range for the wall parameters, their analysis was based on a summary document produced by the "Comitato Termotecnico Italiano Energia e Ambiente". This document suggests the computational values for the main parameters characterizing the walls – among which even u_{wall} and $c_{p,Wall}$ are listed – based on the constructive characteristics of the wall. Each time period is then associated to the typical constructive characteristic adopted for the walls.
  To make the exposition clearer, the typical parameter range for u_{wall} and $c_{p,Wall}$ is further divided into three ages, depending on when the building was constructed:

  - 1930-1975 (Old wall): $c_{p,Wall} \in [57; 65]$ and $u_{Wall} \in [0.98; 1.61]$
  - 1975-2005 (Modern wall): $c_{p,Wall} \in [17; 18]$ and $u_{Wall} \in [0.594; 0.796]$
  - 2005-today (New wall): $c_{p,Wall} \in [13; 13]$ and $u_{Wall} \in [0.28; 0.28]$

  These ranges are synthetically represented in Tab. 4.1.

WALLS				
Year	CpWall [kJ/m2K]	uWall [W/m2]	Average CpWall [kJ/m2K]	Average uWall [W/m2]
1930-1975	57<>65	0,98<>1,61	61	1,28
1975-2005	18<>17	0,594<>0,706	17,5	0,65
2005-today	13	0,28	13	0,28

Tab. 4.1: Walls parameters range

For each of these ranges, the average value was computed in order to define three representative values for the of walls, which will be used in section 4.a.3:

- 1930-1975 (Old wall): $c_{p,Wall} = 61 \left[\frac{kJ}{m^2K}\right]$ and $u_{Wall} = 1.295 \left[\frac{W}{m^2K}\right]$
- 1975-2005 (Modern wall): $c_{p,Wall} = 17.5 \left[\frac{kJ}{m^2K}\right]$ and $u_{Wall} = 0.65 \left[\frac{W}{m^2K}\right]$
- 2005-today (New wall): $c_{p,Wall} = 13 \left[\frac{kJ}{m^2K}\right]$ and $u_{Wall} = 0.28 \left[\frac{W}{m^2K}\right]$

In the same figure it is possible to notice the strong non-continuity of these ranges, both for $c_{p,Wall}$ and u_{Wall}. The final range adopted in this work is then taken by considering the lowest and highest value among the presented ones, resulting in:

- $c_{p,Wall} \in [13; 65]$
- $u_{Wall} \in [0.28; 1.61]$

in order to theoretically cover all the typical values adopted from the last century on.

- PAVEMENT:

Four different type of screed have been considered to establish a reasonable range for the pavement parameters, each one associated to a specific market brand and material. Without reporting the brand name, the four example and their associated values are represented in Tab. 4.2.

PAVEMENT (SCREED)																	
Type	Average convective heat transfer coefficient uPav [W/m2]									Specific heat CpPav [kJ/m2K]							
	Height [cm]									Height [cm]							
	2	3	4	5	6	7	8	9	10	2	3	4	5	6	7	8	9	10
Type 1	93,5	62,33	46,75	37,4	31,17	26,71	23,38	20,78	18,7	36	54,01	72,01	90,01	108,01	126,02	144,02	162,02	180,02
Type 2	64	42,67	32	25,6	21,33	18,29	16	14,22	12,8	33,48	50,22	66,96	83,7	100,44	117,18	133,92	150,66	167,4
Type 3	55	36,67	27,5	22	18,33	15,71	13,75	12,22	11	36	54	72	90	108	126	144	162	180
Type 4	37,5	25	18,75	15	12,5	10,71	9,38	8,33	7,5	34	51	68	85	102	119	136	153	170
Average	*62,5*	*41,6675*	*31,25*	*25*	*20,8325*	*17,855*	*15,6275*	*13,8875*	*12,5*	*34,87*	*52,3075*	*69,7425*	*87,1775*	*104,613*	*122,05*	*139,485*	*156,92*	*174,355*
Grouping	*45,13916667*			*21,22916667*			*14,005*			*52,30666667*			*104,6133333*			*156,92*		

Tab. 4.2: Pavement parameters range

For each type of screed, the $c_{p,Pav}$ and u_{Pav} values have been computed on different screed height, ranging from 2cm to 10cm. Then the average was computed along the four types of screed for each value of the screed height, obtaining nine different values. These nine values were then grouped 3 by 3 in order to define three types of pavement, similarly to what was done with the three age of the walls:

- 2-4 cm height (Small screed): $c_{p,Pav} \in [35; 70]$ and $u_{Pav} \in [31; 62]$
- 5-7 cm height (Medium screed): $c_{p,Pav} \in [87; 122]$ and $u_{Pav} \in [18; 25]$
- 8-10 cm height (Big screed): $c_{p,Pav} \in [140; 174]$ and $u_{Pav} \in [12; 16]$

For each of these ranges, the average value was computed in order to define three representative values for the pavement, which will be used in section 4.a.3:

- 2-4 cm height (Small screed): $c_{p,Pav} = 52.3 \left[\frac{kJ}{m^2K}\right]$ and $u_{Pav} = 45.139 \left[\frac{W}{m^2K}\right]$
- 5-7 cm height (Medium screed): $c_{p,Pav} = 104.6 \left[\frac{kJ}{m^2K}\right]$ and $u_{Pav} = 21.229 \left[\frac{W}{m^2K}\right]$
- 8-10 cm height (Big screed): $c_{p,Pav} = 157 \left[\frac{kJ}{m^2K}\right]$ and $u_{Pav} = 14.005 \left[\frac{W}{m^2K}\right]$

Since these ranges present the same problem on non-continuity of the walls, the range considered for $c_{p,Pav}$ and u_{Pav} was then selected to enclose all the 9 values obtained:

- $c_{p,Pav} \in [34; 175]$
- $u_{Pav} \in [12; 63]$

4.a.3 Representative rooms and limit cases

The three kind of pavements “Small screed Ss”, “Medium screed Ms” and “Big screed Bs” are now combined with the three kind of walls “Old wall Ow”, “Modern wall Mw” and “New wall Nw” to define 9 representative rooms, represented in Tab. 4.3.

ROOM	CpWall [kJ/m2K]	uWall [W/m2]	CpPav [kJ/m2K]	uPav [W/m2]
Ow - Ss	61	1,28	52,3	45,139
Ow - Ms	61	1,28	104,6	21,229
Ow - Bs	61	1,28	157	14,005
Mw - Ss	17,5	0,65	52,3	45,139
Mw - Ms	17,5	0,65	104,6	21,229
Mw - Bs	17,5	0,65	157	14,005
Nw - Ss	13	0,28	52,3	45,139
Nw - Ms	13	0,28	104,6	21,229
Nw - Bs	13	0,28	157	14,005

Tab. 4.3: Parameters of the 9 representative rooms

The values associated to these rooms have no specific importance in the adaptive algorithms, which will be designed to work along all the range of the four main thermo-physical parameters. These rooms will just serve as a basis to define another set of rooms that covers all the “limit cases”, i.e. a set of rooms characterized by each combination of the extreme values that the four main thermo-physical parameters can assume. This set of “limit cases” is significant because it covers the limit layouts of the room, so that with a restrained number of tests we encircle all the infinite possible combination outcomes. The “limit cases”, together with the “representative rooms”, will be exploited in the next sections to perform a structured testing campaign by which our algorithms will be tuned. The algorithms will then be tested on random-parameters rooms to verify their robustness.

Theoretically, there are 4 parameters - $c_{p,Wall}$, u_{Wall}, $c_{p,Pav}$ and u_{Pav} – that have 6 possible limit values – 2 values for each of the 3 types: old/modern/new for the walls, small/medium/big for the pavement – resulting in a total of $6^4 = 1296$ limit cases to test. These are way too much tests to maintain their physical sense, so it is better to reduce this amount.

First, only the limit values that belong to the same representative rooms will be combined together. This means for example that the lower bound for $c_{p,Wall}$ of the “Old wall” type (57) cannot be combined with the lower bound for u_{Wall} of the “Modern wall” type (0.594), but

only with the upper or lower bound of the "Old wall" type (0.98 or 1.61). With this restriction, the possible limit cases combinations are reduced to $9 * 2^4 = 144$.

Even this is a quite big amount of tests, so a final restriction will be made. The variation of $c_{p,Wall}$ will associated to a specific variation of u_{Wall}, and the same will be done between $c_{p,Pav}$ and u_{Pav}. This association will be made in an inverse sense, meaning that the lower bound (respectively, the upper bound) for $c_{p,Wall}$ will be associated to the upper bound (respectively, the lower bound) for u_{Wall}, and similarly for the pavement parameters $c_{p,Pav}$ and u_{Pav}. This inverse association is chosen because of its logical interpretation: for example, by choosing the upper bound of $c_{p,Wall}$ together with the lower bound of u_{Wall}, the resulting room has a "strong wall" because it is both very insulating and very "thermally heavy". This room will then be more representative of a limit case with respect to a room assuming the upper bound of $c_{p,Wall}$ together with the upper bound of u_{Wall}, that would have a bad insulation on a thermally heavy wall – two factors that compensate each other in terms of protection towards the external environment. Anyway, this further rule restricts the possible combinations to $9 * 2^2 = 36$. Moreover, the "New wall" category doesn't have any upper and lower bounds for both u_{Wall} and $c_{p,Wall}$, so the tests are further reduced to 30.

By combining these 30 limit cases with the 9 central cases of the representative rooms, a total of 39 cases is obtained. These are listed in Tab. 4.4, in which the following notation was adopted:

- "W" means a "strong wall", i.e. the upper bound of $c_{p,Wall}$ and the lower bound of u_{Wall} of the current wall category were adopted.
- "w" means a "weak wall", i.e. the lower bound of $c_{p,Wall}$ and the upper bound of u_{Wall} of the current wall category were adopted.
- "P" means a "massive pavement", i.e. the upper bound of $c_{p,Pav}$ and the lower bound of u_{Pav} of the current pavement category were adopted.
- "p" means a "light pavement", i.e. the lower bound of $c_{p,Pav}$ and the upper bound of u_{Pav} of the current pavement category were adopted.

	ROOM	Limit case	CpWall [kJ/m2K]	uWall [W/m2]	CpPav [kJ/m2K]	uPav [W/m2]
1	Ow - Ss		61	1,28	52,3	45,139
2		W P	65	0,98	70	31
3		W p	65	0,98	35	62
4		w P	57	1,61	70	31
5		w p	57	1,61	35	62
6	Ow - Ms		61	1,28	104,6	21,229
7		W P	65	0,98	122	18
8		W p	65	0,98	87	25
9		w P	57	1,61	122	18
10		w p	57	1,61	87	25
11	Ow - Bs		61	1,28	157	14,005
12		W P	65	0,98	174	12
13		W p	65	0,98	140	16
14		w P	57	1,61	174	12
15		w p	57	1,61	140	16
16	Mw - Ss		17,5	0,65	52,3	45,139
17		W P	18	0,594	70	31
18		W p	18	0,594	35	62
19		w P	17	0,706	70	31
20		w p	17	0,706	35	62
21	Mw - Ms		17,5	0,65	104,6	21,229
22		W P	18	0,594	122	18
23		W p	18	0,594	87	25
24		w P	17	0,706	122	18
25		w p	17	0,706	87	25
26	Mw - Bs		17,5	0,65	157	14,005
27		W P	18	0,594	174	12
28		W p	18	0,594	140	16
29		w P	17	0,706	174	12
30		w p	17	0,706	140	16
31	Nw - Ss		13	0,28	52,3	45,139
32		P	13	0,28	70	31
33		p	13	0,28	35	62
34	Nw - Ms		13	0,28	104,6	21,229
35		P	13	0,28	122	18
36		p	13	0,28	87	25
37	Nw - Bs		13	0,28	157	14,005
38		P	13	0,28	174	12
39		p	13	0,28	140	16

Tab. 4.4: Parameters of the 39 representative rooms and limit cases

The numeration of these 39 representative rooms and limit cases respects the order by which the rooms are tested in the following chapters.

4.b G(s), H(s) and M(s) analysis

The purpose of this section is to deduce the greatest amount of information on the plant transfer functions G(s) and H(s), in the first part 4.b.1. These information will then be used in 4.b.2 to deduce some characteristics about the outside air compensator M(s). These conclusions will then be used in the next chapter 5 to develop the tuning algorithms for the outside air compensator M(s).

4.b.1 G(s) and H(s)

Any possible relationship between the two transfer functions can be very useful in understanding how the compensator $M(s) = \frac{H(s)}{G(s)}$ comes out, especially since the M(s) adopted (which was proposed in section 3.e.3) is the 1-pole 1-zero approximation.

First, the conclusions on the poles and zeroes of both G(s) and H(s) are presented:

- Poles: the poles of G(s) are equal to the poles of H(s) for any parameter configuration of our model. This conclusion is justifiable by the fact that the whole MISO (Multiple Input Single Output) system – considering the ON state-space system presented in section 2.b.3 – is completely observable and controllable, so the poles of the system, including their multiplicity, coincide with the eigenvalues of the matrix A [22].
- Zeroes: the same conclusion cannot be drawn for the zeroes. It is even impossible for the zeroes of G(s) to be equal to the zeroes of H(s), because it would mean that the effect of the outside air temperature T_{OA} on the zone temperature T_Z has the same dynamics of the effect of the inlet water temperature T_M on T_Z, which is known to be different from experience.
  Over all the cases analyzed, both G(s) and H(s) are characterized by one or two zeroes, depending on the physical parameters configuration. The second zero, if present, is always positioned at a definitely high frequency and can thus be neglected.

The gain of G(s) and H(s) is considered separately because there is a particular relationship linking these two quantities. Now it will be proven that, for the model adopted, the following relationship holds:

$$G_0 + H_0 = 1$$

Where G_0 and H_0 are the gain of G(s) and H(s) respectively.

This property can be proven with the support of the electrical equivalent modeling [23].The electrical equivalent will be obtained considering the final model adopted in section 2.d, i.e.:

$$\begin{cases} C_Z\dot{T_Z} = U_{wi}(T_W - T_Z) + U_{pav}(T_{Pav} - T_Z) \\ C_{Wall}\dot{T_W} = U_{wi}(T_Z - T_W) + U_{we}(T_{OA} - T_W) \\ C_{Pav}\dot{T_{Pav}} = U_{Pav}(T_Z - T_{Pav}) + U_1A_pL(\frac{1-e^{-\alpha}}{\alpha})(T_M - T_{Pav}) \\ C_{Pi}\dot{T_{Pi}} = [U_1A_pL\left(\frac{1-e^{-\alpha}}{\alpha}\right) + wC_{p-aq}(e^{-\alpha} - \frac{1-e^{-\alpha}}{\alpha})](T_{Pav} - T_M) + wC_{p-aq}(T_M - T_{Pi}) \end{cases}$$

Its electrical equivalent is represented in Fig 4.2.

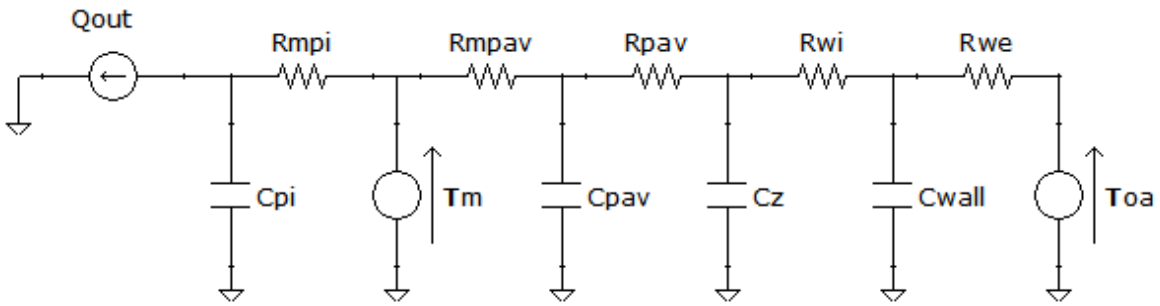

Fig 4.2: System electrical equivalent

with:

- $Q_{out} = 1/[U_1A_pL\left(\frac{1-e^{-\alpha}}{\alpha}\right) + wC_{p-aq}(e^{-\alpha} - \frac{1-e^{-\alpha}}{\alpha})](T_{Pav} - T_M)$
- $R_{mpi} = 1/wC_{p-aq}$
- $R_{mpav} = 1/U_1A_pL(\frac{1-e^{-\alpha}}{\alpha})$

To compute the gain of G(s) and H(s), the system is considered in its steady state form. This means that the electric capacities are turned into open circuits, as shown in Fig 4.3.

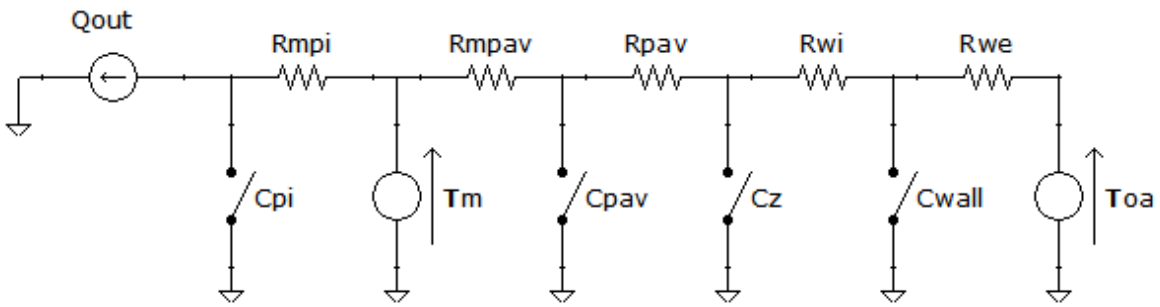

Fig 4.3: System electrical equivalent in steady state

Then ,to compute the gain of G(s) in particular, the other sources are turned off (Fig 4.4) and the ratio $\frac{T_z}{T_M}$ is computed.

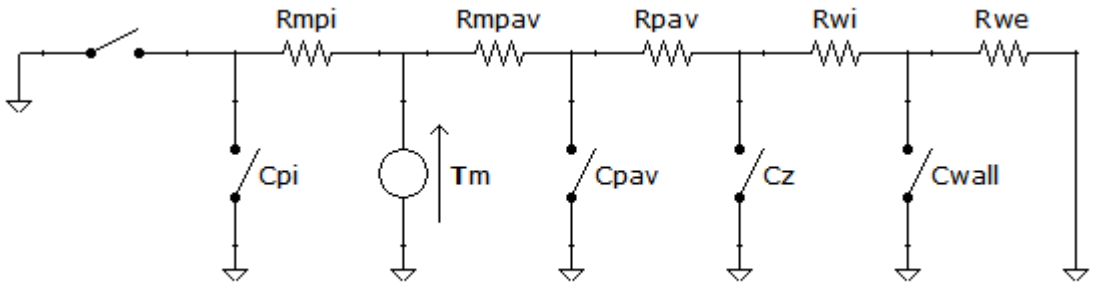

Fig 4.4: System electrical equivalent in steady state, only inlet water temperature input acting on the system

The ratio $\frac{T_z}{T_M}$ can be found by simply applying the voltage divider formula, i.e.

$$G_0 = \frac{T_z}{T_M}(s=0) = \frac{R_{wi} + R_{we}}{R_{wi} + R_{we} + R_{pav} + R_{mpav}}$$

Then, the gain of H(s) is found in an analogous way (Fig 4.5).

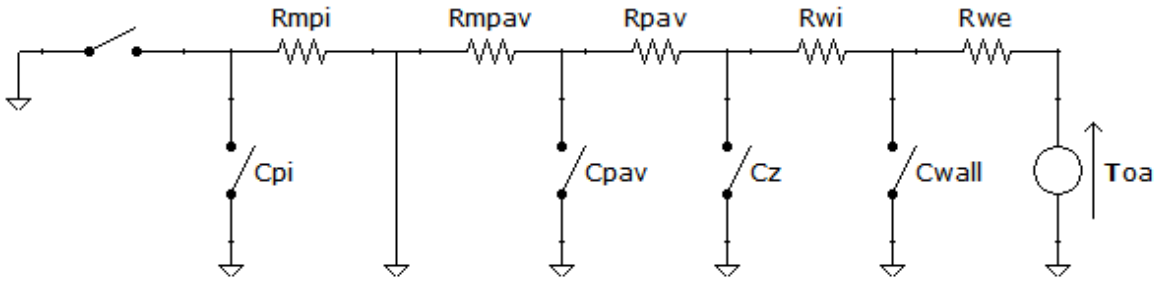

Fig 4.5: System electrical equivalent in steady state, only outside air temperature input acting on the system

Even this ratio $\frac{T_z}{T_{OA}}$ can be found by simply applying the voltage divider formula, i.e.

$$H_0 = \frac{T_z}{T_{OA}}(s=0) = \frac{R_{pav} + R_{mpav}}{R_{wi} + R_{we} + R_{pav} + R_{mpav}}$$

It is now possible to verify that:

$$G_0 + H_0 = \frac{R_{wi} + R_{we}}{R_{wi} + R_{we} + R_{pav} + R_{mpav}} + \frac{R_{pav} + R_{mpav}}{R_{wi} + R_{we} + R_{pav} + R_{mpav}} = 1$$

4.b.2 M(s)

Following the conclusions drawn in the previous section about the singularities of G(s) and H(s), in the $M(s) = \frac{H(s)}{G(s)}$ ratio the only singularities that will survive are the zeroes of both G(s) and H(s). This means that the poles of M(s) will be the zeroes of G(s) and the zeroes of M(s) will be the zeroes of H(s). Moreover, the compensator adopted in this work is the 1-zero 1-pole approximation of the ideal compensator $M(s) = \frac{H(s)}{G(s)}$ (see section 3.e.3), meaning that there are only three parameters to tune for this compensator:

$$M(s) = \mu_M \frac{1 + sT_M}{1 + s\tau_M}$$

that is the gain μ_M, the zero time constant T_M and the pole time constant τ_M.
About these three parameters, it can be concluded that:

- τ_M will be the dominant zero of G(s).
- T_M will be the dominant zero of H(s).
- μ_M will be the ratio between the gain of G(s) and of H(s)

A sensitivity analysis was conducted with respect to the variation of the four main thermo-physical parameters $c_{p,Wall}$, u_{Wall}, $c_{p,Pav}$ and u_{Pav}. The results are listed below:

- τ_M, that is the dominant zero of G(s), is affected only by the variation of $c_{p,Wall}$ and u_{Wall}. This conclusion was extensively tested on numerous random rooms. It might be sound counter-intuitive that the dominant zero of G(s), which is the transfer function from T_M and T_Z and thus is more involved with the pavement, is affected only by the parameters of the walls. This fact can however be interpreted in the following way. The zeroes of the transfer functions are generally associated to the dynamics of the sub-system that is not on the direct path of the transfer function in question. It is like the zeroes represent the effect of the complementary dynamics of the transfer function. In this case, the direct path of the transfer function G(s) is constituted by the pavement, while the complementary sub-system is represented by the walls.
  By means of the symbolic computation equipped on Matlab, the four main thermo-physical parameters were expressed in a symbolic form and the transfer functions H(s) and G(s) were computed. Then, the analytical form of τ_M was obtained:

$$\tau_M = \frac{20.000U_{Wall} + 2.600{U_{Wall}}^2}{10.000C_{p,Wall} + 2.600U_{Wall}C_{p,Wall} + 169{U_{Wall}}^2C_{p,Wall}}$$

Beside the particular numerical values expressed, that are related to the nominal values of the other room parameters, it can be seen that $c_{p,Pav}$ and u_{Pav} cannot be found in that expression, confirming the point on τ_M.

- T_M, that is the dominant zero of H(s), is affected only by the variation of $c_{p,Wall}$ and u_{Wall}. Even this conclusion was extensively tested on numerous random rooms. The same explanation proposed in the previous point holds.

This sensitivity analysis lays the basis for the tuning algorithms proposed in chapter 5. The dependency of the compensator parameters on the respective thermo-physical parameters will be exploited to define the correlation functions which are the backbone of the tuning algorithms. Each compensator parameter will be associated to a specific identified quantity of the plant – such as the time constant of G(s) – depending on their mutual dependency on the main thermo-physical parameters. Then, each compensator parameter will be tuned according to the value of the relative identified quantity.

4.c Plant identification

In this section, the procedures focused on the identification of the plant transfer functions G(s) and H(s) are presented. These identification will serve the control tuning algorithms that are presented in the next chapter 5.

First, the mathematics behind the identification is presented 4.c.1. Then three different procedures are presented for the identification of G(s) in 4.c.2. A method to refine the gain of the estimated G(s) is defined in 4.c.3, which will serve to the H(s) identification procedure presented in 4.c.4.

4.c.1 Identification algorithm

The identification algorithm here proposed is the one adopted to perform the identification of both G(s) and H(s). Each identification method for G(s) and H(s) will differ in the application of this algorithm, that however is the mathematical basis of all of them.

Since all the work on the adaptive part of this thesis was done on a simulation environment employing Simulink, the Matlab identification functions were exploited. In particular, to

identify the transfer function receiving a certain set of measured input data u and outputting another set of measured data y the function "tfest" was used [19]. The sampling time adopted to collect the data in any identification task was set to 30 seconds.

The Matlab function "tfest" was asked to return – for the identification of both G(s) and H(s) transfer functions – a transfer function characterized by only one pole. Regarding the functioning of "tfest", a combination of instrument variables based on subspace estimation approaches are used to initialize the transfer function coefficients. The initialized coefficients are then passed on a nonlinear least-squares solver to iteratively minimize the prediction error (PEM method). The focus of this work, however, is not on the identification algorithms per se. For further information, it is possible to refer to [24] and [25].

4.c.2 G(s) estimation

To identify this transfer function, three different methods are proposed:

- Closed loop identification 4.c.2.1
- Open loop identification 4.c.2.2
- Open loop identification by exploiting the estimation of H(s) 4.c.2.3

In all of these methods, the effect of the outside temperature T_{OA} will be somehow compensated, since it is not possible to shut off this disturbance during the G(s) identification. Luckily, the effect of G(s) is realistically stronger than the effect of H(s), so the result of the identification will be affected only marginally by the outside temperature.

4.c.2.1 G(s) Closed loop

This identification procedure is performed, as said, in closed loop. This means that both the outer control loop of T_Z and the inner control loop of T_M are closed and functioning, together with the outside temperature compensator M(s). The tuning adopted for these controllers during the identification procedure is explained below:

- The PI regulator of the inner loop is related to the mixing valve only, so its nominal tuning will be adopted and left unvaried after the identification.
- The tuning of the PID regulator of the outer loop depends on the plant instead. During this closed loop identification, initially an average tuning is adopted for the PID. To compute this average tuning, the average room was considered: the average

room is the room characterized by the average values for each of the four main thermo-physical parameters, i.e. $c_{p,Wall}$, u_{Wall}, $c_{p,Pav}$ and u_{Pav}. Those average values are taken as the middle of each range:

- $c_{p,Wall} \in [13; 65]$ has average 39 $\left[\frac{kJ}{m^2K}\right]$
- $u_{Wall} \in [0.28; 1.61]$ has average 0.945$\left[\frac{W}{m^2K}\right]$
- $c_{p,Pav} \in [34; 175]$ has average 104.5$\left[\frac{kJ}{m^2K}\right]$
- $u_{Pav} \in [12; 63]$ has average 37.5$\left[\frac{W}{m^2K}\right]$

The PID tuning resulting from this room configuration is:

- $P = 3.25$
- $I = 1.3 * 10^{-4}$
- $D = 8.96 * 10^{3}$
- $N = 1000$

- Even for the outside temperature compensator M(s) the adopted configuration is tuned according to the average room expressed in the previous point. Its parameters read:
  - $\mu_M = 0.4$
  - $T_M = 9.67 * 10^{3}$
  - $\tau_M = 2.36 * 10^{4}$

This identification procedure exploits the "tfest" Matlab function (introduced in the previous section) to compute the 1-pole estimation of G(s):

$$\hat{G}(s) = \widehat{\mu_G} \frac{1}{1 + s\tau_G}$$

To compute this estimated transfer function, the "tfest" function receives the input data set "u" and the output data set "y" as follows:

- $u = T_M + T_{M,rif,M(s)}$
- $y = T_Z$

with $T_{M,rif,M(s)}$= output signal of the compensator M(s). This particular choice of the input data set "u" has to be explained. In fact, by simply taking $u = T_M$ and $y = T_Z$ the effect of the outside temperature on T_Z would have been unduly attributed to T_M, while with this correction everything is rebalanced – assuming that M(s) is the ideal compensator $M(s) = \frac{H(s)}{G(s)}$. This can be proven by the following relationships:

$$y = T_Z = G(s)T_M + H(s)T_{OA}$$

$$u = T_M + T_{M,rif,M(s)} = T_M + \frac{H(s)}{G(s)} T_{OA}$$

$$G(s) * u = G(s)T_M + G(s) * \frac{H(s)}{G(s)} T_{OA} = G(s)T_M + H(s)T_{OA} = y$$

A simple steady-state example can be used to clarify the above considerations:

> The zone temperature T_Z has settled to 20°C with an inlet water temperature T_M of 30°C and an outside temperature T_{OA} of 0°C. In this case, the G(s) gain is trivially equal to $\frac{\overline{T_Z}}{\overline{T_M}} = \frac{20}{30} = \frac{2}{3}$. Then let us assume a variation in the outside temperature, that passes from 0°C to 10°C. This rise of T_{OA} will correspond to a decrease of the T_M – in particular to 25°C – since to maintain the same zone temperature $T_Z = 20^\circ\ C$ less effort is required. This would lead the identification procedure with $u = T_M$ and $y = T_Z$ to think that the gain of G(s) is equal to $\frac{\overline{T_Z}}{\overline{T_M}} = \frac{25}{30} = \frac{5}{6}$ instead of the correct value $\frac{2}{3}$. It is then necessary to account for the action of the outside temperature, now that its contribution is non-null. To do so, the method adopted in this procedure is to consider a virtual increase in the effort "u", i.e. $T_{M,rif,M(s)}$: this value represents the additional effort that T_M should have done to obtain the same effect that T_{OA} has on T_Z. In the steady state example of before, the effect of T_{OA} on T_Z is $T_{OA} * H_0 = 10 * \frac{1}{3} = \frac{10}{3}^\circ\ C$. To have the same effect from T_M on T_Z, T_M should be equal to $\frac{10}{3} * \frac{1}{G_0} = \frac{10}{3} * \frac{3}{2} = 5^\circ\ C$. This value is exactly the output $T_{M,rif,M(s)}$ of the compensator $M(s) = \frac{H(s)}{G(s)} \rightarrow T_{M,rif,M(s)} = \frac{H_0}{G_0} T_{OA} = \frac{\frac{1}{3}}{\frac{2}{3}} * 10 = 5^\circ\ C$. Note that, by considering $u = T_M + T_{M,rif,M(s)} = 25^\circ\ C + 5^\circ\ C = 30^\circ\ C$ the G(s) gain identified is correct.

Now that the control structure of the test is defined, an explanation on the identification procedure phases is due. The procedure starts by imposing a zone temperature set-point $T_{Z,rif}$ greater than the initial zone temperature $T_Z(0)$. This set-point causes a heating response from the PID regulator, that slowly brings the zone temperature to its set-point. During this heating phase, the data previously defined is collected. The identified model $\hat{G}(s)$ is then computed. The procedure is algorithmically presented as:

1. Impose a zone temperature set-point $T_{Z,rif}$
2. Collect the data T_Z and T_M for two days

3. Use the collected data to identify the $\hat{G}(s)$ transfer function

An example of the heating phase during which the data set is collected is represented in Fig 4.6.

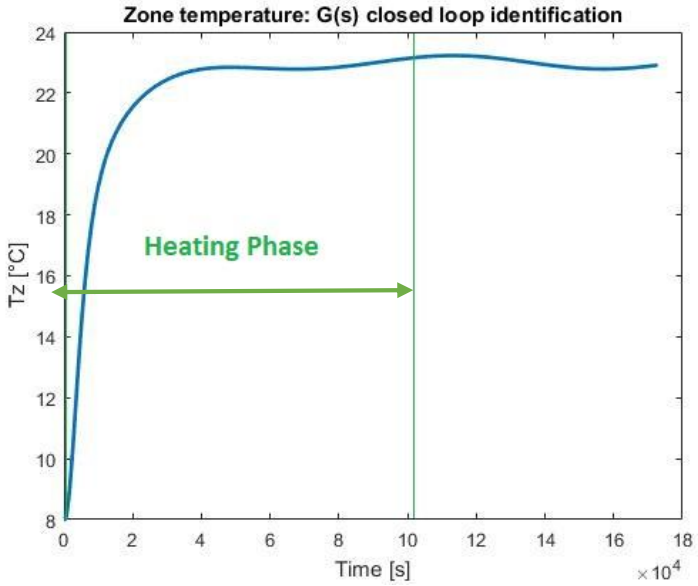

Fig 4.6: Closed loop G(s) estimation exemplificative zone temperature profile

The quality of the result of this identification procedure depends on three factors:

- The number of days during which the data set are collected.
- The outside temperature profile.
- The difference $T_{Z,rif} - T_Z(0)$

The effect of these three factors is analyzed in depth in the simulation chapter 8. In the end, this procedure is recommended when there is a big difference $T_{Z,rif} - T_Z(0)$ – for example when the heating system is started for the first time in a uninhabited house. For now, a representative result of this procedure is presented in Fig 4.7: the step response and the Bode diagrams of the real G(s) are compared with the ones of the identified $\hat{G}(s)$.

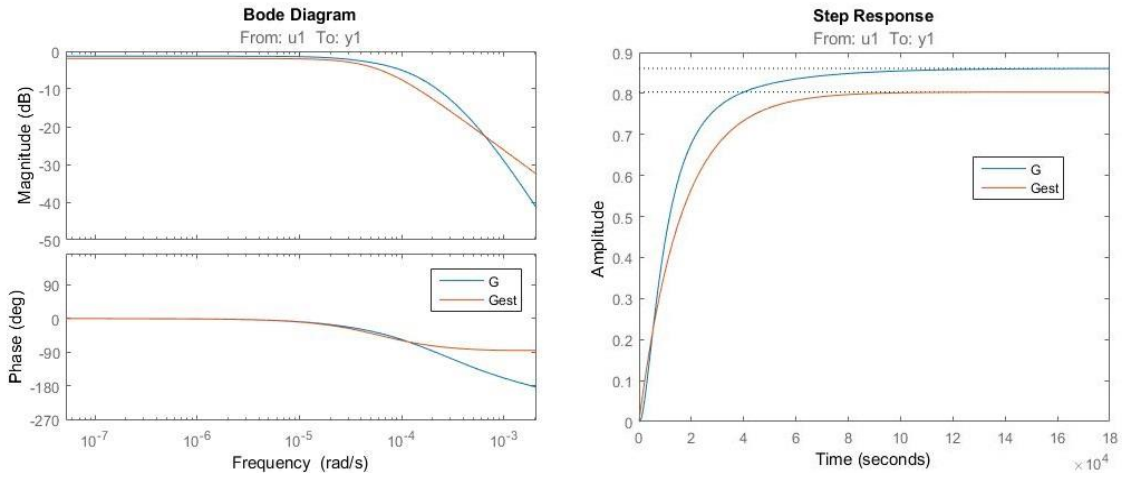

Fig 4.7: Bode diagrams comparison between G(s) and its identified 1-pole approximation

The choice of adopting an "average compensator" M(s) instead of no compensator at all was tested. The comparison between the "average compensator" and "no compensator" cases in terms of accuracy of the identified μ_G and τ_G are presented in Fig 4.8 and Fig 4.9. This figure presents 39 tests conducted on the 39 representative rooms and limit cases introduced in section 4.a.3.

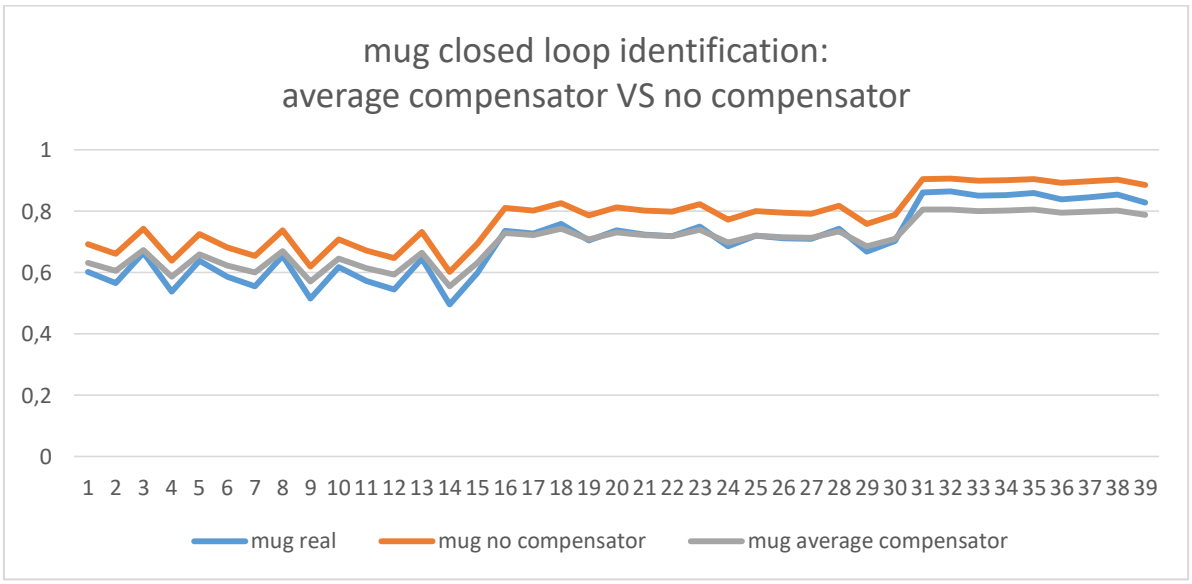

Fig 4.8: Quality of the identified G(s) gain with the closed loop identification procedure

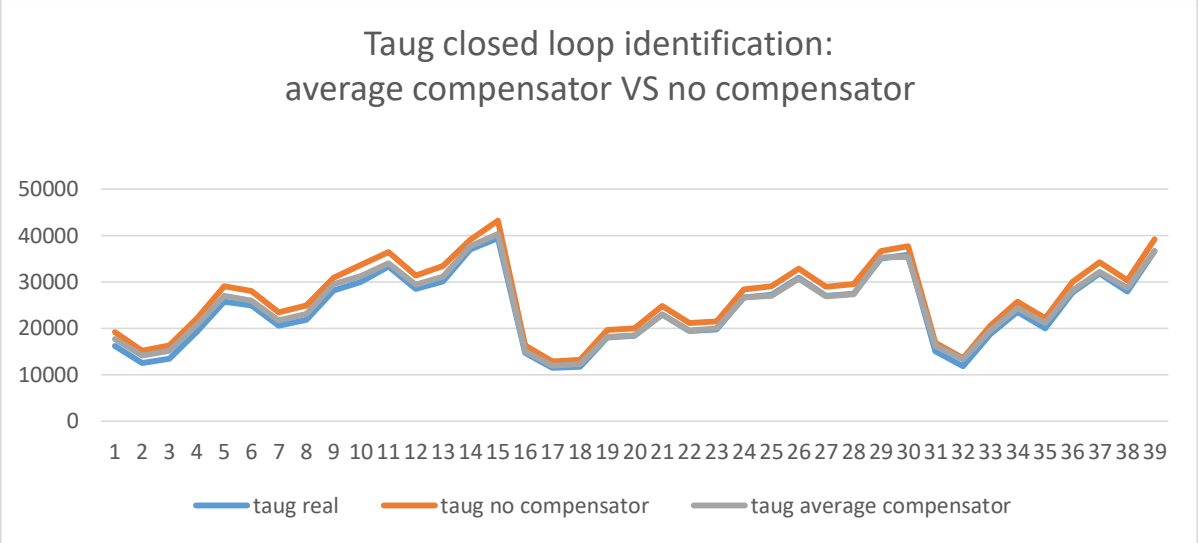

Fig 4.9: Quality of the identified G(s) time constant with the closed loop identification procedure

The μ_G is compared to the real gain of G(s), while τ_G is compared to $\tau_{G,real}$: this is the value of τ_G resulting from an identification with no disturbance T_{OA} acting on the system, i.e. a "perfect" identification of G(s). As it can be seen, the use of the average compensator is preferable, for both μ_G and τ_G.

4.c.2.2 G(s) Open loop

This procedure is adopted as alternative the previous closed loop procedure. The outer control loop is deactivated, so no tuning for the PID is needed. The compensator M(s) doesn't act on the system, but its output is computed and used only numerically in the identification procedure. The configuration adopted for the compensator M(s) is the "average compensator" configuration presented in the previous section, i.e.:

- $\mu_M = 0.4$
- $T_M = 9.67 * 10^3$
- $\tau_M = 2.36 * 10^4$

The identification procedure is now described.

Once the zone temperature set-point $T_{Z,rif}$ has been reached and a sufficient time has passed, the system can be considered in a "pseudo-equilibrium" status. This means that the zone temperature will oscillate around its set-point only because of the outside temperature disturbance. Starting from this pseudo-equilibrium state, the current inlet water temperature set-point $T_{M,rif}$ is memorized and called $T_{M,rif}(0)$. A more robust alternative would choose $T_{M,rif}(0)$ as the average value of T_M of the last 24 hours, in order to increase the chance of

$T_{M,rif}(0)$ to be the value associated to the desired zone temperature $T_{Z,rif}$. Then, an additional signal $T_{M,rif,OL}$ is added to this value:

$$T_{M,rif} = T_{M,rif}(0) + T_{M,rif,OL}$$

This additive signal $T_{M,rif,OL}$ is a composed signal designed empirically to obtain the best performances in this identification procedure. $T_{M,rif,OL}$ is the output of a VCO (Voltage Controlled Oscillator) tuned as follows:

- Output amplitude: 2V
- Quiescent frequency: $\frac{3}{2} * \frac{1}{86400}$
- Input sensitivity: $\frac{1}{86400}$
- Input signal: a triangle wave with amplitude ± 2 and frequency $\frac{3}{5} * \frac{1}{86400}$

The resulting $T_{M,rif,OL}$ signal is represented in Fig 4.10.

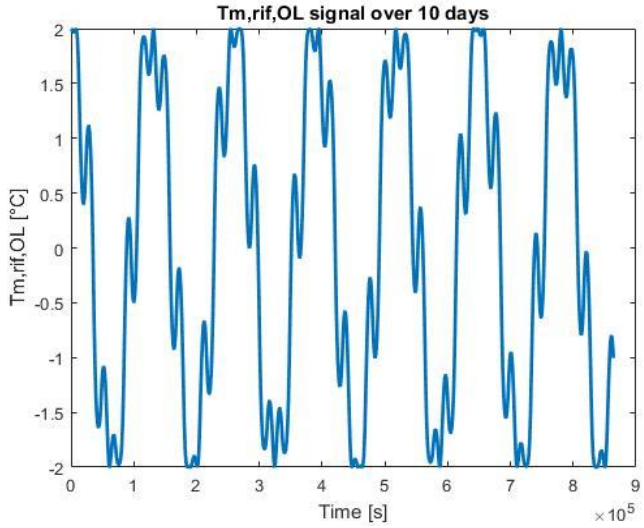

Fig 4.10: Profile used for the G(s) open loop identification procedure

The input data set "u" and the output data set "y" to feed to the "tfest" function are defined as in the G(s) closed loop identification procedure, i.e.:

- $u = T_M + T_{M,rif,M(s)}$
- $y = T_Z$

The reason why the term $T_{M,rif,M(s)}$ is added in the input data set "u" was explained in the previous section 4.c.2.1. An example of the T_Z profile resulting from this procedure is presented in Fig 4.11. As it can be seen, the effect of this test is contained in a $\pm 1.5°C$ interval around the zone temperature set-point, so the thermal discomfort is limited. Since

the effect of the test would violate the safety hysteresis introduced in section 3.d, it is recommendable to turn the safety hysteresis OFF during this identification procedure.

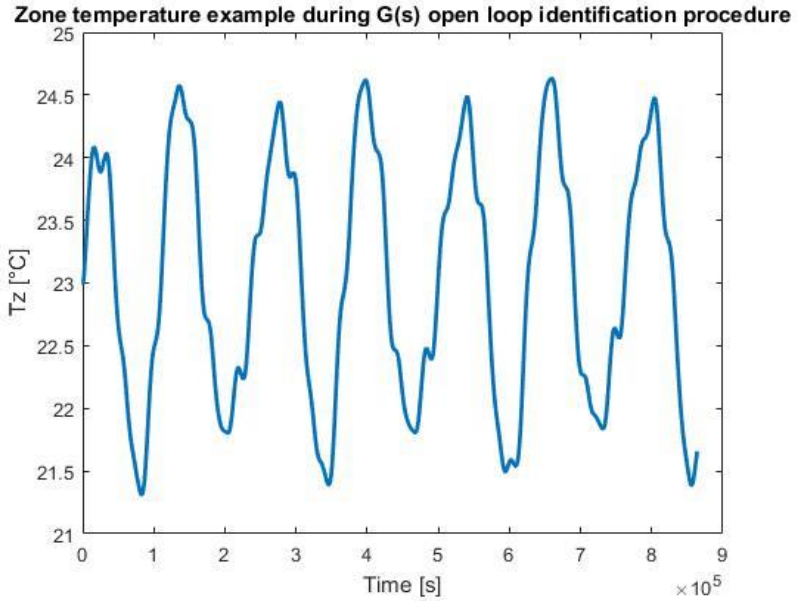

Fig 4.11: Zone temperature during the open loop identification procedure

The procedure is algorithmically presented as:

1. The value $T_{M,rif}(0)$ is set as current inlet water temperature set-point $T_{M,rif}$, or alternatively is computed as the average value of the T_M of the last 24 hours
2. For the days needed by the data collection phase (3 days) the inlet water temperature set-point $T_{M,rif}$ is imposed as $T_{M,rif} = T_{M,rif}(0) + T_{M,rif,OL}$. The data T_Z and T_M is collected
3. Use the collected data to identify the $\hat{G}(s)$ transfer function

The quality of the result of this identification procedure depends on two factors:

- The number of days during which the data set are collected.
- The outside temperature profile

The effect of these two factors is analyzed in depth in the simulation chapter 8. In the end, this procedure is recommended when it was not possible to apply the G(s) closed loop identification procedure – for example when the system first start wasn't suitable to perform the closed loop procedure, and now the pseudo-equilibrium state has been reached. The performance of this procedure is shown in Fig 4.12.

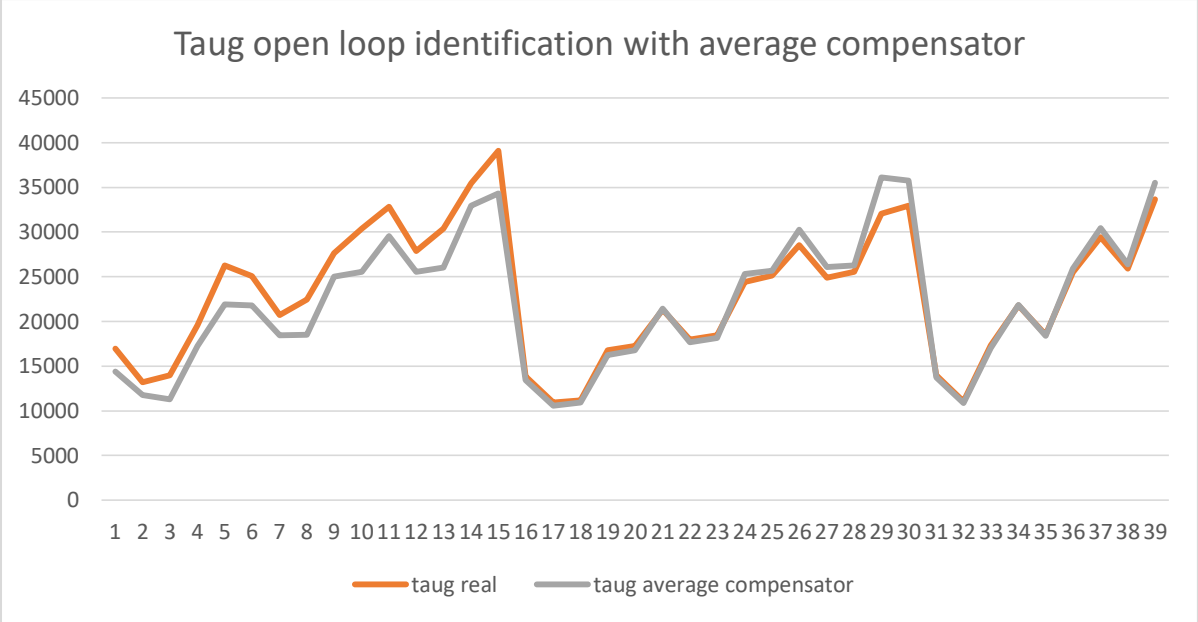

Fig 4.12: Quality of the identified G(s) time constant with the open loop identification procedure

4.c.2.3 G(s) estimation in open loop exploiting H(s) estimation

The same G(s) open loop identification procedure proposed in the previous section can be improved if the estimation of H(s) has already been performed. The estimation of H(s) is reported in the following section 4.c.4. In the input data set "u" of the G(s) open loop identification procedure the term $T_{M,rif,M(s)}$ was added to account for the effect of the outside temperature. However, by knowing an estimation of H(s) it is possible to account for the effect of T_{OA} in a more efficient way. The data sets "u" and "y" are chosen as follows:

- $u = T_M$
- $y = T_Z - \hat{H}(s) * T_{OA}$

In this way, the estimated effect of T_{OA} on T_Z is removed directly from the measured output T_Z. The improvement with respect to the simple G(s) open loop identification procedure – which used the average compensator to account for T_{OA} – can be seen in Fig 4.13. The τ_G identified in open loop with the average compensator is compared to the τ_G identified in open loop with the H(s) estimation in terms of accuracy with respect to the value $\tau_{G,real}$. This comparison is performed on the 39 representative rooms and limit cases 4.a.3.

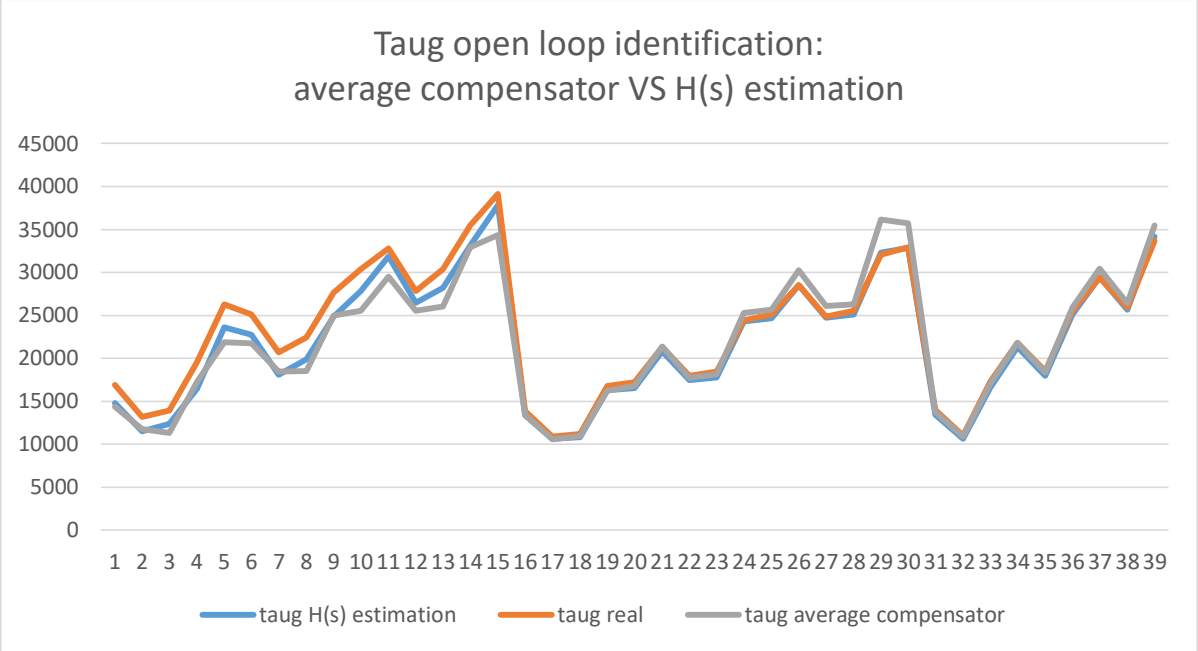

Fig 4.13: Quality of the identified G(s) time constant exploiting the H(s) estimation

The quality of the result of this identification procedure depends on three factors:

- The number of days during which the data set are collected.
- The outside temperature profile
- The quality of the exploited H(s) estimation

The effect of these two factors is analyzed in depth in the simulation chapter 8. Briefly, the use of a reasonably accurate H(s) results always in an estimation quality improvement. Moreover, the data collection phase can be reduced from 3 days to 2 days.

4.c.3 G(s) gain estimation refinement

All the G(s) identification procedures proposed does not provide a perfect estimation of the G(s) gain G_0 By exploiting the complementarity of G(s) and H(s) gains proved in section 4.b.1, it is possible to compute a refined estimation of G_0.

Considering a steady state case – which is physically impossible in practice due to the continuous action of the variable disturbance T_{OA} – the zone temperature equation results:

$$\overline{T_Z} = G_0\overline{T_M} + H_0\overline{T_{OA}}$$

Combining this equation with:

$$G_0 + H_0 = 1$$

The following formula is obtained:

$$G_0 = \frac{\overline{T_Z} - \overline{T_{OA}}}{\overline{T_M} - \overline{T_{OA}}}$$

Since our system never reaches a perfect steady state, the constant quantities $\overline{T_Z}$, $\overline{T_{OA}}$ and $\overline{T_M}$ can be generalized to their average over a long period of time, like two days. The formula is then simply corrected as:

$$G_0 = \frac{mean(T_Z) - mean(T_{OA})}{mean(T_M) - mean(T_{OA})}$$

This refined estimation of G_0 will be exploited especially in the H(s) estimation procedure presented in the next section.

In our simulation campaign, the efficiency of this formula is extremely high – the estimation accuracy is always around the 99.9% – so that a representative figure of the results would not be significant. However, this efficiency is due to the lack of other modeled disturbances. As it will be pointed out in the conclusion chapter, a sensibility study with respect to other typical disturbances should be carried out to assess its robustness. A discussion on the theoretical effect of the solar radiation on this procedure is carried out in chapter 6.

4.c.4 H(s) estimation

As previously said, the effect on T_Z of H(s) is realistically smaller than the effect of G(s). This means that, if the loop correlated to G(s) – i.e. the outer loop on T_Z – is left active, the effect of H(s) will be too small to allow a good identification of this transfer function. However, since the G(s) input (T_M) is controllable, it is possible to isolate the effect of H(s) from the effect of G(s) – as it will be explained soon – and use the function "tfest" to compute the estimation of H(s):

$$\widehat{H}(s) = \widehat{\mu_H} \frac{1}{1 + s\tau_H}$$

As for the G(s) open loop identification procedure, the pseudo-equilibrium state is reached after that the zone temperature set-point $T_{Z,rif}$ had been reached for a sufficiently long time. After reaching this pseudo-equilibrium state, the current inlet water temperature set-point $T_{M,rif}$ is memorized and fixed – alternately, the last 24 hours average of T_M as proposed in the G(s) open loop identification procedure 4.c.2.2. In this way, the effect of the daily thermal excursion of T_{OA} is unvaried by an eventual damping action of the PID, and so the

following equation can be written:

$$T_Z = G_0 T_M + H(s) T_{OA}$$

The effect of T_M is computed only on the gain of G(s), because its value has been fixed during this procedure. It is then easier to remove the T_M effect from the measured T_Z. In fact, by adopting the following data sets:

- $u = T_{OA}$
- $y = T_Z - \widehat{G_0} * T_M$

the effect of T_M is completely removed in case of perfect estimation of G_0. However, even a small error on $\widehat{G_0}$ can lead to very bad results in this H(s) estimation procedures. In Fig 4.14 it is possible to see the result of this H(s) identification starting from an excessively wrong estimation of G_0. The identified H(s) is very different from the real one, and such estimation results are not acceptable for the tuning algorithms that will be presented in chapter 5. It is then necessary to perform this identification with a good $\widehat{G_0}$. The G(s) gain estimation refinement proposed in the previous section 4.c.2 can solve this problem. By adopting this refined $\widehat{G_0}$ for the H(s) estimation, a very good result is obtained as shown in the same figure Fig 4.14.

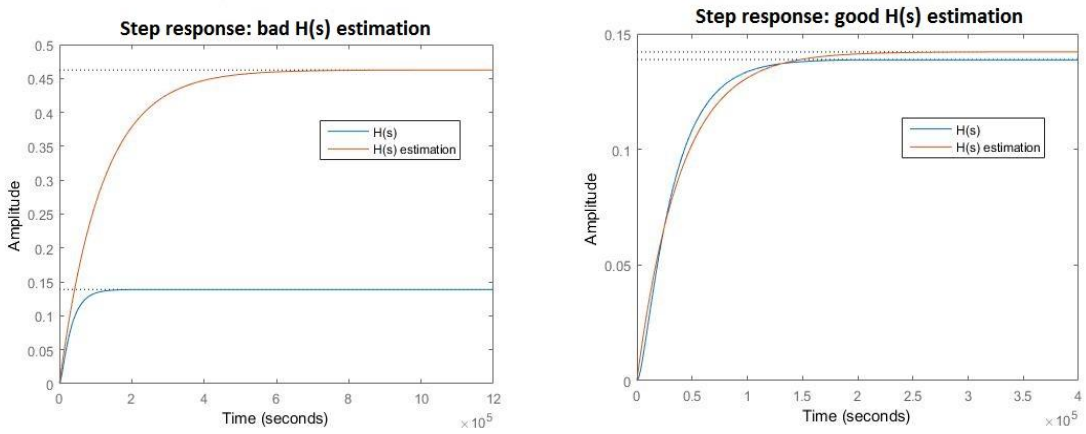

Fig 4.14: Bad H(s) estimation caused by an excessively wrong G(s) estimated gain (left) and good H(s) estimation (right)

4.d Estimated G(s) and H(s) analysis

Now that different methods for the estimation of G(s) and H(s) have been laid out, it is time to analyze their sensitivity with respect to the four main thermo-physical parameters, like it has been done for the compensator M(s) in section 4.b.2. In particular, the sensitivity of the identified time constants τ_G and τ_H is analyzed.

The sensitivity of M(s) turned out to be completely biased: the pole is influenced only by $c_{p,Wall}$ and u_{Wall} while the zero is influenced only by $c_{p,Pav}$ and u_{Pav}. However, this is not the case for τ_G and τ_H: both of these quantities are influenced by all the four main thermo-physical parameters. A test was designed to find out by which parameter τ_G and τ_H are mostly influenced.

This test exploited the 39 representative rooms and limit cases of section 4.a.3. For both τ_G and τ_H and along the 39 cases, two scatterplots were represented with the quantities:

- τ_G (or τ_H) and $\frac{c_{p,Wall}}{u_{Wall}} = "Wall"$, representing the influence of the wall parameters on τ_G (or τ_H).
- τ_G (or τ_H) and $\frac{c_{p,Pav}}{u_{Pav}} = "Pav"$, representing the influence of the pavement parameters on τ_G (or τ_H).

These scatterplots were then supported by a plot of τ_G (or τ_H), $\frac{c_{p,Wall}}{u_{Wall}}$, and $\frac{c_{p,Pav}}{u_{Pav}}$, along the 39 test in order to visually verify eventual correlations.

The results of this analysis are proposed below:

- τ_G sensitivity:

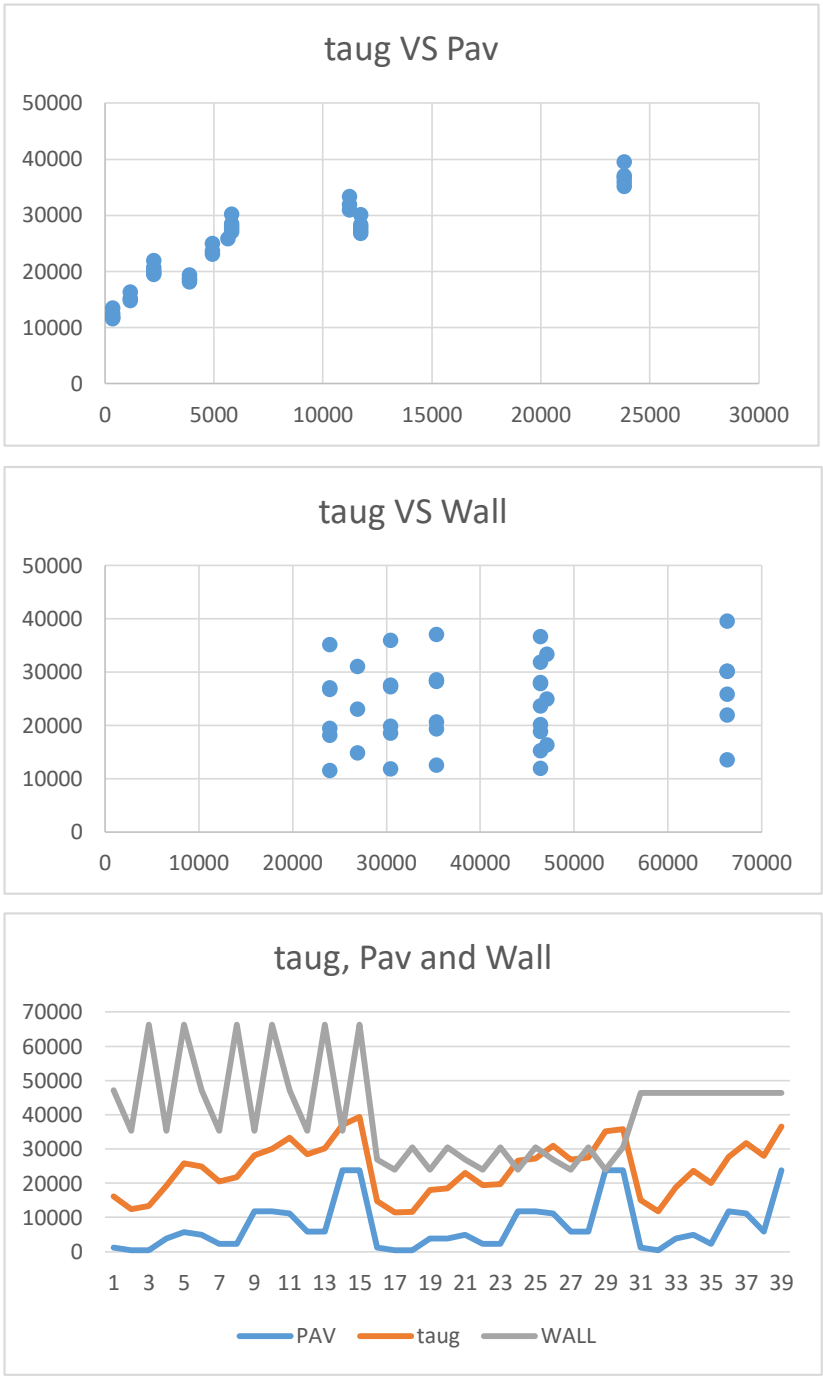

Fig 4.15: scatterplot of G(s) time constant VS Pavement ratio (upper)
scatterplot of G(s) time constant VS Wall ratio (central)
G(s) time constant, Pavement ratio and Wall ratio (lower)

The figures show a marked dependency of τ_G on the pavement quantities. This behavior reflects our intuition, since it is reasonable to assume that the time constant associated to the heating transfer function G(s) (i.e. τ_G) is mainly influenced by the characteristics of the pavement.

- τ_H sensitivity:

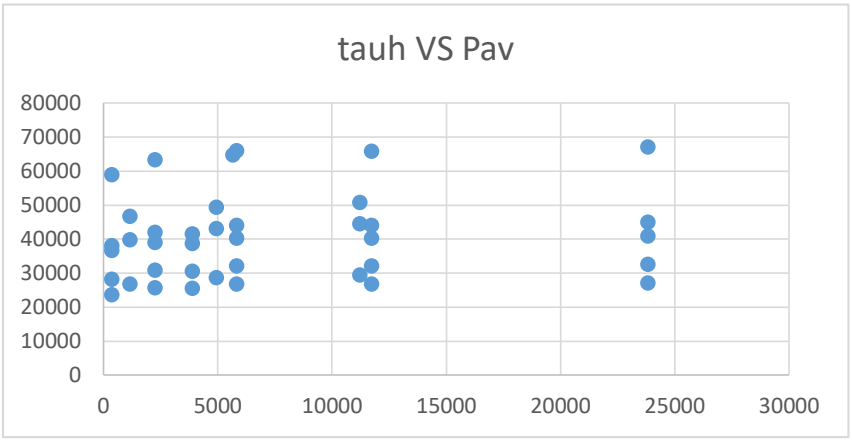

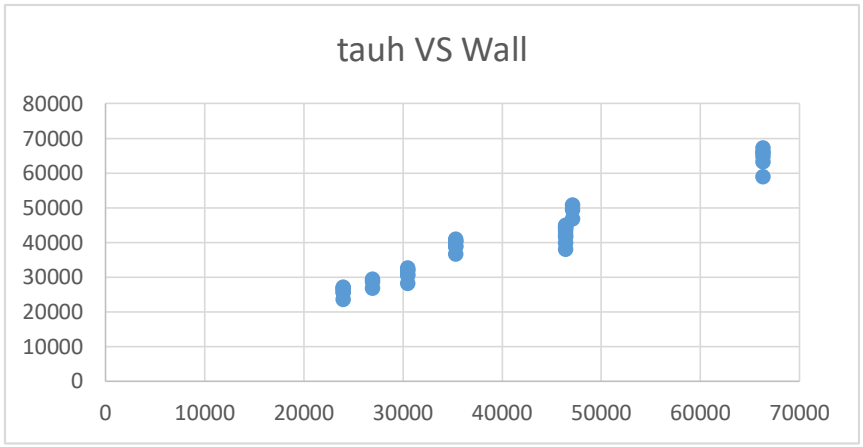

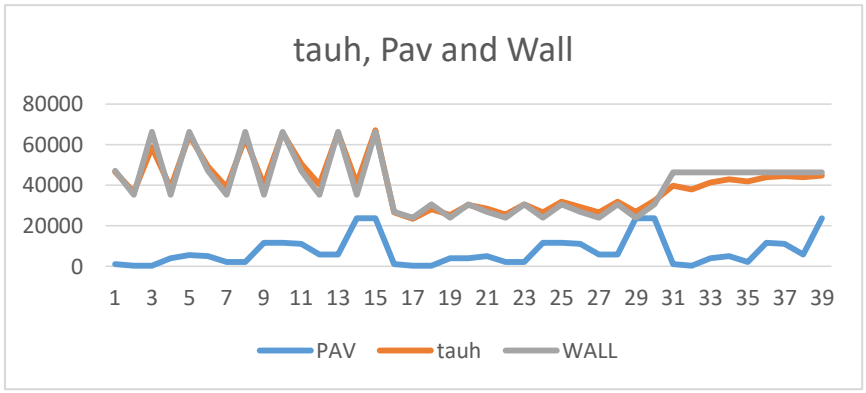

Fig 4.16: scatterplot of H(s) time constant VS Pavement ratio (upper)
scatterplot of H(s) time constant VS Wall ratio (central)
H(s) time constant, Pavement ratio and Wall ratio (lower)

On the contrary, here the figures show a marked dependency of τ_H on the wall quantities. Even this behavior reflects our intuition, since it is reasonable to assume that the time constant associated to the transfer function describing the effect of the outside temperature H(s) (i.e. τ_H) is mainly influenced by the characteristics of the wall.

4.e Chapter 4 conclusions

In this chapter, the variability of four model parameters – called main thermo-physical parameters – was introduced. The control tuning needs an adaptation strategy to face these parameters changes. This adaptation strategy is presented in the next chapter, while this chapter is meant to lay the basis for the next one. In particular, the transfer functions G(s) and H(s) were analyzed, together with the outside air compensator M(s). The identification procedures for the plant transfer functions G(s) and H(s) were then proposed. Finally, a sensitivity analysis of all the transfer functions involved – G(s), H(s), M(s), $\hat{G}(s)$ and $\hat{H}(s)$ – with respect to the four main thermo-physical parameters was carried out.

All these analyses and identification are not finalized to anything yet. However all these information will be combined together in the next chapter to define a variety of adaptive tuning strategies for the PID and the compensator M(s). The key concepts to keep in mind for the next chapter, beside the different methods to identify G(s) and H(s), are the conclusions of the sensitivity analysis:

- The compensator pole τ_M is influenced only by $C_{p,Wall}$ and u_{Wall}
- The compensator zero T_M is influences only by $C_{p,Pav}$ and u_{Pav}
- The identified τ_G is influenced mainly by $C_{p,Pav}$ and u_{Pav}
- The identified τ_G is influenced mainly by $C_{p,Wall}$ and u_{Wall}

PAGE INTENTIONALLY LEFT BLANK

5. ADAPTIVE TUNING

All the pieces of conclusions from the previous chapters are put together in this chapter in order to define a series of adaptive tuning algorithms for both the outer loop PID regulator and the outside air temperature compensator M(s).

First, a section of the chapter is dedicated to the PID adaptive tuning 5.a. This section is relatively small since the PID re-tuning is quite straightforward thanks to the tuning strategy proposed in section 3.a. The following section 5.b is then dedicated to the adaptive tuning of the compensator M(s) and is divided into three sub-sections, presenting a tuning strategy for each parameter of M(s). Moreover, two additional methods are proposed for the tuning of the compensator pole. All this tuning methods are based on the correlation between some identifiable plant quantities – like τ_G and τ_H – and the variation of some not easily identifiable room parameters – i.e. the main thermo-physical parameters.

After the definition of these individual adaptive tuning methods, seven different sequences of these methods – called tuning algorithms – are presented in section 5.c. A final section 5.d is then dedicated to the applicability limits of these methods.

5.a PID adaptive tuning

The initial configuration of the PID regulator is the one associated to the average room, which was first presented in section 4.c.2.1. The average room has parameters:

- $c_{p,Wall} \in [13; 65]$ has average 39 $\left[\frac{kJ}{m^2K}\right]$
- $u_{Wall} \in [0.28; 1.61]$ has average 0.945$\left[\frac{W}{m^2K}\right]$
- $c_{p,Pav} \in [34; 175]$ has average 104.5$\left[\frac{kJ}{m^2K}\right]$
- $u_{Pav} \in [12; 63]$ has average 37.5$\left[\frac{W}{m^2K}\right]$

and the resulting PID tuning reads:

- $P = 3.25$
- $I = 1.3 * 10^{-4}$
- $D = 8.96 * 10^{3}$
- $N = 1000$

This configuration, although robust for most of the room possible configuration, can present some performance issues. In Fig 5.1, the performance of the initial average PID configuration is evaluated on the “New walls” & ” Big screed” representative room. That performance is compared with the one resulting from a correct PID tuning. Recalling that the average PID configuration is tuned on an average room – regarding both the walls and the pavement – the small overshoot phenomenon is explained.

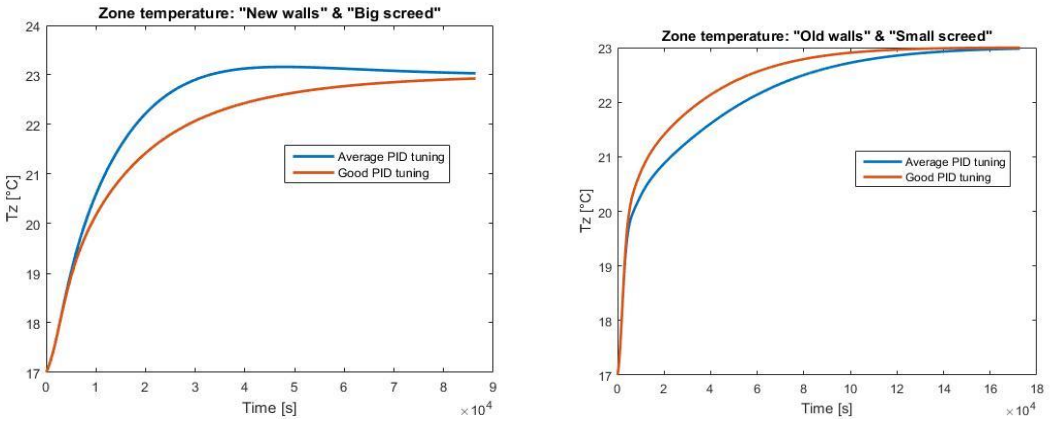

Fig 5.1: Performance of the average PID tuning on the "New walls" & "Big screed" representative room (left) and performance of the average PID tuning on the "Old walls" & "Small screed" representative room (right)

In the same figure Fig 5.1, the performance of the initial average PID configuration is evaluated on the “Old walls” & ”Small screed” representative room instead. In this case, the performance drop is on settling time, which is bigger than the one obtained with a suitable PID tuning.

It is then advisable to correct the PID tuning based on the estimation of the working plant. Recalling the PID tuning exposed in section 3.a, the four parameters are tuned as follows:

- $I = k$
- $N = \frac{1}{\tau_3}$
- $P = \frac{(\tau_1+\tau_2)*N*I-I}{N}$
- $D = \frac{(\tau_1*\tau_2)*N*I-P}{N}$

With:

- $\tau_1 = \tau_G$
- $\tau_2 = \frac{\tau_G}{5}$
- $\tau_3 = \frac{1}{1000}$

- $k = \frac{2}{\mu_G}$

Once the G(s) identification has been performed, the PID tuning is immediate: just by substituting the identified μ_G and τ_G, an adapted PID configuration will result. The positive effects of this adapted configuration are visible in Fig 5.2, where the performances of the average initial PID configuration are compared with the performance of the adapted PID configuration fed with μ_G and τ_G with an estimation error of 10%. The room under example is the "Old walls" & "Small screed" representative room.

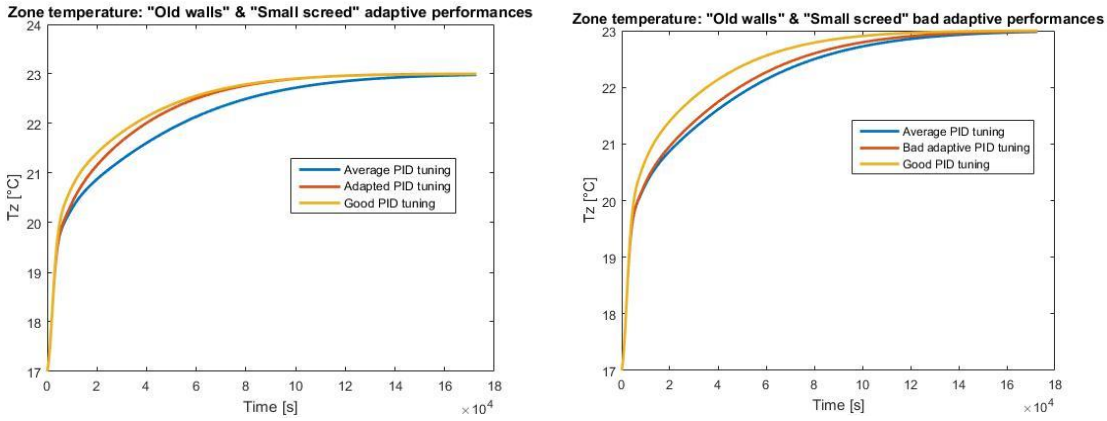

Fig 5.2: Effect of the adaptive PID tuning in case of good G(s) identification (left) and bad G(s) identification (right)

Of course, the performance of the adapted PID configuration is related to the quality of the G(s) estimation. In the same figure it is possible to see the performance resulting from a PID tuned on an excessively wrong estimation of G(s) – in this case, an error of 40% on μ_G and 70% on τ_G. In this case, the improvement with respect to the average PID configuration is marginal.

5.b M(s) adaptive tuning

Even the outside air temperature compensator M(s) has its initial configuration tuned on the average room. However, the efficiency of this average compensator can turn out to be very poor. Considering for example Fig 5.3, the performance of the average compensator is compared to the performance of the system without any compensator. In this case, the compensator action is just slightly better than the "no compensator" case. As for the PID, even the compensator M(s) would benefit from an adaptive tuning.

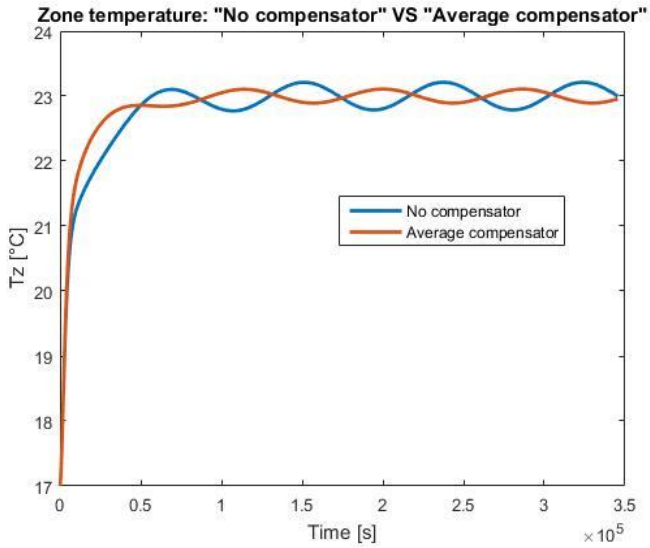

Fig 5.3: Effect of the average compensator on the outside air temperature disturbance rejection

The tuning of the three parameters of M(s) are presented separately in the next three sub-sections. For each of these parameters, the tuning strategy will aim at selecting a value that is the closest possible to the one of the corresponding ideal compensator, i.e.:

$$M(s) = \frac{H(s)}{G(s)} = \mu_{M,ideal} \frac{1 + sT_{M,ideal}}{1 + s\tau_{M,ideal}}$$

5.b.1 M(s) gain

This parameter is the easiest to tune, since $\mu_{M,ideal} = \frac{\mu_H}{\mu_G}$, with μ_G and μ_H the real gains of G(s) and H(s) respectively. The gain of M(s) will just be set:

$$\mu_M = \frac{\widehat{\mu_H}}{\widehat{\mu_G}}$$

with $\widehat{\mu_G}$ and $\widehat{\mu_H}$ the gains of the estimated $\hat{G}(s)$ and $\hat{H}(s)$ respectively. As it will be explained later, there are alternative adaptive tuning strategies that don't need the estimation of H(s): the quantity $\widehat{\mu_H}$ would not be available. In that case, by exploiting the complementarity of the gains proved in section 4.b.1 it is possible to set:

$$\mu_M = \frac{1 - \widehat{\mu_G}}{\widehat{\mu_G}}$$

The accuracy of this μ_M tuning depends only on the identified gains $\widehat{\mu_G}$ and $\widehat{\mu_H}$. By exploiting the G(s) gain estimation refinement, both $\widehat{\mu_G}$ and $\widehat{\mu_H}$ (or $1 - \widehat{\mu_G}$ if H(s) identification had not been performed) present an incredible level of accuracy, resulting in an almost perfect tuning of μ_M. This performance is due to the lack of other modeled

disturbances, as it was said in section 4.c.3. To have an idea of the accuracy level obtained, in Fig 5.4 it is possible to see an example the result of the adaptive tuning of μ_M on the 39 representative rooms and limit cases.

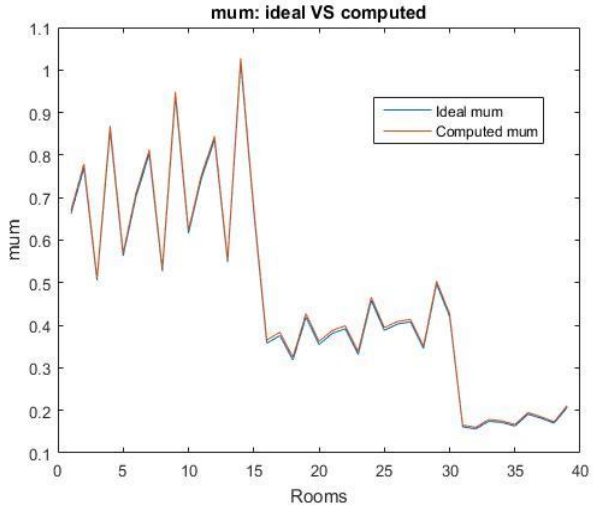

Fig 5.4: Compensator gain estimated with the complementary gain formula

5.b.2 M(s) zero

The tuning strategy for this parameter is not as straightforward as for the M(s) gain. This is because the H(s) identification procedure returns a transfer function:

$$\widehat{H}(s) = \widehat{\mu_H}\frac{1}{1+s\tau_H}$$

with only one pole, while the zero of the compensator M(s) has been proven to be the dominant zero of H(s) (see section 4.b.2). A simple solution might seem to extend the order of H(s) identification – for example with two poles and one zero – reading something like:

$$\widehat{H}(s) = \widehat{\mu_H}\frac{1+sT_H}{(1+s\tau_{H1})(1+s\tau_{H2})}$$

The problem however is that the identified zero is set almost casually by the identification procedure. This is a known problem in the identification literature and can hardly be solved.

At this point, it is clear that a direct tuning of M(s) zero T_M is not possible. A solution was found by exploiting the results of the sensitivity functions carried out in the previous chapter. In particular, the M(s) zero T_M was found out to be influenced only by two main thermo-physical parameters: $C_{p,Pav}$ and u_{Pav}. Moreover, the quantity τ_G – i.e. the time constant of the identified G(s) – was found out to be influenced mainly by the same two parameters

$C_{p,Pav}$ and u_{Pav}. Since both of these quantities are bounded to $C_{p,Pav}$ and u_{Pav}, it is possible that a correlation exists between them. By plotting a scatterplot (Fig 5.5) of the quantities T_M and τ_G (τ_G on the x-axis, T_M on the y-axis) this correlation is verified.

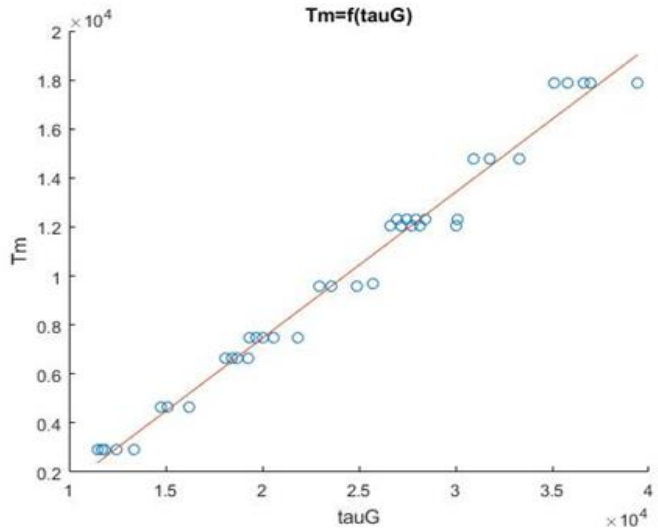

Fig 5.5: Correlation function between the compensator zero and the G(s) time constant

To exploit this correlation, a linear regression was performed on this scatterplot. The graphical result is presented in the same figure Fig 5.5, while the analytical form of this regression reads:

$$T_M = f(\tau_G) = 0.599\tau_G - 3862$$

The goodness of fit of this regression is evaluated through the Root Mean Square Error (RMSE) [26]. This value will be computed for all the following regressions as well.

$$RMSE = 649.8$$

With this formula, the identified time constant τ_G can be used to tune the zero of M(s). In Fig 5.6 the accuracy of this tuning is presented over the usual 39 representative rooms and limit cases, assuming that τ_G was estimated in the best conditions (i.e. no outside air temperature disturbance acting on the system).

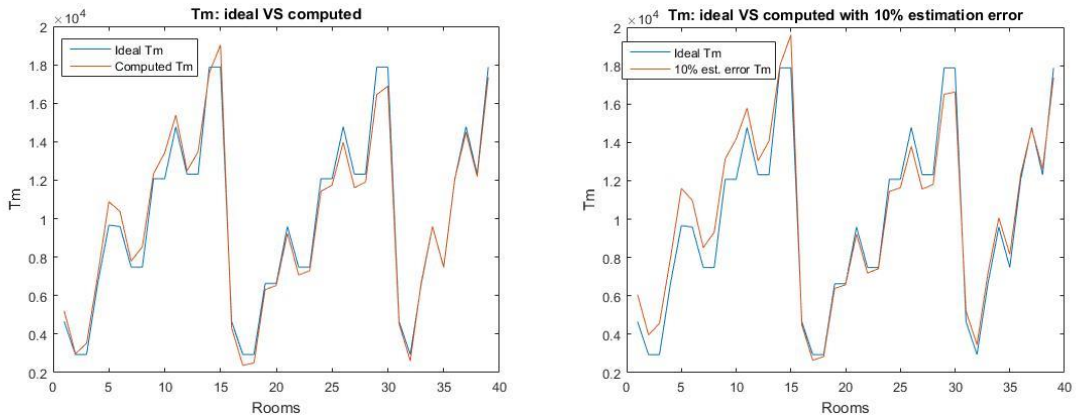

Fig 5.6: Accuracy of the compensator zero tuned with the proposed correlation function (left) and accuracy of the compensator zero using a G(s) time constant with 10% error (right)

The accuracy of the tuned T_M would of course drop in correspondence of an estimation error on τ_G. In the same figure Fig 5.6 the same formula was used to tune T_M but using a τ_G characterized by a random $\pm 10\%$ error, still resulting in a good tuning.

5.b.3 M(s) pole

For this parameter, three different tuning methods are proposed. The first is similar to the zero tuning of the previous section, while the other two are related to the well-known concept of thermal lag [27].

5.b.3.1 Using H(s) identified time constant

This method is the analogous of the zero tuning method of section 5.b.2. Since there is no reliable way to estimate the dominant zero of G(s) – i.e. the pole of M(s) – it is necessary to tune this parameter by exploiting other identifiable quantities.

In particular, the M(s) pole τ_M was found out to be influenced only by two main thermo-physical parameters: $C_{p,Wall}$ and u_{Wall}. Moreover, the quantity τ_H – i.e. the time constant of the identified H(s) – was found out to be influenced mainly by the same two parameters $C_{p,Wall}$ and u_{Wall}. Since both of these quantities are bounded to $C_{p,Wall}$ and u_{Wall}, it is possible that a correlation exists between them. By plotting a scatterplot (Fig 5.7) of the quantities τ_M and τ_H (τ_G on the x-axis, τ_M on the y-axis) this correlation is verified.

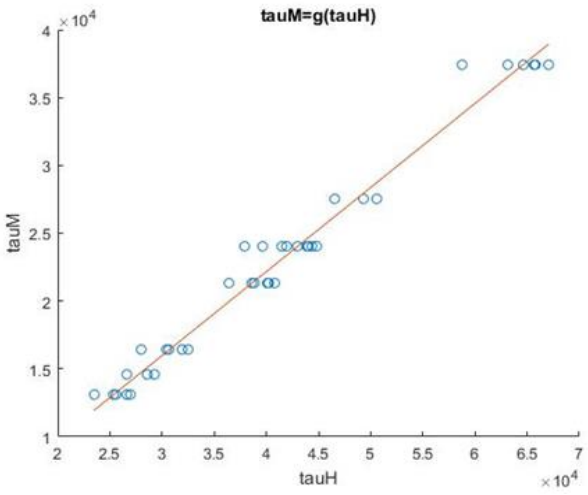

Fig 5.7: Correlation function between the compensator pole and the H(s) time constant

To exploit this correlation, a linear regression was performed on this scatterplot. The graphical result is presented in the same figure Fig 5.7, while the analytical form of this regression reads:

$$\tau_M = g(\tau_H) = 0.6592\tau_H - 3147$$

$$RMSE = 1213$$

With this formula, the identified time constant τ_H can be used to tune the pole of M(s), just like the identified time constant τ_G was used to tune its zero. In Fig 5.8 the accuracy of this tuning is presented over the usual 39 representative rooms and limit cases, assuming that τ_H was estimated in the best conditions.

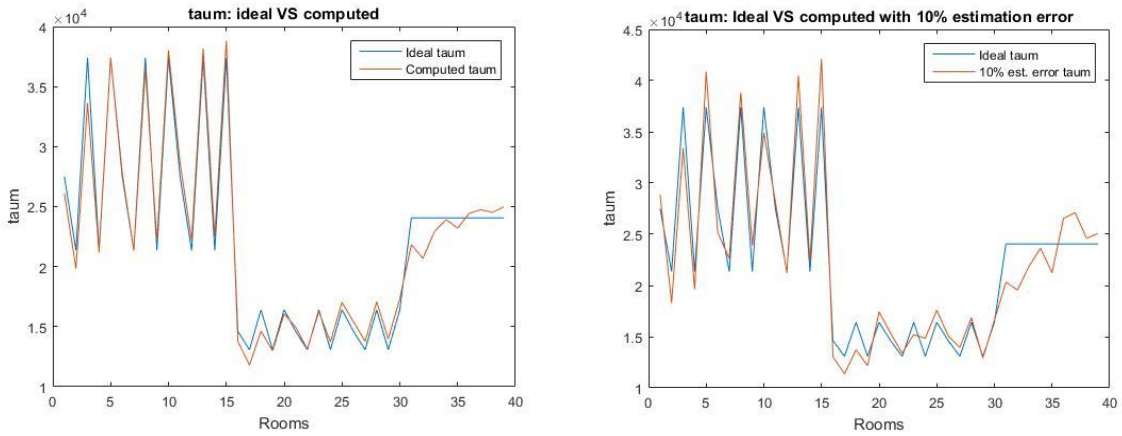

Fig 5.8: Accuracy of the compensator pole tuned with the proposed correlation function (left) and accuracy of the compensator pole using a H(s) time constant with 10% error (right)

The accuracy of the tuned τ_M would of course drop in correspondence of an estimation error on τ_H. In the same figure Fig 5.8 the same formula was used to tune τ_M but using a τ_H characterized by a random $\pm 10\%$ error, still resulting in a good tuning.

5.b.3.2 Using open loop thermal lag

This method is the first of the two methods which exploit the thermal lag. Before introducing the tuning method itself, let's give a brief description of the thermal lag phenomenon.

First, it is assumed for simplicity that the outside air temperature profile is a sinusoid of period 24 hours:

$$T_{OA} = A * \sin(\frac{2\pi}{86400} t)$$

and the system is in open loop with a constant inlet water temperature T_M. His configuration is analogous to the one used in section 4.c.4 to perform the open loop H(s) identification. Under this configuration, the effect of the daily thermal excursion of T_{OA} on T_Z is visible in Fig 5.9.

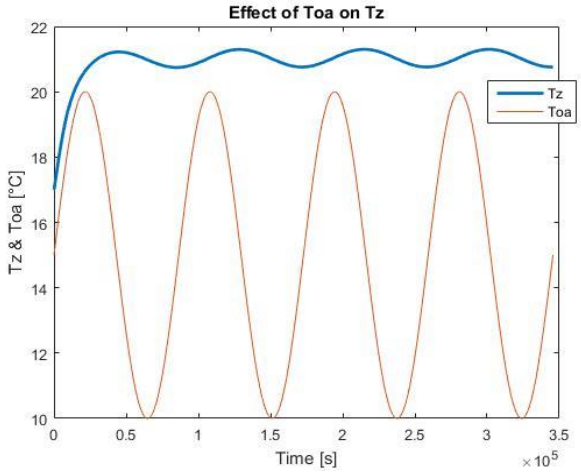

Fig 5.9: Sinusoidal outside air temperature profile effect on zone temperature

As it can be seen, this effect is a sinusoid itself that has been shrunk and delayed in time. This is the result of the filtering action of H(s). The effect on T_Z reads in fact:

$$T_Z = A * \left\| H\left(j\frac{2\pi}{86400}\right) \right\| \sin\left(\frac{2\pi}{86400} t + phase\left(H\left(j\frac{2\pi}{86400}\right)\right)\right)$$

and since the typical Bode diagram of H(s) is represented in Fig 5.10, the filtering action is explained.

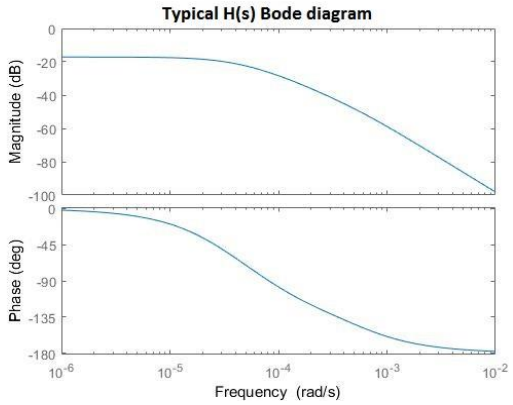

Fig 5.10: Typical H(s) Bode diagrams

This phenomenon takes the name of "thermal lag" in building lexicon. In this explanation, the outside air temperature profile is simply a sinusoidal wave, but the thermal lag concept is usually generalized to any shape of the T_{OA} profile. However, the effect of this thermal lag is not straightforward for some outside air temperature profiles. For example, by choosing the T_{OA} profile derived in section 3.e.2, the resulting T_Z profile shape turns out slightly modified (Fig 5.11). This is because each frequency contribution of the whole T_{OA} signal is filtered according to different values of magnitude and phase of H(s), so the final shape can potentially lose completely the similarity with the input one.

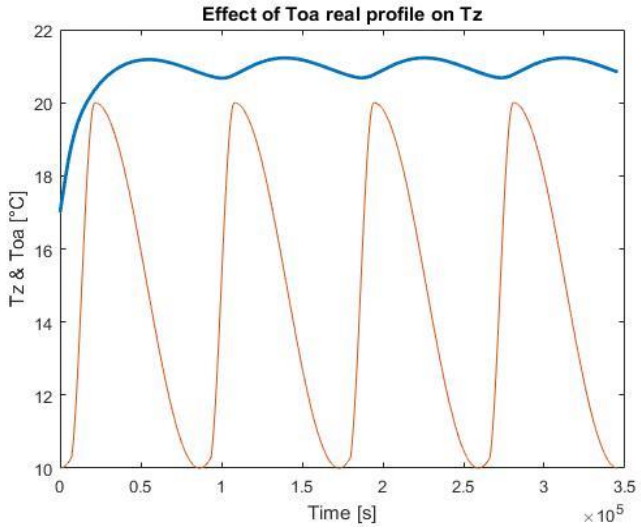

Fig 5.11: Realistic outside air temperature profile effect on zone temperature

In this thesis, the outside air temperature profile is assumed sinusoidal when applying this tuning method. This simplification is done in order to define a clear and easy quantity for the thermal lag, i.e. the time registered between the temperature peak of T_{OA} and the correspondent temperature peak on T_Z. This time delay will be called Δ_{OA} from now on. In

case of a real shape of the T_{OA} profile, it could be necessary to define another numerical quantity to associate to Δ_{OA}. This is because a peak on a real T_{OA} profile – that could even not exist – is not granted to correspond to a peak on the resulting T_Z profile because of the different filtering action applied to each frequency of the T_{OA} signal. It should then be necessary to define a signal processing procedure to recognize some specific more robust quantities. For example, these quantities could be the phase delay imposed by H(s) on the T_{OA} 24 hours frequency or an average delay of the whole T_{OA} shape and so on. However such digression is far from the purpose of the thesis, that is to define the correlation between some measurable quantities and some unmeasurable ones and test them in an adaptive tuning scenario.

The focus will now be moved to the definition of the tuning procedure. Similarly to what was done for the open loop H(s) identification, this procedure starts when the system has reached the pseudo-equilibrium point. The last inlet water temperature set-point – or alternatively the last 24 hours average of T_M – is memorized and fixed. Then the time between the temperature peak of T_{OA} and the correspondent temperature peak on T_Z is registered and called $\Delta_{OA,OL}$ (where "OL" stands for Open Loop).

Now, under the sinusoidal T_{OA} profile hypothesis, it is possible to interpret the measured $\Delta_{OA,OL}$ as:

$$\Delta_{OA,OL} = \frac{86400}{360} * \left| phase\left(H\left(j\frac{2\pi}{86400}\right)\right)\right|$$

where the term $\frac{86400}{360}$ is used to convert the value of $phase\left(H\left(j\frac{2\pi}{86400}\right)\right)$ from degrees to seconds. Therefore, since this registered thermal lag is caused by the action of H(s), it is reasonable to assume that its value $\Delta_{OA,OL}$ is sensible to the same main thermo-physical parameters $C_{p,Wall}$ and u_{Wall} that affect τ_H – i.e. the identified time constant of H(s). If this is the case, then there could be a correlation between $\Delta_{OA,OL}$ and τ_M, since the first is affected mainly by $C_{p,Wall}$ and u_{Wall} and the second is affected only by the same two parameters. Such correlation is verified Fig 5.12, where a scatterplot of the quantities τ_M and $\Delta_{OA,OL}$ ($\Delta_{OA,OL}$ on the x-axis, τ_M on the y-axis) has been plotted.

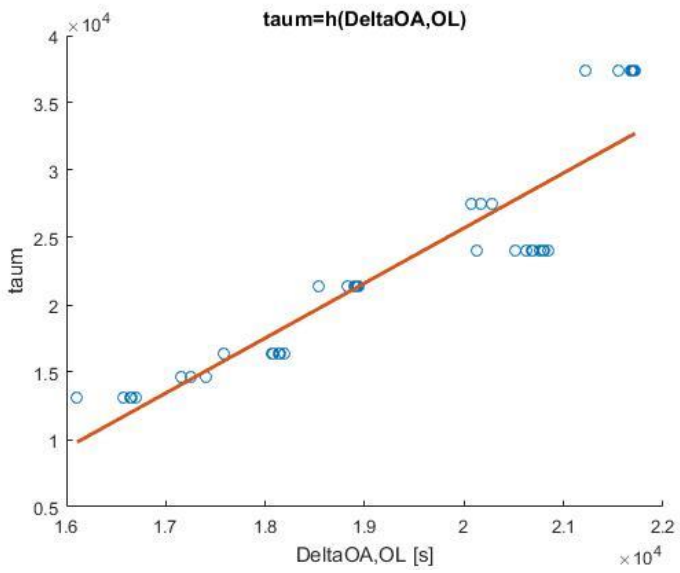

Fig 5.12: Correlation function between the compensator pole and the open loop thermal lag

To exploit this correlation, a linear regression was performed on this scatterplot. The graphical result is presented in the same figure Fig 5.12, while the analytical form of this regression reads:

$$\tau_M = h(\Delta_{OA,OL}) = 4.088\Delta_{OA,OL} - 56050$$

$$RMSE = 3190$$

With this formula, the measured thermal lag $\Delta_{OA,OL}$ can be used to tune the pole of M(s), just like the identified time constant τ_H was used to tune the same parameter. In Fig 5.13 the accuracy of this tuning is presented over the usual 39 representative rooms and limit cases, assuming that $\Delta_{OA,OL}$ was measured perfectly. The accuracy of the tuned τ_M would of course drop in correspondence of a measurement error on $\Delta_{OA,OL}$. In the same figure Fig 5.13 the same formula was used to tune τ_M but using a $\Delta_{OA,OL}$ characterized by a random $\pm 10\%$ error, still resulting in a good tuning.

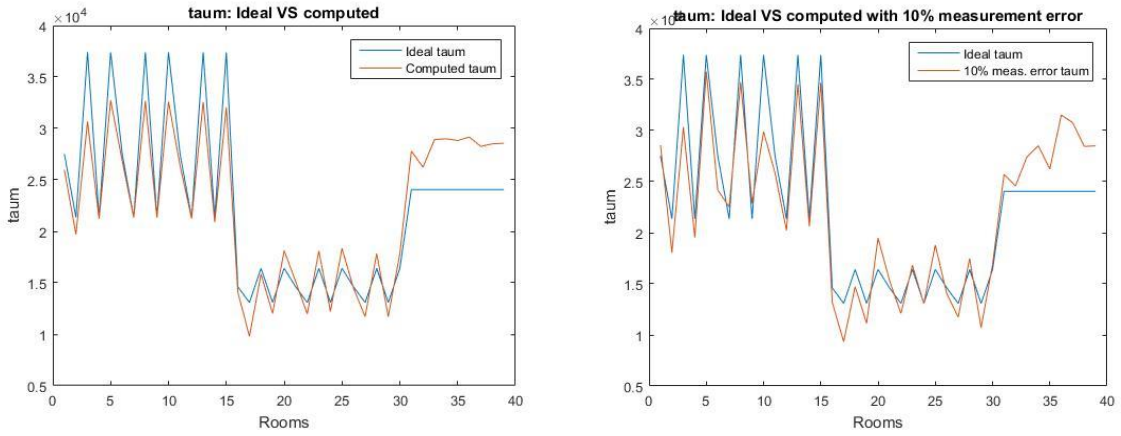

Fig 5.13: Accuracy of the compensator pole tuned with the proposed correlation function (left) and accuracy of the compensator pole using a open loop thermal lag with 10% error (right)

Since this tuning strategy has lower performances with respect to the τ_H-based one of section 5.b.3.1, the use of this thermal lag quantity $\Delta_{OA,OL}$ is preferable to the identification of H(s) transfer function when the latter is not possible. This might happen when: the number of days needed by the H(s) identification procedure is unacceptable; the controller is not capable of performing such computation; the effect of the solar radiation is not negligible and some other conditions are met (see chapter 6 for more details).

5.b.3.3 Using closed loop thermal lag

Both the τ_M tuning strategies presented before need the system to act in open loop. This means that the effect of the daily thermal excursion of T_{OA} acts on T_Z undisturbed, without the damping effect of the PID outer control loop. The persistence of the resulting thermal discomfort $T_Z - T_{Z,rif}$ however could be unacceptable. In this case, it is possible to make use of this third τ_M tuning strategy.

In this case, the system is left in closed loop and with the compensator M(s) turned off. Under this configuration, the transfer function between the outside air temperature T_{OA} and the zone temperature T_Z reads:

$$\frac{T_Z(s)}{T_{OA}(s)} = \frac{H(s)}{1 + PID(s) * G(s)}$$

The damping effect of the outer loop is caused by the denominator of this transfer function. Still assuming a sinusoidal profile for T_{OA}, the time between the temperature peak of T_{OA} and the correspondent temperature peak on T_Z is registered and called $\Delta_{OA,CL}$ (where "CL" stands for Closed Loop). This value, because of the action of the PID outer control loop, will

be different from the value that would have been registered in open loop, i.e. $\Delta_{OA,OL}$. Definitely, $\Delta_{OA,CL}$ value is affected not only by H(s) but even by G(s) and PID(s). The identified time constant of H(s) τ_H has been found mainly influenced by $C_{p,Wall}$ and u_{Wall}, opposed to the identified time constant of G(s) τ_G that has been found mainly influenced by $C_{p,Pav}$ and u_{Pav}. This means that the value $\Delta_{OA,CL}$ might be affected by the parameters that affect τ_M (i.e. $C_{p,Wall}$ and u_{Wall}) or the parameters that affect T_M (i.e. $C_{p,Pav}$ and u_{Pav}) as well, so it is hard to decide how to exploit this parameter for now. In Fig 5.14 it is possible to see the scatterplot of the quantities τ_M and $\Delta_{OA,CL}$ ($\Delta_{OA,OL}$ on the x-axis, τ_M on the y-axis) and the scatterplot of the quantities T_M and $\Delta_{OA,CL}$ ($\Delta_{OA,CL}$ on the x-axis, T_M on the y-axis).

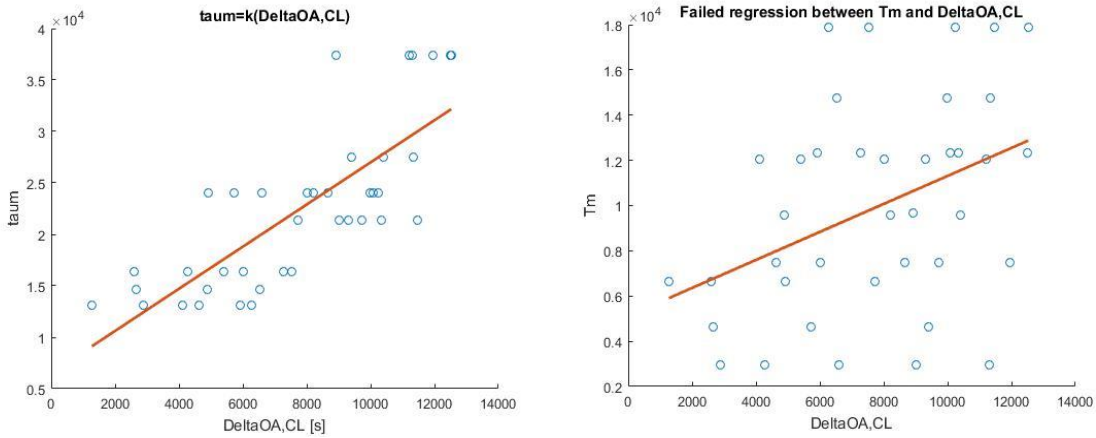

Fig 5.14: Correlation function between the compensator pole and the closed loop thermal lag (left) and correlation function between the compensator zero and the closed loop thermal lag (right)

It can be seen that $\Delta_{OA,CL}$ is more correlated to τ_M than to T_M. The analytical form of the associated linear regression is presented below:

$$\tau_M = k(\Delta_{OA,CL}) = 2.048\Delta_{OA,CL} + 6518$$

$$RMSE = 4983$$

However, this correlation is not strong enough to grant high tuning accuracy, whose result are presented in Fig 5.15.

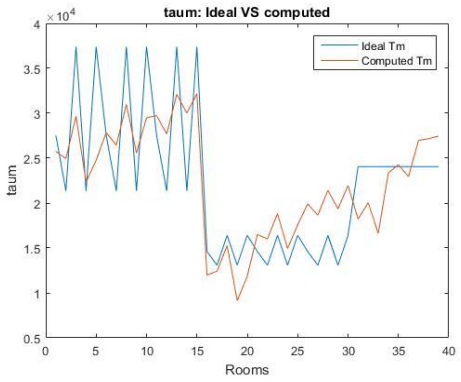

Fig 5.15: Accuracy of the compensator pole tuned with the correlation function between the compensator pole and the closed loop thermal lag

Exploiting the sinusoidal profile of T_{OA} hypothesis, it is possible to estimate the contribution of the outer control loop and correct the measure $\Delta_{OA,CL}$. Since the frequency of the input T_{OA} and the transfer function $\frac{T_Z(s)}{T_{OA}(s)}$ are known, it is possible to rewrite $\Delta_{OA,CL}$ as:

$$\Delta_{OA,CL} = \frac{86400}{360} * \left| phase\left(H\left(j\frac{2\pi}{86400}\right)\right) - phase\left(Den\left(j\frac{2\pi}{86400}\right)\right)\right|$$

with $Den(s) = 1 + PID(s) * G(s)$. Theoretically, if the term $phase\left(Den\left(j\frac{2\pi}{86400}\right)\right)$ was identified and removed, the open-loop quantity $\Delta_{OA,OL}$ would be obtained and then it would be possible to apply the correlation function $\tau_M = h(\Delta_{OA,OL})$ computed in the previous section 5.b.3.2. The perfect identification of that term is impossible, but its estimation can be obtained instead. By knowing the PID(s) transfer function and the estimated G(s) transfer function, i.e. $\hat{G}(s)$, it is then possible to compute the estimation of the Den(s) transfer function:

$$\widehat{Den}(s) = 1 + PID(s) * \hat{G}(s)$$

and, by that, the estimation of the phase term as:

$$phase\left(\widehat{Den}\left(j\frac{2\pi}{86400}\right)\right)$$

By correcting the $\Delta_{OA,CL}$ term with this estimation, a new term is obtained:

$$\Delta_{OA,CLC} = \frac{86400}{360} * \left| phase\left(H\left(j\frac{2\pi}{86400}\right)\right)\right| - phase\left(\widehat{Den}\left(j\frac{2\pi}{86400}\right)\right)$$

where "CLC" stands for Closed Loop Corrected.

The correlation of this new quantity with τ_M is tested in the scatterplot of τ_M and $\Delta_{OA,CLC}$ ($\Delta_{OA,CLC}$ on the x-axis, τ_M on the y-axis) in Fig 5.16.

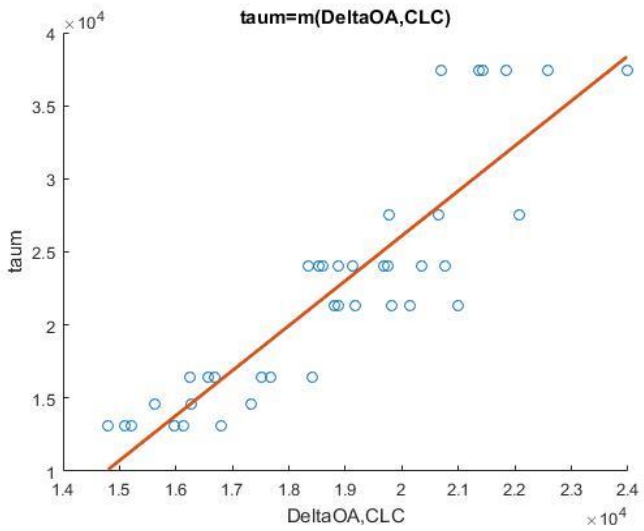

Fig 5.16: Correlation function between the compensator pole and the closed loop corrected thermal lag

Comparing this figure with the figure Fig 5.14 "taum=k(DeltaOA,CL)" it is possible to see an improvement on the level of correlation. The analytical form of this new linear regression is presented below:

$$\tau_M = m(\Delta_{OA,CLC}) = 3.075\Delta_{OA,CLC} - 35390$$

$$RMSE = 3692$$

and in Fig 5.17 the accuracy of this tuning is presented over the usual 39 representative rooms and limit cases, assuming that $\Delta_{OA,CLC}$ was obtained with a perfect measurement of $\Delta_{OA,CL}$ and the best possible 1-pole estimation of G(s).

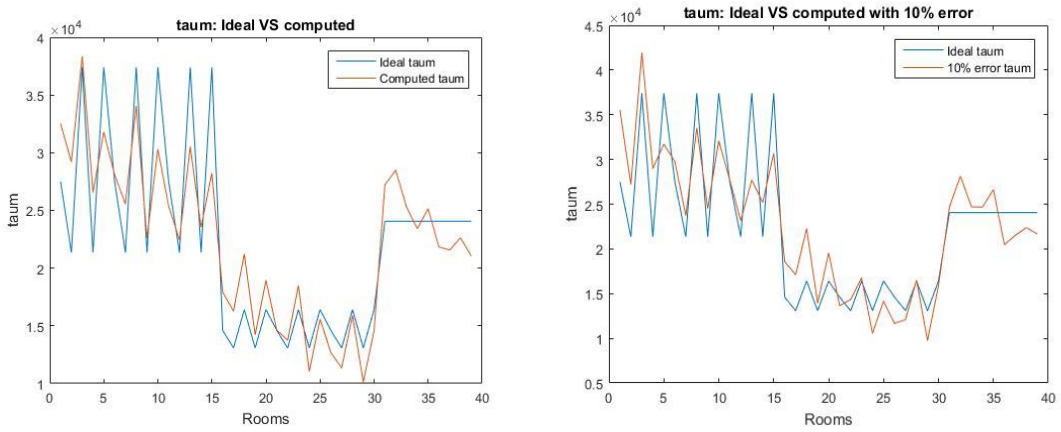

Fig 5.17: Accuracy of the compensator pole tuned with the proposed correlation function (left) and accuracy of the compensator pole using a closed loop corrected thermal lag with 10% error (right)

A visual comparison with the correspondent $\Delta_{OA,OL}$ figure (Fig 5.13) can be hard, so the mean square error MSE was computed for figure Fig 5.13, Fig 5.15 and Fig 5.17 with the following result, which proves that the CLC case is better than the CL case but worse than

the OL case:

$$MSE_{\Delta_{OA,OL}} = 9.6347 * 10^5$$

$$MSE_{\Delta_{OA,CL}} = 4.584 * 10^6$$

$$MSE_{\Delta_{OA,CLC}} = 1.676 * 10^7$$

The accuracy of the tuned τ_M would of course drop in correspondence of a measurement error on $\Delta_{OA,CL}$ and/or an estimation error on $\hat{G}(s)$. In the same figure Fig 5.17 the same formula was used to tune τ_M but using a $\Delta_{OA,CLC}$ characterized by a random $\pm 10\%$ error with respect to the ideal case. This error is the consequence of a measurement error on $\Delta_{OA,CL}$ and/or an estimation error on $\hat{G}(s)$.

5.c Adaptive tuning algorithms

All the individual tuning methods have been listed in the previous sections. Here, the possible sequences of these methods are combined to form the whole adaptive tuning algorithms. The ideal case in which applying each algorithm is explained in the list below.

To see the performances of these algorithms under different working conditions, refer to the simulation chapter 8. The algorithms are here listed in order of overall performances, starting from the most performing:

1. *G(s) closed loop identification [T_M] → G(s) estimated gain refinement [PID] → H(s) open loop identification [τ_M] [μ_M]:*
   These tuning methods refer respectively to 4.c.2.1, 4.c.3 and 4.c.4.
   The exact process scale of this algorithm reads:
   I. Initialize the PID and the compensator M(s) with the average configuration presented in section 5.a.
   II. Perform the G(s) closed loop identification when there is a sufficient difference $T_{Z,rif} - T_Z(0)$ is measured, for example at the first functioning of the system.
   III. Use the identified time constant of G(s) τ_G to tune of the M(s) compensator zero T_M through the correlation function $T_M = f(\tau_G) = 0.599\tau_G - 3862$.
   IV. Perform the G(s) gain refinement procedure applying the formula $G_0 = \frac{mean(T_Z) - mean(T_{OA})}{mean(T_M) - mean(T_{OA})}$.

V. Use the identified time constant τ_G and the refined G(s) gain estimation G_0 to tune the PID parameters according to the tuning strategy presented in section 3.a. Then, apply this new PID configuration.

VI. After reaching the pseudo-equilibrium state, memorize and fix the last value of $T_{M,rif}$ registered and then perform the H(s) open loop identification.

VII. Use the identified time constant of H(s) τ_H to tune the M(s) compensator pole τ_M through the correlation function $\tau_M = g(\tau_H) = 0.6592\tau_H - 3147$.

VIII. If the estimation of H(s) has been performed (like in this case), tune the compensator M(s) gain μ_M with the formula $\mu_M = \frac{\widehat{\mu_H}}{\widehat{\mu_G}}$. Else, use the formula gain μ_M with the formula $\mu_M = \frac{1+\widehat{\mu_G}}{\widehat{\mu_G}}$.

IX. Configure a new compensator M(s) using its three computed parameters and apply it to the system.

This algorithm is suggested when it is possible to perform a G(s) closed loop identification – i.e. when the difference $T_{Z,rif} - T_Z(0)$ is big enough, for example in a first auctioning of the heating system – and when it is possible to perform an H(s) open loop identification – i.e. when the effect of the daily thermal excursion of T_{OA} on T_Z can be sustained for the time needed to the H(s) identification procedure, which is 3 days on average. This algorithm is the one that returns the highest overall performances, as it will be seen in chapter 8, so if the conditions previously listed are met, it should be the first choice. Because of the potential invasiveness of the H(s) estimation procedure, this algorithm could be used for example in an holiday home in two phases: the first phase for G(s) identification and gain refinement during the first functioning of the system and a second phase for H(s) when the house becomes uninhabited again.

2. *G(s) closed loop identification [T_M] → G(s) estimated gain refinement [PID] → Open loop thermal lag [τ_M] [μ_M]:*

These tuning methods refer respectively to 4.c.2.1, 4.c.3 and 5.b.3.2.

The exact process scale of this algorithm reads (NOTE: only the steps VI and VII differ from the algorithm 1):

I. Initialize the PID and the compensator M(s) with the average configuration presented in section 5.a.

II. Perform the G(s) closed loop identification when there is a sufficient difference $T_{Z,rif} - T_Z(0)$ is measured, for example at the first functioning of the system.

III. Use the identified time constant of G(s) τ_G to tune of the M(s) compensator zero T_M through the correlation function $T_M = f(\tau_G) = 0.599\tau_G - 3862$.

IV. Perform the G(s) gain refinement procedure applying the formula $G_0 = \frac{mean(T_Z) - mean(T_{OA})}{mean(T_M) - mean(T_{OA})}$.

V. Use the identified time constant τ_G and the refined G(s) gain estimation G_0 to tune the PID parameters according to the tuning strategy presented in section 3.a. Then, apply this new PID configuration.

VI. After reaching the pseudo-equilibrium state, memorize and fix the last value of $T_{M,rif}$ registered and then perform the open loop thermal lag measurement.

VII. Use the measured thermal lag $\Delta_{OA,OL}$ to tune the M(s) compensator pole τ_M through the correlation function $\tau_M = h(\Delta_{OA,OL}) = 4.088\Delta_{OA,OL} - 56050$.

VIII. If the estimation of H(s) has been performed (not in this case), tune the compensator M(s) gain μ_M with the formula $\mu_M = \frac{\widehat{\mu_H}}{\widehat{\mu_G}}$. Else, use the formula gain μ_M with the formula $\mu_M = \frac{1+\widehat{\mu_G}}{\widehat{\mu_G}}$.

IX. Configure a new compensator M(s) using its three computed parameters and apply it to the system.

This algorithm is suggested when it is possible to perform a G(s) closed loop identification and when it is not possible to perform an H(s) identification, i.e.: the number of days needed by the H(s) identification is too big; the controller is not capable of performing such computation; the effect of the solar radiation is not negligible and some other conditions are met (see chapter 6 for more details). Generally speaking, this algorithm could be used when the first functioning of the system presents a big difference $T_{Z,rif} - T_Z(0)$ (to identify G(s)) and it's quickly needed a complete compensator tuning with a short impact on the thermal comfort (1 day test to measure the open loop thermal lag).

3. *G(s) closed loop identification [T_M] → G(s) estimated gain refinement [PID] → Closed loop thermal lag [τ_M] [μ_M]:*

These tuning methods refer respectively to 4.c.2.1, 4.c.3 and 5.b.3.3.

The exact process scale of this algorithm reads (NOTE: only the steps VI and VII differ from the algorithm 2):

I. Initialize the PID and the compensator M(s) with the average configuration presented in section 5.a

II. Perform the G(s) closed loop identification when there is a sufficient difference $T_{Z,rif} - T_Z(0)$ is measured, for example at the first functioning of the system.

III. Use the identified time constant of G(s) τ_G to tune of the M(s) compensator zero T_M through the correlation function $T_M = f(\tau_G) = 0.599\tau_G - 3862$.

IV. Perform the G(s) gain refinement procedure applying the formula $G_0 = \frac{mean(T_Z) - mean(T_{OA})}{mean(T_M) - mean(T_{OA})}$.

V. Use the identified time constant τ_G and the refined G(s) gain estimation G_0 to tune the PID parameters according to the tuning strategy presented in section 3.a. Then, apply this new PID configuration.

VI. Keeping the system in closed loop with the new PID configuration, deactivate the average M(s) compensator and measure the closed loop thermal lag.

VII. Use the measured thermal lag $\Delta_{OA,CLC}$ to tune the M(s) compensator pole τ_M through the correlation function $\tau_M = m(\Delta_{OA,CLC}) = 3.075\Delta_{OA,CLC} - 35390$.

VIII. If the estimation of H(s) has been performed (not in this case), tune the compensator M(s) gain μ_M with the formula $\mu_M = \frac{\widehat{\mu_H}}{\widehat{\mu_G}}$. Else, use the formula gain μ_M with the formula $\mu_M = \frac{1+\widehat{\mu_G}}{\widehat{\mu_G}}$.

IX. Configure a new compensator M(s) using its three computed parameters and apply it to the system.

This algorithm is suggested when it is possible to perform a G(s) closed loop identification and when it is not possible to impose the open loop system functioning, most likely because of the resulting thermal discomfort. In this case, the only tuning method left for the M(s) compensator pole τ_M is the closed loop thermal lag one, that is the least performing of the τ_M tuning methods.

Definitely, this algorithm could be used when the first functioning of the system allows a closed loop G(s) identification – i.e. has a big $T_{Z,rif} - T_Z(0)$ difference – and when the switching of the system in open loop is not possible.

4. *G(s) gain refinement → H(s) open loop estimation [τ_M] → G(s) open loop identification exploiting H(s) identification [T_M] [PID] [μ_M]:*

   These tuning methods refer respectively to 4.c.2.3, 4.c.3 and 4.c.4.

   The exact process scale of this algorithm reads:

   I. Initialize the PID and the compensator M(s) with the average configuration presented in section 5.a.

   II. Perform the G(s) gain refinement procedure applying the formula $G_0 = \frac{mean(T_Z) - mean(T_{OA})}{mean(T_M) - mean(T_{OA})}$.

   III. After reaching the pseudo-equilibrium state, memorize and fix the last value of $T_{M,rif}$ registered and then perform the H(s) open loop identification.

   IV. Use the identified time constant of H(s) τ_H to tune the M(s) compensator pole τ_M through the correlation function $\tau_M = g(\tau_H) = 0.6592\tau_H - 3147.$

   V. Starting from the pseudo-equilibrium state, register the last value of $T_{M,rif}$ and perform the G(s) open loop identification exploiting the H(s) estimation.

   VI. Use the identified time constant of G(s) τ_G to tune of the M(s) compensator zero T_M through the correlation function $T_M = f(\tau_G) = 0.599\tau_G - 3862.$

   VII. Use the identified time constant τ_G and the refined G(s) gain estimation G_0 to tune the PID parameters according to the tuning strategy presented in section 3.a. Then, apply this new PID configuration.

   VIII. If the estimation of H(s) has been performed (like in this case), tune the compensator M(s) gain μ_M with the formula $\mu_M = \frac{\widehat{\mu_H}}{\widehat{\mu_G}}$. Else, use the formula gain μ_M with the formula $\mu_M = \frac{1+\widehat{\mu_G}}{\widehat{\mu_G}}$.

   IX. Configure a new compensator M(s) using its three computed parameters and apply it to the system.

   This algorithm differs completely from the first three presented. Its use is recommended in case that the closed loop G(s) identification procedure is not possible – for example, this is not the first functioning of the system and/or the difference $T_{Z,rif} - T_Z(0)$ is too small – but the open loop H(s) identification procedure is applicable. In this case, unlike the first three algorithms, the first transfer function identified is H(s). Before this identification, however, it is necessary to perform the G(s) gain refinement (called so even if in this case no estimation of G(s)

has been done yet) to obtain a reliable H(s) identification, as exposed in section 4.c.4. The H(s) identification is then exploited in the open loop G(s) identification procedure to obtain a better result in a shorter time.

This algorithm could be applied when there is no big difference $T_{Z,rif} - T_Z(0)$ to perform the closed loop estimation of G(s) and when it is possible to perform an open loop estimation of H(s).

5. *G(s) open loop identification [T_M] → G(s) estimated gain refinement [PID] → H(s) open loop identification [τ_M] [μ_M]:*

   These tuning methods refer respectively to 4.c.2.2, 4.c.3 and 4.c.4.

   The exact process scale of this algorithm reads (NOTE: apart from the step II, this algorithm is equal to the algorithm 1):

   I. Initialize the PID and the compensator M(s) with the average configuration presented in section 5.a.

   II. Starting from the pseudo-equilibrium state, register the last value of $T_{M,rif}$ and perform the G(s) open loop identification.

   III. Use the identified time constant of G(s) τ_G to tune of the M(s) compensator zero T_M through the correlation function $T_M = f(\tau_G) = 0.599\tau_G - 3862$.

   IV. Perform the G(s) gain refinement procedure applying the formula $G_0 = \frac{mean(T_Z) - mean(T_{OA})}{mean(T_M) - mean(T_{OA})}$.

   V. Use the identified time constant τ_G and the refined G(s) gain estimation G_0 to tune the PID parameters according to the tuning strategy presented in section 3.a. Then, apply this new PID configuration.

   VI. After reaching the pseudo-equilibrium state, memorize and fix the last value of $T_{M,rif}$ registered and then perform the H(s) open loop identification.

   VII. Use the identified time constant of H(s) τ_H to tune the M(s) compensator pole τ_M through the correlation function $\tau_M = g(\tau_H) = 0.6592\tau_H - 3147$.

   VIII. If the estimation of H(s) has been performed (like in this case), tune the compensator M(s) gain μ_M with the formula $\mu_M = \frac{\widehat{\mu_H}}{\widehat{\mu_G}}$. Else, use the formula gain μ_M with the formula $\mu_M = \frac{1+\widehat{\mu_G}}{\widehat{\mu_G}}$.

   IX. Configure a new compensator M(s) using its three computed parameters and apply it to the system.

The application of this algorithm has the same requirements of the algorithm 4 presented before, which returns a better overall performance with respect to the current one. In this way, it seems that the application of this algorithm instead of the other is never useful. However, some particular cases can exist in which this algorithm is preferable. For example, the effect of the open loop H(s) identification procedure on the thermal comfort can be more relevant than the effect of the open loop G(s) identification. This is the case when the room presents high wall conductance and/or when the daily thermal excursion of the outside air temperature is relevant. Under these conditions, it could be preferable to first perform the open loop G(s) estimation and wait for a period during which the room is uninhabited to perform the H(s) open loop estimation.

6. *G(s) open loop identification [T_M] → G(s) estimated gain refinement [PID] → Open loop thermal lag [τ_M] [μ_M]:*

   These tuning methods refer respectively to 4.c.2.2, 4.c.3 and 5.b.3.2.

   The exact process scale of this algorithm reads (NOTE: apart from the step VI and VII, this algorithm is equal to the algorithm 5):

   I. Initialize the PID and the compensator M(s) with the average configuration presented in section 5.a.
   II. Starting from the pseudo-equilibrium state, register the last value of $T_{M,rif}$ and perform the G(s) open loop identification.
   III. Use the identified time constant of G(s) τ_G to tune of the M(s) compensator zero T_M through the correlation function $T_M = f(\tau_G) = 0.599\tau_G - 3862$.
   IV. Perform the G(s) gain refinement procedure applying the formula $G_0 = \frac{mean(T_Z) - mean(T_{OA})}{mean(T_M) - mean(T_{OA})}$.
   V. Use the identified time constant τ_G and the refined G(s) gain estimation G_0 to tune the PID parameters according to the tuning strategy presented in section 3.a. Then, apply this new PID configuration.
   VI. After reaching the pseudo-equilibrium state, memorize and fix the last value of $T_{M,rif}$ registered and then perform the open loop thermal lag measurement.
   VII. Use the measured thermal lag $\Delta_{OA,OL}$ to tune the M(s) compensator pole τ_M through the correlation function $\tau_M = h(\Delta_{OA,OL}) = 4.088\Delta_{OA,OL} - 56050$.

VIII. If the estimation of H(s) has been performed (not in this case), tune the compensator M(s) gain μ_M with the formula $\mu_M = \frac{\widehat{\mu_H}}{\widehat{\mu_G}}$. Else, use the formula gain μ_M with the formula $\mu_M = \frac{1+\widehat{\mu_G}}{\widehat{\mu_G}}$.

IX. Configure a new compensator M(s) using its three computed parameters and apply it to the system.

The use of this algorithm is recommended in case that the closed loop G(s) identification procedure is not possible – for example, this is not the first functioning of the system and/or the difference $T_{Z,rif} - T_Z(0)$ is too small – and even the open loop H(s) identification procedure is not acceptable.
Generally speaking, this algorithm could be used when the system is already functioning – or its first functioning presents a small difference $T_{Z,rif} - T_Z(0)$ – and a complete compensator tuning with a short impact on the thermal comfort is needed (1 day test to measure the open loop thermal lag).

7. *G(s) open loop identification [T_M] → G(s) estimated gain refinement [PID] → Closed loop thermal lag [τ_M] [μ_M]:*

These tuning methods refer respectively to 4.c.2.2, 4.c.3 and 5.b.3.3.
The exact process scale of this algorithm reads (NOTE: apart from the step VI and VII, this algorithm is equal to the algorithm 6):

I. Initialize the PID and the compensator M(s) with the average configuration presented in section 5.a.

II. Starting from the pseudo-equilibrium state, register the last value of $T_{M,rif}$ and perform the G(s) open loop identification.

III. Use the identified time constant of G(s) τ_G to tune of the M(s) compensator zero T_M through the correlation function $T_M = f(\tau_G) = 0.599\tau_G - 3862$.

IV. Perform the G(s) gain refinement procedure applying the formula $G_0 = \frac{mean(T_Z) - mean(T_{OA})}{mean(T_M) - mean(T_{OA})}$.

V. Use the identified time constant τ_G and the refined G(s) gain estimation G_0 to tune the PID parameters according to the tuning strategy presented in section 3.a. Then, apply this new PID configuration.

VI. Keeping the system in closed loop with the new PID configuration, deactivate the average M(s) compensator and measure the closed loop thermal lag.

VII. Use the measured thermal lag $\Delta_{OA,CLC}$ to tune the M(s) compensator pole τ_M through the correlation function $\tau_M = m(\Delta_{OA,CLC}) = 3.075\Delta_{OA,CLC} - 35390$.

VIII. If the estimation of H(s) has been performed (not in this case), tune the compensator M(s) gain μ_M with the formula $\mu_M = \frac{\widehat{\mu_H}}{\widehat{\mu_G}}$. Else, use the formula gain μ_M with the formula $\mu_M = \frac{1+\widehat{\mu_G}}{\widehat{\mu_G}}$.

IX. Configure a new compensator M(s) using its three computed parameters and apply it to the system.

The use of this algorithm is recommended in case that the closed loop G(s) identification procedure is not possible and it is not possible to impose an open loop functioning on the system.
Generally speaking, this algorithm could be used when the system is already functioning – or its first functioning presents a small difference $T_{Z,rif} - T_Z(0)$ – and the user wants to keep the system in closed-loop to benefit from a bigger thermal comfort.

5.d Applicability limits

The adaptive tuning algorithms have been developed by considering some room model parameters constant and some others – the main thermo-physical parameters u_{wall}, $c_{p,Wall}$, u_{Pav} and $c_{p,Pav}$ – variable. These four quantities are the room thermal characteristics on which the adaptive tuning is designed on. They have been chosen among all the room parameters mainly because of their low identifiability. The performance of the tuning algorithms on the variation of these four parameters has been proved in this chapter (further tests are conducted in the simulations chapter 8). The range along which these parameters are allowed to vary has been chosen big enough to grant the functioning of the algorithms on any reasonable variation of such parameters.

Other quantities – i.e. the room dimensions and the parameters of the radiant panel system – have been kept fixed to their nominal value, listed in section 4.a. These parameters are or controllable in the design/installation phase (radiant panel system) or easily identifiable manually (room dimensions). However, their variation with respect to the nominal value affect the ideal control tuning as well. This means that, by introducing a variation of these quantities together with the formerly considered variation of the four main thermo-physical

parameters, the efficiency of the adaptive tuning algorithm is gradually reduced. The numerical coefficients of such algorithms have been developed referring to the nominal value of the room dimensions and radiant panel characteristics. The only parameter that is not affected by these further variations is the compensator M(s) gain μ_M: this parameter is tuned with a formula that has no numerical calibration, unlike the other correlation formulae used for the M(s) pole and zero.

In this section, these two new variations – i.e. room dimensions and radiant panel characteristics – and their effect on the adaptive tuning algorithm performances is treated differently in two separate sub-sections.

5.d.1 Room dimensions

In section 4.a.1 the variation of S_{Wall} (respectively, S_{Pav}) was defined as assimilable to a variation of u_{Wall} (respectively, u_{Pav}). Since the variation of the room dimensions is correlated to the variation of S_{Wall} and S_{Pav} it seems unlikely for any problem to arise, since the adaptive tuning algorithms have been verified on the variation of u_{Wall} and u_{Pav}. However, the variation of the room dimensions introduce two problems:

- In addition to the variation of S_{Wall} and S_{Pav}, it is correlated to the variation of the zone volume too.
- An excessive variation of S_{Wall} (respectively, S_{Pav}) can of course be assimilated to a variation of u_{Wall} (respectively, u_{Pav}), but the resulting variation on u_{Wall} (respectively, u_{Pav}) would be too high. For example, a variation of +300% on the average value of u_{Wall} is supported correctly by the tuning algorithms, but an additional variation of +300% on S_{Wall} would lead to a resulting variation of +600% on u_{Wall}, which is too high to maintain the same adaptive tuning performances.

Regarding the variation of the room dimensions from their nominal value, two results are presented in this sub-section. First, the maximum variation range of these parameters to maintain a good tuning performance is found. Then, the numerical correlation is proven to exist even under different values of the room dimensions.

5.d.1.1 Maximum range

The variation of the height of the room has a different impact than the variation of its width or length. This fact can be explained by analyzing the ratio between the pavement surface S_{Pav} and the walls surface S_{Wall}. A variation in the length or width of the room reasonably corresponds to a similar variation in both S_{Pav} and S_{Wall}. Since the variation rate of the ratio between S_{Pav} and S_{Wall} is reduced, it will take big variations of the width or length of the room before to cause a relevant drop in the adaptive tuning performances. The situation is different considering the variation of the room height. In this case, only S_{Wall} varies resulting in an equivalent variation of the S_{Wall} to S_{Pav} ratio and a quicker drop in the adaptive tuning performances.
Some indicative limits for the three room dimensions have been tested and found:

- Height: [2 ; 4] meters.
- Width and length: [2 ; 8] meters each.

To prove the robustness of the tuning algorithms with respect to these boundaries, a test campaign was conducted over all the individual tuning strategies. For each tuning strategy, 40 random rooms were tested characterized by the following parameter ranges:

- Room dimensions: randomly picked with height $\in$ [2 ; 4], width $\in$ [2 ; 8] and length $\in$ [2 ; 8].
- Main thermo-physical parameters: randomly picked inside their formerly defined boundaries, i.e. $c_{p,Wall} \in [13; 65]$, $u_{Wall} \in [0.28; 1.61]$, $c_{p,Pav} \in [34; 175]$ and $u_{Pav} \in [12; 63]$

The quantity used for each tuning (for example τ_G, $\Delta_{OA,CLC}$ and so on) is assumed to have been perfectly identified/measured. Any identification/measurement error would cause a further performance drop, but this section is meant to prove the robustness of the tuning algorithms with respect to the rooms dimensions variation.
The results of these test are presented in Fig 5.18.

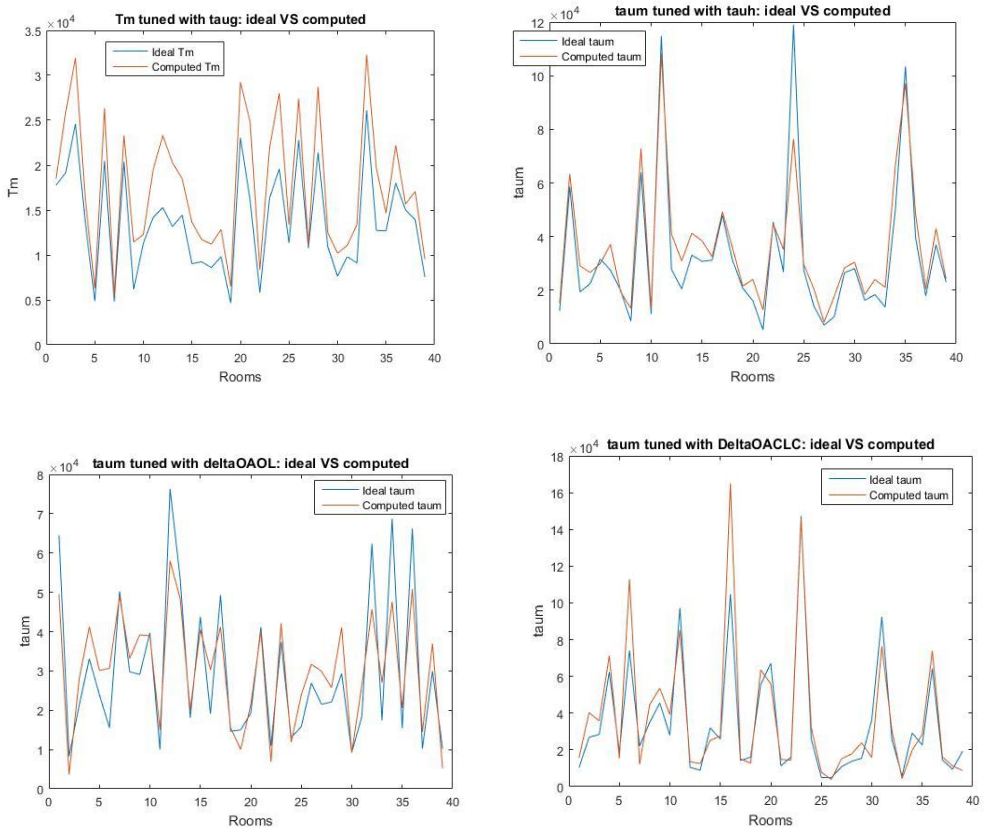

Fig 5.18: Correlation functions accuracy even under different room dimensions:
compensator zero with G(s) time constant (upper left), compensator pole with H(s) time constant (upper right) compensator pole with open loop thermal lag (lower left) and compensator pole with closed loop corrected thermal lag (lower right)

5.d.1.2 Existence of numerical correlation

Similarly to what was done when introducing the individual tuning methods, a scatterplot is presented in each case to prove the existence of a correlation. This time however, this scatterplot will be produced starting from different values of the room dimensions instead of the nominal ones. For each tuning strategy – i.e. tuning T_M using τ_G, tuning τ_M using τ_H, tuning τ_M using $\Delta_{OA,OL}$ and tuning T_M using $\Delta_{OA,CLC}$ – three different room dimensions [height,width,length] are considered: [3,6,6], [4,8,8] and [4.5,10,10]. The results of these test are presented in Fig 5.19 (*tuning T_M using τ_G*), Fig 5.20 (*tuning τ_M using τ_H*), Fig 5.21 (*tuning τ_M using $\Delta_{OA,OL}$*) and Fig 5.22 (*tuning T_M using $\Delta_{OA,CLC}$*).

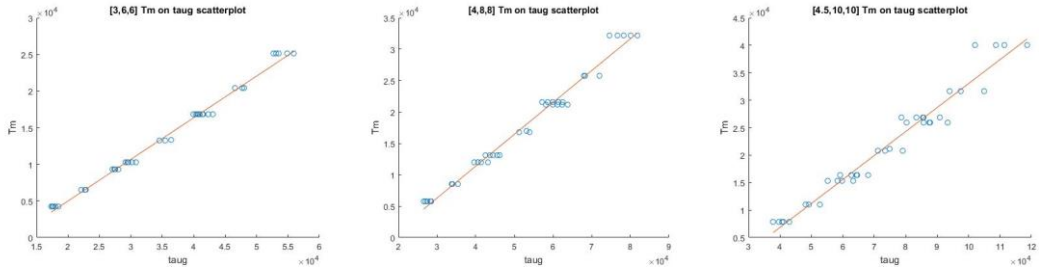

Fig 5.19: Existence of the correlation function [compensator zero | G(s) time constant] even with different room dimensions

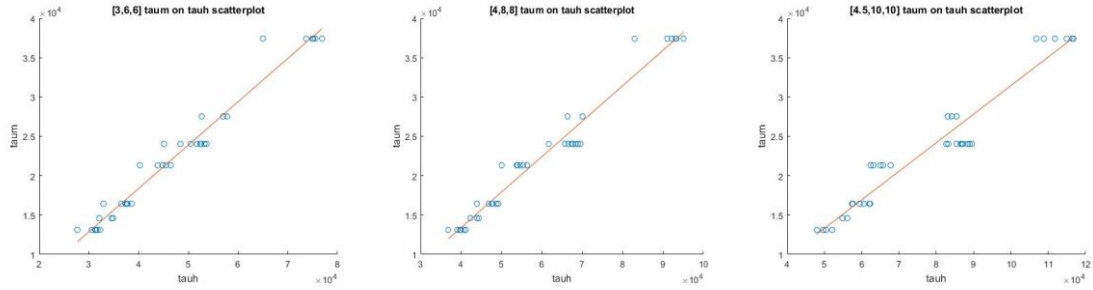

Fig 5.20: Existence of the correlation function [compensator pole | H(s) time constant] even with different room dimensions

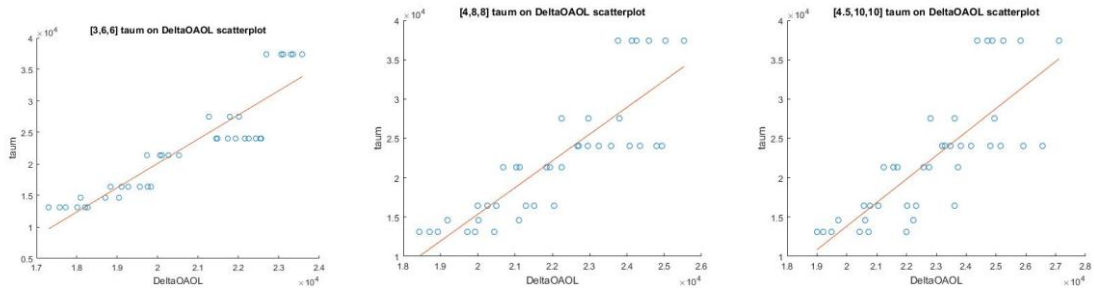

Fig 5.21: Existence of the correlation function [compensator pole | open loop thermal lag] even with different room dimensions

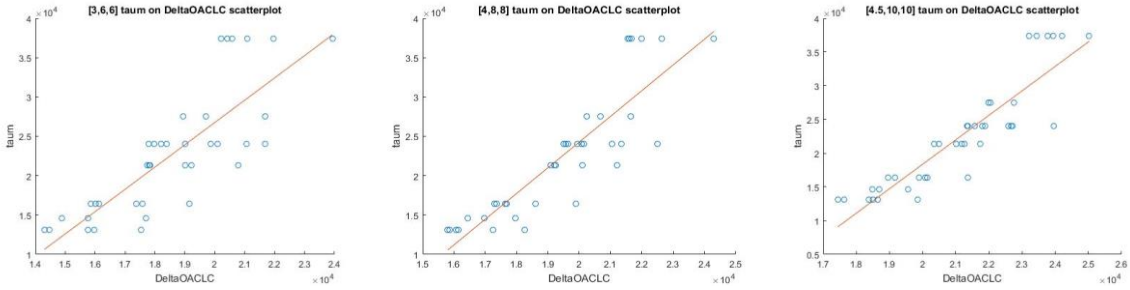

Fig 5.22: Existence of the correlation function [compensator pole | closed loop corrected thermal lag] even with different room dimensions

The resulting correlation functions are listed below, compared to the ones resulting from the nominal room dimensions:

- Nominal dimensions.:
  - $T_M = f(\tau_G) = 0.599\tau_G - 3862$
  - $\tau_M = g(\tau_H) = 0.6592\tau_H - 3147$
  - $\tau_M = h(\Delta_{OA,OL}) = 4.088\Delta_{OA,OL} - 56050$
  - $\tau_M = m(\Delta_{OA,CLC}) = 3.075\Delta_{OA,CLC} - 35390$
- [3,6,6] dimensions:
  - $T_M = f(\tau_G) = 0.5685\tau_G - 6380$
  - $\tau_M = g(\tau_H) = 0.551\tau_H - 3662$
  - $\tau_M = h(\Delta_{OA,OL}) = 3.850\Delta_{OA,OL} - 56917$
  - $\tau_M = m(\Delta_{OA,CLC}) = 2.833\Delta_{OA,CLC} - 28985$
- [4,8,8] dimensions:
  - $T_M = f(\tau_G) = 0.507\tau_G - 8902$
  - $\tau_M = g(\tau_H) = 0.451\tau_H - 4647$
  - $\tau_M = h(\Delta_{OA,OL}) = 3.398\Delta_{OA,OL} - 52629$
  - $\tau_M = m(\Delta_{OA,CLC}) = 3.267\Delta_{OA,CLC} - 41080$
- [4.5,10,10] dimensions:
  - $T_M = f(\tau_G) = 0.436\tau_G - 10612$
  - $\tau_M = g(\tau_H) = 0.363\tau_H - 4844$
  - $\tau_M = h(\Delta_{OA,OL}) = 2.990\Delta_{OA,OL} - 45960$
  - $\tau_M = m(\Delta_{OA,CLC}) = 3.629\Delta_{OA,CLC} - 54214$

5.d.2 Radiant panel parameters

Unlike the analysis carried out for the room dimensions variation, in this case no maximum range of the radiant panel parameters will be defined. This choice is due to two reasons:

- These parameters are decidable during the design/installation phase, so theoretically no adaptation will ever be required if this adaptive system is associated to a specific radiant panel system.
- These parameters are much more than the three room dimensions and their nature is variegated. It would be hard to define a significant maximum range for all of them especially for the possible interactions that each variation can have with another one.

For the radiant panel parameters, the only action taken is to prove the existence of the exploited numerical correlation even under a different configuration of the radiant panel. This proof will be done by presenting the usual scatterplots under three non-nominal configurations of the radiant panel parameters. The radiant panel parameters related to the water thermal properties will be kept constant because of their physical nature:

- ρ : 996 [kg/m^3]
- C_{p-aq} : 4180 [J/kgK]

The other parameters have been configured as follows. The symbol "a→b" means that the second quantity "b" is automatically decided once the value of the first quantity "a" is set. In the end, there are 5 degrees of freedom in this radiant panel configuration:

- Config. 1:
  - $L = S_{Pav}/0.1$ [m]
  - D_e : 0.027 m → A_p : 0.085 [m^2]
  - D_i : 0.023 m → C_{Pi} : 155630 [J/K]
  - θ : 0.2 [m/s] → w : 2.5 [kg/s]
  - U_1 : 30 [W/K]
- Config. 2:
  - $L = S_{Pav}/0.2$ [m]
  - D_e : 0.022 m → A_p : 0.069 [m^2]
  - D_i : 0.020 m → C_{Pi} : 58839 [J/K]
  - θ : 0.212 [m/s] → w : 0.0664 [kg/s]
  - U_1 : 25 [W/K]
- Config. 3:
  - $L = S_{Pav}/0.15$ [m]
  - D_e : 0.027 m → A_p : 0.053 [m^2]

- D_i : 0.027 m → C_{Pi} : 33140 [J/K]
- θ : 0.377 [m/s] → w : 0.05 [kg/s]
- U_1 : 24.741 [W/K]

The results of these test are presented in Fig 5.23 (*tuning T_M using τ_G*), Fig 5.24 (*tuning τ_M using τ_H*), Fig 5.25 (*tuning τ_M using $\Delta_{OA,OL}$*) and Fig 5.26 (*tuning T_M using $\Delta_{OA,CLC}$*).

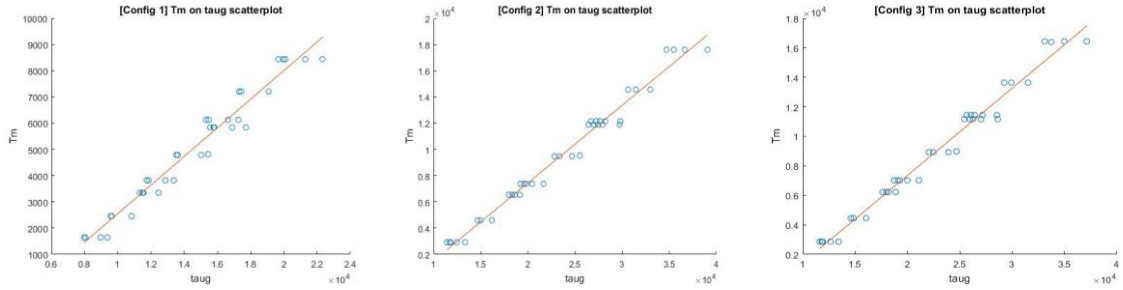

Fig 5.23: Existence of the correlation function [compensator zero | G(s) time constant]
even with different radiant panel parameters

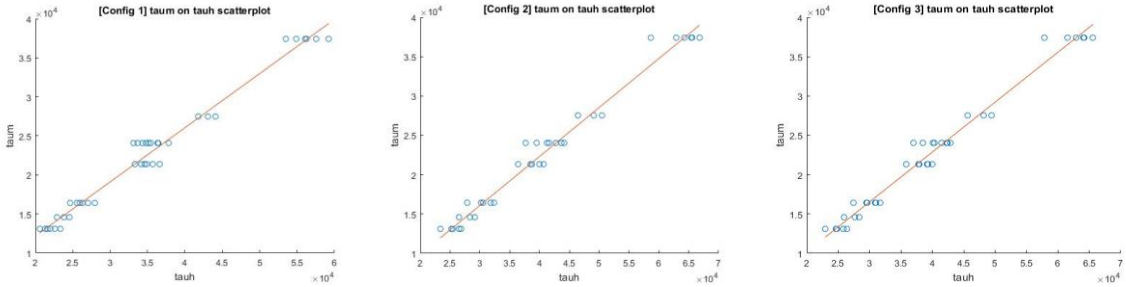

Fig 5.24: Existence of the correlation function [compensator pole | H(s) time constant]
even with different radiant panel parameters

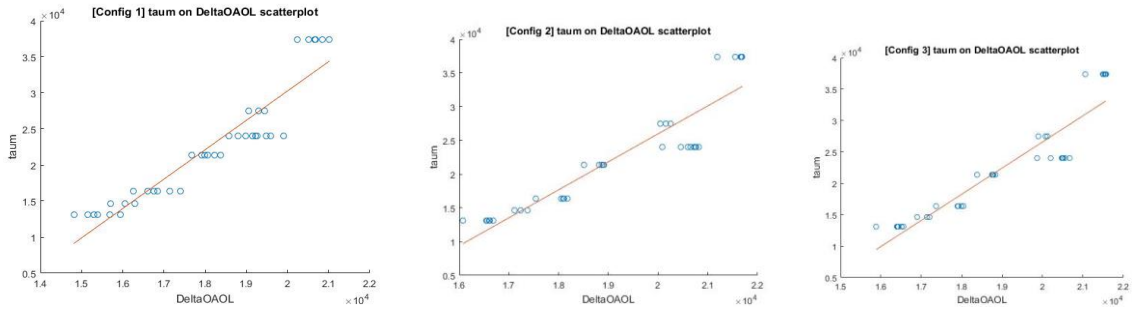

Fig 5.25: Existence of the correlation function [compensator pole | open loop thermal lag]
even with different radiant panel parameters

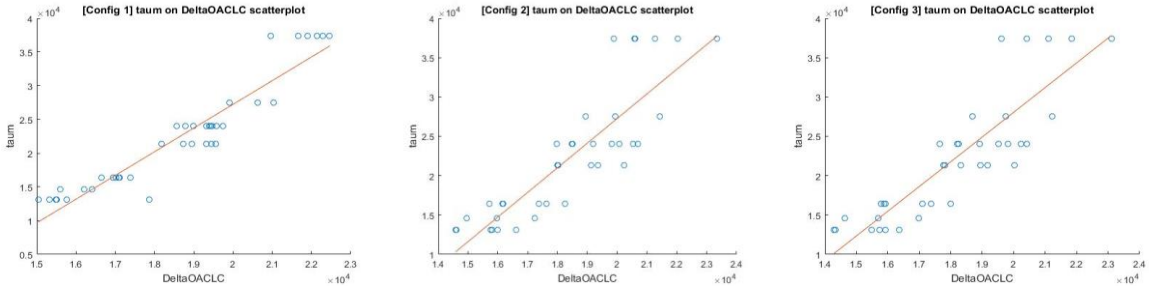

Fig 5.26: Existence of the correlation function [compensator pole | closed loop corrected thermal lag] even with different radiant panel parameters

The resulting correlation functions are listed below, compared to the ones resulting from the nominal system configuration:

- Nominal config.:
  - $T_M = f(\tau_G) = 0.599\tau_G - 3862$
  - $\tau_M = g(\tau_H) = 0.6592\tau_H - 3147$
  - $\tau_M = h(\Delta_{OA,OL}) = 4.088\Delta_{OA,OL} - 56050$
  - $\tau_M = m(\Delta_{OA,CLC}) = 3.075\Delta_{OA,CLC} - 35390$
- Config. 1:
  - $T_M = f(\tau_G) = 0.5458\tau_G - 2906$
  - $\tau_M = g(\tau_H) = 0.6939\tau_H - 1713$
  - $\tau_M = h(\Delta_{OA,OL}) = 4.073\Delta_{OA,OL} - 51208$
  - $\tau_M = m(\Delta_{OA,CLC}) = 3.513\Delta_{OA,CLC} - 43026$
- Config. 2:
  - $T_M = f(\tau_G) = 0.592\tau_G - 4409$
  - $\tau_M = g(\tau_H) = 0.6222\tau_H - 2587$
  - $\tau_M = h(\Delta_{OA,OL}) = 4.15\Delta_{OA,OL} - 57021$
  - $\tau_M = m(\Delta_{OA,CLC}) = 3.131\Delta_{OA,CLC} - 35980$
- Config. 3:
  - $T_M = f(\tau_G) = 0.590\tau_G - 4472$
  - $\tau_M = g(\tau_H) = 0.635\tau_H - 2485$
  - $\tau_M = h(\Delta_{OA,OL}) = 4.166\Delta_{OA,OL} - 56710$
  - $\tau_M = m(\Delta_{OA,CLC}) = 3.153\Delta_{OA,CLC} - 34815$

5.d.3 Conclusions on the applicability limits

Based on the result of the previous tests, it can be said that the correlation functions on which the adaptive tuning has been based exist even for different values of the room dimensions and the radiant panel parameters. This means that the developed tuning algorithms are not just the product of some lucky combination of the nominal room parameters. Based on the

model adopted in this thesis, the existence of the correlation functions under different reasonable room models has been proved.

To extend the applicability of such tuning algorithms to rooms with dimensions really far from the nominal case, it would be necessary to identify manually the dimension scale of the room and then to apply the correct numerical values to the correlation functions used for the adaptive tuning. An excessive precision in this room dimensions estimation is not necessary, since a good robustness with respect to the room dimensions has been proved in these tests. Different numerical values can be developed to accommodate different radiant panel configurations too. In this thesis, only one numerical set of correlation functions has been developed (in this chapter) because the aim is to present the potentiality of the whole adaptive approach without entering too much into detail on the range of different numerical sets.

5.e Chapter 5 conclusions

This chapter is the core of the thesis. Here, all the adaptive tuning methods are proposed individually, starting from the easy adaptive tuning of the PID and continuing with the adaptive tuning methods for the compensator M(s) parameters. After this, the complete tuning algorithms were composed out of the single tuning methods and the applicability limits of those algorithms were defined.

The main contribution for the adaptive tuning field is constituted by the correlation functions used for the pole and zero of M(s). These correlation function allow the compensator M(s) to adapt to the variation of the four main thermo-physical parameters – which are the most influent and unidentifiable parameters of the room model – by exploiting some easily identifiable quantities, such as the time constants of G(s) and H(s) and the thermal lag measurement. These correlation functions have proved their robustness with respect to the room dimensions. Moreover, the existence of such correlation functions has been proved even in rooms characterized by a radiant panel configuration and/or different room dimensions different from the nominal values considered: the only change is in the coefficients to use in those correlation functions.

6. SOLAR RADIATION

In the modeling chapter 2 some disturbances that are known to affect the buildings thermal behavior have been neglected. This was done after the model testing of section 2.d because the model could be verified only with the outside air temperature disturbance acting on the system. The neglected disturbances are: solar radiation, ground temperature and internal gains. Among these three, the one that has the highest possibilities of being studied and compensated is the solar radiation.

In this chapter, the solar radiation disturbance is re-introduced in the room model, following the first energy balance equations listed in section 2.b.3. In section 6.a the transfer functions associated to the solar radiation are studied. Then, a discursive section 6.b is dedicated to the estimated effect of the solar radiation on the adaptive tuning algorithms presented in the previous chapter 5. In the end, a theoretical suggestion for a solar radiation compensator is exposed in section 6.c.

6.a Transfer functions analysis

This section is dedicated to the analysis of the two transfer functions associated to the solar radiation disturbance. This disturbance is assumed to affect the walls and pavement energy balance equations, as formerly presented in section 2.b.3. The associated transfer functions are:

$$-> J(s) = \frac{T_z(s)}{P_{Wall}(s)} \; with$$

$$P_{Wall}(s) = k_{Wall} \sum_{i=N,S,W,E,Ceil} W_{Sol,i} S_{Op,i} + \frac{1}{2} k_{Sol,Tr} * \sum_{i=N,S,W,E,Ceil} W_{Sol,i} S_{Tr,i}$$

$$-> K(s) = \frac{T_z(s)}{P_{Pav}(s)} \; with$$

$$P_{Pav}(s) = \frac{1}{2} k_{Sol,Tr} \sum_{i=N,S,W,E,Ceil} W_{Sol,i} S_{Tr,i}$$

These two transfer function have been defined though the introduction of two reformulated inputs, i.e. $P_{Wall}(s)$ and $P_{Pav}(s)$. This choice was done in order to simplify the following

analyses. The transfer functions J(s) and K(s) can be considered respectively as the effect of the solar radiation passing through the wall on T_z and the effect of the solar radiation passing through the pavement on T_z.

By introducing the two reformulated inputs $P_{Wall}(s)$ and $P_{Pav}(s)$, an easy upgrade of the electric equivalent circuit presented in section 4.b.1 can be done to account for the effect of the solar radiation as well. The resulting circuit – on which the analyses of the following sections will be performed – is presented in Fig. 6.1.

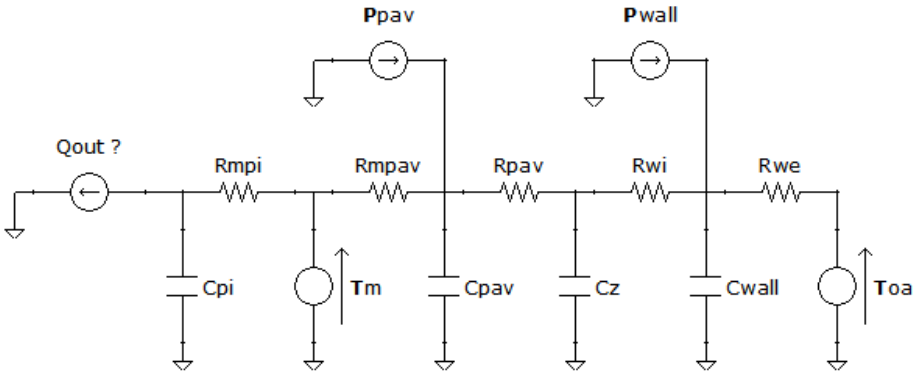

Fig. 6.1: System electrical equivalent extended with the solar radiation disturbance

6.a.1 J(s) analysis

The electric equivalent just presented will be quickly manipulated in order to find a correlation between the transfer function J(s) and H(s). Focusing on the input P_{Wall}, the voltage source associated to T_{OA} is turned off. In this way, the current source associated to the input P_{Wall} is in parallel to the resistance R_{we}. These two components can be associated together and transformed into its Thevenin equivalent (Fig. 6.2).

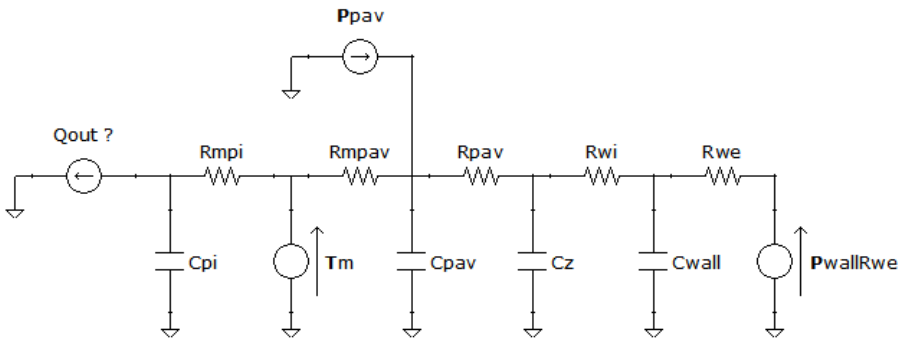

Fig. 6.2: System electrical equivalent, J(s) analysis

It is now possible to see that the obtained tension generator $P_{Wall} * R_{we}$ is in the same exact configuration of the tension generator associated to the outside air temperature T_{OA}. This means that the transfer function from $P_{Wall} * R_{we}$ to T_Z is the same that exists from T_{OA} to T_Z, i.e. H(s), resulting in:

$$J(s) = \frac{T_z(s)}{P_{Wall}(s)} = \frac{T_z(s)}{P_{Wall}(s) * R_{we}} * R_{we} = H(s) * R_{we}$$

In conclusion, the transfer function J(s) is equivalent to the transfer function H(s) with a different gain. This property was verified manually on the transfer functions computed with Matlab.

6.a.2 K(s) analysis

The same procedure applied for J(s) cannot be repeated in this case: the current source associated to P_{Pav} is not directly associable to any resistance. However, it is possible to proceed in the analysis by introducing a simplification. In particular, by neglecting the dynamics associated to the pipes, the resulting circuit would read as Fig. 6.3.

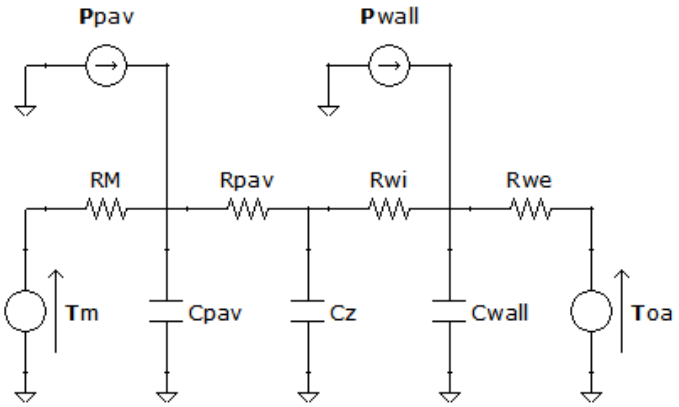

Fig. 6.3: System electrical equivalent neglecting the pipe dynamics

In this case, the new resistance R_M would assume a different value from the corresponding resistance R_{mpav} of the real equivalent circuit, but we are not interested in its particular value for this analysis. In this new simplified circuit, it is possible to perform the same passages done for J(s) and obtain the circuit in Fig. 6.4.

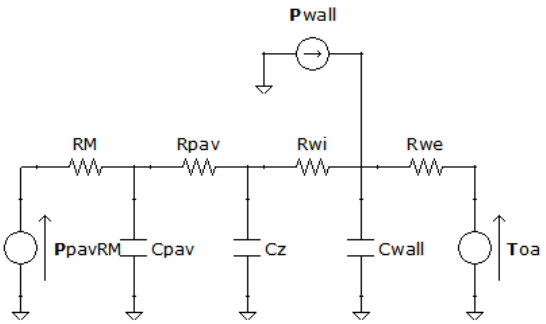

Fig. 6.4: System electrical equivalent, K(s) analysis

By following similar conclusions, it can be said that:

$$K(s) = \frac{T_z(s)}{P_{Pav}(s)} = \frac{T_z(s)}{P_{Pav}(s) * R_M} * R_M = G(s) * R_M$$

Of course, this relationship is not truly valid in our model, because it could be obtained only by neglecting the pipe dynamics. However, if those dynamics were negligible, the transfer function K(s) would result equal to the known transfer function G(s) but with a different gain. Now, it can be said that the dynamics of the pipe are associated to the high frequency component of the transfer function G(s): this is because after a change in the inlet water temperature T_M – that is the input of G(s) – the pipe is the thermal body that changes its temperature faster than any other thermal body. It is possible then that by neglecting the pipe dynamics, the equivalence $K(s) = G(s) * R_M$ is valid but only in the low frequency domain.

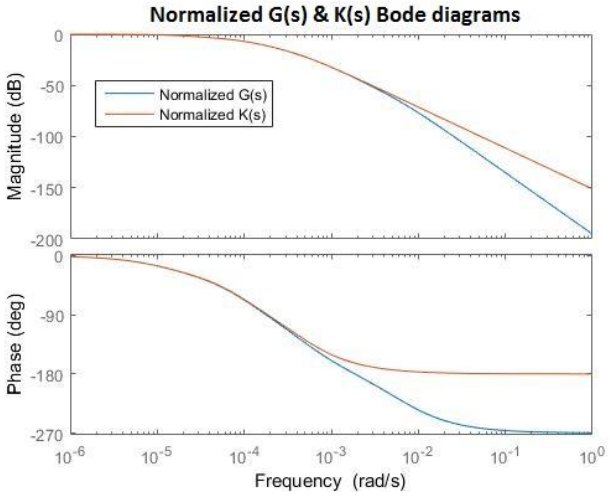

Fig. 6.5: Comparison of the dynamic part of G(s) and K(s)

The result in Fig. 6.5 supports this last statement. In this figure the Bode diagrams of $\frac{G(s)}{G_0}$ and of $\frac{K(s)}{K_0}$ – i.e. the transfer functions normalized on their respective gains – of a random

room have been plotted. As it can be seen, those diagrams are equivalent in a low frequency range. However, to validate completely the $K(s) \approx \alpha G(s)$ approximation, a test campaign was conducted over the 39 representative rooms and limit cases. For each room, the frequency at which the difference between the two Bode diagrams reached the 10% was found, for both the magnitude and the phase diagrams. The results are presented in Fig. 6.6.

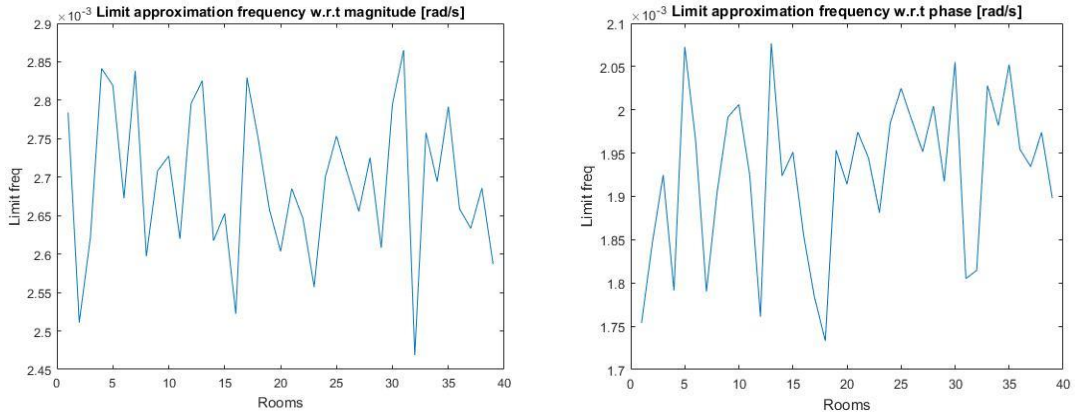

Fig. 6.6: Limit frequency to approximate the dynamics of K(s) to the dynamics of G(s)

The phase diagram poses a more stringent bound on the maximum frequency by which the approximation $K(s) \approx \alpha G(s)$ can be made with respect to the magnitude diagram. Anyway, each room has a small variation on its relative limit frequency. By taking an overall limit frequency of $1.7 * 10^{-3}\ {}^{rad}/_{s}$, the approximation $K(s) \approx \alpha G(s)$ can be accepted. The last significant frequency of the real outside air temperature profile analyzed in section 3.e.2 was $4{,}4e^{-4}\,{}^{rad}/_{s}$. Even if the P_{Pav} dynamics can result faster than the T_{OA} dynamics, the overall limit frequency $1.7 * 10^{-3}\ {}^{rad}/_{s}$ is higher enough to allow the proposed approximation in a simplified approach.

6.a.3 Conclusions on the solar radiation transfer functions

From the previous analyses, it can be concluded that the effect of the solar radiation can be approximated with the dynamics of the known G(s) and H(s) transfer functions. In particular, the dynamics of effect of the solar radiation through the walls (respectively, the pavement) – represented by P_{Wall} and its transfer function J(s) (respectively, P_{Pav} and K(s)) – can be approximated with the dynamics of H(s) (respectively, G(s)). This approximation concerns only the dynamic part of the transfer functions, since their gain is always changed.

A summary scheme of the system affected by the three inputs T_M, T_{OA} and W_{Sol} is presented in Fig. 6.7, with $V(t) = \frac{P_{Pav}(t)}{W_{Sol}(t)}$ and $W(t) = \frac{P_{Wall}(t)}{W_{Sol}(t)}$.

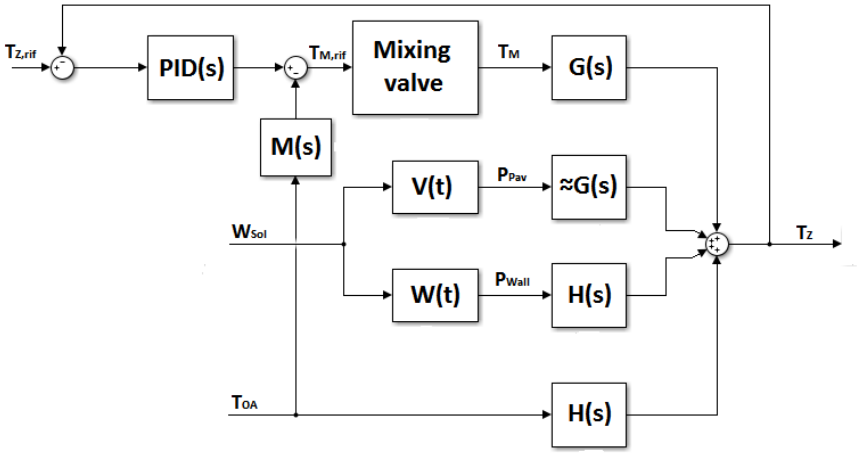

Fig. 6.7: Block diagram of the system affected even by the solar radiation disturbance

The system is then approximately characterized by only two transfer functions – G(s) and H(s) – when considering the two disturbances T_{OA} and W_{Sol}. This conclusion will serve to present the solar radiation compensator concept in section 6.c and can lay the basis to a deeper study of the compensation of this disturbance.

6.b Solar radiation effect on M(s)

This discursive section is dedicated to the possible effects that the solar radiation can have on the adaptive tuning algorithms presented in chapter 5. For time reasons, these effects will not be simulated and tested, but only discussed to serve as a possible future development of this topic. The section is divided into three sub-sections, each one focused on a compensator M(s) parameter tuning. A fourth sub-section is then used to wrap up all the analyses and give a summary conclusion.

6.b.1 M(s) gain

Referring to the tuning strategy of section 5.b.2, this parameter is tuned by exploiting the complementarity of G_0 and H_0 with the formula:

$$G_0 = \frac{mean(T_Z) - mean(T_{OA})}{mean(T_M) - mean(T_{OA})}$$

The complementarity of these two gains is still valid after the introduction of the solar

radiation disturbance. This can be easily verified in the equivalent circuit presented in Fig. 6.1 of the previous section. The introduction of the two current generators related to P_{Wall} and P_{Pav} doesn't change the proof of the complementarity of the gains discussed in section 4.b.1. However, the balance $\overline{T_Z} = G_0\overline{T_M} + H_0\overline{T_{OA}}$ used to develop the G_0 refinement formula is no more valid. The steady state of $\overline{T_Z}$ is not influenced only by $\overline{T_M}$ and $\overline{T_{OA}}$ but also by the solar radiation contribution, resulting in the balance:

$$\overline{T_Z} = G_0\overline{T_M} + H_0\overline{T_{OA}} + J_0\overline{P_{Wall}} + K_0\overline{P_{Pav}}$$

By computing the gain G_0 from the combination of this balance and the relationship $G_0 + H_0 = 1$, the following formula is obtained:

$$G_0 = \frac{mean(T_Z) - mean(T_{OA})}{mean(T_M) - mean(T_{OA})} - \frac{J_0 mean(P_{Wall}) + K_0 mean(P_{Pav})}{mean(T_M) - mean(T_{OA})}$$

that has an additional term $-\frac{J_0 mean(P_{Wall}) + K_0 mean(P_{Pav})}{mean(T_M) - mean(T_{OA})}$ with respect to the formerly presented formula. This term, however, is not computable. It means that the only formula that is practically applicable is $G_0 = \frac{mean(T_Z) - mean(T_{OA})}{mean(T_M) - mean(T_{OA})}$ by neglecting the additional term. This will for sure lead to an error in the resulting G_0. The objective should be to minimize this error, and this can be done by performing the computation $G_0 = \frac{mean(T_Z) - mean(T_{OA})}{mean(T_M) - mean(T_{OA})}$ when the disturbances P_{Wall} and P_{Pav} are negligible, i.e. in a cloudy/rainy day.

6.b.2 M(s) zero

The tuning strategy presented for the compensator zero T_M in section 5.b.2 is based on the correlation between this quantity and the identified time constant τ_G. This latter parameter is unlikely to be relevantly affected by the solar radiation, thus its accuracy should not be compromised, even in presence of non-negligible P_{Wall} and P_{Pav} disturbances. Anyway, performing the G(s) identification procedures when P_{Wall} and P_{Pav} are negligible would improve the quality of the result, so this approach should be preferred when possible.

6.b.3 M(s) pole

To tune this compensator parameters, two different approaches have been proposed. One is based on the identified time constant τ_H (section 5.b.3.1) and the other is based on the thermal lag, that is measured in open loop (section 5.b.3.2) or in closed loop (section 5.b.3.3).

The τ_H based approach is vulnerable to the solar radiation effect. This is because, to properly perform the open loop identification of H(s), a good estimation of the gain of G(s) is needed. This estimation, however, is done with the formula $G_0 = \frac{mean(T_Z) - mean(T_{OA})}{mean(T_M) - mean(T_{OA})}$, that turned out to be incorrect in case of non-negligible solar radiation contribution (section 6.b.1). Depending on the result of this G(s) gain estimation, the quality of the H(s) estimation can result unacceptable. Unless a good estimation of G_0 is granted – for example, the gain G_0 has been estimated during a cloudy day – this tuning method is not recommended.

The other approach to tune the pole τ_M exploits the thermal lag measurement. The thermal lag can be influenced by the solar radiation as well. This is because the different disturbances acting on T_Z could deviate its maximum temperature peak so that the thermal lag measured will not be related only to H(s). In this section, a study on a simplified case is presented to exemplify the effect of the solar radiation on the thermal lag.

First, some simplification hypotheses are introduced:

- The P_{Wall} disturbance is a sinusoid isofrequential to the outside air temperature sinusoidal profile, i.e. 24 hours.
- The P_{Pav} disturbance is negligible with respect to the other inputs.

Under these hypotheses, let's represent the two disturbances as:

$$T_{oa} = a * \sin(\omega t)$$
$$P_{wall} = b * \sin(\omega t + \varphi)$$

For simplicity, the phase of T_{oa} has been set to zero. The effect of these two disturbances on T_Z with the system in open loop can be written as:

$$T_z|_{Toa} = c * \sin(\omega t + phase\big(H(j\omega)\big)) \quad with\ c = a * |H(j\omega)|$$
$$T_z|_{Pwall} = d * \sin(\omega t + \varphi + phase\big(J(j\omega)\big)) \quad with\ d = b * |J(j\omega)|$$

Now, since the dynamic part of J(s) has been proven to be equal to the dynamic part of H(s), the following equivalence holds:

$$phase\big(H(j\omega)\big) = phase\big(J(j\omega)\big) = \delta$$

It is possible to rewrite the complete T_Z profile as:

$$T_z = T_z|_{Toa} + T_z|_{Pwall} = c * \sin(\omega t + \delta) + d * \sin(\omega t + \varphi + \delta)$$

Since T_z is composed of two isofrequential sinusoids, it is possible to combine them together as:

$$T_z = A * \sin(\omega t + \theta + \delta)$$

with $A = \sqrt{c^2 + d^2 + 2cd * \cos(\tau)}$ and $\theta = arctg(\frac{d*sen(\varphi)}{c+d*\cos(\varphi)})$.

If the term θ is negligible, the measured thermal lag between T_{oa} and T_Z will be δ, i.e. the thermal lag due to the action of H(s) only. Let's analyze the behavior of θ in function of the parameter φ – i.e. the phase delay between the T_{oa} and P_{wall} sinusoids – and the ratio between the amplitude of $T_z|_{Toa}$ and $T_z|_{Pwall}$ – i.e. $\frac{d}{c}$. The term $\frac{d}{c}$ represents the ratio between the magnitude effect of P_{wall} on T_Z and the magnitude effect of T_{oa} on T_Z, meaning that a low $\frac{d}{c}$ ratio represents the prevalence of the effect of T_{oa} with respect to P_{wall}.

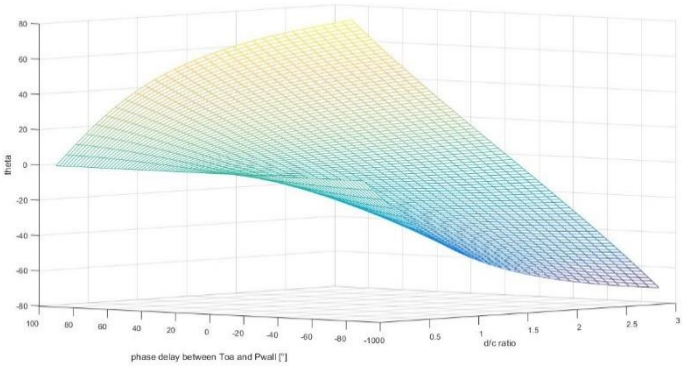

Fig. 6.8: Analysis of the theta term in function of phi and d/c

The Fig. 6.8 represents the tridimensional surface of the function $\theta = f(\varphi, \frac{d}{c})$. The combination of high values of both $\frac{d}{c}$ and φ can result in high values of θ. In Fig. 6.9 the combinations $[\varphi, \frac{d}{c}]$ returning a value $\theta < 10°$ - i.e. a negligible value of θ –are presented in red. If the phase difference φ is less than 20°C (corresponding to 1 hour and 20 minutes) then the parameter θ results negligible for any value of the $\frac{d}{c}$ ratio.

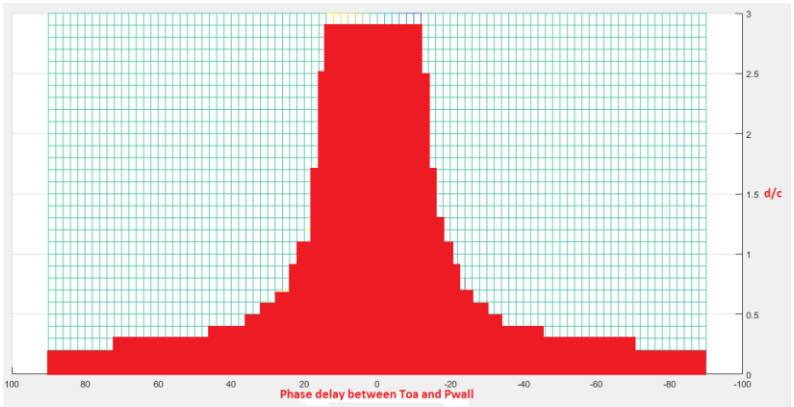

Fig. 6.9: combinations of phi and d/c that return a negligible theta term

6.b.4 Conclusions on the solar radiation effect on M(s)

From the previous sub-sections, different issues have been highlighted. The T_M tuning procedure is reasonably not affected by the solar radiation, while the thermal lag based τ_M tuning procedure can be more or less affected. The formula for the estimation of G(s) gain, however, has shown a possible weakness to the solar radiation effect. This estimated gain is used both for the compensator gain tuning and for the H(s) open loop identification.

In conclusion, the tuning strategies presented in this thesis should be tested on a system affected by the solar radiation to verify its robustness and in case be updated. However, the tuning strategies remain valid under the hypothesis of negligible solar radiation contribution, so they can be simply used as long as the weather remains cloudy during the measurement phase.

6.c Solar radiation compensator idea

In this section, a suggestion for a solar radiation compensator is proposed. For time reasons, this topic was not treated more in depth and no actual tests were done to evaluate the performances of such compensator. However, its concept is explained in order to lay the basis for an eventual future development. The proposed compensator is capable of rejecting only one of the two disturbances P_{Wall} and P_{Pav} related to the solar radiation. In case that the compensator is working on the P_{Wall} disturbance, the P_{Pav} disturbance effect must be negligible with respect to P_{Wall} and vice versa. In this section, the case of a compensator for P_{Wall} (i.e. neglecting P_{Pav}) is presented. The same can be done for P_{Pav} (neglecting P_{Wall}), even if this latter case is realistically not so frequent.

Recalling the conclusions of section 6.a.1, the dynamics of J(s) are equal to the dynamics of H(s), while their gains are different:

$$J(s) = \beta * H(s)$$

Assuming the disturbance P_{Wall} measurable, an open loop compensator $-\frac{J(s)}{G(s)}$ similar to the one used for T_{OA} could be adopted. However, the gain of J(s) is still not known. Moreover, the hypothesis of measurability of P_{Wall} is not realistic: the disturbance that can be assumed measurable by a pyranometer is W_{Sol}. Knowing W_{Sol} is just the first step to reconstruct the disturbance P_{Wall}. An estimation of the solar radiation absorption coefficients k_{Wall} and

$k_{Sol,Tr}$, the surfaces $S_{Op,i}$ and $S_{Tr,i}$ (i = north, south, east, west, ceiling) invested by the radiation and the subdivision of the solar radiation $W_{Sol,i}$ (i = north, south, east, west, ceiling) are necessary to compute P_{Wall} from W_{Sol}. This multitude of estimation is too hard to perform with the reduced measures available to our system. Some approximations of $W_{Sol,i}$ have been developed in the literature [REFERENCE tesi Mantovani] but the other parameters would still be unknown. Now, a theoretical procedure to estimate the contribution of all these uncertainties is presented.

First, let's introduce the quantity:

$$VarGainJ(t) = \frac{P_{Wall}(t)}{W_{Sol}(t)} * J_0$$

this quantity is composed of the gain of the transfer function J(s) multiplied by all the factors that transform the measured $W_{Sol}(t)$ into the disturbance $P_{Wall}(t)$. The combination of all these factors is not constant in time because of the varying orientation of the sun. This means that this quantity VarGainJ(t) is not a single value but a time sequence of value defined over 24 hours. This length has been chosen because realistically the sequence would repeat itself over the 2 hours, i.e. the sun travel the same path from one day to another. This path is known to change over the year, but let's assume it constant for the sake of the explanation.

The time sequence VarGainJ(t) will now be estimated. The purpose of this estimation is not to identify separately the contribution of all the components constituting VarGainJ(t), but only the time sequence values themselves. The knowledge of this time sequence VarGainJ(t) combined to the knowledge of H(s) is sufficient to tune the open loop compensator for the solar radiation effect through the walls. This compensator reads:

$$C(s) = -\frac{VarGainJ(t) * \frac{H(s)}{H_0}}{G(s)}$$

It is fed with the measured signal W_{Sol} and its output is added to the output of the PID controller, as it was done with the M(s) compensator of T_{OA}. At the numerator, the quantity $\frac{H(s)}{H_0}$ is used to describe the dynamic part of H(s), which is equal to the dynamic part of J(s).

To identify the time sequence VarGainJ(t), the following hypotheses must hold:

- The disturbance T_{OA} has been sufficiently compensated by M(s) so that its contribution can be considered negligible with respect to P_{Wall}.

- The disturbance P_{Pav} is negligible with respect to P_{Wall}.
- The system can be considered linear.

After this, the steps for the VarGainJ(t) identification are presented:

1. First, the system will eventually reach the pseudo-equilibrium state, i.e. the state in which the only residual oscillations on the zone temperature T_Z are caused by the disturbance P_{Wall} (remember that the other two disturbances P_{Pav} and T_{OA} are considered negligible). In this state, the system is switched to the open loop by memorizing and fixing the last measured value of $T_{M,rif}$. The zone temperature is then writeable as:

$$T_Z = T_M * G_0 + P_{Wall} * J(s)$$

2. The effect of P_{Wall} on T_Z can be isolated and named:

$$T_{Z,PWall} = T_Z - T_M * \widehat{G_0} = P_{Wall} * J(s) = W_{Sol} * VarGainJ(t) * \frac{H(s)}{H_0}$$

3. A fictitious profile is now computed assuming that VarGainJ(t)=1. In that case, the effect of W_{Sol} on T_Z would read:

$$T_{Z,VJ1} = W_{Sol} * \frac{H(s)}{H_0}$$

   and this profile is obtainable by combining the measurement of W_{Sol} and the estimation of $H(s)$.

4. If the system under analysis is linear, then by changing the input by a scale factor, the output will change only by a scale factor too. In this case, the system is $\frac{H(s)}{H_0}$ that has been fed one time with the input $W_{Sol} * VarGainJ(t)$ to obtain the output $T_{Z,PWall}$ and another time with the input W_{Sol} to obtain the output $T_{Z,VJ1}$. Thus, the following relationship holds:

$$T_{Z,PWall} = VarGainJ(t) * T_{Z,VJ1}$$

   It is then possible to compute the time sequence VarGainJ(t) from the ratio between the two profiles $T_{Z,PWall}$ and $T_{Z,VJ1}$, as representatively reported in Fig. 6.10.

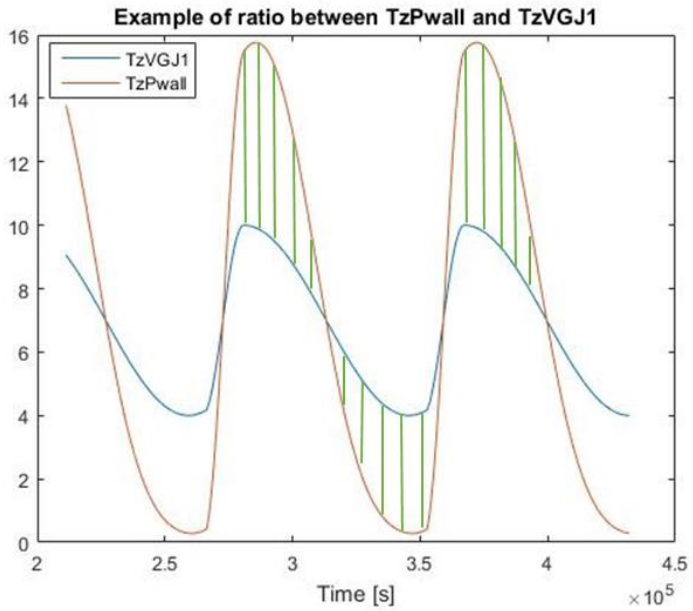

Fig. 6.10: Graphic representation of the VarGainJ(t) term

6.d Chapter 6 conclusions

The two transfer functions associated to the solar radiation impact on the room model have been studied in section 6.a, concluding that the dynamic part of both of them are equal (or approximated at low frequency) to the already known G(s) and H(s) transfer functions. This conclusion was exploited to suggest an idea for the solar radiation compensation in section 6.c. The expected effect of the solar radiation on the adaptive tuning algorithms of chapter 5 has been described in section 6.b. It was concluded that some tuning methods (T_M with τ_G and τ_M with thermal lag, under some conditions) should be robust to the introduction of this new disturbance, while others might turn out inadequate (G_0 estimation refinement failure→ impossible to estimate H(s) and tune τ_M with τ_H). Since the tuning strategies require between 1 to 3 days to be successfully completed, it is advisable to perform them with a cloudy or rainy weather. Any improvement of the robustness of the procedures to the solar radiation can be studied in a future development, starting from the considerations presented in this chapter.

PAGE INTENTIONALLY LEFT BLANK

7. FAULTS

The current chapter is dedicated to the analysis of the radiant panel heating system under some specific faults. In all the thesis work an hypothesis of perfect measurement has been implied, meaning that the sensors for T_Z, T_M and T_{OA} were considered infallible and exact. This hypothesis will be maintained in the first fault analysis of section 7.a, which concerns the mixing valve. The second section 7.b will then deal with a fault on the T_M sensor. Many undesired behaviors can result from a fault on that sensor, thus concluding the high importance of its good functioning.

The fault of the T_Z and T_{OA} sensors will not be considered because their effect is easily deducible and impossible to detect without some sensor redundancy or internal measurement reliability identification. One easy way to detect a possible malfunctioning of one of the three sensors T_Z, T_M and T_{OA} is quickly presented here. That is the persistence of one of the following relationships:

$$1.)\ T_Z > T_M > T_{OA}\ or\ T_Z > T_{OA} > T_M$$
$$2.)\ T_Z < T_M < T_{OA}\ or\ T_Z < T_{OA} < T_M$$

The first couple would imply that the zone temperature T_Z has been heated up by a third input/heat source not considered in our model, while the second couple would imply that the zone temperature T_Z has been heated up by a third input/cooling source.

In this chapter, equality relationships such as $T_{M,rif} = T_M$ will be used frequently. This equality notation is not to be intended strictly, because it would be impossible to have a perfect equivalence between two real values. It is always implicit a reasonably small margin for the equivalence to be verified.

7.a Mixing valve fault

This section is dedicated to the fault of the mixing valve, in particular to the impossibility to reach a desired valve position $X_{V,rif} \in [0,1]$. This kind of fault will be referred to as "valve stuck fault" from now on. It is made no difference whether this fault is caused by a mechanical jam, an electronic failure or any other factor.

First, it is assumed that there is no feedback information on the position of the valve, i.e. the valve actuator receives the valve position set-point $X_{V,rif}$ and operates in open loop to generate the actual valve position X_V. If such feedback was available, then to verify an eventual mixing valve fault it would just be necessary to check whether the X_V value eventually reaches $X_{V,rif} \in [0,1]$ or it stabilizes to a constant value $\overline{X_V} \neq X_{V,rif} \in [0,1]$. By assuming that this feedback is not available, to establish a valve stuck fault it will be necessary to refer to the other available measures of the system. However, the symptoms associated to this fault can be caused by other factors, thus generating an indecision in the diagnosis which will soon be analyzed.

The valve stuck fault can occur in two different modalities, each one characterized by its symptoms: "valve stuck open", when $\overline{X_V} > X_{V,rif}$ causing an overheating of the system with respect to the desired behavior, and "valve stuck closed" when $\overline{X_V} < X_{V,rif}$. The analysis of these two modalities of the valve stuck fault is carried on below:

- Valve stuck open: in this case, the inlet water temperature measure and set point will reflect the relationship $T_M > T_{M,rif}$ and, if the set point $T_{M,rif}$ is consistent with the desired zone temperature set point, the system will overheat and cause a thermal discomfort. The intensity of this discomfort will be directly related to the gap between $\overline{X_V}$ and $X_{V,rif}$. As the fault persists, the inlet water temperature set point $T_{M,rif}$ will reach its lower bound $T_{M,rif,MIN} = 20°C$. That is because the PID will be constantly fed with a negative error $e = T_{Z,rif} - T_Z$ that will cause its integral action saturation. This in turn will correspond to a valve position set point $X_{V,rif} = 0$. When this scenario $T_M > T_{M,rif} = 20°C$ && $X_{V,rif} = 0$ is persisting from a sufficiently long period, the fault can be declared. The period chosen for the fault to be identified is weighted on two factors: a short time leads to a quicker fault detection, but in turn increases the possible occurrence of false alarms. That is

because, recalling the mixing valve functioning, it is not possible to force a cooling action on the inlet water temperature T_M. If a cooling action is desired, it will be necessary to wait for the heat dispersion from the pipeline to the zone temperature to occur. This process can take a variable amount of time depending on the environmental conditions. Anyway, in case that the fault alarm is not a bothering factor for the user – for example, a simple alarm icon is displayed on the control panel – a relatively short diagnosis time is preferable.

The symptomatology of this valve stuck open fault can however be confused with another scenario. By setting the zone temperature to an unacceptably low value, the inlet water temperature set point $T_{M,rif}$ will still saturate to its lower bound $T_{M,rif,MIN} = 20°C$ even if the valve position as actually reached the value $\overline{X_V} = X_{V,rif} = 0$. The problem is not the mixing valve but the unobtainable zone temperature request. An extreme exemplificative scenario sees a zone temperature set point of 18°C in a room full of people during a sunny day with an average outside air temperature of 17°C. These circumstances will for sure lead to a zone temperature greater than 18°C, causing the previously described symptoms.

- Valve stuck closed: in this case, the inlet water temperature measure and set point will reflect the relationship $T_M < T_{M,rif}$. The intensity of the resulting discomfort will be directly related to the gap between $\overline{X_V}$ and $X_{V,rif}$. Similarly to the previous scenario, as the fault persists the inlet water temperature set point $T_{M,rif}$ will reach its upper bound $T_{M,rif,MAX} = 40°C$ because of the constantly positive error $e = T_{Z,rif} - T_Z$ feeding the PID controller. This in turn will correspond to a valve position set point $X_{V,rif} = 1$.

  Similar considerations can be done about the period in which the conditions $T_M < T_{M,rif} = 40°C$ && $X_{V,rif} = 1$ must hold to declare a fault state of the system. The period related to this fault can however be significantly lower than the period related to the previous fault. This is because in this case the mixing valve has the capability of performing an heating action on the inlet water temperature T_M. A persistence of the condition $T_M < T_{M,rif} = 40°C$ means that the mixing valve is failing to perform its heating action. The period chosen to declare the system fault can be a small multiple of the valve actuator settling time, for example:

$$6 * T_{Settling} = 3 * 5\tau_{Valve} = 30\ minutes$$

This valve stuck closed fault can be confused with a different fault, that is related to the boiler hydraulic circuit. If the boiler provides a water too cold for the mixing valve to perform its action, then the inlet water temperature set point $T_{M,rif}$ will not be respected even if the valve position is kept at its maximum value $X_{V,rif} = 1$. For example, if $T_{M,rif} = 35°C$ starting from a pipeline temperature of 25°C and with a boiler supply water of 30°C, the same symptomatology previously described will sooner or later appear.

It is worth noticing that the valve stuck closed fault cannot be confused with a "zone temperature set point $T_{Z,rif}$ too high" scenario. In fact, if the zone temperature is set to an impossibly high value – for example $T_{Z,rif} = 35°C$ with an average outside temperature of 10°C and one window has been left open – the inlet water temperature T_M will reach its set point $T_{M.rif} = 40°C$ since the mixing valve theoretically has the capability of heating the water to a desired value $\in$[20 , 40]°C range. This scenario can be signaled separately to the user, encouraging him to reduce the zone temperature set point and/or to verify the presence of big heat dispersions – such as an open window.

In conclusion, the valve stuck open case presents the $T_M > T_{M,rif} = 20°C \;\&\&\; X_{V,rif} = 0$ symptoms and can be confused with a "zone temperature set point $T_{Z,rif}$ too low" scenario, while the valve stuck closed case presents the $T_M < T_{M,rif} = 40°C \;\&\&\; X_{V,rif} = 1$ symptoms and can be confused with a "boiler supply water too cold" scenario. The "zone temperature set point $T_{Z,rif}$ too high" scenario is easily identifiable by the persistence of the combination $T_M = T_{M,rif} = 40°C \;\&\&\; T_{Z,rif} > T_Z$.

7.b Inlet water temperature sensor fault

The inlet water temperature T_M sensor fault presents an unexpectedly wide casuistry. The combination of the intensity of the sensor fault and the desired behavior of the system produces a multitude of consequences, which will be listed in this section. For simplicity, the only T_M sensor fault considered is the measurement bias, i.e. the measured value $T_{M,meas}$ differs of a constant offset Δ_M from the real value $T_{M,real}$. The two cases $\Delta_M > 0$ and $\Delta_M < 0$ will be treated separately in section 7.b.1 and 7.b.2 respectively. There is a strong parallelism between the two cases, but a generalization of the two cases into one needs an

complex mathematical notation that would make the comprehension uselessly difficult. A final section 7.b.3 will collect the conclusions on this topic.

This study is built on an explicit reference to the numerical values of the system. These values are:

- Inlet water temperature set point lower bound $T_{M,rif,MIN} = 20°C$
- Inlet water temperature set point upper bound $T_{M,rif,MAX} = 40°C$
- Boiler supply water temperature $T_B = 52°C$

Moreover, to analyze the consequences of this fault on the system performances, a steady state is always considered. The nature of this thermal system rarely allows a steady state to exist, but the conclusions presented are more easily comprehended by assuming this condition. The conclusion are, however, generalizable to a non-steady state scenario.

7.b.1 Positive offset

Two new quantities are defined together with the three values $T_{M,rif,MIN} = 20°C$, $T_{M,rif,MAX} = 40°C$ and $T_B = 52°C$. These two new values are the upper and lower bounds $T_{M,rif,MIN}$ and $T_{M,rif,MAX}$ shifted of the measurement offset Δ_M. During its normal functioning, the system is allowed to set the T_M value in the range [20 , 40]°C. However, when a Δ_M fault occurs, the range in which T_M will take value is [20+Δ_M, 40+Δ_M]°C instead, i.e. contained in the two new quantities introduced before. A graphic representation of these quantities is presented in Fig. 7.1.

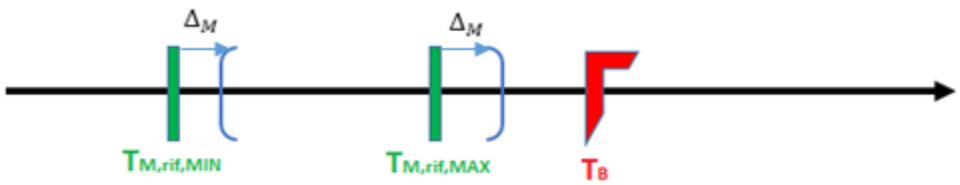

Fig. 7.1: Graphic representation of the effect of the measurement offset

Four different cases are defined depending on the amplitude of the measurement offset $\Delta_M > 0$:

A. $0 < \Delta_M < 12°C$
B. $12 < \Delta_M < 20°C$
C. $20 < \Delta_M < 32°C$
D. $\Delta_M > 32°C$

In each of the four cases, the sensor fault can have different consequences depending on the inlet water temperature that is needed to achieve the zone temperature set point. This ideal value for the inlet water temperature is from now on called $T_{M,needed}$. Different behaviors of the system will result depending on the position of $T_{M,needed}$. The straight line presented in Fig. 7.1 is now updated in Fig. 7.2 with the relative casuistry and thus divided into segments. It is assumed for simplicity that $T_{M,needed}$ cannot be higher than the boiler supply water temperature T_B, because that would occur only if the radiant panel system has been dimensioned very poorly on the room.

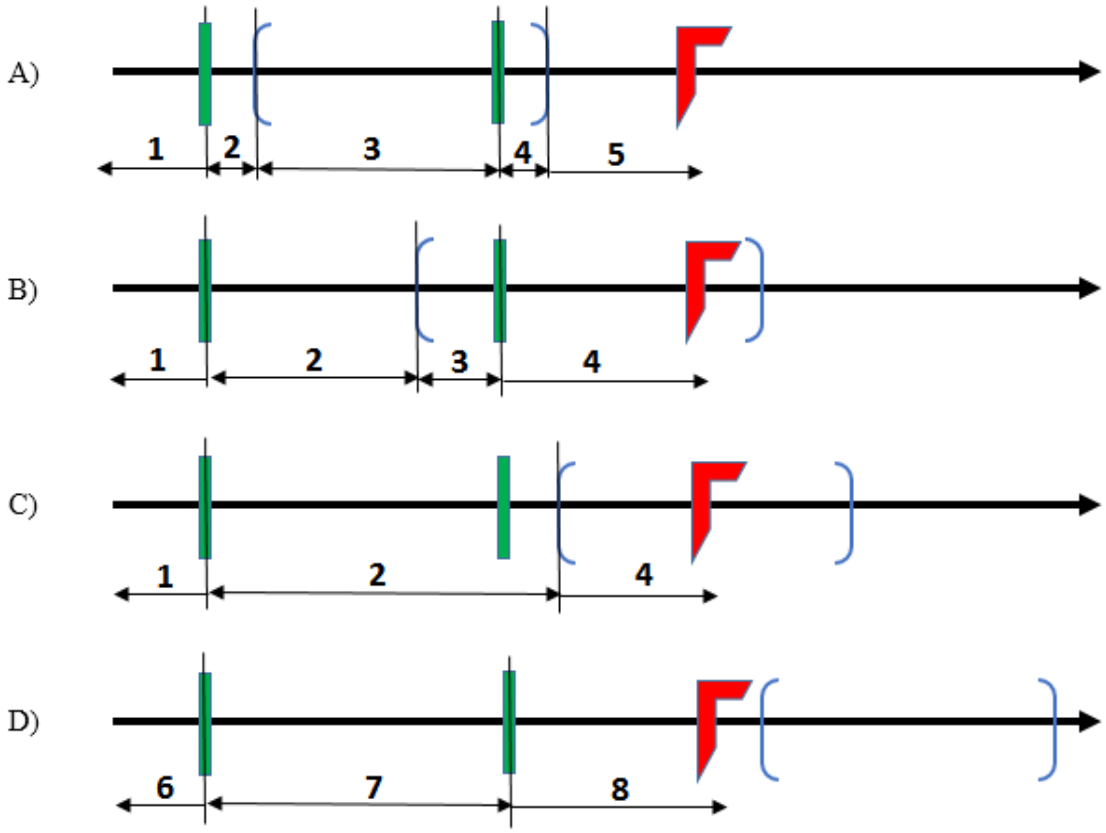

Fig. 7.2: Fault casuistry with positive measurement offset depending on the offset measurement (A-D) and the value of Tm,needed (1–8)

Depending on the position of $T_{M,needed}$ on these straight lines, a particular behavior of the system will follow together with its relative symptomatology. For example, if $0 < \Delta_M < 12°C$ and $T_{M,needed} = 30°C$ the "type 2" behavior will result. The different behaviors are listed in the following Tab. 7.1. The symptomatology ($T_{M,meas}$ and T_Z values) is implicitly related to a persistent state of these relationships: for example, "$T_{M,rif} = T_{M,meas}$" means

that the measured value $T_{M,meas}$ has been found very close to its set point $T_{M,rif}$ for a reasonably long period. The definition of the length of such period is beyond the scope of this analysis.

#	$T_{M,meas}$	T_Z	Description	Detect.
1	$T_{M,rif} = T_{M,meas}$	$T_{Z,rif} < T_Z$	The requested $T_{Z,rif}$ is too low to be obtained even in the "no Δ_M fault" case. However, the obtained performance is poorer because of the Δ_M fault.	NO
2	$T_{M,rif} = T_{M,meas}$	$T_{Z,rif} < T_Z$	The requested $T_{Z,rif}$ can be obtained, but the Δ_M fault impedes it.	NO
3	$T_{M,rif} = T_{M,meas}$	$T_{Z,rif} = T_Z$	The requested performances are fulfilled and the Δ_M fault is masked by the control loop action.	NO
4	$T_{M,rif} = T_{M,meas}$	$T_{Z,rif} = T_Z$	The requested $T_{Z,rif}$ cannot be obtained in a "no Δ_M fault", but the system is pushed beyond its safety limits because of Δ_M and the requested performances are fulfilled.	NO
5	$T_{M,rif} = T_{M,meas}$	$T_{Z,rif} > T_Z$	The system is pushed beyond its safety limits because of Δ_M but the requested $T_{Z,rif}$ is still not obtained.	NO
6	$T_{M,rif} > T_{M,meas}$	$T_{Z,rif} < T_Z$	The same consequences of case #1, but the symptoms are different.	YES
7	$T_{M,rif} > T_{M,meas}$	$T_{Z,rif} < T_Z$	The same consequences of case #2, but the symptoms are different.	YES
8	$T_{M,rif} > T_{M,meas}$	$T_{Z,rif} < T_Z$	The same consequences of case #5, but the symptoms are different.	YES

Tab. 7.1: Fault diagnosis casuistry with positive measurement offset

In the following table Tab. 7.1, a representative numerical case for each combination of Δ_M amplitude (A-D) and resulting consequences (1-8) is presented:

	A	B	C	D
1	$T_{M,need} = 16°C$ $T_{M,rif} = 20°C$ $T_{M,meas} = 20°C$ $T_{M,real} = 25°C$	$T_{M,need} = 16°C$ $T_{M,rif} = 20°C$ $T_{M,meas} = 20°C$ $T_{M,real} = 35°C$	$T_{M,need} = 16°C$ $T_{M,rif} = 20°C$ $T_{M,meas} = 20°C$ $T_{M,real} = 35°C$	
2	$T_{M,need} = 22°C$ $T_{M,rif} = 20°C$	$T_{M,need} = 22°C$ $T_{M,rif} = 20°C$	$T_{M,need} = 22°C$ $T_{M,rif} = 20°C$	

	$T_{M,meas} = 20°C$ $T_{M,real} = 25°C$	$T_{M,meas} = 20°C$ $T_{M,real} = 35°C$	$T_{M,meas} = 20°C$ $T_{M,real} = 45°C$	
3	$T_{M,need} = 38°C$ $T_{M,rif} = 33°C$ $T_{M,meas} = 33°C$ $T_{M,real} = 38°C$	$T_{M,need} = 38°C$ $T_{M,rif} = 23°C$ $T_{M,meas} = 23°C$ $T_{M,real} = 38°C$		
4	$T_{M,need} = 42°C$ $T_{M,rif} = 37°C$ $T_{M,meas} = 37°C$ $T_{M,real} = 42°C$	$T_{M,need} = 42°C$ $T_{M,rif} = 27°C$ $T_{M,meas} = 27°C$ $T_{M,real} = 42°C$	$T_{M,need} = 48°C$ $T_{M,rif} = 23°C$ $T_{M,meas} = 23°C$ $T_{M,real} = 48°C$	
5	$T_{M,need} = 12°C$ $T_{M,rif} = 20°C$ $T_{M,meas} = 20°C$ $T_{M,real} = 15°C$			
6				$T_{M,need} = 42°C$ $T_{M,rif} = 20°C$ $T_{M,meas} = 12°C$ $T_{M,real} = 52°C$
7				$T_{M,need} = 22°C$ $T_{M,rif} = 40°C$ $T_{M,meas} = 45°C$ $T_{M,real} = 10°C$
8				$T_{M,need} = 12°C$ $T_{M,rif} = 40°C$ $T_{M,meas} = 45°C$ $T_{M,real} = 10°C$

Tab. 7.2: Fault examples casuistry with positive measurement offset

Some of the cases presented in table Tab. 7.2 will now be explained in detail to understand the behavior of this fault:

- Case 1A: as explained for the "type 1 consequence" in table Tab. 7.1, the requested $T_{Z,rif}$ is too low to be obtained even in the "no Δ_M fault" case but the obtained

performance is poorer because of the Δ_M fault. This is because, considering a $\Delta_M = 5°C$ case, the system will see a $T_{M,real} = 25°C$ as a $T_{M,meas} = 20°C$. The value for T_M cannot be set lower than 20°C so the system will stuck the $T_{M,ref}$ at this point, being convinced that it is doing the best it can. The needed $T_{M,need}$ is too low to be imposed anyway, but with a $T_{M,real} = 20°C$ (i.e. with no Δ_M fault) the obtained performance would have been better.

- Case 2B: as explained for the "type 2 consequence" in table Tab. 7.1, the requested $T_{Z,rif}$ can be obtained but the Δ_M fault impedes it. This case is similar to the previous analyzed case 1A, but here the $T_{M,need}$ value is acceptable – i.e. belongs to the [20 , 40]°C range – so this case is impeding an otherwise obtainable performance.
- Case 3A: if the radiant panel has been dimensioned correctly and the offset Δ_M is small, this is the case that will mostly occur. As explained for the "type 3 consequence" in table Tab. 7.1, the requested performances are fulfilled and the Δ_M fault is masked by the control loop action. This is because, considering a $\Delta_M = 5°C$ case, the system will be able to set a $T_{M,real} = 38°C = T_{M,need}$ because it measures a $T_{M,meas} = 33°C$ that is contained in the boundaries range [20 , 40]°C of $T_{M,rif}$.
- Case 4C: as explained for the "type 4 consequence" in table Tab. 7.1, the requested $T_{Z,rif}$ cannot be obtained in a "no Δ_M fault", but the system is pushed beyond its safety limits because of Δ_M and the requested performances are fulfilled. This case is similar to the previous analyzed case 3A, but here the $T_{M,real} = T_{M,need}$ is set to a theoretically unacceptable value of 48°C.
- Case 5A: as explained for the "type 5 consequence" in table Tab. 7.1, the system is pushed beyond its safety limits because of Δ_M but the requested $T_{Z,rif}$ is still not obtained. Thanks to the $\Delta_M = 5°C$ measurement offset, the measured $T_{M,meas} = 40°C$ appears to be acceptable even if the real value is $T_{M,real} = 45°C$, thus theoretically unacceptable. However, this boundary violation is still not enough to fulfill the request $T_{M,need} = 48°C$.
- Case 6D/7D/8D: apart from the request $T_{M,need}$ value, the dynamic in these cases is the same. Because of the elevated measurement offset $\Delta_M = 40°C$, any value set from the PID to $T_{M,rif}$ will cause the valve PI to be fed with a positive error $e = T_{M,rif} - T_{M,meas}$. That is because $T_{M,real}$ cannot be bigger than the boiler supply water temperature $T_B = 52°C$, and thus the measured $T_{M,meas}$ cannot be bigger than $52 -$

$\Delta_M = 12°C$. The positive error feeding the valve PI will make the valve set to a fully open position $X_V = 1$, causing for sure a system overheating.

In conclusion, the detectability of each case is discussed:

- The symptoms of the "type 1" and "type 2" cases can be caused by an excessively low $T_{Z,rif}$ value. The range of the obtainable $T_{Z,rif}$ values depends on the physical characteristics of the whole room system, so there is no a priori way to decide if the symptoms were caused by a sensor fault or by an excessively low $T_{Z,rif}$.
- The "type 3" and "type 4" cases cannot be detected since the measurement error Δ_M is masked.
- The symptoms of the "type 5" case can be caused by an excessively high $T_{Z,rif}$ value, resulting in an indecisive diagnosis similar to the "type 1" and "type 2" cases.
- The fault with $\Delta_M > 32°C$ ("type 6", "type 7" and "type 8" cases) is the only one that can be detected and isolated thanks to the logic conflict of its symptoms $T_{M,rif} > T_M$ and $T_{Z,rif} > T_Z$.

7.b.2 Negative offset

This case will be treated in a less discursive way because of its strong parallelism with the "positive offset" case.

Four different cases are defined depending on the amplitude of the measurement offset $\Delta_M > 0$:

A. $-10 < \Delta_M < 0°C$
B. $-20 < \Delta_M < -10°C$
C. $-30 < \Delta_M < -20°C$
D. $\Delta_M < -30°C$

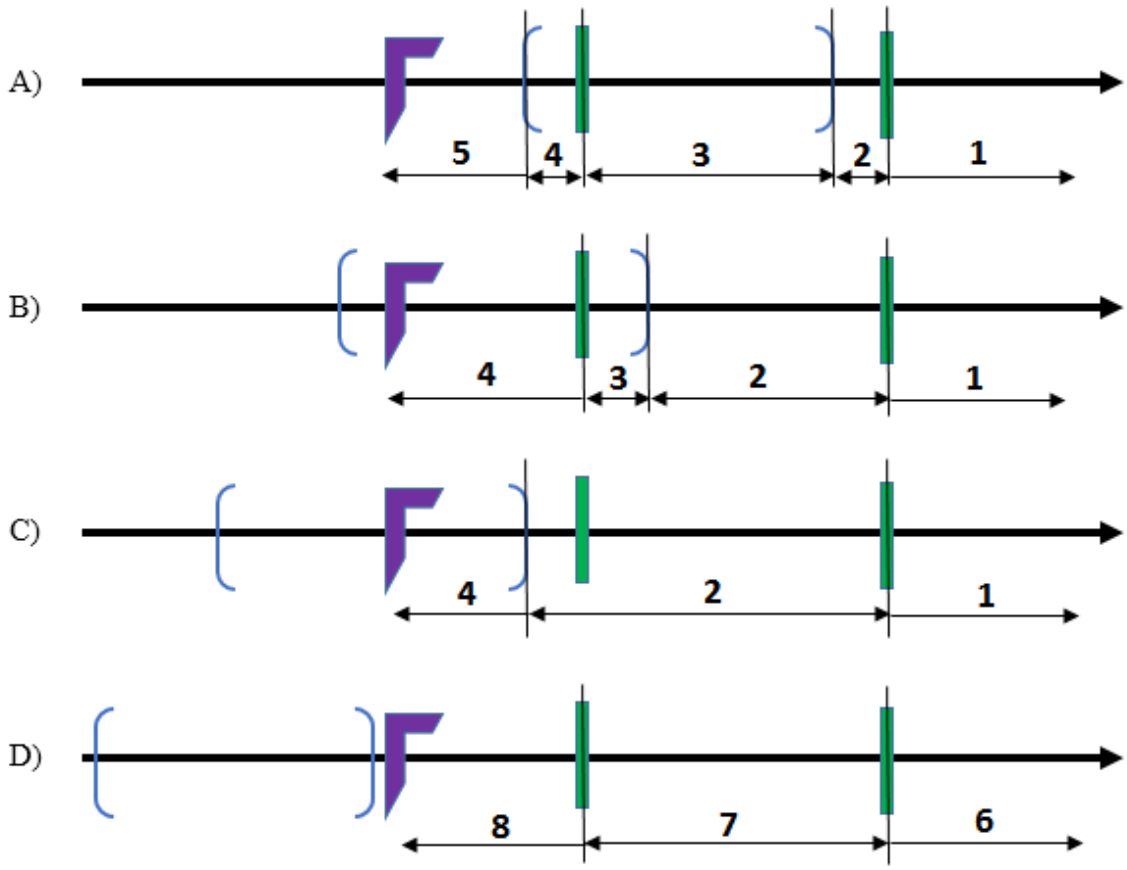

Fig. 7.3: Fault casuistry with negative measurement offset depending on the offset measurement (A-D) and the value of Tm,needed (1–8)

These four cases are represented in Fig. 7.3. In each of these four cases, the sensor fault can have different consequences depending on the inlet water temperature that is needed to achieve the zone temperature set point, i.e. $T_{M,needed}$. It is assumed for simplicity that $T_{M,needed}$ cannot be lower than a certain T_{MIN} value that is the temperature that the whole

room would reach if the system was turned off . This T_{MIN} value can be interpreted as the maximum cooling temperature reachable by T_M, i.e. the symmetrical of the T_B temperature exploited in the "positive offset" analysis which was the maximum heating temperature reachable by T_M.

Depending on the position of $T_{M,needed}$ on these straight lines, a particular behavior of the system will follow together with its relative symptomatology. These behaviors are perfectly symmetrical with respect to the "positive offset" casuistry. The only difference with respect to the table Tab. 7.3: Fault diagnosis casuistry with negative measurement offsetTab. 7.3 of section 7.b.1 is in the T_Z and $T_{M,meas}$ symptom columns.

#	$T_{M,meas}$	T_Z	Description	Detect.
1	$T_{M,rif} = T_{M,meas}$	$T_{Z,rif} > T_Z$	The requested $T_{Z,rif}$ is too **high** to be obtained even in the "no Δ_M fault" case. However, the obtained performance is poorer because of the Δ_M fault.	NO
2	$T_{M,rif} = T_{M,meas}$	$T_{Z,rif} > T_Z$	The requested $T_{Z,rif}$ can be obtained, but the Δ_M fault impedes it.	NO
3	$T_{M,rif} = T_{M,meas}$	$T_{Z,rif} = T_Z$	The requested performances are fulfilled and the Δ_M fault is masked by the control loop action.	NO
4	$T_{M,rif} = T_{M,meas}$	$T_{Z,rif} = T_Z$	The requested $T_{Z,rif}$ cannot be obtained in a "no Δ_M fault", but the system is pushed beyond its safety limits because of Δ_M and the requested performances are fulfilled.	NO
5	$T_{M,rif} = T_{M,meas}$	$T_{Z,rif} < T_Z$	The system is pushed beyond its safety limits because of Δ_M but the requested $T_{Z,rif}$ is still not obtained.	NO
6	$T_{M,rif} < T_{M,meas}$	$T_{Z,rif} > T_Z$	The same consequences of case #1, but the symptoms are different.	YES
7	$T_{M,rif} < T_{M,meas}$	$T_{Z,rif} > T_Z$	The same consequences of case #2, but the symptoms are different.	YES
8	$T_{M,rif} < T_{M,meas}$	$T_{Z,rif} > T_Z$	The same consequences of case #5, but the symptoms are different.	YES

Tab. 7.3: Fault diagnosis casuistry with negative measurement offset

In the following table Tab. 7.4, a representative numerical case for each combination of Δ_M amplitude (A-D) and resulting consequences (1-8) is presented:

	A	B	C	D
1	$T_{M,need} = 42°C$ $T_{M,rif} = 40°C$ $T_{M,meas} = 40°C$ $T_{M,real} = 35°C$	$T_{M,need} = 42°C$ $T_{M,rif} = 40°C$ $T_{M,meas} = 40°C$ $T_{M,real} = 25°C$	$T_{M,need} = 42°C$ $T_{M,rif} = 40°C$ $T_{M,meas} = 40°C$ $T_{M,real} = 15°C$	
2	$T_{M,need} = 37°C$ $T_{M,rif} = 40°C$ $T_{M,meas} = 40°C$ $T_{M,real} = 35°C$	$T_{M,need} = 37°C$ $T_{M,rif} = 40°C$ $T_{M,meas} = 40°C$ $T_{M,real} = 25°C$	$T_{M,need} = 37°C$ $T_{M,rif} = 40°C$ $T_{M,meas} = 40°C$ $T_{M,real} = 15°C$	
3	$T_{M,need} = 22°C$ $T_{M,rif} = 27°C$ $T_{M,meas} = 27°C$ $T_{M,real} = 22°C$	$T_{M,need} = 22°C$ $T_{M,rif} = 37°C$ $T_{M,meas} = 37°C$ $T_{M,real} = 22°C$		
4	$T_{M,need} = 17°C$ $T_{M,rif} = 22°C$ $T_{M,meas} = 22°C$ $T_{M,real} = 17°C$	$T_{M,need} = 17°C$ $T_{M,rif} = 32°C$ $T_{M,meas} = 32°C$ $T_{M,real} = 17°C$	$T_{M,need} = 12°C$ $T_{M,rif} = 37°C$ $T_{M,meas} = 37°C$ $T_{M,real} = 12°C$	
5	$T_{M,need} = 48°C$ $T_{M,rif} = 40°C$ $T_{M,meas} = 40°C$ $T_{M,real} = 45°C$			
6				$T_{M,need} = 10°C$ $T_{M,rif} = 20°C$ $T_{M,meas} = 12°C$ $T_{M,real} = 52°C$
7				$T_{M,need} = 22°C$ $T_{M,rif} = 20°C$ $T_{M,meas} = 12°C$ $T_{M,real} = 52°C$
8				$T_{M,need} = 48°C$ $T_{M,rif} = 20°C$

				$T_{M,meas} = 12°C$ $T_{M,real} = 52°C$

Tab. 7.4: Fault examples casuistry with negative measurement offset

The reasoning behind this casuistry and its detectability is the same explained in the previous section 7.b.1.

7.b.3 Conclusions on this fault

The previous detailed analysis has shown different undesired behaviors that could result from a measurement offset on the inlet water temperature sensors. Briefly, such behaviors include:

- Impossibility to reach a certain $T_{Z,rif}$ that is otherwise obtainable in a "no fault" case.
- Setting the real value of the inlet water temperature to a value outside the acceptable range [20 , 40]°C;

The detectability of such fault is possible only in case of a massive measurement offset, i.e. when the measurement offset is bigger than $\min\{ (T_B - T_{M,rif,MIN}) , (T_{Z,MIN} - T_{M,rif,MIN}) \}$. In the other cases, the detectability is not possible. In conclusion, despite apparent harmlessness of this inner loop control sensor, it is recommended to take into account and address this system weakness.

7.c Chapter 7 conclusions

The proposed fault analysis is not comprehensive of all the possible faults of the radiant panel heating system. Two of the most common ones have been analyzed. A mixing valve fault can usually be detected mainly thanks to the persistence of the difference between T_M and its set point $T_{M,rif}$. Conversely, a measurement error on the inlet water temperature T_M sensor is almost never identified and can cause some undesired behaviors. Sensor redundancy or internal measurement reliability identification are recommended to address this weakness.

8. SIMULATIONS

This final chapter is dedicated to the presentation of the simulation results. The previous estimation methods and adaptive tuning algorithms are tested in the Simulink simulation environment. The model adopted is of course the model presented in chapter 2.

The first section 8.a is dedicated to the results of the different G(s) estimation methods. The following section 8.b presents the H(s) estimation method and the third final section 8.c is left for the results of all the seven adaptive tuning algorithms.

8.a G(s) estimation

The three different estimation methods presented in chapter 4 are tested in three different sub-sections: 8.a.1 for the closed loop estimation, 8.a.2 for the open loop and 8.a.3 for the open loop exploiting the H(s) estimation. For each method, different outside air temperature profiles are used, combined with different data collection period. A longer data collection corresponds to a higher estimation accuracy, especially in the open loop procedures. However, if the room is inhabited, this conflicts with the thermal comfort of the user. The data collection phase should then be reduced to the minimum possible to grant satisfactory performances. A future development may strengthen these estimation methods so to obtain the same performances but in shorter time.

The quality of the estimated τ_G is presented along the 39 representative rooms and limit cases and compared to the "real" τ_G value, i.e. the τ_G resulting from a clean identification with no T_{OA} disturbance acting on the system. Therefore, this "real" τ_G value is the best 1-pole approximation of the fourth order transfer function G(s).

8.a.1 G(s) Closed loop

As anticipated in section 4.c.2.1, the factors mainly influencing the outcome of this method are:

- The number of days during which the data set are collected.
- The outside temperature profile.
- The difference $T_{Z,rif} - T_Z(0)$

To evaluate the combined effect of these factors, several tests have been conducted among which the most relevant are reported below. In all the tests, the initial state of the system has been chosen as the state that the system reached after being exposed to the outside temperature profile with the heating panels switched OFF. The zone temperature set-point $T_{Z,rif}$ has been kept constant to 23°C. This means that the difference $T_{Z,rif} - T_Z(0)$ depends on the $T_Z(0)$ value, which in turns depends on the average value of the outside air temperature profile. The realistic outside air temperature profile presented in section 3.e.2 has been adopted in these tests.

- Test 1:

$$\begin{cases} T_{OA} \text{ average: } 8°C \\ T_{OA} \text{ daily range: } \pm 5°C \end{cases}$$

Two cases are presented in which the data have been collected for 5 days or 2 days. The identified time constant τ_G of both those cases is compared with the real τ_G value in Fig. 8.1.

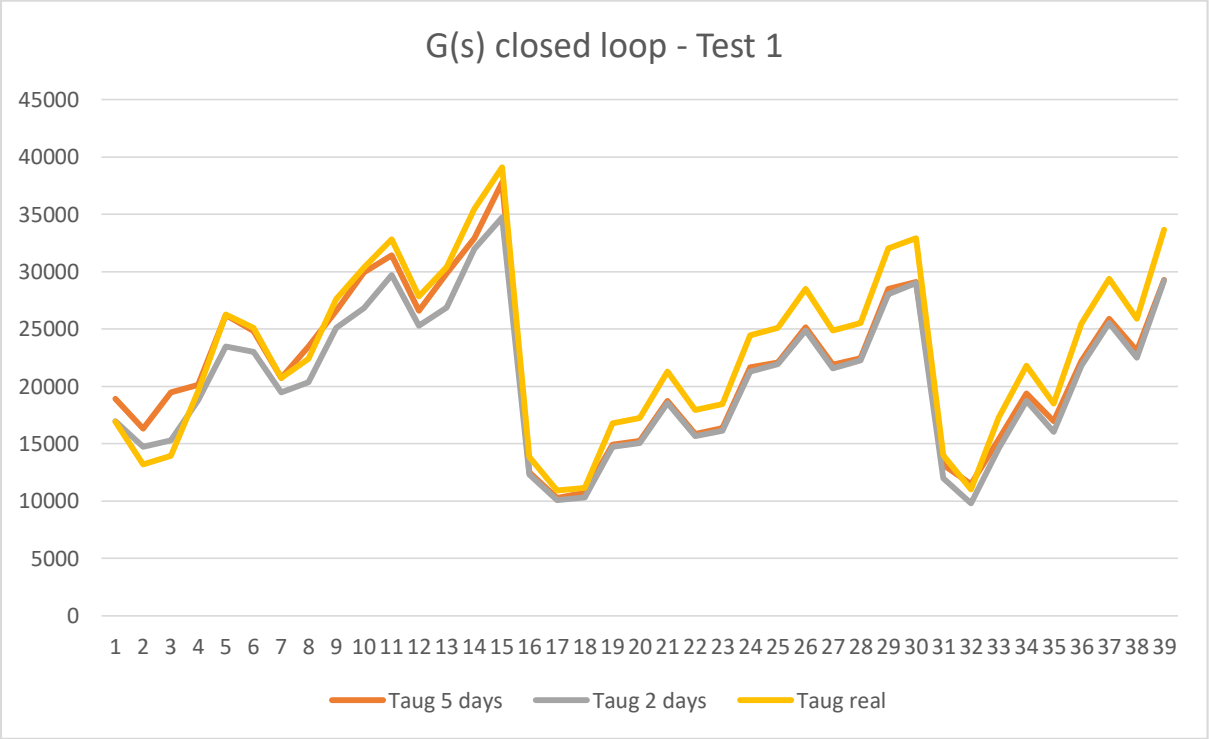

Fig. 8.1: G(s) closed loop estimation, identified time constant accuracy: Test 1

The 5 days data collection grants a better accuracy in almost all the cases, but the improvement is marginal and a 2 days data collection should be preferred.

- Test 2:

$$\begin{cases} T_{OA} \text{ average: } 12°C \\ T_{OA} \text{ daily range: } \pm 6°C \end{cases}$$

This test presents a higher value for the external temperature average and range. This will negatively impact on the estimation, since the initial state $T_Z(0)$ will be higher with respect to the "Test 1" resulting in a smaller difference $T_{Z,rif} - T_Z(0)$.

As for the previous test, two cases are presented in which the data have been collected for 5 days or 2 days. The identified time constant τ_G of both those cases is compared with the real τ_G value in Fig. 8.2.

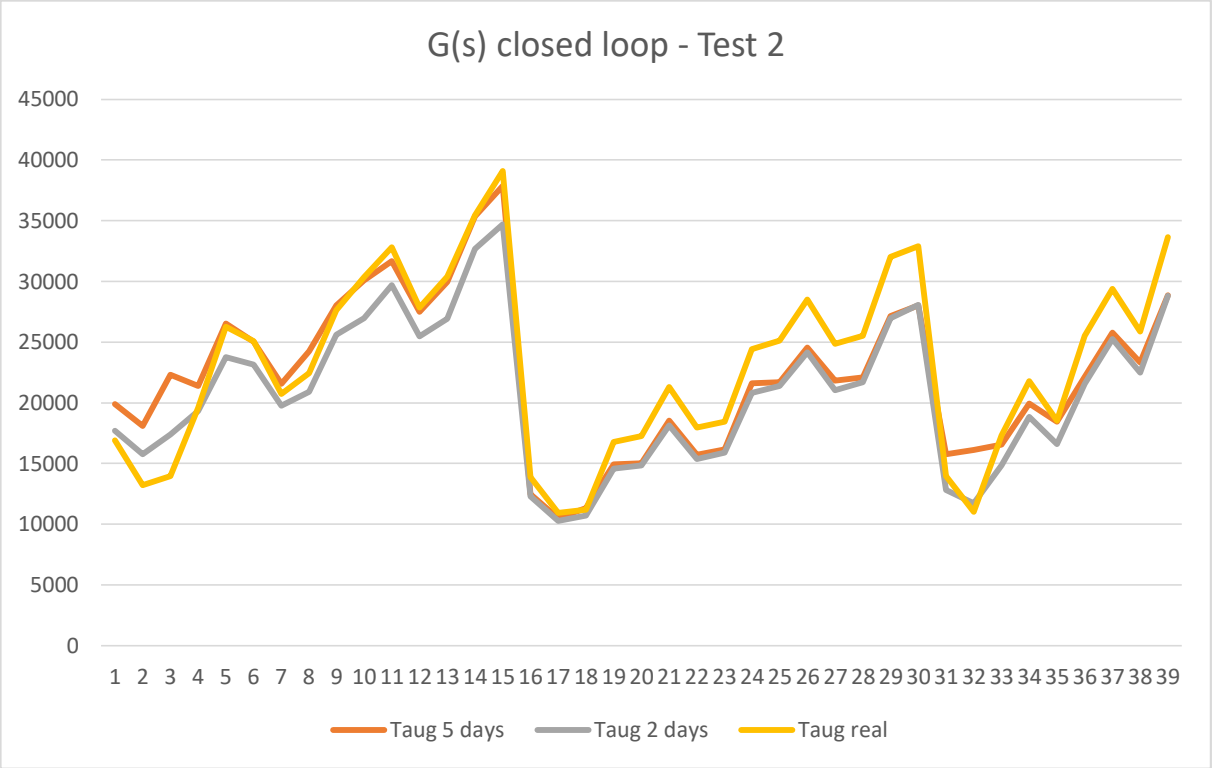

Fig. 8.2: G(s) closed loop estimation, identified time constant accuracy: Test 2

As for the previous test, the 5 days data collection grants a better accuracy in almost all the cases, but the improvement is marginal and a 2 days data collection should still be preferred. The impact of an higher outside air temperature is not too relevant.

In conclusion, the identification performances increase as the difference between the outside air temperature and the zone temperature set point increases. This is because the contribution of the outside air temperature gets confused with the contribution of the radiant panels more easily if they assume a similar value. Moreover, two days are sufficient for the data collection phase.

8.a.2 G(s) Open loop

As anticipated in section 4.c.2.2, the factors that are mainly influencing the outcome of this method – beside any relevant measurement error – are:

- The number of days during which the data set are collected.
- The outside temperature profile

To evaluate the combined effect of these factors, several tests have been conducted among which the most relevant are reported below. The zone temperature set-point $T_{Z,rif}$ has been kept constant to 23°C. The realistic outside air temperature profile presented in section 3.e.3 has been adopted in these tests.

- Test 1:

$$\begin{cases} T_{OA} \text{ average: } 9°C \\ T_{OA} \text{ daily range: } \pm 5°C \end{cases}$$

Two cases are presented in which the data have been collected for 5 days or 2 days. The identified time constant τ_G of both those cases is compared with the real τ_G value in Fig. 8.3.

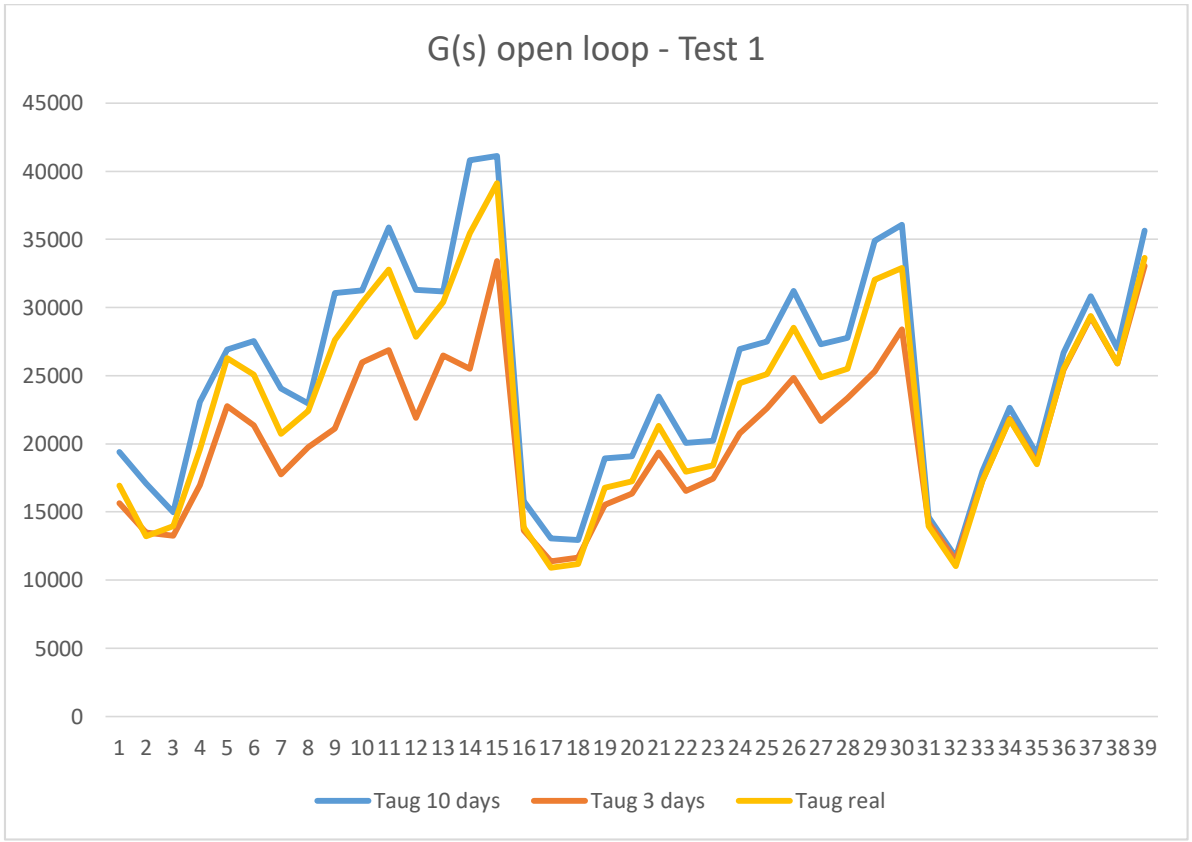

Fig. 8.3: G(s) open loop estimation, identified time constant accuracy: Test 1

The identified τ_G resulting from a 3 days data collection is almost always underestimated, while the identified τ_G resulting from a longer data collection period is usually overestimated and closer to the real value. It is still preferable to adopt a 3 days length for the data collection phase.

- Test 2:

$$\begin{cases} T_{OA} \text{ average: } 9°C \\ T_{OA} \text{ daily range: } \pm 8°C \end{cases}$$

This test presents a bigger daily range value with respect to the previous test. This will negatively affect the identification result because the effect of the T_M open loop profile will mix with the effect of the T_{OA} profile even more. A higher T_{OA} average value would not have affected the identification results since the T_{OA} average is automatically compensated by the PID loop action before reaching the pseudo-equilibrium state. Two cases are presented in which the data have been collected for 5 days or 2 days. The identified time constant τ_G of both those cases is compared with the real τ_G value in Fig. 8.4.

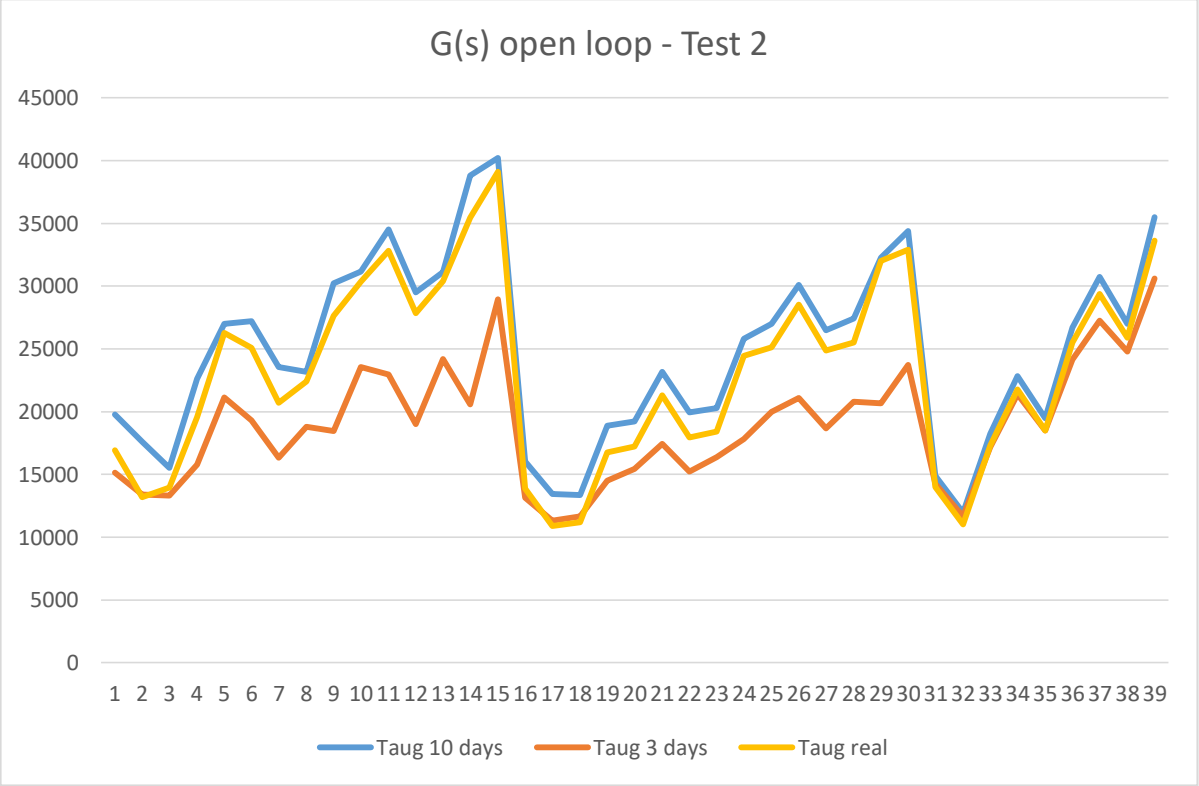

Fig. 8.4: G(s) open loop estimation, identified time constant accuracy: Test 2

This time the accuracy of the identified τ_G resulting from a 3 days data collection is visibly lower than the accuracy of the 10 days data collection one. This means that this wider T_{OA} daily range has impacted significantly on the performances of this

identification method. It is recommended to increase the length of the data collection phase in presence of big thermal excursions.

In conclusion, the factors influencing this identification methods are the length of the data collection phase and the amplitude of the T_{OA} daily excursion. With reasonably small values of the latter (i.e. $\leq 6°C$ ca.), the former can be set to 3 days and still grant good overall identification results.

8.a.3 G(s) estimation in open loop exploiting H(s) estimation

As anticipated in section 4.c.2.3, the factors influencing the outcome of this method – neglecting any relevant measurement error – are:

- The number of days during which the data set are collected.
- The outside temperature profile
- The quality of the exploited H(s) estimation

To evaluate the combined effect of these factors, several tests have been conducted among which the most relevant are reported below. The zone temperature set-point $T_{Z,rif}$ has been kept constant to 23°C. The realistic outside air temperature profile presented in section 3.e.3 has been adopted in these tests.

- Test 1:

$$\begin{cases} T_{OA} \text{ average: } 9°\text{C} \\ T_{OA} \text{ daily range: } \pm 5°\text{C} \\ H(s)\ estimation: ideal \end{cases}$$

  In this test, the exploited H(s) estimation has been developed under ideal conditions, i.e. the real gain and "real" τ_H have been identified. Two cases are presented in which the data have been collected for 2 days or 1 day. The identified time constant τ_G of both those cases is compared with the real τ_G value in Fig. 8.5.

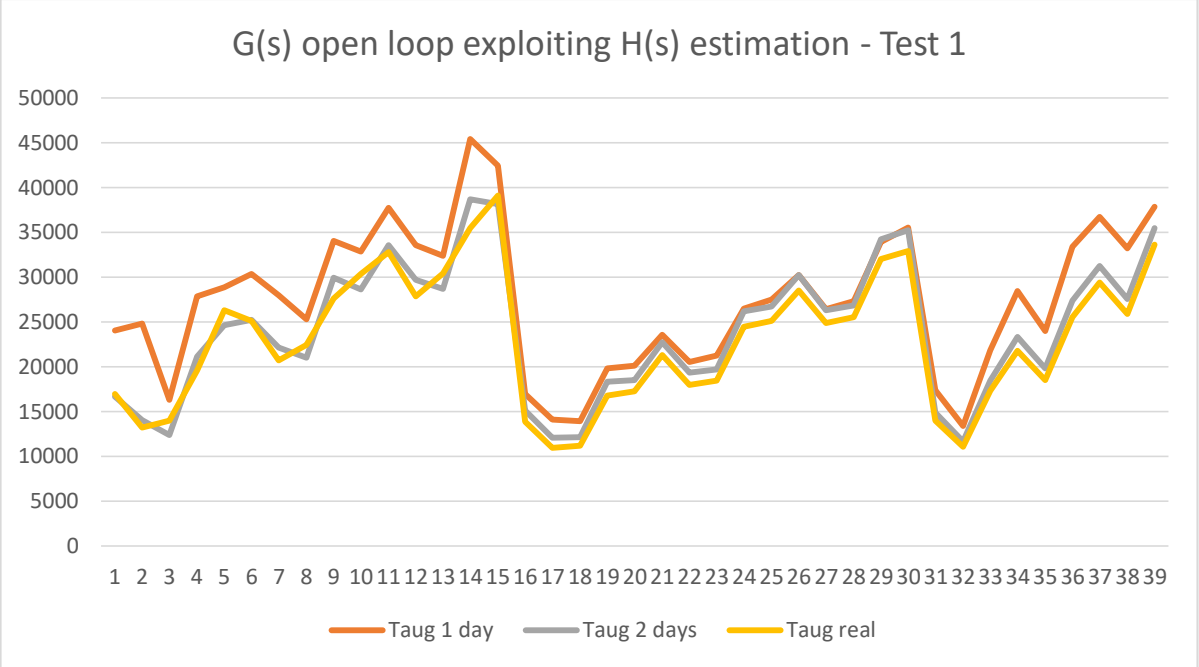

Fig. 8.5: G(s) estimation in open loop exploiting H(s) estimation,
identified time constant accuracy: Test 1

The accuracy resulting from a 2 days data collection phase is visibly better than the one resulting from only 1 day of data collection. The use of H(s) estimation returned better results with respect to the simple open loop G(s) identification performed under the same environmental conditions, i.e. “Test 1” of the previous section.

- Test 2:

$$\begin{cases} T_{OA} \text{ average: } 9°C \\ T_{OA} \text{ daily range: } \pm 8°C \\ H(s)\ estimation: ideal \end{cases}$$

Even in this test the exploited H(s) estimation has been developed under ideal conditions. The T_{OA} daily range has been increased similarly to “Test 2” of the previous section. This change will negatively impact on the identified τ_G for the same reasons explained in “Test 2” of the previous section. Two cases are presented in which the data have been collected for 2 days, 3 days or 1 day. The identified time constant τ_G of both those cases is compared with the real τ_G value in Fig. 8.6.

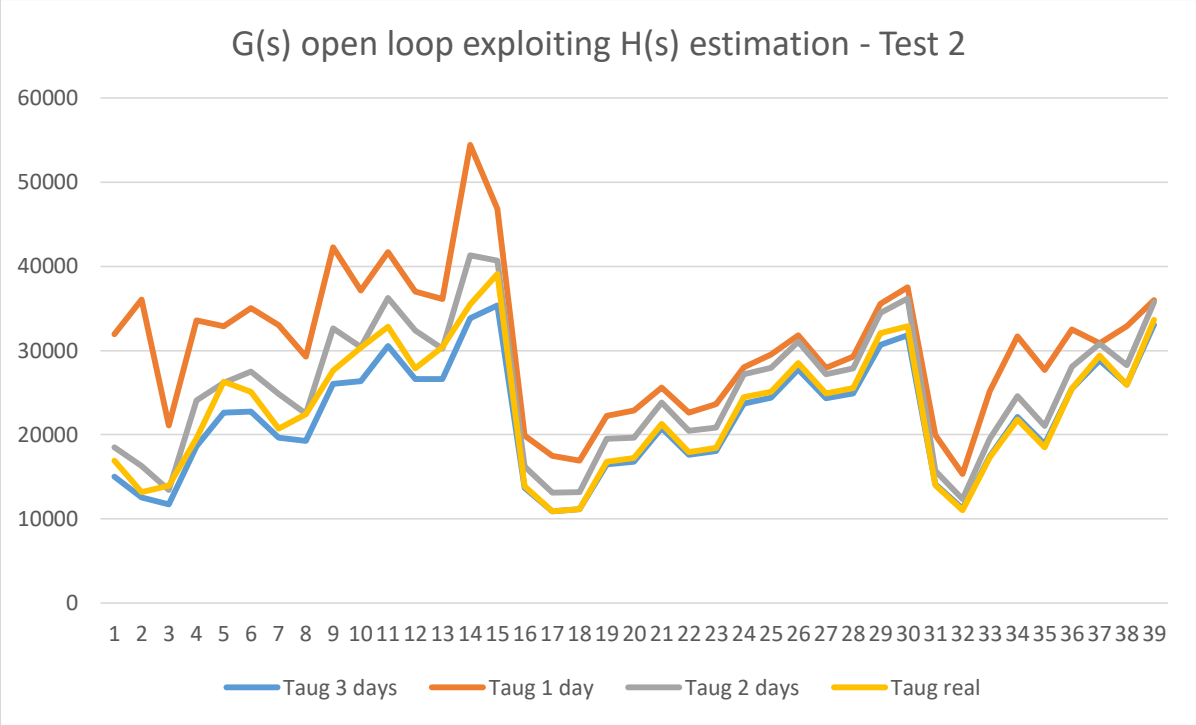

Fig. 8.6: G(s) estimation in open loop exploiting H(s) estimation, identified time constant accuracy: Test 2

The wider T_{OA} daily range has affected the performances of this identification method. The accuracy of the estimation resulting from 1 day data collection is not acceptable, and the 2 days data collection one has been affected too. By extending the data collection phase to 3 days noticeable improvements are obtained. However, a time window of 2 days for the data collection seems a more reasonable trade off between the estimation accuracy and the practical limits of a long estimation period.

- Test 3:

$$\begin{cases} T_{OA} \text{ average: } 9°C \\ T_{OA} \text{ daily range: } \pm 8°C \\ H(s)\ estimation: +30\%\ error \end{cases}$$

In this test the exploited H(s) estimation presents a 30% error on both its gain and time constant τ_H. Two cases are presented in which the data have been collected for 3 days or 2 days. The identified time constant τ_G of both those cases is compared with the real τ_G value in Fig. 8.7.

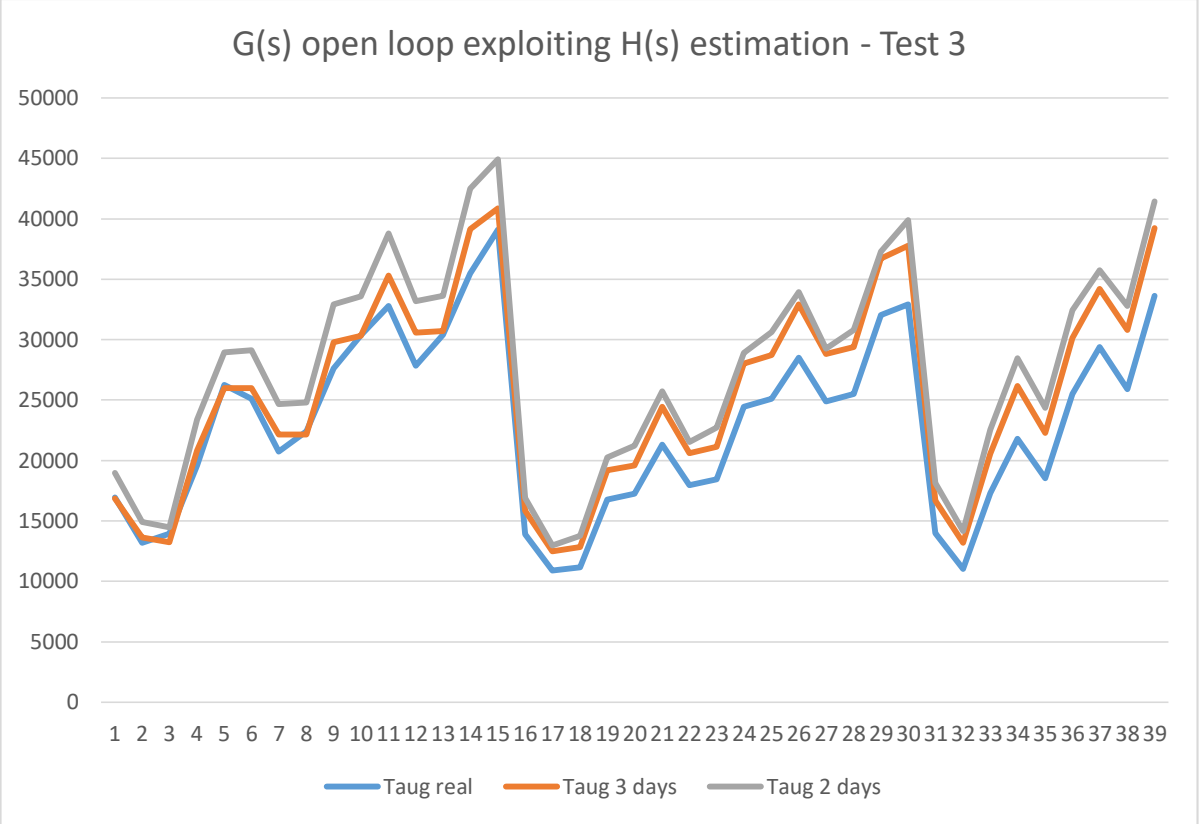

Fig. 8.7: G(s) estimation in open loop exploiting H(s) estimation, identified time constant accuracy: Test 3

The accuracy of the τ_G estimation has been affected in both the 2 days data collection and 3 days data collection cases. Still, a 2 days data collection time window is advised.

In conclusion, the use of H(s) estimation provides better results with respect to the simple open loop G(s) estimation presented in the previous section. Moreover, a shorter data collection phase is required – two days instead of three. Similarly to the simple open loop G(s) estimation, the outside air temperature daily range and the length of the data collection phase affect this estimation method. The quality of the H(s) estimation plays a relevant role too, but the results turned out to be satisfactory even under its 30% error.

8.b H(s) estimation

To estimate the H(s) transfer function only one method was proposed in this thesis, i.e. the open loop method. To recall its reasoning, this choice has been made because of the uncontrollability of the T_{OA} disturbance and the lower impact of H(s) on the measured output T_Z with respect to the heating panel transfer function G(s). As anticipated in section 4.c.4, the outcome of the H(s) open loop estimation method is mainly influenced by the following factors:

- The number of days during which the data set are collected.
- The quality of the exploited G(s) gain estimation

Similarly to the G(s) estimation testing, the quality of the estimated τ_H is presented along the 39 representative rooms and limit cases and compared to the "real" τ_H value, i.e. the τ_H resulting from an ideal estimation of H(s). Therefore, this "real" τ_H value is the best 1-pole approximation of the fourth order transfer function H(s). The ideal estimation of H(s) is obtained when the estimated G(s) gain used for this identification procedure is equivalent to the real G(s) gain. To evaluate the combined effect of these factors, several tests have been conducted. Only one test is reported here.

$$\begin{cases} T_{OA} \text{ average: } 9°\text{C} \\ T_{OA} \text{ daily range: } \pm 5°\text{C} \\ \mu_G \; estimation: +5\% \end{cases}$$

In this test, the estimated G(s) gain used to identify H(s) has a 5% error. Using a perfect G(s) gain estimation would result in a perfect H(s) identification, losing the meaning of the test. Two cases are presented in which the data have been collected for 2 days or 1 day. The identified time constant τ_H of both those cases is compared with the real τ_H value in Fig. 8.8.

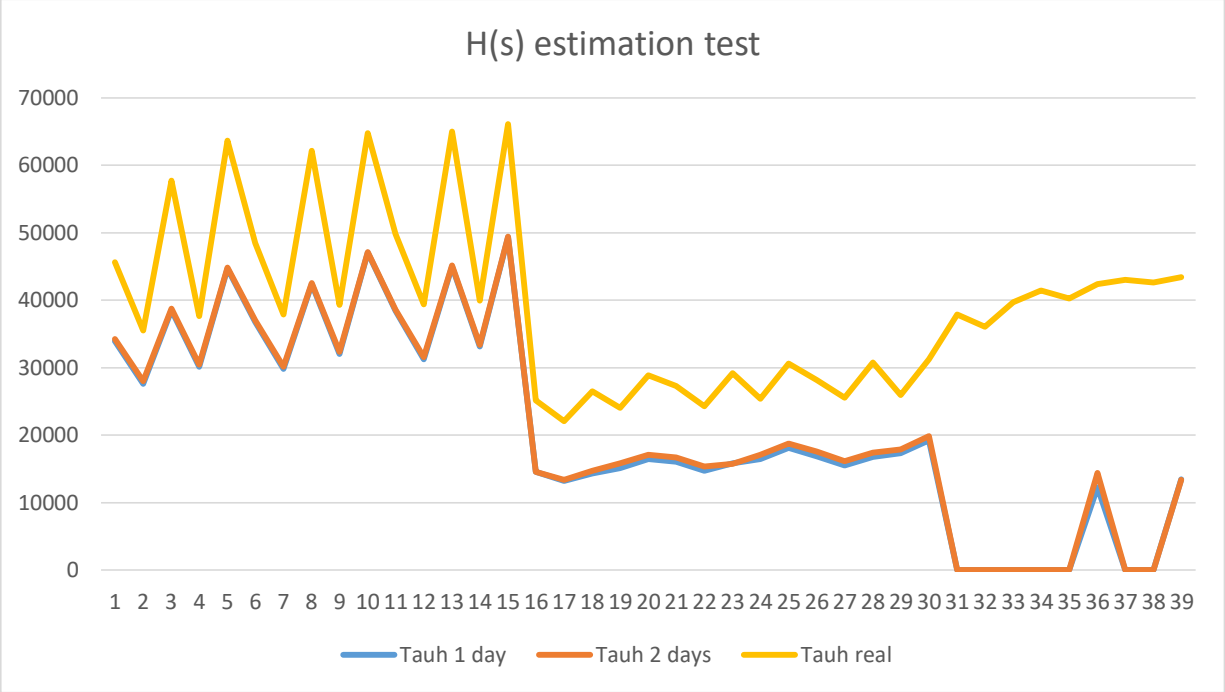

Fig. 8.8: H(s) open loop estimation using an estimated G(s) gain with 5% error, identified time constant accuracy

As it can be seen, the length of the data collection phase is not so relevant for this estimation procedure, since the results for 1 day or 2 days of data collection is almost the same. However, the 5% error on the G(s) gain has drastically reduced the accuracy of the τ_H estimation. The last 9 rooms present an unacceptable value of τ_H or even $\tau_H = 0$ when the identified H(s) resulted unstable ($\tau_H < 0$).

From the results of the presented test, it is clear that the estimation of G(s) gain is of paramount importance for the correct outcome of this procedure. If such condition cannot be met, it is better to forget about the H(s) estimation procedure and exploit the thermal lag measurements to tune the M(s) pole instead. A data collection window of 2 days is more than sufficient to perform such identification.

8.c Adaptive tuning algorithms

In this section, all the seven tuning algorithms presented in section 5.c are tested. A sub-section is dedicated to each tuning algorithm.

As seen in the previous tests, many factors influence the overall performance of the tuning algorithm, which is the result of different identifications and/or measurements. To shorten the presentation of these results, the only considered factor is the very accuracy of the measured/identified quantity used for the tuning. No focus is posed on the multitude of causes that result in the impoverishment of the quality of that measured/identified quantity, because in the end the result of the tuning algorithm depends only on the quality of the measured/identified quantity itself.

For each algorithm, two test sets are presented for each variation of the quality of the measured/identified quantity used for the tuning: one on the 39 representative rooms and limit cases and another one on 40 random rooms. While the 39 representative rooms and limit cases have been defined in section 4.a.3, the 40 random rooms are chosen by randomly assigning the values of the four main thermo-physical parameters, each one from its respective range proposed in section 4.a.2:

- $c_{p,Wall} \in [13; 65]$
- $u_{Wall} \in [0.28; 1.61]$
- $c_{p,Pav} \in [34; 175]$
- $u_{Pav} \in [12; 63]$

In all the following tests, the outside air temperature profile adopted is presented in Fig. 8.9. It is characterized by the realistic shape presented in section 3.e.3 and with the following numerical parameters:

$$\begin{cases} T_{OA} \text{ average: } 9°\text{C} \\ T_{OA} \text{ daily range: } \pm 5°\text{C} \end{cases}$$

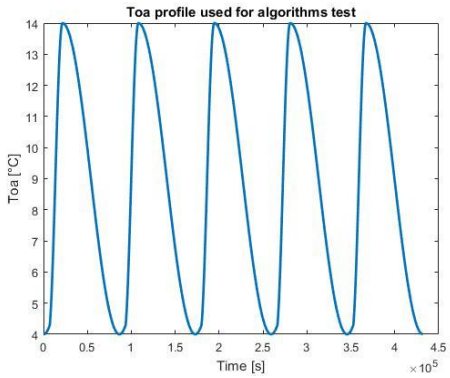

Fig. 8.9: Outside air temperature profile used to test the tuning algorithms

The algorithm performances are represented by computing the Mean Square Error MSE between the zone temperature T_Z and its set point $T_{Z,rif}$ measured for a specified time length (3 days are used, but any other number of days is acceptable) during the pseudo-equilibrium state. Two MSE are presented: one resulting by applying the general compensator M(s) and another one resulting by applying the adaptive algorithm compensator. In this way, the MSE evaluates the capability of the tuned compensator M(s) to reject the disturbance T_{OA}. A representative Fig. 8.10 reports the improvement obtained by applying the compensator resulting from the tuning algorithms with respect to the average compensator.

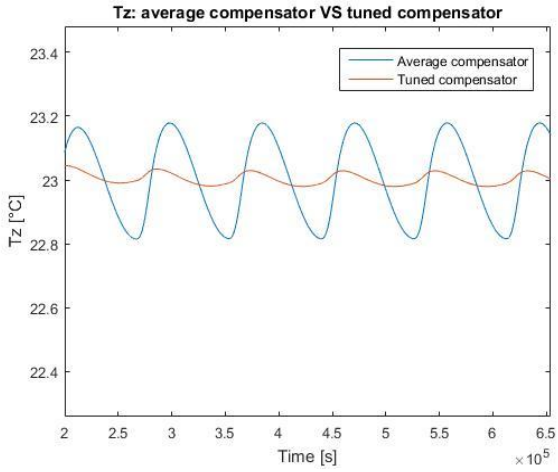

Fig. 8.10: Effect of the tuning algorithms in the outside air temperature disturbance rejection

Among the 39 representative rooms and limit cases, the 14-th room will be neglected in the results because of its peculiarity. This room is the limit case room endowed with the worst combination of walls and pavement, i.e. the lowest $c_{p,Wall}$ and u_{Pav} combined with the highest $c_{p,Pav}$ and u_{Wall}. The result is that the gain of H(s) is bigger than the gain of G(s) and thus the performances are very poor. However, such case is not realistic so it is easily abandoned to allow a better comparison of the performance among the other cases.

8.c.1 Algorithm 1

The current algorithm is summarily represented by the sequence:
G(s) closed loop identification [T_M] → G(s) estimated gain refinement [PID] → H(s) open loop identification [τ_M] [μ_M].

The data collection phase for the G(s) closed loop identification procedure is 2 days and the H(s) open loop identification procedure used 2 days for data collection and an estimated G(s) gain with a 3% error. With the T_{OA} disturbance profile adopted in this section and the resultant estimated/measured tuning quantities $[\tau_G \rightarrow T_M]$, $[\tau_H \rightarrow \tau_M]$ and $[\mu_G \rightarrow \mu_M]$ the results expressed in MSE are reported in Fig. 8.11.

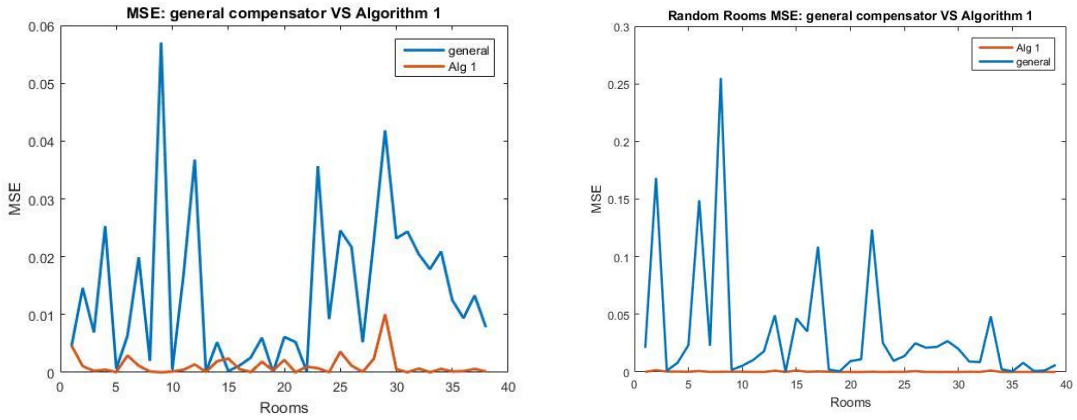

Fig. 8.11: Tuning algorithm 1 tested on the 39 representative rooms and limit cases (left) and on 40 random rooms (right)

Then, an artificial estimation/measurement error of $\pm 20\%$ was added on the tuning quantities and the results expressed in MSE are reported in Fig. 8.12.

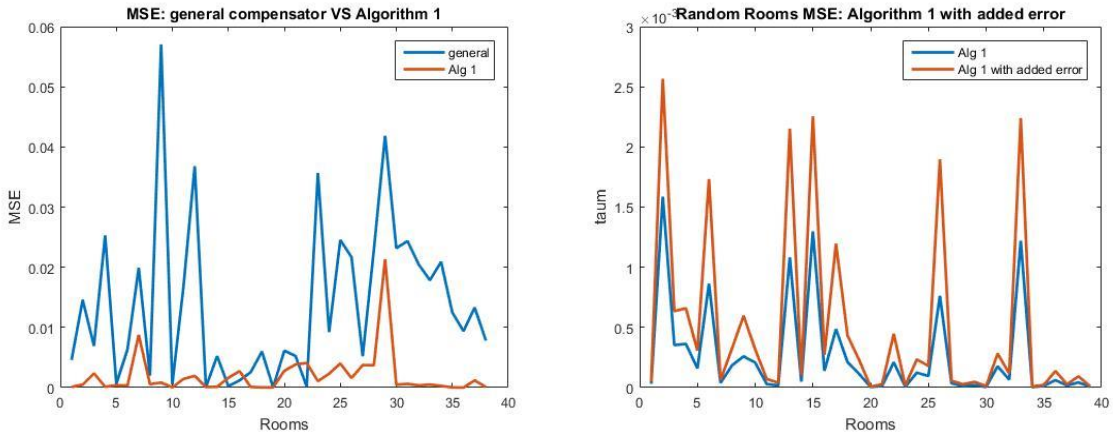

Fig. 8.12: Tuning algorithm 1 tested with an additive estimation/measurement error on the 39 representative rooms and limit cases (left) and on 40 random rooms (right)

8.c.2 Algorithm 2

The current algorithm is summarily represented by the sequence:
G(s) closed loop identification [T_M] → G(s) estimated gain refinement [PID] → Open loop thermal lag [τ_M] [μ_M].

The data collection phase for the G(s) closed loop identification procedure is 2 days. With the T_{OA} disturbance profile adopted in this section and the resultant estimated/measured tuning quantities [$\tau_G \rightarrow T_M$], [$\Delta_{OA,OL} \rightarrow \tau_M$] and [$\mu_G \rightarrow \mu_M$] the results expressed in MSE are reported in Fig. 8.13.

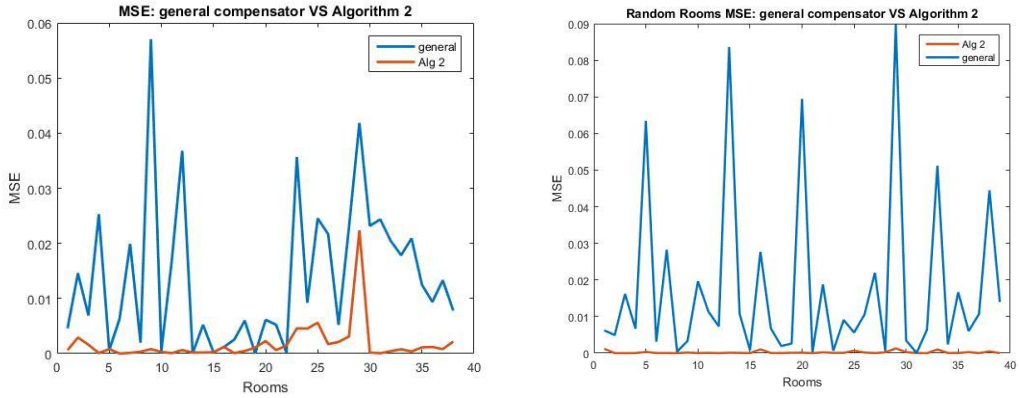

Fig. 8.13: Tuning algorithm 2 tested on the 39 representative rooms and limit cases (left) and on 40 random rooms (right)

Then, an artificial estimation/measurement error of $\pm 20\%$ was added on the tuning quantities and the results expressed in MSE are reported in Fig. 8.14.

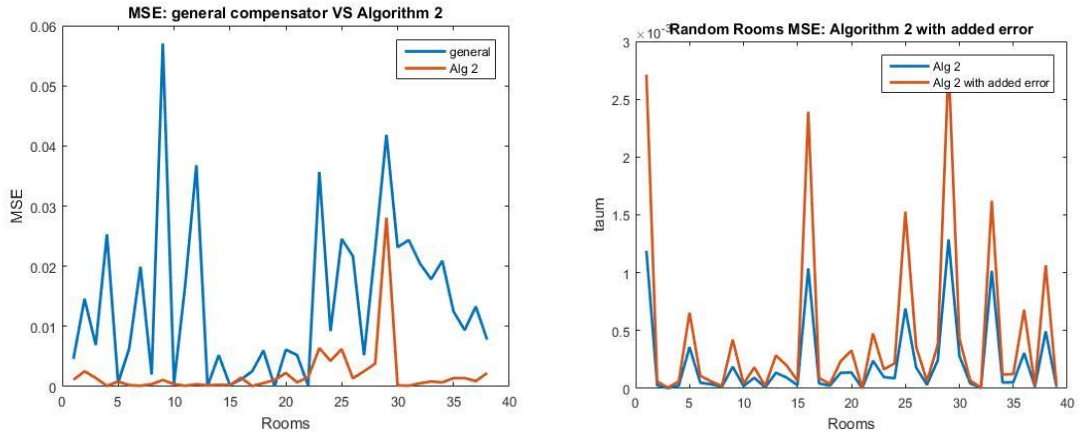

Fig. 8.14: Tuning algorithm 2 tested with an additive estimation/measurement error on the 39 representative rooms and limit cases (left) and on 40 random rooms (right)

8.c.3 Algorithm 3

The current algorithm is summarily represented by the sequence:
G(s) closed loop identification [T_M] → G(s) estimated gain refinement [PID] → Closed loop thermal lag [τ_M] [μ_M].

The data collection phase for the G(s) closed loop identification procedure is 2 days. With the T_{OA} disturbance profile adopted in this section and the resultant estimated/measured tuning quantities [$\tau_G \rightarrow T_M$], [$\Delta_{OA,CLC} \rightarrow \tau_M$] and [$\mu_G \rightarrow \mu_M$] the results expressed in MSE are reported in Fig. 8.15.

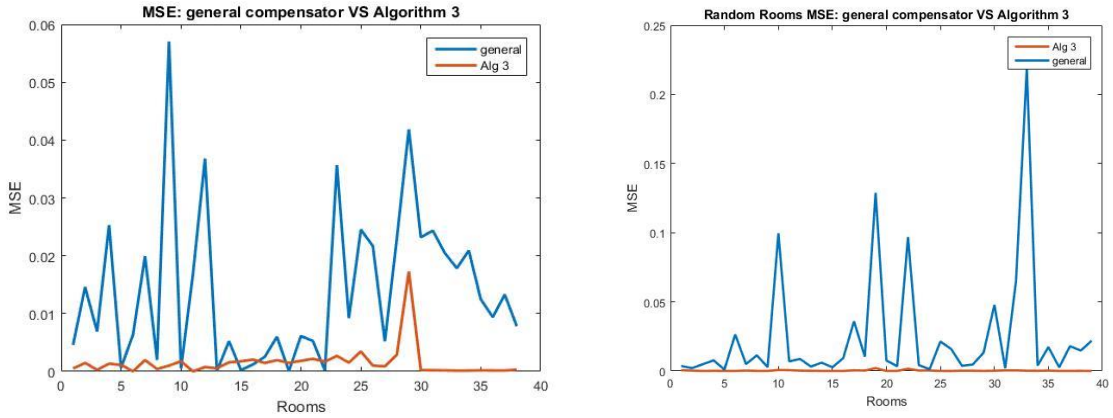

Fig. 8.15: Tuning algorithm 3 tested on the 39 representative rooms and limit cases (left) and on 40 random rooms (right)

Then, an artificial estimation/measurement error of $\pm 20\%$ was added on the tuning quantities and the results expressed in MSE are reported in Fig. 8.16.

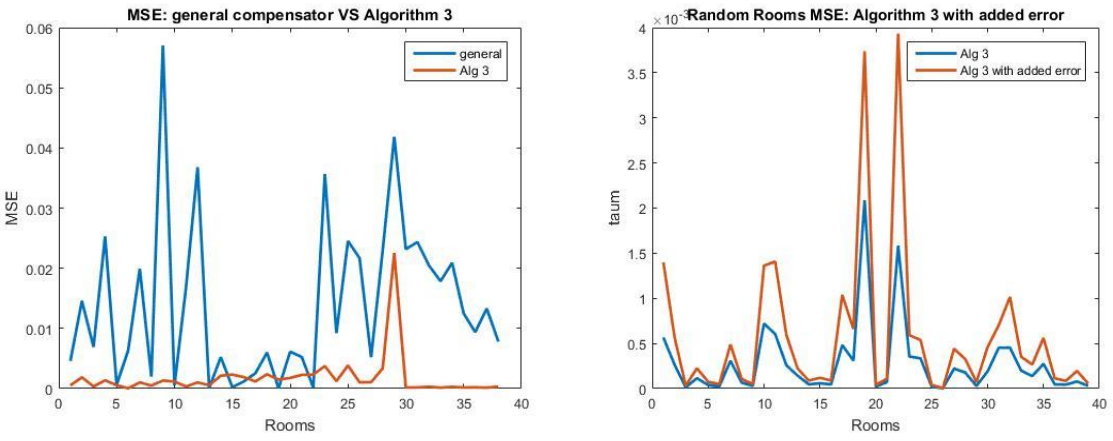

Fig. 8.16: Tuning algorithm 3 tested with an additive estimation/measurement error on the 39 representative rooms and limit cases (left) and on 40 random rooms (right)

8.c.4 Algorithm 4

The current algorithm is summarily represented by the sequence:
G(s) gain refinement → H(s) open loop estimation [τ_M] → G(s) open loop identification exploiting H(s) identification [T_M] [PID] [μ_M].

The data collection phase for the G(s) open loop identification procedure is 2 days and the H(s) open loop identification procedure used 2 days for data collection and an estimated G(s) gain with a 3% error. With the T_{OA} disturbance profile adopted in this section and the resultant estimated/measured tuning quantities $[\tau_G \rightarrow T_M]$, $[\tau_H \rightarrow \tau_M]$ and $[\mu_G \rightarrow \mu_M]$ the results expressed in MSE are reported in Fig. 8.17.

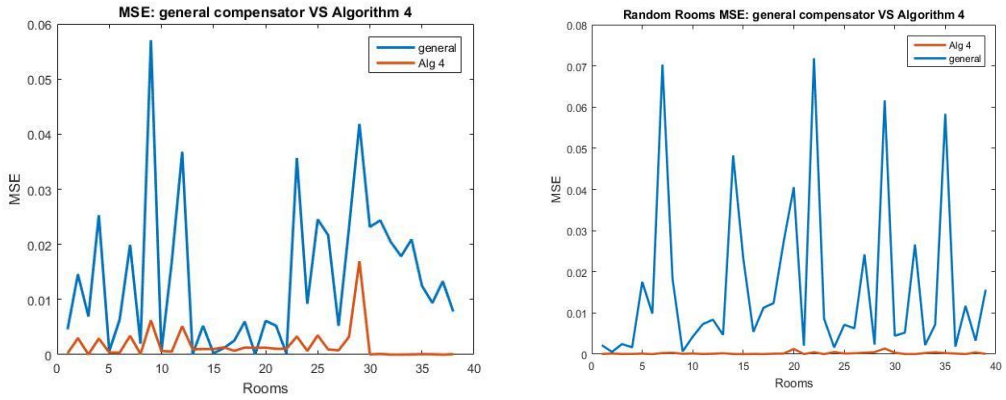

Fig. 8.17: Tuning algorithm 4 tested on the 39 representative rooms and limit cases (left) and on 40 random rooms (right)

Then, an artificial estimation/measurement error of $\pm 20\%$ was added on the tuning quantities and the results expressed in MSE are reported in Fig. 8.18.

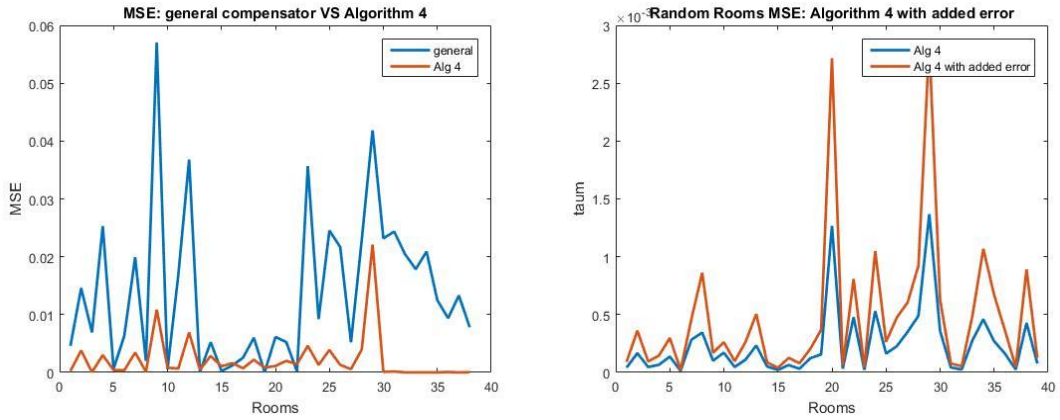

Fig. 8.18: Tuning algorithm 4 tested with an additive estimation/measurement error on the 39 representative rooms and limit cases (left) and on 40 random rooms (right)

8.c.5 Algorithm 5

The current algorithm is summarily represented by the sequence:
G(s) open loop identification [T_M] → G(s) estimated gain refinement [PID] → H(s) open loop identification [τ_M] [μ_M].

The data collection phase for the G(s) open loop identification procedure is 3 days and the H(s) open loop identification procedure used 2 days for data collection and an estimated G(s) gain with a 3% error. With the T_{OA} disturbance profile adopted in this section and the resultant estimated/measured tuning quantities $[\tau_G \rightarrow T_M]$, $[\tau_H \rightarrow \tau_M]$ and $[\mu_G \rightarrow \mu_M]$ the results expressed in MSE are reported in Fig. 8.19.

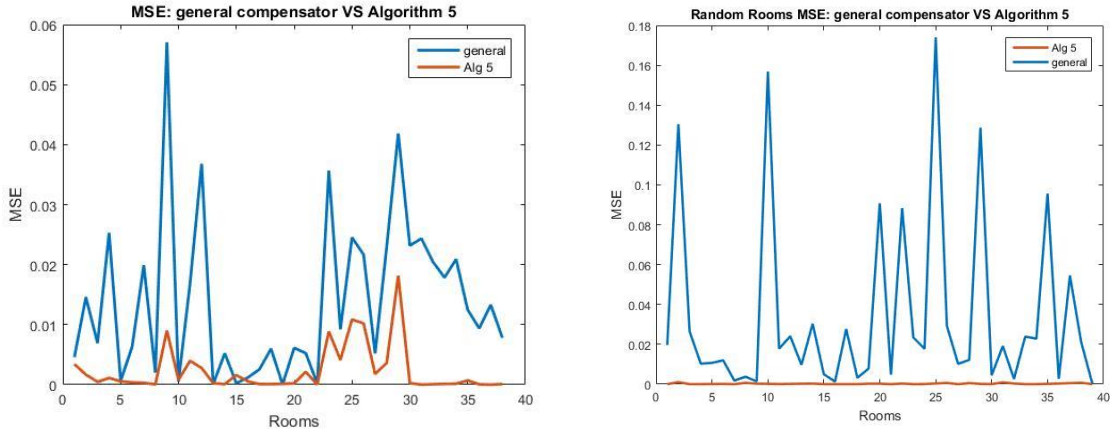

Fig. 8.19: Tuning algorithm 5 tested on the 39 representative rooms and limit cases (left) and on 40 random rooms (right)

Then, an artificial estimation/measurement error of $\pm 20\%$ was added on the tuning quantities and the results expressed in MSE are reported in Fig. 8.20.

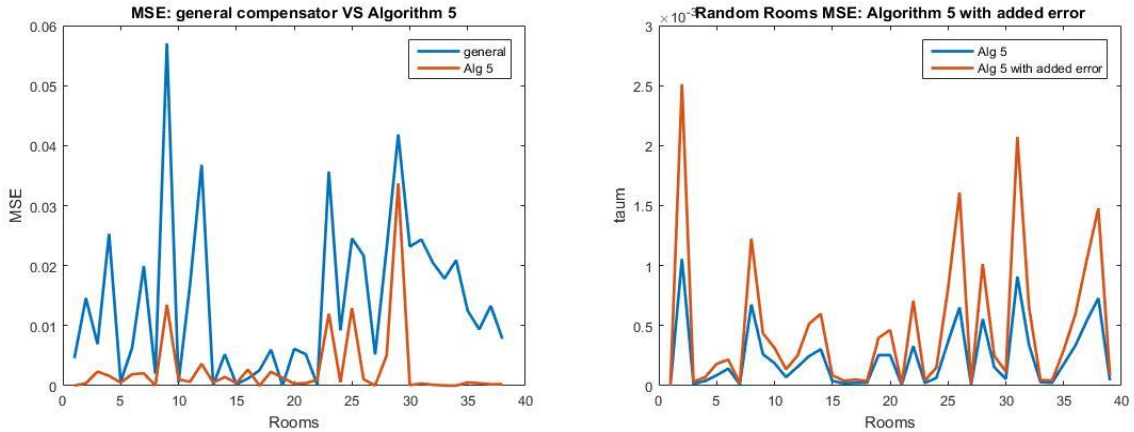

Fig. 8.20: Tuning algorithm 5 tested with an additive estimation/measurement error on the 39 representative rooms and limit cases (left) and on 40 random rooms (right)

8.c.6 Algorithm 6

The current algorithm is summarily represented by the sequence:
G(s) open loop identification [T_M] → G(s) estimated gain refinement [PID] → Open loop thermal lag [τ_M] [μ_M].

The data collection phase for the G(s) open loop identification procedure is 2 days. With the T_{OA} disturbance profile adopted in this section and the resultant estimated/measured tuning quantities [$\tau_G \rightarrow T_M$], [$\Delta_{OA,OL} \rightarrow \tau_M$] and [$\mu_G \rightarrow \mu_M$] the results expressed in MSE are reported in Fig. 8.21.

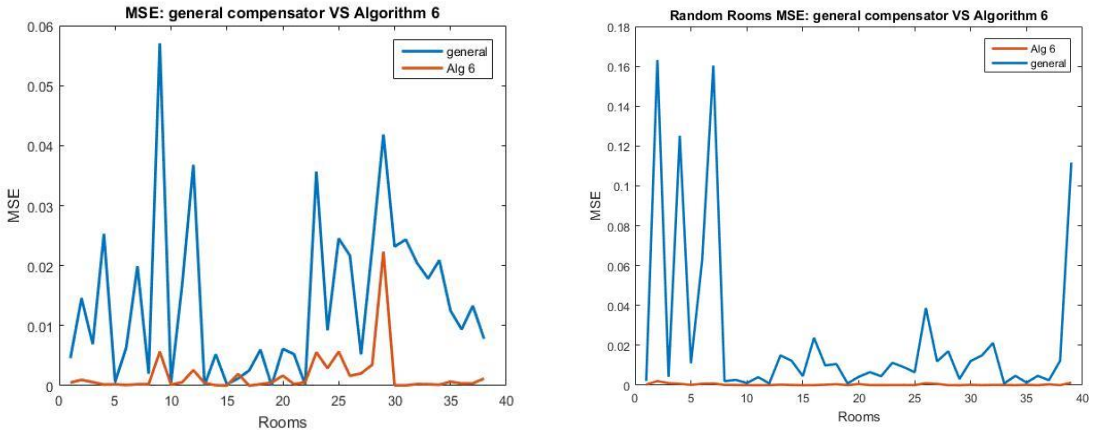

Fig. 8.21: Tuning algorithm 6 tested on the 39 representative rooms and limit cases (left) and on 40 random rooms (right)

Then, an artificial estimation/measurement error of $\pm 20\%$ was added on the tuning quantities and the results expressed in MSE are reported in Fig. 8.22.

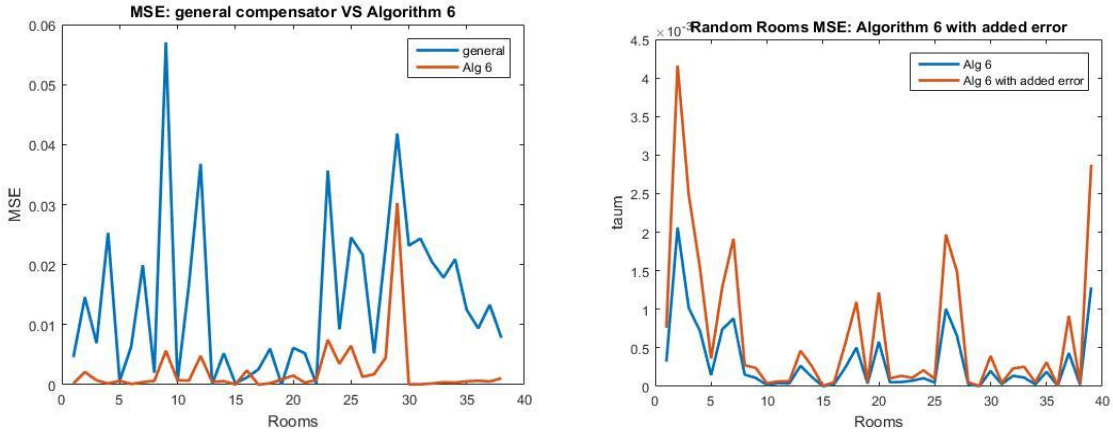

Fig. 8.22: Tuning algorithm 6 tested with an additive estimation/measurement error on the 39 representative rooms and limit cases (left) and on 40 random rooms (right)

8.c.7 Algorithm 7

The current algorithm is summarily represented by the sequence:
G(s) open loop identification [T_M] → G(s) estimated gain refinement [PID] → Closed loop thermal lag [τ_M] [μ_M].

The data collection phase for the G(s) open loop identification procedure is 2 days. With the T_{OA} disturbance profile adopted in this section and the resultant estimated/measured tuning quantities [$\tau_G \rightarrow T_M$], [$\Delta_{OA,CLC} \rightarrow \tau_M$] and [$\mu_G \rightarrow \mu_M$] the results expressed in MSE are reported in Fig. 8.23.

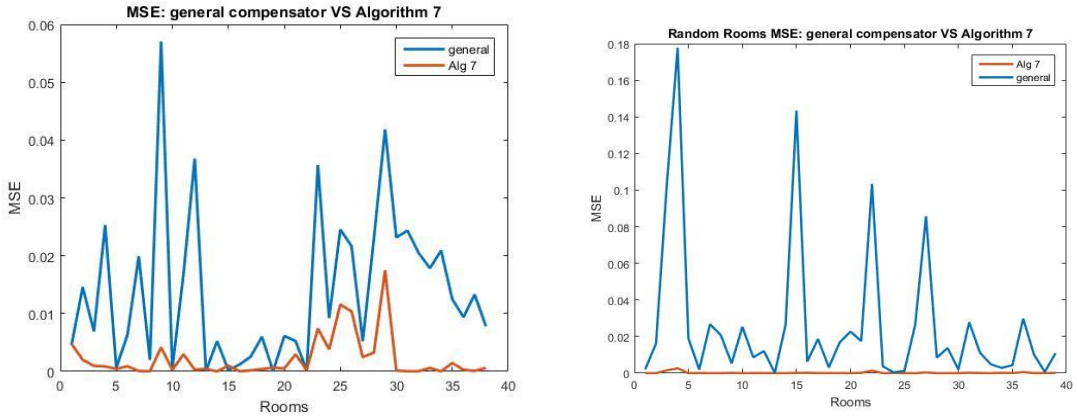

Fig. 8.23: Tuning algorithm 7 tested on the 39 representative rooms and limit cases (left) and on 40 random rooms (right)

Then, an artificial estimation/measurement error of $\pm 20\%$ was added on the tuning quantities and the results expressed in MSE are reported in Fig. 8.24.

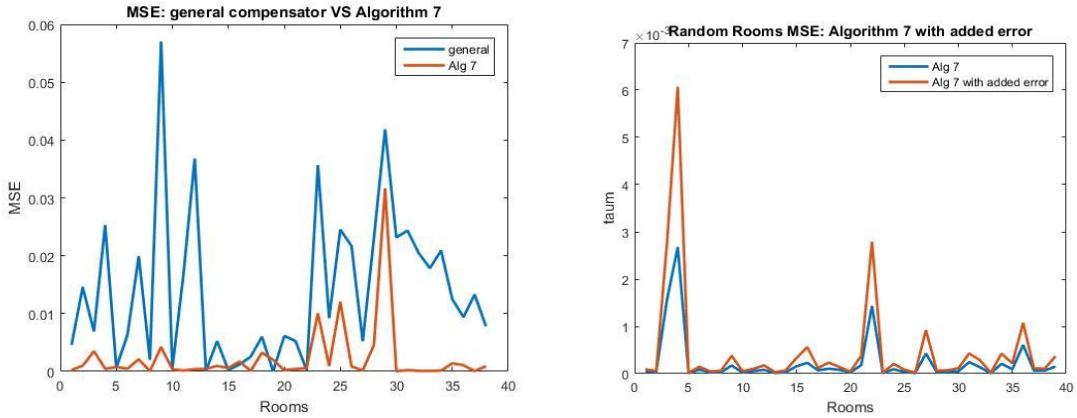

Fig. 8.24: Tuning algorithm 7 tested with an additive estimation/measurement error on the 39 representative rooms and limit cases (left) and on 40 random rooms (right)

8.c.8 Conclusions on the tuning algorithms

The performances resulting from the application of all the seven tuning algorithms presented advantages with respect to the average compensator. Sometimes the average compensator shows a lower MSE with respect to the tuned compensator, but this happens only when both the compensators return a low MSE value, i.e. when the average compensator was already suitable for the room. In those cases, the compensator tuning does not cause any relevant performance drop.

Overall, the improvement with respect to the average compensator is visible especially in the random rooms test. In this test, the average compensator shows less frequently a good behavior. Moreover, the tuned compensator always turned out to have a very low MSE – order of magnitude 10^{-3} – unlike in the 39 representative rooms and limit cases, in which some limit configurations of the room caused a non-optimal tuning of the compensator.

8.d Chapter 8 conclusions

The chapter presented a series of tests for both the identification methods and the tuning algorithms. About the identification methods, specific lengths of the data collection phase were tested showing that this phase should last 2 days more or less for all the methods. The effect of other influent factors was analyzed, such as the outside air temperature profile and the quality of other estimations on which a method may rely. Then the tuning algorithms were tested individually, showing an overall performance net improvement with respect to the use of average compensator, even under reasonable errors on the quantities used for the compensator tuning.

These tests were conducted on a model affected by the outside air temperature disturbance only. To prove the robustness of these methods in a real environment, other known disturbances as the solar radiation and the internal gains should be introduced, as it will be pointed out in the conclusion chapter 9. Anyhow, this chapter has shown the potentiality of exploiting the connections between the estimated/measured quantities and the compensator parameters to tune the latters. By ensuring the robustness of the related estimation/measurement methods it is then possible to exploit these tested connections.

PAGE INTENTIONALLY LEFT BLANK

9. CONCLUSIONS

This final chapter is dedicated to the conclusion of the whole thesis. The main contribution of this work will be described along with its limitations and suggestions for a future development. The main achievements of this research are presented in the first section 9.a, followed by the limitations and future developments section 9.b.

9.a Main achievements

The crucial point of this work is the development of an easy and robust adaptive tuning strategy for the outside air temperature compensator M(s) of a room endowed with a radiant floor heating system. Supported by the control structure presented in chapter 3, this compensator is designed to reduce the thermal discomfort of the controlled room resulting from the outside air temperature disturbance. Beside this compensator, the control structure is simply constituted by two cascaded control loops presenting a PID regulator. This structure has already been widely applied in the literature and thus it does not represent a new contribution by itself.

The adopted open loop compensator presents a 1-pole 1-zero low frequency approximation to grant its feasibility. This approximation has proved to be sufficient to capture the dominant frequency of the disturbance in question, i.e. the outside air temperature. The compensator is then composed by three parameters that need to be tuned according to the actual room system. The compensator correct tuning is greatly affected by the thermo-physical parameters of the controlled room. However, these parameters are both hardly identifiable/measurable from the outside and relevantly affected by uncertainties with respect to their constructive values. This means that imposing an average configuration of the compensator M(s) does not present a satisfying solution in some cases. The proposed adaptive tuning strategy – developed in seven different algorithms – offers to tune the compensator M(s) according to some measurable/identifiable quantities, which in turn are influenced by the same thermo-physical parameters that affect the correct tuning of the compensator itself. In this way, those thermo-physical parameters are indirectly identified so to grant a suitable M(s) tuning. The efficiency of these adaptive tuning algorithms has been proven along a wide range of the main thermo-physical parameters considered. The

identified quantities are used to re-tune even the outer loop PID in order to obtain a more suitable set-point response in terms of settling time and overshooting avoidance.

9.b Limitations and future developments

Since this thesis is focused on the proposal of a new adaptive control tuning strategy for a commercial radiant panel heating system, there are many possible future developments that can be carried out in order to verify the real-world efficiency of such idea. These future developments are listed in this section.

The efficiency of the adaptive tuning algorithms has been validated in chapter 8 by neglecting other known disturbances, such as the solar radiation and the internal gains. The effect of the solar radiation on these algorithms has been only discussed in chapter 6 without performing any test. The first future development should then concern these neglected disturbances, testing its effect and eventually updating the tuning algorithms so to reduce the impact of these other disturbances.

Second, the correlation functions exploited by the tuning algorithms have been obtained by analyzing a room model with fixed dimensions and radiant panel system characteristics. The robustness with respect to reasonable variations of these parameters has been tested in chapter 5. The existence of such correlation functions under very different configurations has been proven too. An idea for an easy future development of this work is to define a set of these transfer functions, each one related to a particular class of controlled rooms and installed heating system.

Third, the assumption of a single controlled room has been made in this thesis. The adaptive algorithms could be extended in a multi-room context depending on the particular physical configuration of the heating system installed.

Fourth, the thermal lag based tuning strategies are now based on the measurement of the difference between the maximum peak of outside air temperature and the correspondent maximum peak of the zone temperature. This simple thermal lag measurement should be extended so to identify the time shift of the whole outside air temperature profile

Fifth, no measurement noise was considered for any sensor. Some identification procedures would realistically be affected by the introduction of the measurement noise, i.e. the open loop based ones. That is because in those procedures the measured zone temperature presents

only small oscillations (around $\pm 1°C$) around its set-point. A consistent measurement noise could compromise the identification outcome. Conversely, the G(s) closed loop identification procedure rely on relevant variations of the measured quantities and thus should not be affected by the measurement noise. Even the thermal lag based tuning strategies, once generalized as said in the fourth point, should not be affected by this measurement noise. So, theoretically, the algorithms 2 and 3 should maintain their overall performances even under relevant measurement noises. The efficiency of other algorithms should be tested so to define their dependency on the sensor quality.

Other possible developments are related to the two analyses started after the presentation of the tuning algorithms, i.e. the development of a solar radiation compensator of chapter 6 and the fault analysis of chapter 7.

PAGE INTENTIONALLY LEFT BLANK

List of figures

Fig. 2.1: Room endowed with radiant panel heating system 19
Fig. 2.2: Open/closed valve switching system 26
Fig. 2.3: Heating test to highlight the effect of the inlet water temperature set-point saturation 32
Fig. 2.4: Cooling test to highlight the effect of the inlet water temperature set-point saturation 33
Fig. 2.5: Mixing valve actuator block diagram 34
Fig. 2.6: Cooling test to highlight the effect of the mixing valve saturation 35
Fig. 2.7: Test room map 36
Fig. 2.8: Sperimental data collected in the fitting phase 38

Fig. 3.1: Block diagram of the outer control loop endowed with a PID regulator 41
Fig. 3.2: Typical shape of the Bode diagrams of the G(s) transfer function 43
Fig. 3.3: Effect of different PID tuning strategies 44
Fig. 3.4: Matlab PIDtune toolbox - comparison between the PID tuning proposed by Matlab and the PID tuning resulting from the proposed strategy 45
Fig. 3.5: Block diagram of the inner control loop endowed with a PI regulator 46
Fig. 3.6: Back-calculation anti-windup scheme 48
Fig. 3.7: Clamping anti-windup scheme 50
Fig. 3.8: Safety hysteresis diagram 51
Fig. 3.9: System behavior if the outer loop PID is left computing while the system if OFF .. 52
Fig. 3.10: System behavior if the outer loop PID is turned OFF while the system if OFF 53
Fig. 3.11: System behavior if the outer loop PID integral action is initialized when the system is turned ON 53
Fig. 3.12: Block diagram of the system until now 54
Fig. 3.13: Effect of the outside air temperature on the zone temperature 55
Fig. 3.14: Block diagram of the system endowed with an open loop outside air temperature compensator 56
Fig. 3.15: Typical outside air temperature profile 57
Fig. 3.16: Realistic approximation of the outside air temperature profile 57
Fig. 3.17: Frequency spectrum of the outside air temperature approximation 58
Fig. 3.18: Typical shape of the Bode diagrams of the ideal compensator M(s) 58
Fig. 3.19: 1-pole 1-zero approximation of the M(s) compensator. The red vertical line represents the last significant frequency of the outside air temperature profile 59
Fig. 3.20: Classic clamping anti-windup block scheme (upper) in comparison with the new clamping anti-windup scheme which accounts for the variable saturation boundaries (lower) 60

Fig 4.1: Variations on the system measured variables caused by different factors 64
Fig 4.2: System electrical equivalent 74
Fig 4.3: System electrical equivalent in steady state 74

Fig 4.4: System electrical equivalent in steady state, only inlet water temperature input acting on the system 75
Fig 4.5: System electrical equivalent in steady state, only outside air temperature input acting on the system 75
Fig 4.6: Closed loop G(s) estimation exemplificative zone temperature profile 81
Fig 4.7: Bode diagrams comparison between G(s) and its identified 1-pole approximation .. 82
Fig 4.8: Quality of the identified G(s) gain with the closed loop identification procedure 82
Fig 4.9: Quality of the identified G(s) time constant with the closed loop identification procedure 83
Fig 4.10: Profile used for the G(s) open loop identification procedure 84
Fig 4.11: Zone temperature during the open loop identification procedure 85
Fig 4.12: Quality of the identified G(s) time constant with the open loop identification procedure 86
Fig 4.13: Quality of the identified G(s) time constant exploiting the H(s) estimation 87
Fig 4.14: Bad H(s) estimation caused by an excessively wrong G(s) estimated gain (left) and good H(s) estimation (right) 89
Fig 4.15: scatterplot of G(s) time constant VS Pavement ratio (upper) scatterplot of G(s) time constant VS Wall ratio (central) G(s) time constant, Pavement ratio and Wall ratio (lower) 91
Fig 4.16: scatterplot of H(s) time constant VS Pavement ratio (upper) scatterplot of H(s) time constant VS Wall ratio (central) H(s) time constant, Pavement ratio and Wall ratio (lower) 92

Fig 5.1: Performance of the average PID tuning on the "New walls" & "Big screed" representative room (left) and performance of the average PID tuning on the "Old walls" & "Small screed" representative room (right) 96
Fig 5.2: Effect of the adaptive PID tuning in case of good G(s) identification (left) and bad G(s) identification (right) 97
Fig 5.3: Effect of the average compensator on the outside air temperature disturbance rejection 98
Fig 5.4: Compensator gain estimated with the complementary gain formula 99
Fig 5.5: Correlation function between the compensator zero and the G(s) time constant 100
Fig 5.6: Accuracy of the compensator zero tuned with the proposed correlation function (left) and accuracy of the compensator zero using a G(s) time constant with 10% error (right) ... 101
Fig 5.7: Correlation function between the compensator pole and the H(s) time constant 102
Fig 5.8: Accuracy of the compensator pole tuned with the proposed correlation function (left) and accuracy of the compensator pole using a H(s) time constant with 10% error (right) ... 102
Fig 5.9: Sinusoidal outside air temperature profile effect on zone temperature 103
Fig 5.10: Typical H(s) Bode diagrams 104
Fig 5.11: Realistic outside air temperature profile effect on zone temperature 104
Fig 5.12: Correlation function between the compensator pole and the open loop thermal lag 106
Fig 5.13: Accuracy of the compensator pole tuned with the proposed correlation function (left) and accuracy of the compensator pole using a open loop thermal lag with 10% error (right) 107
Fig 5.14: Correlation function between the compensator pole and the closed loop thermal lag (left) and correlation function between the compensator zero and the closed loop thermal lag (right) 108

Fig 5.15: Accuracy of the compensator pole tuned with the correlation function between the compensator pole and the closed loop thermal lag 109
Fig 5.16: Correlation function between the compensator pole and the closed loop corrected thermal lag 110
Fig 5. 17: Accuracy of the compensator pole tuned with the proposed correlation function (left) and accuracy of the compensator pole using a closed loop corrected thermal lag with 10% error (right) 110
Fig 5.18: Correlation functions accuracy even under different room dimensions: compensator zero with G(s) time constant (upper left), compensator pole with H(s) time constant (upper right) compensator pole with open loop thermal lag (lower left) and compensator pole with closed loop corrected thermal lag (lower right) 122
Fig 5.19: Existence of the correlation function [compensator zero | G(s) time constant] even with different room dimensions 123
Fig 5.20: Existence of the correlation function [compensator pole | H(s) time constant] even with different room dimensions 123
Fig 5.21: Existence of the correlation function [compensator pole | open loop thermal lag] even with different room dimensions 123
Fig 5.22: Existence of the correlation function [compensator pole | closed loop corrected thermal lag] even with different room dimensions 124
Fig 5.23: Existence of the correlation function [compensator zero | G(s) time constant] even with different radiant panel parameters 126
Fig 5.24: Existence of the correlation function [compensator pole | H(s) time constant] even with different radiant panel parameters 126
Fig 5.25: Existence of the correlation function [compensator pole | open loop thermal lag] even with different radiant panel parameters 126
Fig 5.26: Existence of the correlation function [compensator pole | closed loop corrected thermal lag] even with different radiant panel parameters 127

Fig. 6.1: System electrical equivalent extended with the solar radiation disturbance 130
Fig. 6.2: System electrical equivalent, J(s) analysis 130
Fig. 6.3: System electrical equivalent neglecting the pipe dynamics 131
Fig. 6.4: System electrical equivalent, K(s) analysis 132
Fig. 6.5: Comparison of the dynamic part of G(s) and K(s) 132
Fig. 6.6: Limit frequency to approximate the dynamics of K(s) to the dynamics of G(s) 133
Fig. 6.7: Block diagram of the system affected even by the solar radiation disturbance 134
Fig. 6.8: Analysis of the theta term in function of phi and d/c 137
Fig. 6.9: combinations of phi and d/c that return a negligible theta term 137
Fig. 6.10: Graphic representation of the VarGainJ(t) term 141

Fig. 7.1: Graphic representation of the effect of the measurement offset 147
Fig. 7.2: Fault casuistry with positive measurement offset depending on the offset measurement (A-D) and the value of Tm,needed (1–8) 148
Fig. 7. 3: Fault casuistry with negative measurement offset depending on the offset measurement (A-D) and the value of Tm,needed (1–8) 153

Fig. 8.1: G(s) closed loop estimation, identified time constant accuracy: Test 1 158
Fig. 8.2: G(s) closed loop estimation, identified time constant accuracy: Test 2 159
Fig. 8.3: G(s) open loop estimation, identified time constant accuracy: Test 1.....160
Fig. 8.4: G(s) open loop estimation, identified time constant accuracy: Test 2.....161
Fig. 8.5: G(s) estimation in open loop exploiting H(s) estimation, identified time constant accuracy: Test 1 163
Fig. 8.6: G(s) estimation in open loop exploiting H(s) estimation, identified time constant accuracy: Test 2 164
Fig. 8.7: G(s) estimation in open loop exploiting H(s) estimation, identified time constant accuracy: Test 3 165
Fig. 8.8: H(s) open loop estimation using an estimated G(s) gain with 5% error, identified time constant accuracy.....167
Fig. 8.9: Outside air temperature profile used to test the tuning algorithms.....169
Fig. 8.10: Effect of the tuning algorithms in the outside air temperature disturbance rejection 169
Fig. 8.11: Tuning algorithm 1 tested on the 39 representative rooms and limit cases (left) and on 40 random rooms (right) 170
Fig. 8.12: Tuning algorithm 1 tested with an additive estimation/measurement error on the 39 representative rooms and limit cases (left) and on 40 random rooms (right) 170
Fig. 8.13: Tuning algorithm 2 tested on the 39 representative rooms and limit cases (left) and on 40 random rooms (right) 171
Fig. 8.14: Tuning algorithm 2 tested with an additive estimation/measurement error on the 39 representative rooms and limit cases (left) and on 40 random rooms (right) 171
Fig. 8.15: Tuning algorithm 3 tested on the 39 representative rooms and limit cases (left) and on 40 random rooms (right) 172
Fig. 8.16: Tuning algorithm 3 tested with an additive estimation/measurement error on the 39 representative rooms and limit cases (left) and on 40 random rooms (right) 172
Fig. 8.17: Tuning algorithm 4 tested on the 39 representative rooms and limit cases (left) and on 40 random rooms (right) 173
Fig. 8.18: Tuning algorithm 4 tested with an additive estimation/measurement error on the 39 representative rooms and limit cases (left) and on 40 random rooms (right) 173
Fig. 8.19: Tuning algorithm 5 tested on the 39 representative rooms and limit cases (left) and on 40 random rooms (right) 174
Fig. 8.20: Tuning algorithm 5 tested with an additive estimation/measurement error on the 39 representative rooms and limit cases (left) and on 40 random rooms (right) 174
Fig. 8.21: Tuning algorithm 6 tested on the 39 representative rooms and limit cases (left) and on 40 random rooms (right) 175
Fig. 8.22: Tuning algorithm 6 tested with an additive estimation/measurement error on the 39 representative rooms and limit cases (left) and on 40 random rooms (right) 175
Fig. 8.23: Tuning algorithm 7 tested on the 39 representative rooms and limit cases (left) and on 40 random rooms (right) 176
Fig. 8.24: Tuning algorithm 7 tested with an additive estimation/measurement error on the 39 representative rooms and limit cases (left) and on 40 random rooms (right) 176

List of tables

Tab. 4.1: Walls parameters range....68
Tab. 4.2: Pavement parameters range....69
Tab. 4.3: Parameters of the 9 representative rooms....70
Tab. 4.4: Parameters of the 39 representative rooms and limit cases....72

Tab. 7.1: Fault diagnosis casuistry with positive measurement offset....149
Tab. 7.2: Fault examples casuistry with positive measurement offset....150
Tab. 7.3: Fault diagnosis casuistry with negative measurement offset....154
Tab. 7.4: Fault examples casuistry with negative measurement offset....156

PAGE INTENTIONALLY LEFT BLANK

Bibliography

[1] K. Astrom, B. Wittenmark, “Adaptive control”, 2nd ed., Addison - Wesley, 1995

[2] C. G. Nesler, “Adaptive control of thermal processes in buildings, IEEE Control Systems Magazine, 6(4), pp. 9 - 13, 1986.

[3] L. Bakker, A. Brouwer, R. Babuska, “Integrated predictive adaptive control of heating, cooling, ventilation, daylighting and electrical lighting in buildings”, International Journal of Solar Energy, 21(2-3), pp. 203 - 217, 2007.

[4] J. Moon, “Performance of ANN-based predictive and adaptive thermal-control methods for disturbances in and around residential buildings”, The International Journal of Building Science and its Applications, 48, pp. 15 - 26, 2012

[5] M. Adolph, N. Kopmann, B. Lupulescu, D. Muller, “Adaptive control strategies for single room heating”, Energy and Buildings, 68, pp. 771 - 778, 2014

[6] M. Tanaskovic, L. Fagiano, R. Smith, M. Morari, “Adaptive receding horizon control for constrained MIMO systems”, Automatica, 50, pp. 3019-3029, 2014.

[7] I. Landau, R. Lozano, M. M'saad, A. Karimi, “Adaptive Control, Algorithms, Analysis and Applications”, New York: Springer, 2011

[8] J. Kim, T. Yoon, H. Shim, “Switching adaptive output feedback model predictive control for a class of input-constrained linear plants”, IET Control Theory & Applications, pp. 573 - 582, 2008.

[9] International Organization for Standardization, EN 13790: Energy performance of buildings - Calculation of energy use for space heating and cooling, ISO, 2008.

[10] Ente Italiano di Normazione, UNI TS 11300:2008 – Energy Building Efficiency - Parte 1: Determinazione del fabbisogno di energia termica dell'edificio per la climatizzazione estiva ed invernale, UNI, 2008.

[11] International Organization for Standardization, EN 13789:2007 Thermal performance of buildings - Transmission and ventilation heat transfer coefficients - Calculation method, ISO, 2007.

[12] G. Rios-Moreno, M. Trejo-Perea, R. Castaneda-Miranda, V. Hernandez-Guzman, G. Herrera-Ruiz, “Modelling temperature in intelligent buildings by means of autoregressive models”, Automation in Construction, pp. 713-722, 2007.

[13] S. Wu e S. Jian-Qiao, “A physics-based linear parametric model of room temperature in office buildings”, Building and Environment, vol. 50, pp. 1-9, 2012.

[14] K. Amarasinghe, D. Wijayasekara e M. Manic, “Neural Network Based Downscaling of Building Energy Management System Data”, in IEEE International Symposium on Industrial Electronics (ISIE 2014), Istanbul, Turkey, 2014.

[15] H. Park, M. Ruellan, A. Bouvet, E. Monmasson e R. Bennacer, “Thermal Parameter Identification of Simplified Building Model with Electric Appliance”, in 11th International

Conference on Electrical Power Quality and Utilisation (EPQU), Lisbon, Portugal, 2011.

[16] F. Casella, “Advanced Process Control” course notes, 2016.

[17] M. A.Johnson, M. H.Moradi, “PID Control”, PID Applications, 2005 .

[18] K. J. Åström, T. Hägglund, “Advanced PID Control”, Research Triangle Park, NC: Instrumentation, System and Automation Society, PID Applications, pp. 216-251, 2006.

[19] MathWorks Matlab documentation.

[20] P. Bolzern, R. Scattolini, N. Schiavoni, “Fondamenti di controlli automatici”, Automation Theory, McGraw-Hill, 2008.

[21] www.weatheronline.co.

[22] L. Magni, R. Scattolini, “Advanced and Multivariable Control”, Automation Theory, Pitagora Editrice Bologna, 2014.

[23] A. Leva, “Automation of Energy Systems” course notes, 2016.

[24] Garnier, H., M. Mensler, and A. Richard. "Continuous-time Model Identification From Sampled Data: Implementation Issues and Performance Evaluation" International Journal of Control, 2003, Vol. 76, Issue 13, pp 1337–1357.

[25] Ljung, L. “Experiments With Identification of Continuous-Time Models”, Proceedings of the 15th IFAC Symposium on System Identification. 2009.

[26] T. Chai, R. R. Draxler, “Root mean square error (RMSE) or mean absolute error (MAE)? – Arguments against avoiding RMSE in the literature”, in Geoscientific Model Developement, College Park, MD, USA, 2014.

[27] Concrete Masonry Association of California and Nevada, http://www.cmacn.org.

[28] G. Mantovani, L. Ferrarini, L. Bascetta, “Model predictive control of flexible energy efficient buildings in smart microgrids”, Doctoral Dissertation, 2014.